Metallisation and Structuring of Low Temperature Co-fired Ceramic for Micro and Millimetre Wave Applications

By

Dilshani Rathnayake-Arachchige

PhD Thesis Presented to the

Wolfson School of Mechanical and Manufacturing Engineering

In Partial Fulfilment of the Requirements for the Degree of Doctor of Philosophy of Loughborough University

Loughborough University

Certificate of Originality
Thesis Access Conditions and Deposit Agreement

Students should consult the guidance notes on the electronic thesis deposit and the access conditions in the University's Code of Practice on Research Degree Programmes

Author… Dilshani Rathnayake-Arachchige
Title…… Metallisation and Structuring of Low Temperature Co-fired Ceramic for Micro and Millimetre Wave Applications

I [Dilshani Rathnayake-Arachchige, Loughborough University], "the Depositor",
would like to deposit "Metallisation and Structuring of Low Temperature Co-fired Ceramic for Micro and Millimetre Wave Applications", hereafter referred to as the "Work", once it has successfully been examined in Loughborough University Institutional Repository

Status of access OPEN

Moratorium Period……years,
ending……../……20…….

Status of access approved by (CAPITALS):……

Supervisor (Signature)……...……...

School of Mechanical and Manufacturing Engineering

Author's Declaration *I confirm the following :*

CERTIFICATE OF ORIGINALITY
This is to certify that I am responsible for the work submitted in this thesis, that the original work is my own except as specified in acknowledgements or in footnotes, and that neither the thesis nor the original work therein has been submitted to this or any other institution for a degree

NON-EXCLUSIVE RIGHTS
The licence rights granted to Loughborough University Institutional Repository through this agreement are entirely non-exclusive and royalty free. I am free to publish the Work in its present version or future versions elsewhere. I agree that Loughborough University Institutional Repository administrators or any third party with whom Loughborough University Institutional Repository has an agreement to do so may, without changing content, convert the Work to any medium or format for the purpose of future preservation and accessibility.

DEPOSIT IN LOUGHBOROUGH UNIVERSITY INSTITUTIONAL REPOSITORY
I understand that open access work deposited in Loughborough University Institutional Repository will be accessible to a wide variety of people and institutions - including automated agents - via the World Wide Web. An electronic copy of my thesis may also be included in the British Library Electronic Theses On-line System (EThOS).
I understand that once the Work is deposited, a citation to the Work will always remain visible. Removal of the Work can be made after discussion with Loughborough University Institutional Repository, who shall make best efforts to ensure removal of the Work from any third party with whom Loughborough University Institutional Repository has an agreement. Restricted or Confidential access material will not be available on the World Wide Web until the moratorium period has expired.

- That I am the author of the Work and have the authority to make this agreement and to hereby give Loughborough University Institutional Repository administrators the right to make available the Work in the way described above.
- That I have exercised reasonable care to ensure that the Work is original, and does not to the best of my knowledge break any UK law or infringe any third party's copyright or other Intellectual Property Right. I have read the University's guidance on third party copyright material in theses.
- The administrators of Loughborough University Institutional Repository do not hold any obligation to take legal action on behalf of the Depositor, or other rights holders, in the event of breach of Intellectual Property Rights, or any other right, in the material deposited.

*The statement below shall apply to **ALL** copies:*

This copy has been supplied on the understanding that it is copyright material and that no quotation from the thesis may be published without proper acknowledgement.

Restricted/confidential work: All access and any copying shall be strictly subject to written permission from the University Dean of School and any external sponsor, if any.

Author's signature……..Date……...……...……

user's declaration: for signature during any Moratorium period (Not Open work): ***I undertake to uphold the above conditions:***			
Date	Name (CAPITALS)	Signature	Address

ABSTRACT

The recent developments in Low Temperature Co-fired Ceramic (LTCC) as a substrate material enable it to be used in the micro and millimetre wave range providing low dissipation factors at high frequencies, good dielectric properties and a high degree of integration for further miniaturised devices. The most common metallisation method used in LTCC technology is screen printing with high cost noble metals such as silver and gold that are compatible with the high sintering temperatures (850^0C). However, these techniques require high capital cost and maintenance cost. As the commercial world requires convenient and low cost process technologies for mass production, alternative metallisation methods should be considered. As a result, electroless copper plating of fired LTCC was mainly investigated in this research.

The main goals of this project were to carry out electroless plating of fired LTCC with sufficient adhesion and to extend the process to metallise closed LTCC channel structures to manufacture Substrate Integrated Waveguide (SIW) components. The objectives were focused on electroless copper deposition on fired LTCC with improved adhesion. Electroless deposits on the Sn/Pd activated LTCC surface showed poor adhesion without any surface pre-treatments. Hence, chemical etching of fired LTCC was carried out using concentrated NaOH solution. NaOH pre-treatment of LTCC led to the formation of flake like structures on the LTCC surface. A number of surface and chemical analysis techniques and weight measurements were used to investigate the mechanism of the modification of the LTCC surface. The results showed that the flake like structures were dispersed in the LTCC material and a material model for the LTCC structure was proposed. SEM EDX elemental mapping showed that the flake like structure consisted of aluminium, calcium, boron and oxygen. Further experiments showed that both the concentration of NaOH and the immersion time affect the surface morphology and the roughness of fired LTCC. The measured Ra values were 0.6 μm for untreated LTCC and 1.1 μm for the LTCC sample treated with 4M NaOH for 270 minutes. Adhesion tests including peel test and scratch test were carried out to examine the adhesion strength of the deposited copper and both tests indicated that the NaOH pre-treatment led to an improvement, with the best results achieved for samples treated with 4M NaOH.

A second aspect of the research focused on the selective metallisation of fired LTCC. Excimer laser machining was used to pattern a resist film laminated on the LTCC surface. This process also roughened the substrate and created channels that were characterised with respect to the laser operating parameters. After patterning the resist layer, samples were activated using Sn/Pd catalyst solution followed by the electroless copper deposition. Electroless copper was selectively deposited only on the patterned LTCC surface. Laser parameters clearly affected the copper plating rate. Even with a similar number of shots per area, the tracks machined with higher repetition rate showed relatively more machining depth as well as good plating conditions with low resistance values. The process was further implemented to realize a complete working circuit on fired LTCC. Passive components including a capacitor and an inductor were also fabricated on LTCC using the mask projection technique of the excimer laser system. This was successful for many designs, but when the separation between conductor lines dropped below 18 μm, electroless copper started to deposit on the areas between them.

Finally, a method to deposit copper films on the internal walls of closed channel structures was developed. The method was first demonstrated by flowing electroless copper solutions through silane treated glass capillaries. A thin layer (approx. 60 nm) of electroless copper was deposited only on the internal walls of the glass capillaries. The flow rate of the electroless copper solution had to be maintained at a low level as the copper deposits tended to wash away with higher flow rates. The structures were tested for transmission losses and showed low (<10dB) transmission losses in the terahertz region of the electromagnetic spectrum. The process was further applied to deposit electroless copper on the internal walls of the LTCC closed channel structures to manufacture a LTCC Substrate Integrated Waveguide (SIW).

Key words: Low Temperature Co-Fired Ceramic (LTCC); Electroless copper plating; Excimer laser machining; Dry film photo-resist; LTCC passive components; Substrate Integrated Waveguide (SIW);

ACKNOWLEDGEMENTS

Foremost, I would like to express my sincere gratitude to my supervisors, Dr David Hutt and Professor Paul Conway for their endless support throughout my PhD study and research. Their guidance, motivation and immense knowledge helped me in all the time of research and writing of this thesis.

Of course, this research would not have been possible without the help of the Laboratory support staff. I would like to acknowledge Mr Andy Sandaver, Mr Simon Neal, Mr Jagpal Singh, Mr Peter Wileman, Mr David Britton and Mr Mark Capers for their technical advice and support. I would also like to give special thanks to Dr Keith Yendall and Dr Patricia Cropper from the Materials Department for assisting me with surface characterization techniques. A special thank you goes to Dr John Nunn at the UK National Physical Laboratory for help in scratch testing.

Also I thank my project partners, Mario D'Auria, Dr Stepan Lucyszyn, Razak M. Lee, Professor Ian D. Robertson and Sunday Ayodeji for providing me with the LTCC sample specimens and for valuable discussions.

The financial support of the Innovative Electronics Manufacturing Research Centre (IeMRC) provided under Engineering and Physical Sciences Research Council (EPSRC) grant reference number EP/H03014X/1 is gratefully acknowledged.

My next sincere thanks also go to my parents for encouraging me to pursue a PhD in the first place. Last, but not the least, I would like to thank my loving husband Dilan Amaratunga and my loving son Seth Amaratunga for their great patience and support in all aspects.

Table of Contents

List of Figures

List of Tables

Publications and Awards Arising from this Research

1) **Rathnayake-Arachchige, D.**; Hutt, D.A.; Conway, P.P., "Adhesion improvement of electroless copper (Cu) thin films deposited on Low Temperature Co-fired Ceramics (LTCC)," *4th Electronic System-Integration Technology Conference (ESTC)* pp.1-5, Amsterdam, Sept. 2012

2) **Invited Paper**- **Rathnayake-Arachchige, D.**, Hutt, D.A., Conway, P.P., Excimer Laser Machining of Fired LTCC for Selectively Metallised Open Channel Structures. IMAPS 46th International Symposium on Microelectronics. Orlando 2013 (**Invited to publish in *Journal of Microelectronics and Electronic Packaging*)**

3) **Rathnayake-Arachchige, D.**, Hutt, D.A., Conway, P.P., D'Auria, M., Lucyszyn, S., Lee R.M., Robertson, I.D., Patterning of Electroless Copper Deposition on Low Temperature Co-fired Ceramics. 15th Electronics Packaging Technology Conference, Dec 2013, Singapore

4) **Journal paper** in Preparation for *Journal of Electronic Materials*- **Rathnayake-Arachchige, D.**, Hutt, D.A., Conway, P.P., Effect of NaOH Treatment on the Surface Morphology of Low Temperature Co-fired Ceramic.

Awards

1) **BEST of Session award for the paper (Rathnayake-Arachchige, D.**, Hutt, D.A., Conway, P.P., "Excimer Laser Machining of Fired LTCC for Selectively Metallised Open Channel Structures"**) presented at** IMAPS 46th International Symposium on Microelectronics, Orlando 2013, Session-European Perspective on Packaging Trends

2) **IEEE UL&IR Award** for excellence and potential for commercialization for the project (N. Somjith (presenter), Razak M. Lee, A. Sunday, N. Kapur, P. Steenson, **Dilshani Rathnayake-Arachchige**, David A. Hutt, Paul P. Conway, Mario D'Auria, Stepan Lucyszyn, "3-D microwave and millimetre-wave system-on-substrate using RF-MEMS components" at Research to industry (R2i2) 2013 electronics conference.

Chapter 1 Introduction

1.1 Introduction

The global electronics industry seeks low cost and reliable manufacturing strategies in order to develop miniaturised electronic devices with high performance and long service life [1]. The necessity of developing such devices is becoming increasingly important as other fields, i.e. medical, space, automotive and military, benefit from such developments [2]. Within electronics manufacturing, high frequency microwave and millimetre wave applications such as communication and sensing devices have substantial customer demand and popularity. For example, with the evolution of 3G and 4G communication networks, the customer requirement has moved towards handsets that provide high bandwidth for data communications and internet access.

Electronics packaging has gone through rapid changes in the past few decades, to keep up with the above trends in device miniaturisation and functionality. A limitation of the miniaturisation of millimetre wave electronic devices arises with the inconvenience of integrating passive components such as waveguides and antennas onto the substrate, because these devices are large in size or unable to achieve the required performance when integrated. As frequency increases, the conventional substrates or packaging materials need to be replaced with novel substrate materials to maintain the required performance. In this respect, ceramic materials are a promising candidate for micro and millimetre wave applications due to their excellent characteristics such as dielectric properties and low signal loss at high frequencies. However, in order to use these materials in mass production, convenient methods are needed to metallise them and there is increasing interest in developing novel structures to enable further performance enhancements. With ceramic multilayer technology it is possible to integrate waveguide structures into ceramic substrates to achieve the further miniaturisation of the complete system. Furthermore, it is

one of the promising approaches where traditional system technologies can be replaced by System-on-Substrate (SoS), which is a recent packaging concept and still a subject of research [3],[4]. System-on-Substrate (SoS) is an important concept when employing multilayer miniaturised circuitry, which integrates all the system components onto a single substrate material (Figure 1). The interconnection between system components is achieved through tracks and metallised via holes and the SoS concept fulfils the demand from the electronics sector for further miniaturised system technologies.

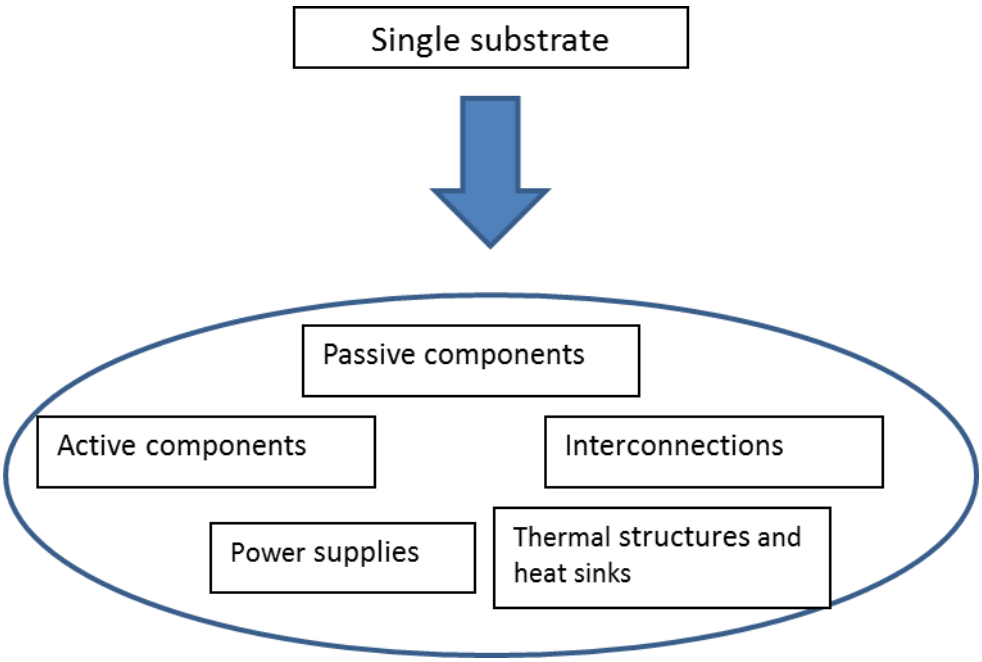

Figure 1 System-on-Substrate (SoS) concept

The research presented here addresses the issues associated with the metallisation of ceramics for use in SoS. This chapter introduces the requirements of substrates for high frequency applications and metallisation techniques which can be alternatively used in those substrates, before describing the context in which the research was conducted.

1.2 Research Background

1.2.1 Microwave and Millimetre Wave Applications

The radio waves in the frequency range of 3-30 GHz are generally defined as microwaves and the term millimetre wave refers to the frequency range of 30-300 GHz [5]. Microwave and millimetre wave devices are used in a wide variety of applications ranging from portable communication systems, satellite transceivers, wireless local area networks, radios etc. The main advantages of moving from the low frequency band towards the microwave and millimetre wave spectrum are that high speed data rates can be achieved, better tolerance to atmospheric attenuation when propagating for long distances and the availability of unused bandwidth. This technology was first reported in 1895, by the Indian physicist J. C. Bose who demonstrated wireless signalling at 60 GHz with various microwave components including waveguides and horn antennas [6]. In recent years many applications in the microwave and millimetre wave region have been employed in the consumer electronics industry. In 2008, Li et al. presented a 24 GHz frequency–modulation continuous-wave radar front end system. This system was used to recognise a stationary metal object which was 2.5 - 5m away from the radar [4]. In 2009, Gautier et al. demonstrated a RF-MEMS phased array antenna on a low loss Low Temperature Co-fired Ceramic (LTCC) substrate for a Kα-band data link [7]: the antenna was demonstrated from 33 GHz up to 40 GHz and beyond with -10dB measured return loss. In 2011, Pursula et al. developed a 60 GHz millimetre-wave identification reader which can be used for accessing tags [8]. In this study, they also used LTCC as the substrate material and all the microwave components were integrated into the module. The VTT research group in Finland has also designed a 77 GHz beam switching antenna on LTCC [9].

1.2.2 Substrate Materials in the Electronics Industry

The primary function of the substrate material in electronic packaging is to provide physical separation between conductors and to regulate or prevent current flow between them. It also provides mechanical support, heat dissipation, thermal shock resistance and a chemically stable environment for conductors [10].

Electronic substrate materials typically require good adhesion for conductors, little variation of properties at high temperatures, low cost and good thermal conductivity.

However, the substrate materials used in high frequency applications should also deliver low loss at high frequencies and little variation of dielectric constant with frequency [11]. Table 1 compares the electrical and thermal properties of typical electronic substrate materials. It can be seen that for high frequency applications the traditional FR4 substrates which are widely used in printed circuit board manufacture should be replaced by substrate materials such as High Temperature Co-fired Ceramic (HTCC) and Low Temperature Co-fired Ceramic (LTCC).

Table 1 Comparison of electrical and thermal properties of typical electronic substrate materials (data compiled from:[12], [13], [14], [15], [16])

Substrate material	**Dielectric constant**	**Dissipation factor (loss tangent)**	**Thermal expansion (ppm/^{0}C)**	**Thermal conductivity (W/m.K)**
LTCC	7.1 @10 GHz	0.0009 @10 GHz	4.4	4.6
HTCC >92% Al_2O_3	9.2 @10 GHz	0.003 @10 GHz	6.8-8	17-35
FR4	4.2 @3 GHz	0.008 @3 GHz	12-16	0.2
Glass	5.7-7.2 @10 GHz	0.006 @10 GHz	9.2	2
Si	12 @10 GHz	0.015 @10 GHz	2.6	120-150
Alumina (94%)	9.1 @ 1 MHz	0.0007 @ 1kHz	6.5-7.2	22-40
PTFE (RO3003)	3 @10 GHz	0.0013 @10 GHz	13	0.5

1.2.3 Low Temperature Co-fired Ceramics

The LTCC technology developed as a combination of high temperature co-fired ceramics where the metallisation was done with high melting point metals such as tungsten (W) and molybdenum (Mo) and thick film technology. Since W and Mo are low conductivity metals, there was a requirement to lower the sintering temperatures of the ceramics in order to use silver and gold which have relatively low melting points and good conducting properties compared to W and Mo. The most effective and inexpensive way to lower the

sintering temperature of the ceramic was to use liquid phase sintering using glass additives [17].

The developments in glass-ceramics in microelectronics packaging started in the 1980s for devices that were used in computers [18]. Since then, research has been constantly carried out to find the correct components and compositions of glass and ceramic systems to achieve the performance required by the electronic packaging industry. Some of these requirements include dielectric constant, mechanical strength, wiring density, metallisation, dimensional control and matching thermal expansion to silicon [19].

In microwave and millimetre wave applications, Low Temperature Co-fired Ceramic has drawn significant attention in the past few decades as a potential substrate material in electronic devices, due to its characteristic features, such as low loss tangent and high degree of integration, low dissipation factors and suitable dielectric properties [17], [20]. Green LTCC is soft and flexible, so cavities and vias can be fabricated in the green state LTCC for further miniaturised electronic systems with high performance. LTCC is favourable over other high density substrate materials such as High Temperature Co-fired Ceramics (HTCC) or organic laminates due to better dielectric properties in the high frequency region of the electromagnetic spectrum [20], [21]. Also, compared to HTCC, which uses high melting point conductors such as molybdenum (melting point-2623^0C) and tungsten (melting point-3370^0C), low temperature sintering allows LTCC to use better conductors such as silver (melting point-1100^0C) and gold (melting point-960^0C) [22].

LTCC is a glass ceramic composite that consists of a glass matrix and Aluminium Oxide crystalline particles as filler material with a typical diameter range of 2 µm - 3 µm. The green state LTCC is a combination of inorganic and organic material. The inorganic part is mainly formed from Alumina (Al_2O_3) and SiO_2-B_2O_3. The organic part is a blend of binder, plasticizer, dispersing agent, solvent and wetting agent. The LTCC green tapes are obtained from tape casting by spreading the ceramic slurry on a moving carrier substrate and removing some of the volatile organics. Then the green tapes are subjected to a soft bake procedure to obtain a final green tape with thickness between 40 µm - 250 µm depending on the requirements[17]. This soft green state LTCC becomes a dense ceramic body with the final liquid phase sintering process [23].

1.2.4 LTCC Multilayer Technology

LTCC offers a high degree of integration for electronic systems and can achieve up to 50 layers. In addition to this, it provides hermeticity, matching of coefficient of thermal expansion with silicon [24], high thermal dissipation compared to other ceramics, high temperature and frequency applications, and reduced size and cost [25]. Multilayer technology is very popular for system level packaging [26]. In multilayer technology, conductors between the ceramic layers are connected through via holes to achieve compact and miniaturised system devices as shown in Figure 2.

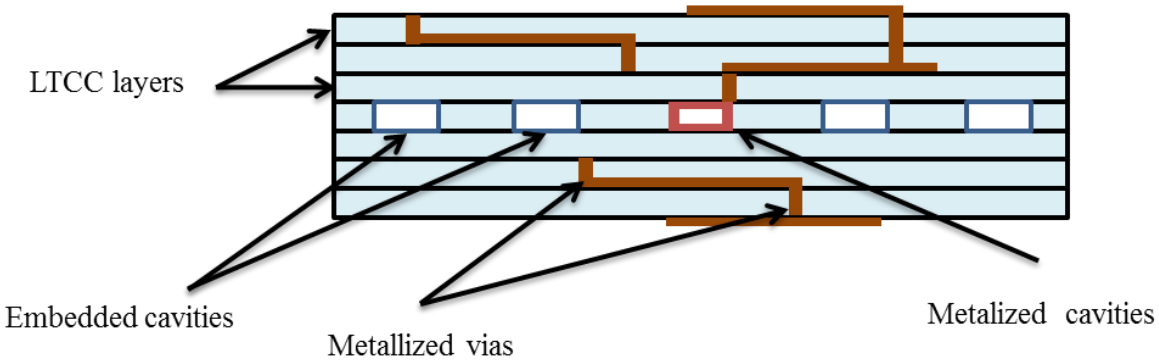

Figure 2 Schematic diagram of LTCC miniaturised device

Multilayer glass-ceramic composites i.e. High Temperature Co-fired Ceramics and Low temperature Co-fired ceramics deliver high density first level (chip to package) and second level (package to board) interconnections [27]. LTCC has been established as a multilayer technology and the state of the art of this technology provides for channel structures and cavities inside the ceramic body. Several LTCC layers can be laminated together and it allows the application of embedded active and passive components as well as microfluidic systems and becomes very attractive for miniaturised electronic devices. To manufacture a multilayer ceramic substrate, several process steps are required that differ from the conventional FR4 PCB manufacture (Figure 3).

Pre-conditioning - This is a thermal treatment which removes any residual solvent and releases any stresses due to the tape casting process.

Via and cavity formation - Vias for electrical connection, cavities for embedded active components such as integrated circuits, RF-MEMS switches, varactors and transistors etc., and channels for microfluidic or waveguide structures are prepared before the tapes

undergo the firing process. Typically, the vias are formed in the green LTCC tapes by mechanical punching or laser drilling, while the cavities and channel structures are formed by laser machining techniques.

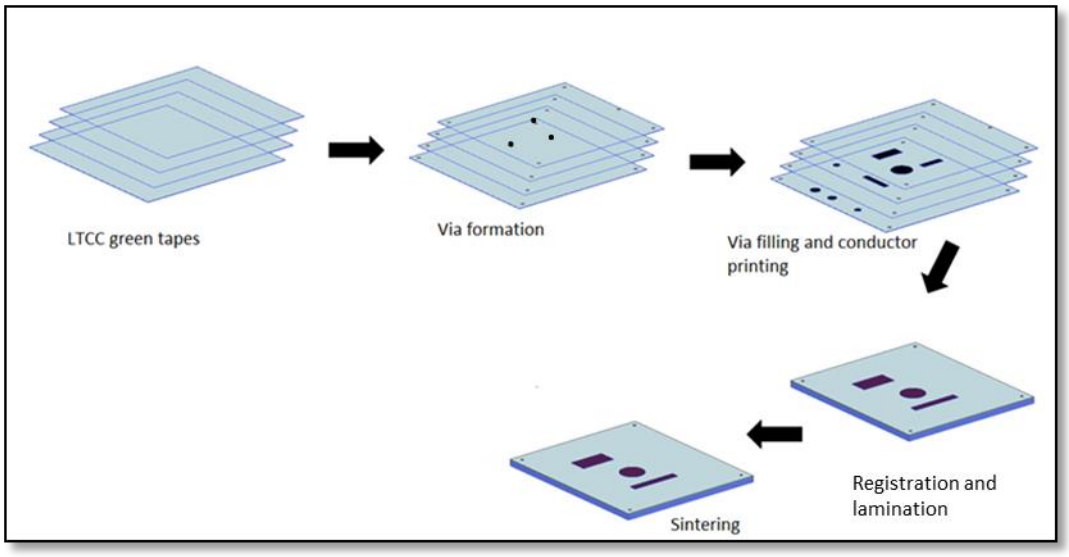

Figure 3 Conventional LTCC Processing

Via filling and conductor printing - The vias are fully filled with via paste and the required conductor patterns are printed using conductor paste which is compatible with the in-plane shrinkage of the ceramic when fired. These pastes are usually obtained by mixing conductive powder in an organic medium that consists of thinning agents, organic binders, plasticizers, and dispersing agents. Via paste is somewhat different to the conductor paste as the viscosity needs to be maintained above a certain value at a particular temperature to achieve void free filling [28]. Planar passive components such as capacitors, inductors, resistors, antennas and sensors which are key elements in signal processing are also printed on green tapes using the screen printing process.

Lamination- The green tapes are stacked and then undergo heat and pressure treatment to complete the lamination process. The lamination process can be two types depending on the method of applying pressure to the green tapes. Uniaxial lamination uses a hydraulic press with heated platens, while isostatic lamination uses a heated water press with the LTCC sealed in a plastic bag. Recommended temperature and pressure values are available, however those values can be altered to get better lamination [29].

Co-firing- The laminated green tapes are then baked in a furnace at a maximum of 850^0C. Each green tape has its own unique firing profile. The organic components in the LTCC

green tapes are evaporated during the firing process around 500^0C [30]. Dissolution and rearrangement of glass and ceramic particles and precipitation of newly formed crystals takes place in the liquid phase sintering process. The final densification is achieved by solid state sintering by further reducing the porosity of the material.

1.3 Metallisation of LTCC

Metallisation is a major requirement for substrate materials in the electronics industry for inter-level connections, integration and assembly of other components to the substrate and fabrication of passive devices. Several metallisation techniques such as inkjet printing, electroplating, sputter deposition, electroless plating and screen printing have been employed for LTCC substrates, depending on whether they are in a fired or unfired condition [31], [32]. Among these techniques screen printing is the most widely used method to metallise unfired LTCC tape as it fits within the conventional LTCC process steps. Green state LTCC contains organic material which is not stable in chemical plating baths and therefore cannot be metallised in this way. However, in cases where post fired metallisation is required for LTCC a range of metallisation techniques as listed above can potentially be applied.

When selecting a suitable metal, many factors have to be considered. The conductors used in the high frequency range generally require low loss, good adherence with the substrate, compatibility with other materials within the circuitry, good bonding properties with other interconnections and must remain corrosion free in harsh environments. Table 2 characterises some of the properties of metals used for microwave and millimetre wave applications.

Table 2 Characteristics of some of the metals used in the electronics industry [11]

Metal	DC resistivity (ρ) relative to Cu	Skin depth at 2 GHz (μm)	Linear Coefficient of thermal expansion $\times 10^6$ (K^{-1})
Ag	0.95	1.4	21
Cu	1	1.5	18
Au	1.36	1.7	15
Al	1.6	1.9	26
Cr	7.6	4	8.5
Ti	27.7	7.8	9
Mo	3.3	2.7	4.6
W	3.2	2.6	6
Pt	6.2	3.6	9

Commonly less reactive metals such as silver and gold are widely used in many electronic manufacturing applications due to their high electrical conductivity, high electromagnetic resistance and low reactivity with other substances such as moisture and air. However these metals are expensive, so the necessity of using low cost metals arises in the electronics manufacturing field. Copper becomes a suitable candidate for metallisation of electronic devices not only for its lower cost, but also its suitability for further assembly and packaging. Copper has a melting point of 1084 °C, which is above the sintering temperature of LTCC, however, oxidation of copper takes place at high temperatures, and therefore it can only be used to metallise the LTCC green tapes with oxygen free sintering conditions. However, another possible solution is to plate or deposit copper onto fired LTCC tapes, thereby making electroless plating a possible solution.

1.4 Limitations of Conventional LTCC Processing

So far, laser cutting [20], [33], [34], powder blasting [35], mechanical punching [36] and hot embossing [37] of green state LTCC have been used to generate cavities and vias. In the LTCC process steps, 3D structures are usually obtained by stacking of individually structured LTCC layers with the aid of registration pins [38]. However, even though the

green state LTCC layers are carefully aligned during lamination, deformation of these structures can occur during the firing process due to the shrinkage properties of the LTCC material. As mentioned above, the conventional way of metallising LTCC is to employ screen printing technology on green tapes. Usually, commercially available silver or gold paste is printed on the green state LTCC using a screen before the firing process when the metallic particles are sintered together. Therefore, tape shrinkage during firing and screen printing capabilities limit the dimensions of features and restrict the passive components that can be fabricated on green state LTCC. For example, the in-plane shrinkage affects the metal lines' width and separation, which are key factors for the performance of structures deposited to form passive components such as capacitors. Also, any non-uniformity in the shrinkage will affect the shape of the metal lines. Furthermore, when realising 3-D structures, for example, Substrate Integrated Waveguides (SIW) in the ceramic body, metallisation of internal vertical walls of LTCC cavity structures is required for which screen printing is not suitable. To meet current and future demands of structures in LTCC substrates, the commercial world requires convenient and low cost process technologies for mass production and therefore alternative metallisation methods and LTCC processing techniques should be considered.

1.5 Research Challenges

This research was conducted as part of an IeMRC funded project in collaboration with The Optical and Semiconductor Devices Group, Electronic and Electrical Engineering Department, Imperial College London and The Institute of Microwaves and Photonics, University of Leeds. The overall aim was to design and fabricate high performance microwave and millimetre wave components in order to fulfil the requirements of the emerging System-on-Substrate concept. The partners from Imperial College carried out the modelling and simulation of RF MEMS, planar passive components and waveguide components, while the University of Leeds fabricated those structures. The role of Loughborough University was to investigate suitable metallisation techniques that can be applied on fired LTCC as an alternative to the conventional metallisation of LTCC.

Metallisation of the vertical walls of LTCC cavity structures was identified as a research problem in the conventional LTCC processing when realising substrate integrated waveguide components and the passive components that can be used in high frequency

applications. A detailed literature survey was carried out to identify the state of the art in metallisation of LTCC and will be presented in later chapters. It was found that very little research has been carried out since the beginning of LTCC technology on developments of alternative metallisation methods. As a result of this, electroless copper plating was selected in this study because it is low cost and it can be a promising solution when metallising LTCC channel structures. Three research challenges were developed accordingly:

1) Electroless copper deposition on fired LTCC was identified as an alternative to the conventional screen printing process. However, poor adhesion was highlighted due to the low surface roughness of the fired LTCC and therefore, there was a need to investigate a suitable method to improve the adhesion between the metal deposit and the substrate.
2) Methods to pattern the electroless copper deposition on fired LTCC were needed in order to fabricate miniaturised passive components and complete circuits.
3) Finally, it was also identified that electroless copper deposition could be a better candidate to selectively metallise the internal walls of open and closed LTCC channel structures. However, this required techniques to be established to selectively deposit electroless copper only on the internal walls of the structures.

1.6 Aims and Objectives

The aim of this research was to develop an electroless copper metallisation technique that could be used to metallise fired LTCC in order to produce integrated passive components, circuit patterns and substrate integrated waveguides. To achieve this aim, a series of objectives were established:

1. Surface modification and activation of fired LTCC to enable electroless copper deposition with good adhesion between metal deposit and substrate.
2. Investigation of the characteristics of the deposited metal layer, in terms of adhesion, thickness, surface morphology and conductivity.
3. Development of a suitable technique to achieve metal patterns on LTCC for passive components and circuit tracks.
4. Development of a method to metallise internal walls of LTCC micro channels

1.7 Research Approach

In this research, electroless copper deposition onto fired LTCC was studied in detail as an alternative to the conventional screen printing process. Figure 4 shows a schematic diagram of the research approach. The two main aspects which were addressed in this research were electroless plating on to pre-designed structures such as substrate integrated waveguides and selective electroless copper deposition on to fired LTCC. Electroless plating of open channel structures as well as closed channel structures was investigated. The main challenge associated with the electroless deposition on to fired LTCC was adhesion between the substrate and the metal deposit. Published methods to modify the LTCC surface to improve adhesion were reviewed and a sodium hydroxide (NaOH) solution surface pre-treatment was identified as a suitable method to modify closed channels. Other surface modification methods such as laser machining were either difficult to apply or impossible to access enclosed geometries. To create the patterns on LTCC substrate, excimer laser machining combined with a dry film photo resist process was used. An advantage of this method was that the excimer laser machining roughened the LTCC surface, while creating the required pattern, leading to better adhesion between substrate and metal deposit. In addition, the excimer laser machining technique was used to remove material from the fired LTCC to create trenches and selective electroless copper deposition was implemented to metallise these structures to achieve 3D passive components. Finally, a technique was developed to metallise internal walls of the LTCC closed channel structures using flow through electroless plating.

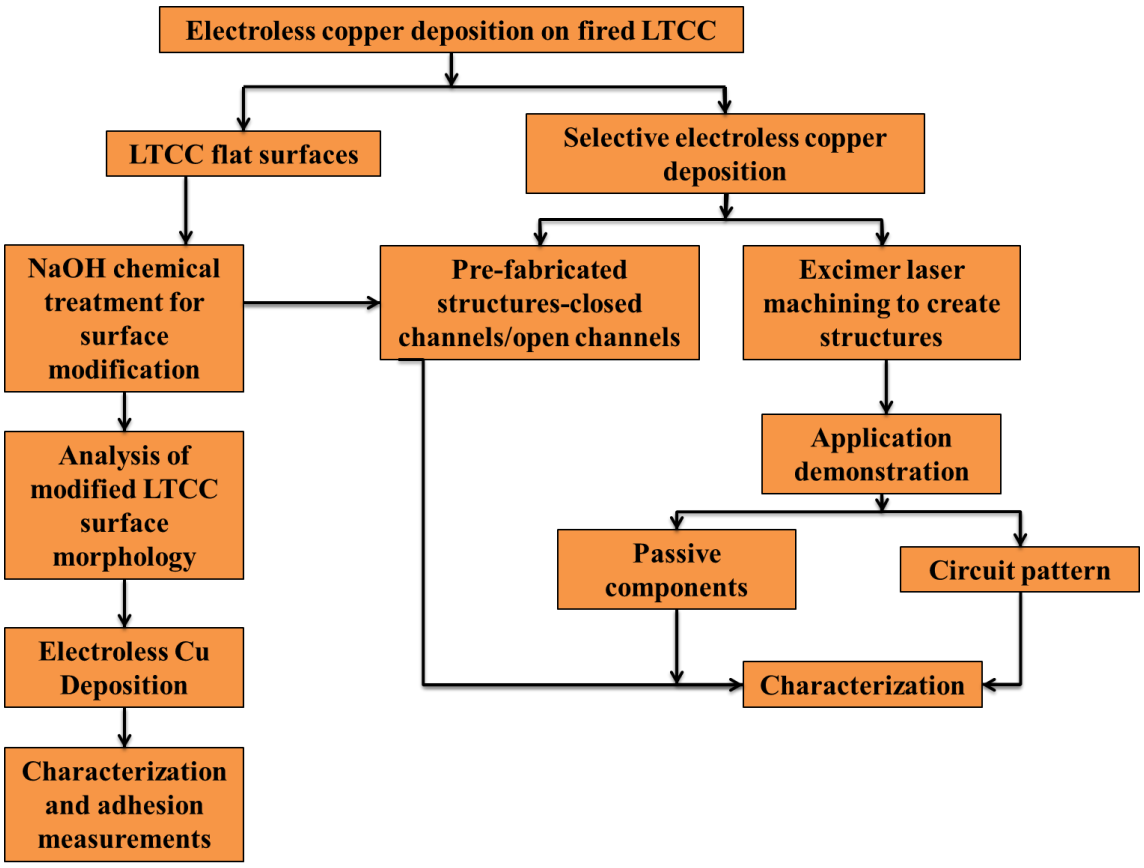

Figure 4 Schematic diagram of the research approach

1.8 Thesis Structure

The research work presented in this thesis mainly focuses on establishing convenient methodologies for electroless copper plating of LTCC substrate materials. This first chapter has introduced low temperature co-fired ceramics, traditional LTCC manufacturing process steps and how the millimetre wave electronic devices benefit from LTCC as an electronic substrate material over other conventional substrates. It has also presented the research problem, motivation for the particular research area, a general overview to the research approach and identified the research novelty. The main objectives and the challenges associated with the research problem are also defined. The second chapter reviews the metallisation techniques available for fired LTCC, explains why the electroless copper plating process was chosen and also presents the initial results of the electroless copper plating on untreated fired LTCC along with associated adhesion problems. The third chapter addresses the surface modification of fired LTCC to improve the adhesion between

deposited electroless copper and the substrate: use of a chemical etching technique to modify the LTCC surface and a detailed study of surface characterization to find the actual etching mechanisms is presented in this chapter. A material model developed for LTCC is introduced in this chapter. Chapter 4 discusses the effect of NaOH solution treatment on the surface roughness of LTCC in terms of NaOH concentration and sample immersion time. In chapter 5, the characterization of electroless copper deposition on flat LTCC is presented. It also contains adhesion results of the deposited copper, characterization of metal deposits and some of the challenges and possible solutions to overcome these problems. Chapter 6 presents excimer laser machining of fired LTCC to create metallised open channel structures. Characterization of machined channels in terms of different laser parameters is addressed here. The sixth chapter also describes the selective metallisation of LTCC tapes and implementation of the process to realize copper circuit patterns, planar and 3-D passive components on fired LTCC. The seventh chapter discusses the development of methods to metallise air-filled substrate integrated waveguide structures with metallic side walls. The approach was demonstrated by metallising the internal walls of glass capillaries. Finally, Chapter 8 gives a summary of the progress made in this research project and offers the work that needs to be done in the future.

Chapter 2 Electroless Copper Deposition on to Fired LTCC

2.1 Introduction

For some time, electroless plating technology has been widely used in the electronics industry for PCB manufacturing and the steel industry for coating applications [39]. One of the inherent features of the electroless plating process is the metallisation of conductive and, more importantly, non-conductive materials without the need to apply an electrical connection to the part. The thickness of the metal layer can be controlled and is an important factor when using high cost metals such as silver and copper. In the electronics industry, the electroless process is mainly used to deposit copper onto an FR4 substrate to metallise vias [40] which is usually reliable as these materials have modified surfaces to enhance the adhesion between the metal deposits and the substrate surface. However, FR4 has its own limitations when used for high frequency applications. In this manner, electroless metal deposition on novel substrate materials such as glass, High Temperature Co-fired Ceramic (HTCC) and LTCC should be considered.

In recent years, electroless plating has been used for LTCC substrates. However, very little information is available in the literature concerning the adhesion of the metal layer to the LTCC, which is an essential criterion for device reliability. Also, no information is available regarding the implementation of electroless plating technology for LTCC when manufacturing electronic devices for real world applications. The capability of achieving selective metallisation patterns with good adhesion and low surface roughness on LTCC substrates using electroless plating is therefore desirable when designing miniature electronic devices. If a well-established process for electroless plating that involves surface activation of the substrate, optimum conditions for maximum adhesion and selective plating for integrating passive components can be achieved, there will be a substantial acceptance by the global electronic industry.

This chapter mainly focuses on establishing the principle of electroless copper plating on LTCC substrate materials. This chapter begins with a literature review of the metallisation techniques available for fired LTCC, the electroless plating process and surface activation, before describing and discussing the experimental results.

2.2 Literature Survey

2.2.1 Metallisation of LTCC

With the limitations of the thick film screen printing technology as described in the first chapter, the recent research has focused on other metallisation techniques available for LTCC. The following table summarises these alternative metallisation techniques.

Table 3 Alternative Metallisation Techniques for Fired LTCC

Year [Ref]	**Metallisation technique**	**Work carried out**	**Challenges**
2005 [41]	Electroless plating	Electroless deposition of Cu, Ag and Au on Nd:YAG laser treated LTCC surface. Area selective metallisation was carried out on laser irradiated areas in order to fabricate metal patterns on fired LTCC. The technique was used to demonstrate basic passive components such as capacitors, coils, resistors and contact pads on fired LTCC using Cu metallisation.	Cu was deposited on LTCC after 4 hours. Thickness of Cu was 150 - 200 nm. Ag particles started to deposit all over the surface without continuity leading to poor conductivity. Au only deposited on glassy LTCC and the surface was attacked and dissolved by the chemical bath.

2008 [32]	Inkjet Printing	Ag nano particle ink was used in this study to form 60-100 μm width patterns on fired LTCC. Electroless nickel was deposited on the Ag patterns to achieve the required metal thickness. This study demonstrated the formation of high aspect ratio micro patterns on fired LTCC.	Width of the conductor lines increased with the plating time. To achieve high aspect ratios, plating was carried out in embossed LTCC channels. The width of the channels were 100 μm.
2011 [31]	Sputtering	Cu films were deposited on LTCC using a sputtering technique. The aim of the study was to investigate the reliability of Cu thin films on fired LTCC as an interesting approach for moderate current density and temperature levels.	The resistivity of 1 μm thick films was 2.8 μΩcm which was higher than the bulk value for Cu (1.7 μΩcm).
2012 [42]	Electroless plating/ electroplating	Both electroplating and electroless plating was carried out on DuPont™ GreenTape™ 9K7 LTCC. Both polished and unpolished LTCC samples were electroplated with copper using a standard TiW seed layer prior to electroless Ni deposition. Another approach was to deposit electroless nickel immersion gold on thick film silver conductors as a surface finish.	Nickel added an additional insertion loss and resulted in higher return loss compared to unplated silver lines. Cu deposited samples had to be fired in an oxygen free environment to prevent copper oxidation.

2.2.2 Electroless Plating Process

Electroless plating of metals such as Cu and Ni has been used as a low cost metallisation method over the years. The wide variety of applications include surface finishes, corrosion protection and under bump metallisation for solder deposition. Electroless plating is widely used in the electronics industry for Printed Circuit Board (PCB) manufacturing and electronic packaging [43]. The common metal ions used in electroless plating are Cu, Ag and Ni depending on the application. Electroless Ni is commonly used as a coating material due to its improved hardness, corrosion resistance, and abrasion resistance [44]. Cu and Ag are extensively used as conductor materials in the electronics industry due to their low bulk resistivity and good thermal stability [45].

2.2.3 Chemistry of Electroless Cu Plating

Electroless Cu plating is an autocatalytic reaction and once the reaction starts it carries on spontaneously until the concentration of reactants in the solution becomes almost zero [46]. The basic chemistry involved with electroless copper plating is an oxidation and reduction reaction (redox reaction) where the electrons are usually provided by formaldehyde (HCHO) reducing the copper ions to their solid metal state: the oxidation state of copper decreases from +2 to zero. The main reactions taking place in an electroless copper bath can be written as follows, with formaldehyde as reducing agent :

$$2HCHO_{(aq)} + 4OH^-_{(aq)} \longrightarrow 2HCOO^-_{(aq)} + 2H_2O_{(aq)} + H_2 + 2e^-$$

$$Cu^{2+}_{(aq)} + 2e^- \longrightarrow Cu_{(s)}$$

These two reactions take place separately on a catalytic surface as shown in Figure 5.

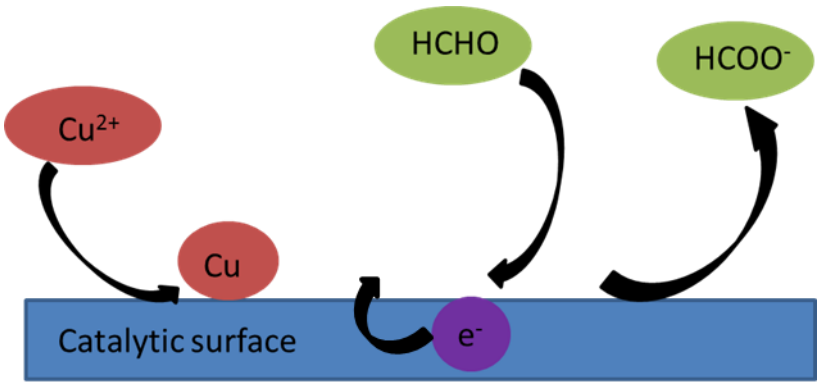

Figure 5 Schematic representation of the electroless process

2.2.4 The Composition of an Electroless Copper Plating Bath

Metal ions and reducing agent are the main components involved in an electroless copper reaction. To optimize the reaction conditions, other chemicals such as stabilizer, complexing agent, accelerator and pH regulator are also added to the reaction mixture [47]. Stabilizers are chemical components that prevent the homogeneous decomposition of the plating solution and inhibit the reaction on non-activated surfaces [44]. Proper control of stabilizer concentration in the plating bath is very important as it will affect the deposition rate, morphology of metal deposit and metal deposition on unwanted areas [46]. Complexing agents such as EDTA can form complexes with metal ions and reduce the free metal ion concentration in the plating bath [47]. Sodium hydroxide is normally added to the solution to control pH between 12.5-13.5 and is required in the oxidation of HCHO [45].

The reaction conditions of the medium directly affect the rate of a chemical reaction. The following factors can be optimized to achieve a better reaction rate [47].

- Temperature- According to the Arrhenius Law, the reaction rate increases with temperature due to increase of molecular vibrations and number of collisions. However, the microstructure of the copper layer changes with temperature. To achieve the required microstructure, the control of temperature in the electroless bath is essential.
- Removal of products from the reaction medium- Usually in an electroless plating bath hydrogen gas is produced in the reaction medium as a by-product. Removal of hydrogen from the reaction medium will increase the reaction rate. Good agitation of the solution is the most effective way of removing hydrogen from the reaction medium.
- Concentration of the reactants- Maintenance of copper ion and formaldehyde concentration is necessary to maintain the reaction rate.

2.3 Surface Activation

Although electroless copper deposition is an autocatalytic reaction, especially for non-conductive materials and in some cases for conductive materials, it is necessary to immerse

the substrate in a catalytic solution to deposit a layer on the surface that can subsequently initiate the electroless reaction. The catalytic pre-treatment of a non-conductive surface for subsequent chemical metal plating is generally known as chemical surface activation. However, there are some cases reported in the literature where laser energy is used to activate dielectric surfaces for electroless metal deposition.

2.3.1 Chemical Surface Activation

The purpose of surface activation is to create a catalytic environment, typically on non-conductive substrate materials for the subsequent electroless plating process. In most electroless plating processes, the formation of a thin palladium catalytic coating on the surface is required. This can be achieved in a one step or two step process.

A. Two Step Method

In some cases, catalytic activity is achieved in a two-step method where the substrate is immersed first in an acidic tin chloride ($SnCl_2$) solution followed by an acidic palladium chloride ($PdCl_2$) solution. In the sensitization step, the Sn^{2+} ions are adsorbed onto the substrate surface. In the activation step, a surface reaction takes place between the Sn^{2+} ions and the Pd^{2+} ions in the catalyst solution [48]. The reactions can be presented as follows:

$$\text{Substrate} + Sn^{2+}{}_{(aq)} \longrightarrow S.Sn^{2+}{}_{ads}$$

$$S.Sn^{2+}{}_{ads} + Pd^{2+}{}_{(aq)} \longrightarrow Sn^{4+}{}_{(aq)} + S.Pd_{\ ads}$$

Where, $S.Sn^{2+}$ represents the Sn^{2+} adsorbed on to the substrate and S.Pd represents the Pd adsorbed on the substrate. Natividad et al. reported a chemical and morphological study to investigate the mechanism of the two step chemical activation for a polycrystalline alumina substrate [49]. X-ray Photoelectron Spectroscopy (XPS), Auger Electron Spectroscopy (AES) and Atomic Force Microscopy (AFM) analysis were carried out to suggest the possible mechanisms. According to their findings, in the sensitization step Sn^{2+} and Sn^{4+} firstly adsorbed on to the alumina surface. Two mechanisms were suggested for the palladium adsorption in the activation step. In the first mechanism the palladium was adsorbed as $PdCl_2$. In the second case it was adsorbed both in metallic (as Pd) and oxidised form (as PdO). The mean roughness (Ra) of the deposited Cu surface achieved was 44% lower in value than the alumina substrate. SEM-EDX analysis was used as a further step to determine the composition of each metal adsorbed on the alumina surface.

B. One Step Method

The two step method cannot be used when plating through-holes on copper–clad boards due to the formation of a non-adherent palladium seed layer on the copper surface [50]. In this case, the catalytic activity is achieved with a mixture of $SnCl_2/PdCl_2$ solution which is also known as one step chemical activation. The Pd^{2+} ions are reduced by the Sn^{2+} ions to form the Pd nuclei in solution which are then adsorbed on the non-metallic surface to activate it [51]. The mechanisms of the catalyst process have been studied in detail in the literature. There are two concepts to describe the catalytic activity of the one step process. The first concept suggests that Sn/Pd colloidal particles are formed and responsible for the catalytic activity, while the second concept claims that the catalytic activity is due to a Sn-Pd solute complex which has the chemical formula $SnPd_7Cl_{18}$ [52]. Different research groups have reported different Sn to Pd atomic ratios in the complex structure. In 1973 Cohen and co-workers carried out a detailed study of the one step Sn/Pd surface activation process including colloid formation, stabilization and particle size distribution by analysing with Mossbauer spectroscopy and centrifugation experiments. Their study suggested that a red-brown Sn-Pd complex which has the stoichiometry of Pd (II).3Sn (II) was formed in the catalytic solution after a few seconds of mixing the Sn and Pd solutions. This complex was then decomposed to the Sn/Pd colloidal system immediately, containing complexed Sn^{4+}, a Sn-Pd alloy core and a small amount of Sn^{2+} [53]. Further studies have suggested a core-shell Pd/Sn colloidal model where $(SnCl_3)^-$ complex forms a shell around the Pd/Sn core to stabilise the system by preventing agglomeration in the solution. Olaf Holderer and co-workers have confirmed that the Sn concentration of the core is less than the Pd concentration at 39 at % [54]. A model of the Pd/Sn catalyst structure on the substrate surface has been proposed by Cui and co-workers [51]. This model was based on detailed study of the surface using X-ray Photoelectron Spectroscopy (XPS) and Secondary Ion Mass Spectrometry (SIMS). According to their model, the conventional Pd-Sn core was further confirmed. However, the idea of $(SnCl_3)^-$ complex was rejected by this model as there was no evidence of fragments of $(SnCl_3)^-$ in the SIMS spectrum. Their results agreed with the model of a Pd-Sn core surrounded by Sn^{4+} ions (Figure 6)

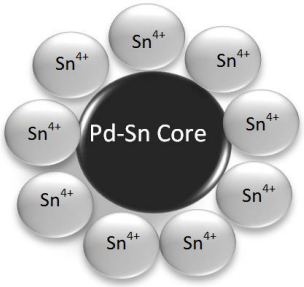

Figure 6 Pd-Sn Core surrounded by Sn^{4+} ions [51]

The surrounding tin ions should be removed from the colloid surface and Pd (0) centres should be exposed to the copper solution in order to achieve the catalytic activity. The tin ions should therefore be dissolved away before the electroless deposition takes place. This can be done by immersing the substrate in an accelerator solution. The accelerator can be an acidic or alkaline solution which has sufficient tin ion solubility and also protects Pd catalytic sites. Typical examples for accelerators are NaOH, H_2SO_4, HCl and NH_4OH etc. [55]. In some of the current electroless systems, the accelerator is in the electroless plating bath itself thereby avoiding an additional process step [47].

C. Other Activation Methods

Jingye Li and co-workers reported a novel method to activate non-metal surfaces using a metal loaded organic solution [56]. In this research, palladium and copper were extracted to an organic solution from an aqueous metal ion solution. Then the non-metallic substrates (Carbon nanotubes, polished alumina and plastic) were immersed in the organic solution to activate the surface followed by subsequent electroless Cu plating. One of the advantages of this method was the use of glyoxylic acid as the reducing agent instead of formaldehyde which is known to be a carcinogenic substance. Also the method has been successful as a single step surface activation method for non-metallic substrates; however the process requires some additional steps in metal extraction. The reaction mechanism of the catalytic process was not mentioned in the article.

The type of surface is also important in catalyst adhesion. For example, it is very difficult to activate the surface of glass for subsequent electroless plating without any surface pre-treatments [16]. In many cases, Self-Assembled Monolayers have been used to enhance the Pd adhesion on to the substrate surface. Atsushi and research group used (NH_2)-terminated organosilane self-assembled monolayer (SAM) on a polyimide substrate in order to activate

the surface with $PdCl_2$ solution. The adsorption of Pd was confirmed by the XPS results and the adsorbed Pd acted as catalytic sites for electroless deposition [57]. Cui and co-workers studied the silanisation of glass using (3-aminopropyl) trimethoxysilane in order to improve the electroless copper glass adhesion [51]. An investigation of the glass surface composition after APTS treatment was carried out using XPS. The N peak observed in the APTS treated glass surface revealed the attachment of the (3-aminopropyl) trimethoxysilane molecules forming a SAM layer. This was also confirmed with the different Si peaks observed in both treated and untreated glass samples. Another study [58] reported electroless copper deposition on glass modified with polyethylenimine. The surface was catalytically activated using $PdCl_2$ solution and the XPS spectrum confirmed the chemically bound Pd^{2+} on the glass surface.

2.3.2 Laser Surface Activation of Ceramic Surfaces

Laser technology is being developed for surface activation of non-conductive materials for electroless plating. In 1994, Folser carried out investigations on direct electroless Cu plating using an excimer-laser (wavelength of 248 nm and 308 nm) to irradiate alumina [50]. Circular and rectangular areas of polished alumina samples were irradiated and the samples were examined using electron induced X-ray spectroscopy and the ablated depths were measured using a stylus profilometer. The plating activity did not change for different wavelength used or for different pulse repetition frequencies. The plating activity only changed with the size of the irradiated area. Large irradiated areas showed higher plating activity. A major drawback of this method was that the edges of the irradiated area showed faster deposition than the inside area. This may lead to uneven surfaces of metallisation on the substrate and will cause higher roughness.

In 1998, G.A. Shafeev reported the activation of several dielectric materials i.e. Alumina, Cerium Oxide, ZrO_2, SiC and Diamond, with UV excimer laser and pulsed CO_2 laser [59]. In previous studies it was found that the surface of AlN ceramics decomposed to Al metal with laser ablation and become activated for electroless Cu. However, some dielectric materials such as diamond can also be activated with laser ablation and these dielectrics do not contain any metals. Shafeev also suggested that the activation mechanism of Alumina is due to the oxygen vacancies formed on the ceramic surface once exposed to the laser. He also suggested that to stabilize the structure, these vacancies tend to form aluminium and silicon nanoclusters. These electron rich environments enhance the reduction of metal ions

so that the surface is activated for the metal deposition. Experimental results showed that the laser irradiated dielectric surfaces are activated for electroless plating for a long time and the catalytic activity only disappears when those surfaces are heated in an oxygen environment.

In recent years, laser surface activation has been used to metallise circuit lines and via holes on AlN substrates [60]. The formation of Aluminium on the ablated AlN surface has further been confirmed by XPS data. Metallisation of via holes did not show a uniform metal layer and the thickness of the metal layer was thicker on the top part of the via than the bottom. This was due to the ablating effect on the top part of the via being greater than the bottom. This problem may be overcome if the substrate is rotated 180^0 and drilled through the same via hole from the other side of the substrate.

In 2005, K. Kordas and co-workers activated an LTCC substrate for electroless metal plating using a Nd:YAG laser (wavelength of 1064 nm). In contrast with the previous studies their results showed that the laser annealed surfaces gave better activity than the ablated areas. Several metals i.e. Cu, Ag, and Au were deposited on activated surfaces and the first Cu metal seeds formed after a period of 4 hours, while Ag and Au metal seeds appeared on the activated surfaces just after immersion in the electroless baths without any incubation time. After one hour of plating, silver metal seeds started to deposit all over the surface without continuity and sufficient thickness could not be achieved for good conductivity. For Au the metal seeds only appeared on the top of the LTCC glassy phase [41].

Laser surface activation of dielectric materials for subsequent electroless plating is a low cost alternative method to lithographic masks when selective metallisation is required. However, in the case of LTCC, the process needs some improvements to reduce the plating time. Furthermore, it can only be used on areas that can be easily accessed with the laser beam and therefore not suitable for closed channel structures.

2.4 Methodology and Experimental Procedures

In these initial experiments, to provide a benchmark for later comparison, electroless copper was deposited on to fired LTCC samples which were only subjected to cleaning procedures, without any other surface treatments. Adhesion tests were carried out using a tape test to

investigate the adhesion between the copper deposit and the LTCC substrate. Initial characterization of the copper deposits was also carried out in terms of thickness and temperature dependence of the surface microstructure.

2.4.1 LTCC Substrate Material

The DuPont™ GreenTape™ 9K7 low temperature co-fired ceramic (single layer for most experiments unless otherwise stated) was used in these experiments and this material was selected due to its low loss properties at frequencies in the high GHz range including wireless and mobile applications and high speed digital applications (Table 4) [61]. LTCC which was fired according to the recommended 26.5 hours firing profile in a static furnace was used and the firing process was carried out by the project partners at the University of Leeds. The fired samples were then subjected to cleaning procedures, surface pre-treatments and surface activation followed by subsequent electroless copper plating.

Table 4 Material Properties of DuPont™ GreenTape™ 9K7 [61]

Property	Value
Unfired thickness, (μm)	254, +/- 14
X, Y, Shrinkage, (%)	9.1, +/- 0.3
Z Shrinkage, (%)	11.8, +/- 0.5
TCE, (23^0- 300^0 C)	4.4
Density, (g/cm^3)	3.1
Surface roughness, (μm)	0.52
Thermal conductivity, (W/ m-K)	4.6
Flexural strength, (MPa)	230
Young's modulus, (GPa)	145
Poisson's ratio	0.25
Dielectric constant, (10 GHz)	7.1 +/- 0.2
Loss tangent, (10 GHz)	0.0010
Insulation resistance, (Ohms)	$>10^{12}$
Breakdown voltage, (kV/25 μm)	>/= 1100

2.4.2 Electroless Copper Plating on Fired LTCC

A. Substrate Cleaning

Sample cleaning is an essential step prior to the electroless copper deposition process. Cleaning usually removes the impurities from the substrate surface leading to better adhesion between the deposited metal and the substrate. The LTCC samples were dipped in 200 ml of 10 vol% Decon 90 solution in deionized (DI) water (a standard industrial cleaner for glass and ceramic materials) at room temperature for 24 hours. The samples were then rinsed with de-ionized water and dried in air with a specimen dryer.

B. Preparation of Solutions for Electroless Copper Deposition

Pre-dip and Circuposit^{TM} Catalyst 3344/4444 from Rohm and Haas chemical company were prepared according to their technical data sheets. Pre-dip is an acidic solution (pH<1) and has similar pH to the catalyst solution. Sample immersion in the pre-dip is usually carried out prior to the catalytic activation as it enhances the wettability of the substrate and prevents contaminants being dragged in to the costly catalyst solution. To prepare the pre-dip solution, 54.0 g of the Circuposit pre-dip 3340/4400 was dissolved in 168 ml of de-ionized water and the volume was made up to 200 ml with de-ionized water.

Catalyst activation of non-conductive substrates is a vital step in the electroless process. Catalyst adsorption on the samples usually takes place when the samples are immersed in a Sn/Pd catalyst solution for a few minutes. To prepare the catalyst solution, 54.0 g of the Circuposit pre-dip 3340/4400 was measured and dissolved in 168.0 ml of de-ionized water. 5.0 ml of the Circuposit catalyst 3344/4444 was then added to the solution mixture and the volume was made up to 200 ml with de-ionized water.

C. Electroless Copper Bath

The electroless bath consists mainly of copper solution, formaldehyde, NaOH and EDTA. The electroless Cu bath Circuposit^{TM} 3350-1 (Rohm and Haas) was prepared according to Table 4. According to the technical data sheets provided by Rohm and Haas, the plating rate was ~0.5 µm for a 10 minute plating period (i.e. ~0.05 µm / min) at 42 ^{0}C.

Table 5 Preparation of electroless copper plating bath

Chemical	Amount/ ml
Deionized water	162.4
Circuposit 3350M-1	30.0
Circuposit 3350A-1	2.0
Cuposit Z-1	2.1
Cuposit Y-1	2.3

2.4.3 Electroless plating of fired LTCC tapes

The cleaned LTCC samples were immersed in the pre dip solution for two minutes. Then these samples were dipped in the catalyst solution for 2 minutes then removed and rinsed with de-ionized water. Rinsed samples were then immersed in the electroless bath for one hour plating time. The samples were then taken out from the plating bath and rinsed with de-ionized water and dried with a specimen drier. The temperature of the plating bath could be ranged from 30 ^{0}C to 55 ^{0}C and controlled using a hot plate equipped with a temperature probe immersed in the electroless solution. The electroless deposition process is illustrated in Figure 7.

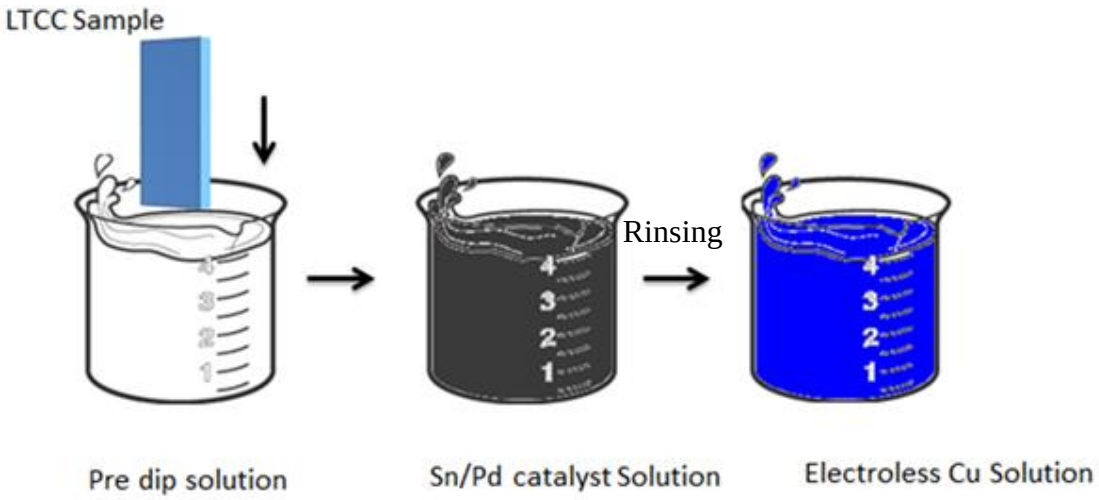

Figure 7 Electroless copper plating process

2.4.4 Cross Section Analysis

A section of the plated LTCC substrate was encapsulated into a compression mounting resin. Then the grinding of the specimen was carried out manually using abrasive papers of 240, 400, 600 and 1200 grit. Grinding was done for 2 minutes at each abrasive paper until the grinding striations on the specimen surface indicated that the grit had completely removed a layer of material. Then polishing of the mounted specimen was carried out to planarize the specimen and to reduce the damage created by sectioning. To do this, the specimen was pressed against polishing wheels loaded with 6 μm and 1 μm diamond paste until the fine scratches were removed from the specimen surface. The cross section of the specimen was then analysed by optical microscope in order to measure the thickness of the deposited copper.

2.4.5 Adhesion Tests- Tape test

A tape test is a qualitative way of measuring the adhesion strength. A number of factors including peel rate, peel strength, type of tape and peel angle directly influence the tape test results [62]. Thus, it is essential to maintain these factors in each test for consistent results. In this study, a test procedure was predefined to maintain the consistency of each test. The test substrate was attached to a work stage using a double sided adhesive tape (Figure 8). The test samples were prepared in a way that the whole area of the sample was smaller than the section of the test tape. Then the test tape (3M 56-7305-2240 adhesive tape) was pressed thoroughly on to the substrate which had been electroless plated. Then the tape was subsequently peeled off manually with fast movement keeping the tape perpendicular to the substrate surface. The surface was then inspected to see what damage had occurred during the peeling process.

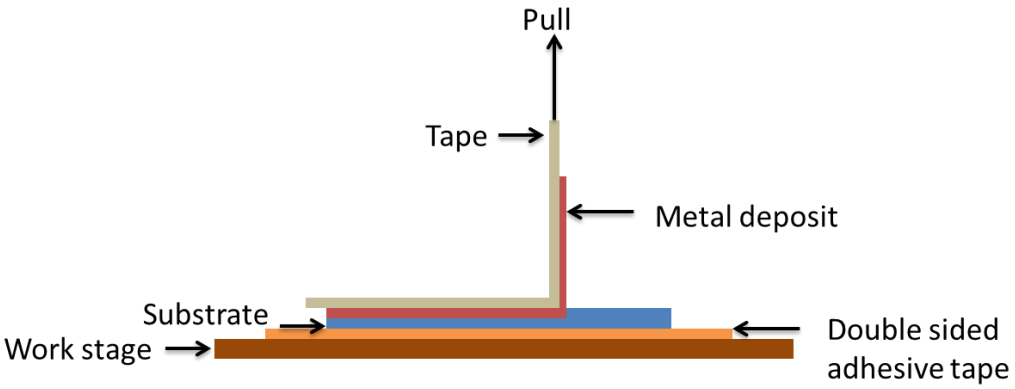

Figure 8 Tape test set up

2.4.6 Microstructure and Morphology Assessment methods

A. Zygo NewView 5000 CSI

The Zygo NewView 5000 CSI uses scanning white light interferometry to image and measure the microstructure and topography of surfaces without contacting the substrate surface. Light from the microscope divides within the interferometric objective, one portion reflects from the test structure and another portion reflects from an internal high quality reference surface in the objective. Then both portions are directed to a solid state camera where they interfere thereby providing information on the topography [63]. The NewView analyses and quantifies the surface topography of parts with a depth of 100 μm with 0.1 nm resolution and these are displayed as solid images, plots and numeric representations of the surface.

B. Field Emission Gun Scanning Electron Microscope (FEGSEM)

A LEO 1530VP Field Emission Gun Scanning Electron Microscope was used to analyse the LTCC surface morphology and the morphology of the deposited copper. Specimens were mounted on aluminium stubs using double sided adhesive and electrically-conductive carbon tape. The bare LTCC samples were gold coated prior to the analysis to achieve the required conductivity using a sputter coater. The energy of the electron beam of the SEM was set at 5 kV and the current of the electron beam was set at 30 pA.

C. Nikon Optiphot Optical Microscope

A Nikon Optiphot optical microscope with GT visio GXcam 5 software was used to obtain optical micrographs of the polished LTCC cross section and other surface structures.

2.5 Results and Discussion

2.5.1 Characterization of LTCC

Figure 9 shows an SEM micrograph of the as-received fired LTCC sample after cleaning as described above. The surface showed a general roughness with some grainy particles

over the surface. Different sizes of particles were seen and the size of the large particles was approximately 5 μm. Some voids were also seen on the surface. The particle size of the alumina grains in LTCC (Dupont 951) material has been reported in the literature and the typical diameter of these alumina grains was in the range of 2-3 μm [23].

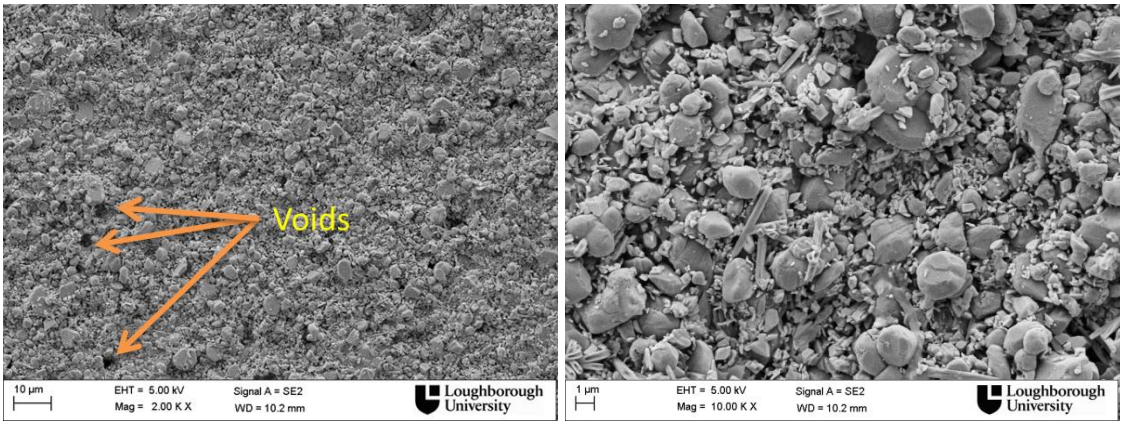

Figure 9 SEM images of the LTCC surface after cleaning

Surface roughness of the fired LTCC sample was measured using the Zygo NewView 5000. The area measured was ~500 x 600 μm and three random locations on the sample were measured to get the average value. The average Ra of the fired LTCC was ~0.65 μm. Figure 10 (a and b) shows 2-D and 3-D surface topography plots. Similar to the SEM results the surface showed uniform roughness over the measured surface. The 2-D profile of the sample exhibited strong valleys and discontinuities at some points and these could correspond with the voids which were presented in the SEM micrograph.

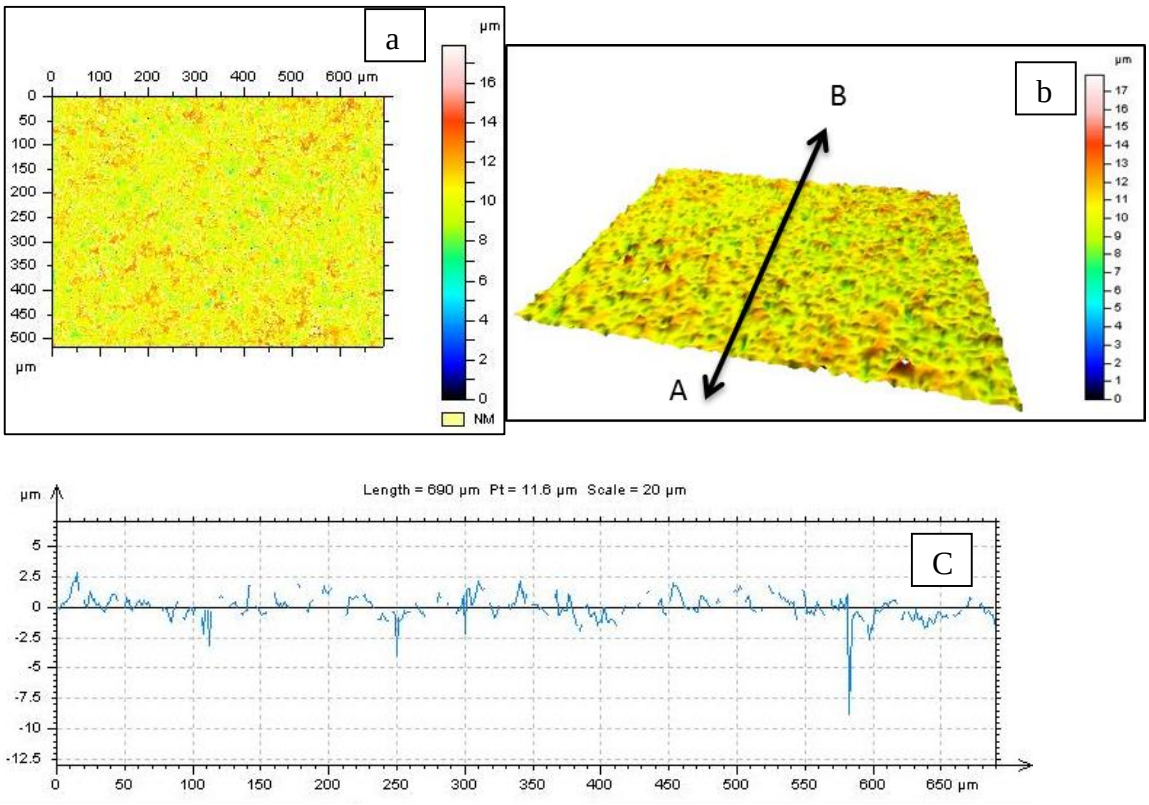

Figure 10 LTCC surface (a) 2-D map (b) 3-D map (c) profile A-B

2.5.2 Electroless Copper Plating of Untreated LTCC

Following the catalyst pre-treatment, the electroless process was observed to start on all samples within the first thirty seconds after immersion in the bath and a continuous Cu layer was achieved on the LTCC surface after a few minutes and started to grow further with the increase in plating time. Figure 11 shows the LTCC sample before and after electroless plating for one hour.

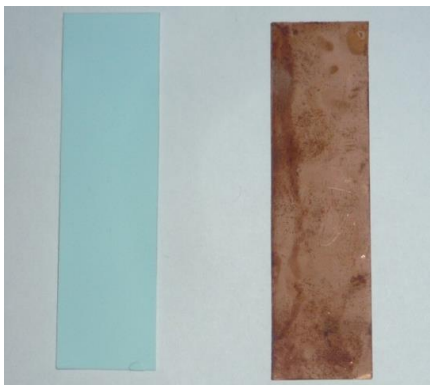

Figure 11 LTCC sample before and after electroless copper deposition

2.5.3 Effect of Temperature on Surface Morphology of Cu Deposits

Surface roughness of the deposited metal is a key factor for high frequency applications to reduce the signal loss. Surface roughness of the metal deposition should be maintained at a low value to achieve better signal propagation. Even though increasing the temperature of the electroless bath enhances the rate of deposition, it can affect the surface morphology of the deposited copper. Commercial electroless baths come with optimum temperature conditions, however, these can be varied depending on the substrate material and the size of the bath. To determine the suitable bath temperature for a fine microstructure, electroless Cu plating was carried out at three different temperatures including the specified temperature for the bath (42 ^{0}C), a low temperature of 30 ^{0}C, and high temperature of 55 ^{0}C. The temperature of the electroless bath was controlled using a temperature probe which was attached to the hot plate. All samples were plated for one hour: this is expected to lead to different Cu thicknesses for the three temperatures. The surface morphology of the copper deposited at different temperatures was analysed using SEM (Figure 12).

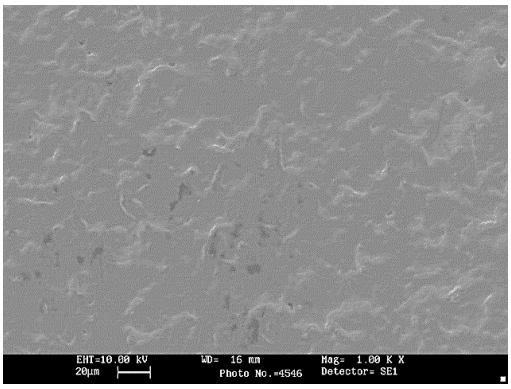

(a)

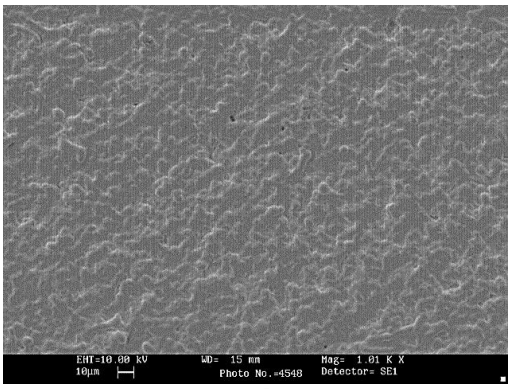

(b)

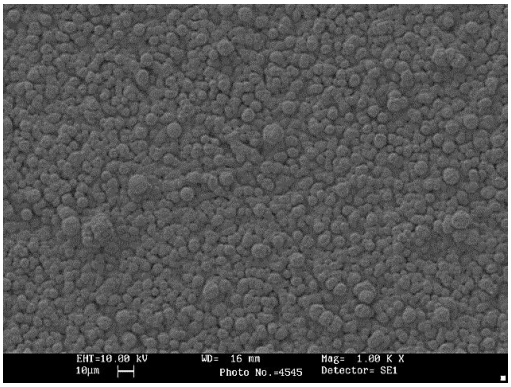

(c)

Figure 12 Temperature dependence of Cu deposits (a) plating temperature 30 ^{0}C, (b) plating temperature 42 ^{0}C, (c) plating temperature 55 ^{0}C

The micrographs in Figure 12 reveal that lower surface roughness was obtained from low temperature electroless baths. Figure 12 (a) shows a smooth surface while Figure 12 (c) shows a nodular structure. The growth mechanism of the electroless copper was reported in previous studies [64], [65], [66] and the surface morphology of the deposited copper obtained at different temperatures can be explained by the theory presented by Sard [65]. According to his theory, the first three dimensional copper nucleation occurs at the catalytic sites. These copper particles (300 Å in size) were not single crystals but aggregates of smaller crystallites (diameter of 25-50 Å). When the deposition time increases, these larger aggregates tend to form continuous chain like structures separated by regions where the film is thinner and this could be observed in the current deposits obtained at 30 ^{0}C and 42 ^{0}C (Figure 12 (a) and (b)). After a certain point, these aggregates become energetically unstable and lead to recrystallization which eliminates the interior boundaries and form larger single grains. The grainy micro-structure in the copper deposit at 55^0 C is thought to be due to the above mentioned process. This provides a contradictory result to the surface morphology obtained for the electroless copper growth on a glass substrate which was explained using the Volmer-Weber mode [16]. However, Nakahara and co-workers [66] reported that the nucleation and the growth patterns of electroless copper depend on the type of substrate and explain the contradictory results.

If a smoother surface could be obtained at lower temperatures, the question then was whether a sufficient thickness of the deposited metal could be obtained. The thickness of the copper deposited at 30^0 C was measured by taking a cross section (Figure 13). Continuous Cu deposition was achieved with 2-3 µm of approximate thickness in one hour plating time. The deposit built up accordingly with the morphology of the surface. Some Cu particles could be seen deep into the LTCC material but it is thought that the polishing process caused the particles to be spread across the interface.

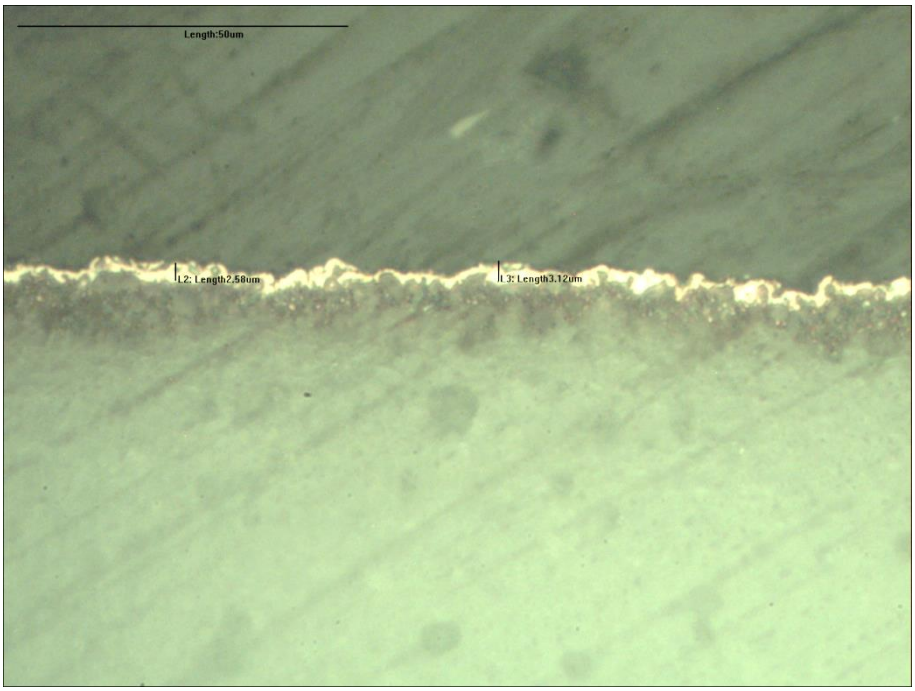

Figure 13 Cross section of the deposited copper on LTCC

2.5.4 Surface Roughness of Cu Deposits

The surface roughness of the deposited copper at 30 ^{0}C was obtained using the Zygo NewView 5000 CSI. Figure 14 shows the 3-D and 2-D profile of the deposited electroless copper. The 3-D profile shows a fairly uniform roughness across the surface. The Ra value was taken at three different locations on the sample surface and the average Ra value was found to be 0.9 μm. The average surface roughness (Ra) was relatively higher compared to the surface roughness of the bare LTCC surface which gave an average Ra of 0.65 μm.

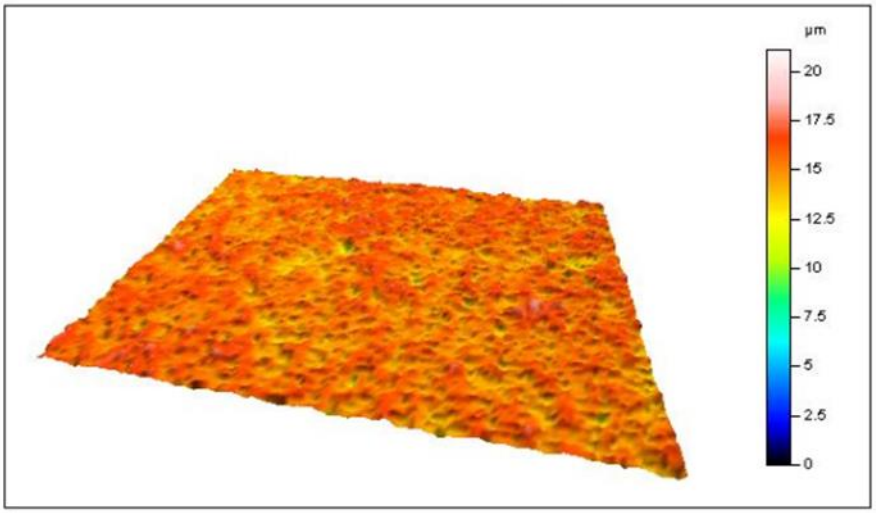

(a)

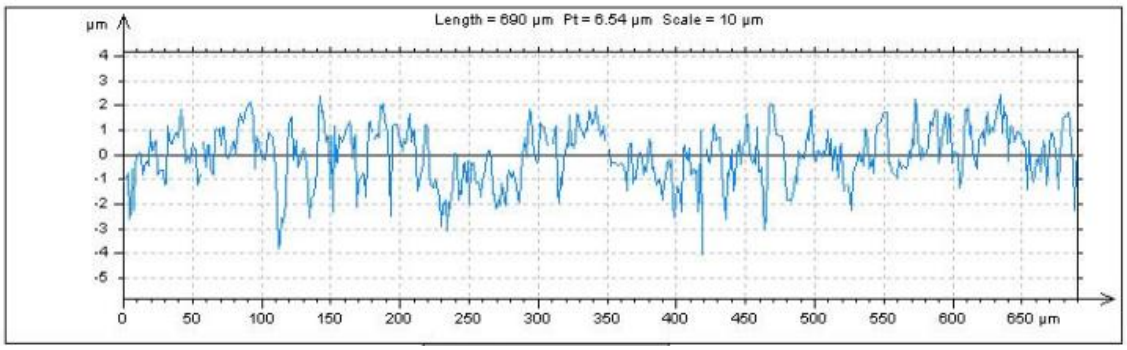

(b)

Figure 14 Surface profile of electroless copper deposits (a) 3-D profile (area ~500 x 700 µm) and (b) 2-D profile

2.5.5 Initial Tape Test Results

Tape test results (Figure 15) showed that the electroless Cu plated on the LTCC surfaces without any surface modification had relatively poor adhesion. The measured surface roughness values showed a relatively low Ra value of ~ 0.65 µm for the fired LTCC and the low surface roughness may have contributed to a low degree of mechanical interlocking between the deposited copper and the LTCC surface leading to poor adhesion. Failure can occur from the interface between catalyst and substrate or the copper / catalyst interface. As seen in Figure 15, almost all the deposited copper was peeled off on to the tape.

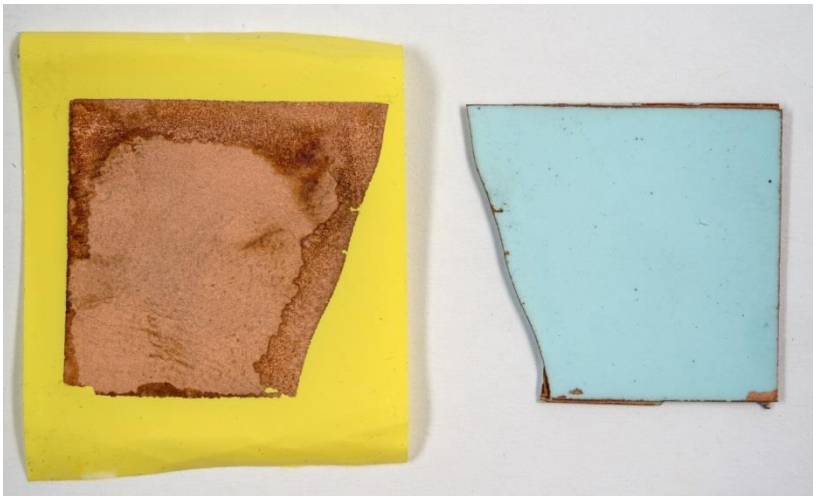

Figure 15 LTCC sample (right) and the adhesive tape (left) after the tape test

2.6 Conclusions

In this chapter, the deposition of electroless copper on to fired LTCC was demonstrated. Initial analysis was carried out on both the bare untreated LTCC surface and electroless copper deposits. According to the SEM analysis, the surface of untreated LTCC showed different sizes of particles and the size of the larger particles was approximately 5 μm. The measured Ra value of the untreated LTCC was approximately 0.65 μm. A lower electroless plating bath temperature of 30 ^{0}C was found to give smoother Cu deposits, which is an essential requirement in microwave and millimetre wave applications and this was used for all future plating trials. A tape test was carried out to find the interfacial adhesion between the electroless copper and untreated LTCC substrate and the results showed poor adhesion indicating an area for further investigation.

Chapter 3 Chemical Surface Pre-treatment of LTCC

3.1 Introduction

As described in the previous chapters, electroless copper deposition on to fired LTCC is a promising solution to overcome the limitations of the screen printing process. However, adhesion of metal films on a substrate is a crucial issue when considering the device reliability and performance. Some of the applications which are operating in harsh environment conditions such as automobile, satellite and military require especially good adhesion. However, the adhesion strength depends on the physical and chemical properties of the substrate as well as the deposited metal.

The initial experiments carried out in chapter 2 revealed that adhesion between the fired LTCC and the deposited copper was poor. It was therefore necessary to discover the potential methods that can be applied to improve the interfacial adhesion of electroless copper to LTCC. Literature on the surface modification of fired LTCC was reviewed and a NaOH solution pre-treatment was identified as a potential method especially suitable to modify the internal walls of closed channels where other methods such as laser machining could not be applied. This chapter therefore mainly focuses on chemical etching of fired LTCC substrate material using NaOH solution with the aim to give improved interfacial adhesion between the electroless copper and LTCC substrate. Furthermore a detailed study of the NaOH surface pre-treatment is also reported to determine the mechanisms of the etching process.

3.2 Literature Survey

A literature survey was conducted to study the adhesion mechanisms and possible techniques that are available to improve interfacial adhesion between two surfaces. The literature was further reviewed to find the surface pre-treatment techniques that have been used to modify the fired LTCC surface which can be a promising solution to improve the electroless copper adhesion.

3.2.1 Adhesion mechanisms

Bonding of two surfaces can occur due to electrostatic attraction, chemical bond formation, molecular entanglement or mechanical interlock. These bonding processes are shown schematically in Figure 16.

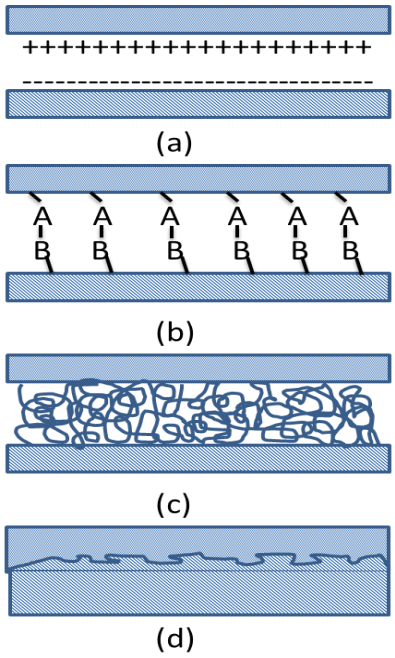

Figure 16 Schematic diagram of two bonding surfaces: (a) electrostatic attraction, (b) chemical bond formation, (c) molecular entanglement and (d) mechanical interlock [67]

Comyn introduced [68] five theories of adhesion and summarises these as follows:

- **Physical adsorption**- The Van der Waals forces due to permanent and induced dipoles across the interface.
- **Chemical bonding**- Ability to form ionic, covalent or hydrogen bonding between the surfaces.

- **Electrostatic force**- If two metallic surfaces are placed in contact the electrons can be distributed between each metal surface to form positive and negative charge leading to an electrostatic attraction.
- **Mechanical interlocking**- If the surface has a rough and porous structure, the materials can make a strong mechanical interlock which gives better adhesion.
- **Removal of weak boundary layer**- Cleaning of the substrate surface to remove oil or grease. This factor is not an adhesion mechanism, but enhances the above mentioned mechanisms.

3.2.2 Improving Metal Film Adhesion to Substrates

The above mechanisms suggest that the adhesion between the substrate and the metal can be improved by increasing the dipole on the surface, adequate cleaning of the surface, attaching new chemical components on the surface and roughening the surface.

Surface energy plays a key role in forming bonds between two surfaces. According to the Dupre equation (Equation 3.1 [69]), work of adhesion (W_{adh}) depends on the surface energy of surface 1 (γ_1), surface energy of surface 2 (γ_2) and the interfacial energy of the two surfaces (γ_{12}).

$$W_{adh} = \gamma_1 + \gamma_2 - \gamma_{12} \qquad 3.1$$

If the surface energy is high at each individual surface and they have low interfacial energy, the work of adhesion is higher i.e. the two surfaces have good interfacial adhesion.

Roughening the surface is a common way of enhancing the bonding strength by increasing the mechanical interlock between two surfaces. Roughening the surface also leads to a larger surface area for effective bonding. Furthermore, an increase in surface roughness can introduce physico-chemical changes which may change the surface energy and wettability of the substrate [70]. Adhesion of a metal deposit to a substrate is therefore likely to be improved by increasing the surface roughness of the substrate through interlocking. On the other hand, the adhesion of the metal deposit and ceramic substrate are typically due to only weak Van der Waals forces and the number of these forces can be enhanced by increasing the bonding area of the interface [71]. Plasma treatments [72], chemical etching, mechanical abrasion, sand and bead blasting and laser machining have been used in the literature to roughen the material surfaces by material removal [63]. However, etching of

the substrate surface using chemicals is a convenient and cost effective way of increasing the roughness. In some cases, surface chemical pre-treatment can also increase the surface energy and change the surface chemistry for better adhesion [73].

A. Chemical Pre-treatment

In many cases, both acidic and basic solutions have been used for etching of ceramic materials. The purpose of etching can be to create a rougher surface or make the material more porous for certain applications. Tetsuya et al. [74] used 0.1 M NaOH solution to etch an AlN substrate. The purpose of the study was to increase the adhesion between the substrate and electroless Ni-P. They concluded that the process started initially as a selective etching of the substrate surface followed by homogeneous etching after a certain period of time. The adhesion strengths increased sharply in the first stage and then decreased accordingly as the homogeneous etching occurred. Jardiel et al. [75] studied the chemical etching of $Bi_4Ti_3O_{12}$ ceramics to improve the microstructure for better electrical response. In this study, a $HF/NH_4F/H_2O$ system with molar ratio 2:1.2:3 was used for different etching times and temperatures. The study found that the best etching was obtained at 50 ^{0}C for 3 minutes in terms of obtaining clear and sharp grain boundaries and preferential etching on certain crystallographic directions. Chemical etching of glass ceramic was reported by Laurent and co-workers [76] for the purpose of creating a porous layer to increase the infrared transmission of the materials. The surface porosity created by chemical etching acted as an anchorage site for silane molecules and enhanced the silane functionalization. Both acidic and basic solutions were used in the etching process. The study reported the selective etching of the glassy phase with 0.1 M NaOH solution and homogeneous etching of the material with an acidic solution which contained 70% of concentrated H_2SO_4 (98%) and 30% of H_2O_2 (35%).

Achin and co-workers used hot phosphoric acid as a chemical etchant to obtain a porous structure on LTCC. The purpose of the study was to modify the permittivity of the material, hence to achieve a low dielectric constant. The LTCC substrate has a chemical structure of alumina particles covered by the glass matrix due to the liquid phase sintering process [24]. The results of the SEM and μ-XRD measurements showed the anorthite crystals in the glass phase near the alumina grains were etched away due to the reaction with hot phosphoric acid. Feng Yuan reported a similar etching procedure using a series of chemicals i.e. 1 wt% HCl, 2 wt% HF, 10 wt% HNO_3, 19 wt% NaOH [77]. Yuan found that NaOH selectively

etched the glass phase leaving a porous LTCC surface, while acidic solutions showed unselective material removal. This study further confirmed that the glass phase can be selectively removed by a chemical etchant and the dielectric properties can be improved by achieving a porous structure.

B. Laser Pre-Treatment for Surface Modification

Laser pre-treatment of the substrate surface has been reported on many occasions in order to create rougher surfaces to improve interfacial adhesion between substrate and coatings. Horn and co-workers [78] investigated the effect of KrF excimer (wavelength = 248 nm and maximum energy per pulse = 600 mJ) laser irradiation of polymers on the adhesion of electroless Ni. This study revealed that laser irradiation improved the adhesion between the polymer substrate and the Ni deposit even at fluences below the material removal threshold and the results were confirmed with tape and peel tests. They suggested that the increase in adhesion strength at the fluences below the material removal threshold may be due to the chemical modification of the irradiated polymer surface. They also suggested that the adhesion improvement at the fluences above the material removal thresholds were due to the mechanical anchoring of the rough polymer surface and the Ni deposit.

Li and co-workers [79] studied pulsed XeCl excimer laser (wavelength = 308 nm and maximum energy per pulse = 450 mJ) pre-treatment of cobalt-cemented tungsten carbide to improve diamond coating adhesion. Samples irradiated with different numbers of laser shots were coated with diamond film using an electronically aided hot filament chemical vapour deposition. Adhesion of test samples was investigated with an indentation test. The number of laser shots was varied between 100 and 700 and the best adhesion was obtained with 300 laser shots. They suggested that the deep drop pits created with 300 laser shots were responsible for improved adhesion. The adhesion of the diamond coating started to drop with a higher number of laser shots due to the formation of uniform surface structure with clear grain boundaries.

Laser pre-treatment has been used to modify ceramic surfaces over many years. In 1998, Tonshoff and research group [80] used KrF excimer (wavelength 248 nm) laser to irradiate silicon carbide ceramics. In this study, selective material removal at the grain boundaries and rounding of grains to create spherical caps on the ceramic surface was observed with the increase in laser pulses. However, above a certain number of pulses these spherical caps

connected each other due to a thin layer of molten phase of sintered additives and caused a less rough surface. Vilar and co-workers [81] also used KrF (wavelength = 248 nm) excimer laser to modify the Al_2O_3–TiC ceramics. Surface roughness (Ra) of the ceramic surfaces was obtained using a stylus instrument for various laser pulses and fluences. The Ra values increased with the number of laser pulses and reached a constant value after 200. The study also revealed that the Ra value increased with the laser fluence. SEM micrographs on the surface indicated uniform globular features dispersed on the ceramic surface after the laser irradiation. The area covered by these features and the diameter of the globules were initially increased with the laser pulses and then reached a constant level and this explained the variation of the Ra values described earlier.

It is clear from the above studies that for each material to obtain the best surface modification for particular applications, different laser parameters and optimum conditions need to be found in each case.

3.3 Research Methodology and Experimental procedures

Fired LTCC tapes have relatively low surface roughness (~0.65 μm) and hence cause adhesion problems for metal deposits. The adhesion of metal deposits on LTCC requires significant attention as this will have a huge impact on device reliability. Among other surface pre-treatment techniques, chemical etching has its own advantages such as low cost and ease of use and also, in some cases, can enhance the dielectric properties of the material as mentioned earlier.

The above mentioned chemical etching techniques can preferably be applied to obtain rougher surfaces of LTCC for adhesion improvements. Chemical etching is especially considered for the fired LTCC samples which required large area metallisation and metallisation of closed channel structures where the laser processing is not possible for surface modification. According to the literature, various acid and base systems have been used to etch ceramic materials. Among these systems, surface modification of the LTCC substrate using concentrated NaOH solution to improve adhesion was selected because concentrated NaOH has the ability to selectively etch the glassy phase from the LTCC surface and was mainly studied in this aspect of the research. Investigation of surface morphology and etching mechanisms using different analysis techniques such as SEM,

SEM-EDX, optical microscopy, X-ray diffraction, X-ray photoelectron spectroscopy and ion coupled plasma emission spectroscopy was carried out.

3.3.1 Experimental

The fired 9K7 LTCC was cleaned using the procedure described in section 2.4.2 A. These samples were then subjected to surface pre-treatments and surface activation followed by subsequent electroless copper plating.

A. Surface Pre-treatment

Surface treatment was carried out by etching with NaOH solution. Several concentrations (3M, 4M, 5M, 6M, and 7M) of NaOH in de-ionized water were prepared to observe the effect of concentration on etching. The LTCC samples were immersed in the NaOH solutions and kept at room temperature for different time intervals. They were then removed, rinsed with de-ionized water and dried using a specimen drier.

3.3.2 Analysis techniques

Analysis techniques were carried out using the Zygo NewView 5000 CSI, Nikon Optiphot optical microscope and FEGSEM as described in section 2.4.6. In addition, X-Ray Photoelectron Spectroscopy (XPS), Leica DM 6000 M optical microscope, Scanning Electron Microscopy combined with Energy Dispersive X-ray Spectroscopy (SEM-EDX), X-Ray Diffraction (XRD), and Ion Coupled Plasma Emission Spectrometer (ICPE-9000) were used to investigate the etching mechanism in detail.

3.3.3 Optical Microscope study

A Leica DM 6000 M optical microscope with LAS 4.2 software was used to take optical micrographs of the LTCC samples treated with NaOH solution.

3.3.4 Scanning Electron Microscopy Combined with Energy Dispersive X-ray Spectroscopy (SEM-EDX)

A LEO 1530VP Field Emission Gun Scanning Electron Microscope was used to analyse the LTCC surface morphology. The energy of the electron beam was set at 5 kV and the

current of the electron beam was set at 30 pA. Further analysis was carried out using Energy Dispersive Spectroscopy with an Oxford Instruments X-Max 80 mm^2 detector, to find the change in chemical composition on the surface. In this case the energy of the electron beam was set to 20 kV and current was set at 9.09 nA.

3.3.5 X-Ray Diffraction (XRD)

The purpose of this analysis technique was to find the possible crystalline phases present in the LTCC material. X-ray diffraction spectra of the LTCC 9k7 were obtained using the D2 PHASER system with reflection geometry theta-theta and a one dimensional LYNXEYE detector. X-rays were generated at 30 kV / 10 mA with wavelength of 1.542 nm due to the Cu 2p-1s transition. The data was collected at 0^0-90^0 at a scan step of 0.02^0.

3.3.6 X-Ray photoelectron spectroscopy (XPS)

X-ray photoelectron spectroscopy is a very sensitive surface (5-10 nm depth) analysis technique which gives information about elements present in the surface, their chemical environment and their oxidation state. In this technique, the photoelectrons are generated by sample irradiation with X-ray energy. These photoelectrons are analysed for their kinetic energy which is characteristic of the binding energy of electrons in a particular element. These characteristic energies allow identification of the chemical elements present on the surface of a sample. A Thermo Scientific K-Alpha system with 180^0 double focussing hemispherical analyser and 128 channel detector was used in this experiment. The X-ray source was monochromatic Al k-alpha with spot size ranging from 30 μm to 400 μm in 5 μm steps and with energy of 1486.65 eV. The survey scans were collected from 0 eV to 1300 eV with 8-10 scans and with pass energy of 200 eV while high resolution spectra were taken with 5 scans and pass energy of 50 eV. The step size of the survey scan and the high resolution spectra was 1 eV and 0.1 eV respectively.

3.6.7 Ion Coupled Plasma Emission Spectrometer (ICPE-9000)

The ion coupled plasma emission spectrometer can be used to analyse chemical elements present in a solution. In this instrument, the solution is converted to aerosols by a nebulizer and these aerosols are ionised by Argon plasma which contains a high concentration of free electrons and argon ions. Due to the high energy in the plasma the electrons of the ions are

excited and travel to higher energy levels. Excited electrons then emit radiation with specific wavelength in the UV region when they return back to lower energy levels, which gives the emission spectrum. In this study, a system was used with radio frequency power of 1.6 kW and sample introduction rate of approximately 1 ml/min. The system has an Echelle spectrometer which operates at 167 nm - 800 nm wavelength, a large-scale 1-inch charge coupled device (CCD) detector, coaxial type nebulizer mini-plasma torch and a cyclone sample mixing chamber.

3.4 Results and Discussion

3.4.1 Surface Modification of LTCC with NaOH Pre-treatment

A. Effect of NaOH Concentration on Surface Morphology

The effect of NaOH concentration on the surface morphology of the LTCC substrate was investigated using a series of NaOH concentrations (3M, 4M, 5M, 6M and 7M). The first batch of samples was immersed in 3M, 4M and 5M NaOH solutions for 24 hours at room temperature, and another batch of samples was immersed in 6M and 7M NaOH for 7.5 hours at room temperature. The surface morphology of the samples was analysed using SEM.

The SEM micrographs of Figure 17 show that the concentration of NaOH had a clear impact on the etching mechanism. The surface morphology of the unetched control sample (Figure 17 (a)) showed a flat surface with a general roughness. However, a flake like structure formed on all LTCC samples treated with NaOH as seen in Figures 17 (b), (c), (d), (e) and (f) and showed different surface structures to the control sample confirming the effect of NaOH. In addition to the flake structures, the morphology of the background surface also varied with the NaOH concentration. Increasing the NaOH concentration further and reducing the immersion time to 7.5 hours, led to the structures shown in Figure 17 (e), (f).

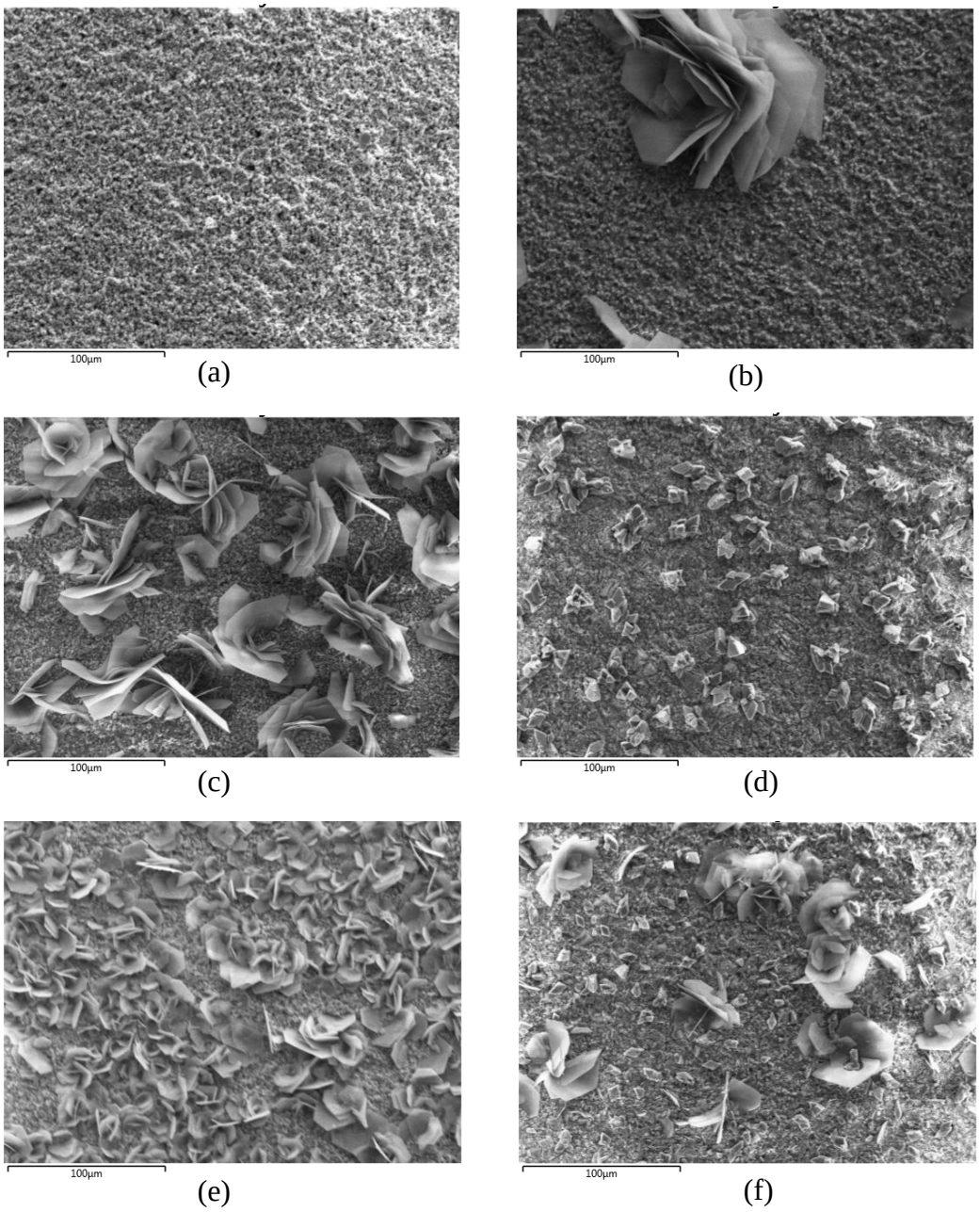

Figure 17 (a) LTCC control sample. LTCC samples immersed in NaOH solution, (b) 3M (24 hrs), (c) 4M (24 hrs), (d) 5M (24 hrs), (e) 6M (7.5 hrs), (f) 7M (7.5 hrs).

According to the scale of the SEM images, the width of the flake like structure shown in Figure 17 (b) was more than 100 μm. Coverage of these features relatively increased in the sample treated with 4M NaOH compared to the sample treated with 3M NaOH for the same time period. However, these flake like structures disappeared from the surface of the sample treated with 5M NaOH. This sample showed uniformly distributed grainy particles on the surface. The sample etched with 7M NaOH with less immersion time (7.5 hrs) (figure 2b) had a surface morphology which was a combination of surface morphology of samples etched with 4M and 5M NaOH for 24 hours. It can be suggested that the flaky structure of

the sample etched with 7M NaOH started to collapse with high concentration of NaOH. The sample treated with 6M NaOH showed similar flake like features to the sample treated with 4M NaOH however the coverage of these features was increased.

B. Effect of Immersion Time on Surface Morphology

From the initial experiments it was found that the immersion time in the NaOH solution affected the surface morphology of the LTCC. To investigate this further one particular concentration (4M NaOH) was selected and samples were immersed for different time periods. The 4M NaOH solution was selected for this study as it gave uniformly distributed flake like features as described above. Figures 18 and 19 show the high and low magnification SEM images of the surface morphology of the specimens. The first sample was taken out from the NaOH solution after 5 minutes. It is very clear from the SEM images (Figure 18 (b)), that even after a short period of time, the surface morphology changed with the NaOH solution exposure, with a significant change in the sample (Figure 18 (d)) taken out after 30 minutes. The grains which were present in the control sample disappeared from the surface and flake like features started to come out from the surface. The flake like crystals seen earlier formed on the surface of the LTCC sample taken out from the NaOH solution after only 50 minutes. It was also noticed that grains reappeared in the background surface. According to the scale of the SEM images, the size of the flake like features could go up to approximately 25 µm depending on immersion time and the concentration of NaOH solution and these structures had a hexagonal shape (Figure 18 (f)). After 75 minutes of immersion time, the coverage of these features increased with the immersion time and at the same time some flakes which were not attached to the bulk could also be seen in Figure 18 (j). The coverage of these flake features decreased in Figure 18 (k) which was immersed in the NaOH solution for 105 minutes.

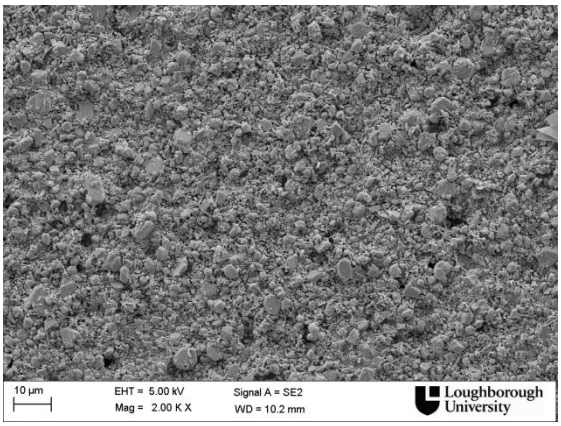
10 µm
EHT = 5.00 kV
Mag = 2.00 K X
Signal A = SE2
WD = 10.2 mm
Loughborough University

(a)

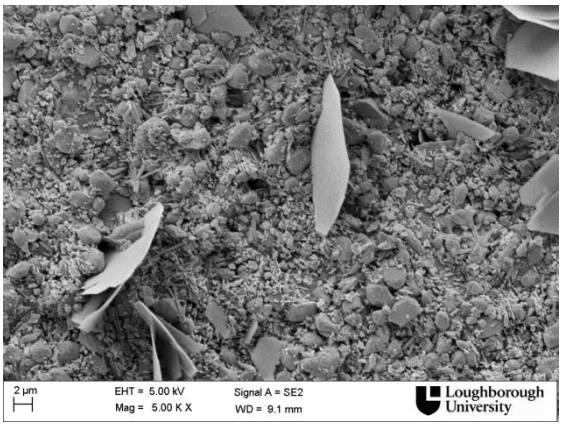
2 µm
EHT = 5.00 kV
Mag = 5.00 K X
Signal A = SE2
WD = 9.1 mm
Loughborough University

(e)

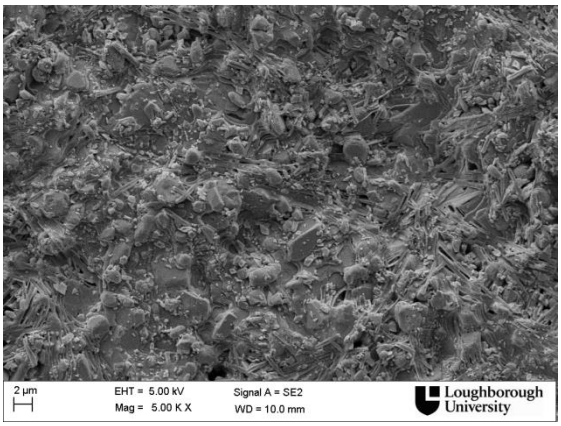
2 µm
EHT = 5.00 kV
Mag = 5.00 K X
Signal A = SE2
WD = 10.0 mm
Loughborough University

(b)

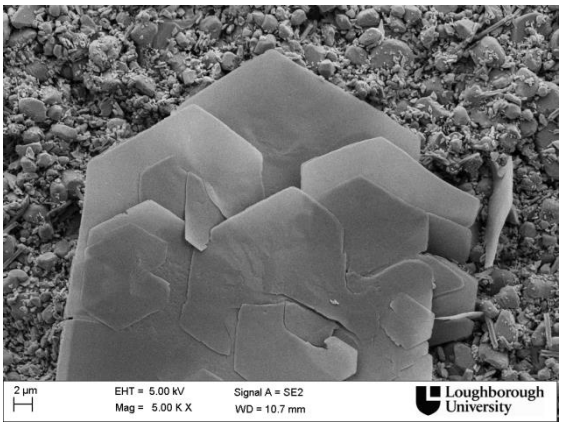
2 µm
EHT = 5.00 kV
Mag = 5.00 K X
Signal A = SE2
WD = 10.7 mm
Loughborough University

(f)

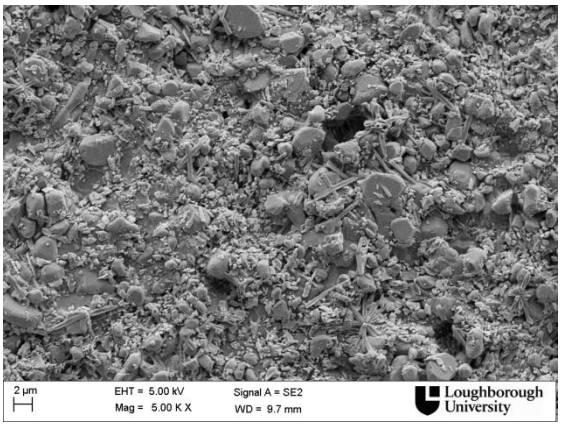
2 µm
EHT = 5.00 kV
Mag = 5.00 K X
Signal A = SE2
WD = 9.7 mm
Loughborough University

(c)

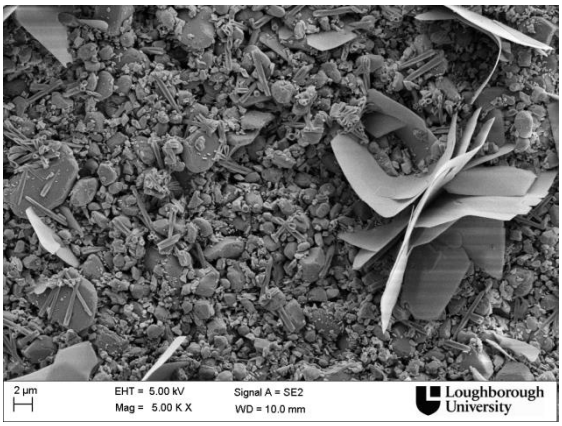
2 µm
EHT = 5.00 kV
Mag = 5.00 K X
Signal A = SE2
WD = 10.0 mm
Loughborough University

(g)

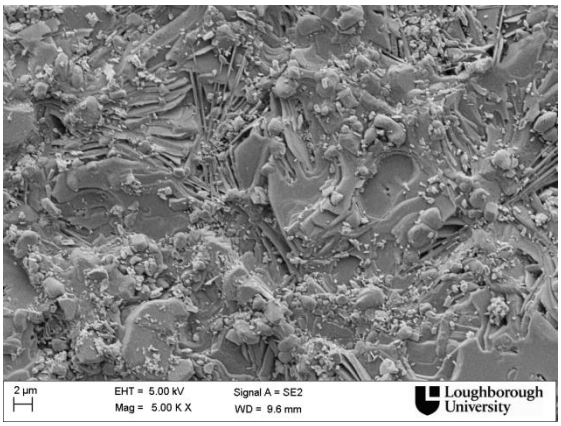
2 µm
EHT = 5.00 kV
Mag = 5.00 K X
Signal A = SE2
WD = 9.6 mm
Loughborough University

(d)

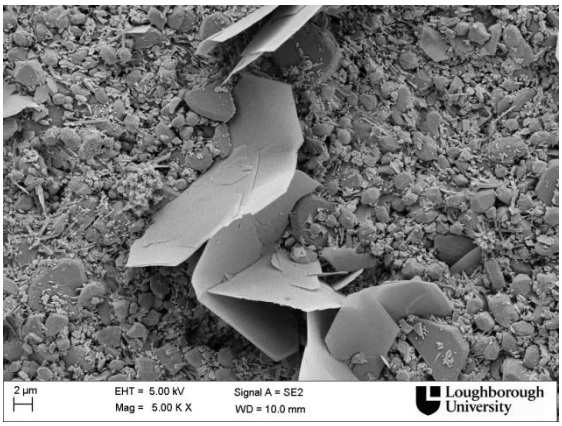
2 µm
EHT = 5.00 kV
Mag = 5.00 K X
Signal A = SE2
WD = 10.0 mm
Loughborough University

(h)

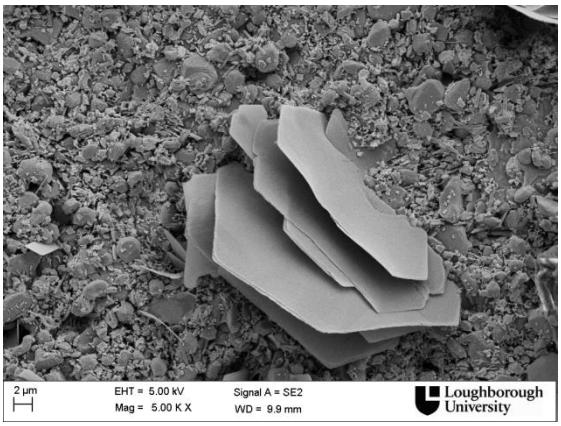

(i)

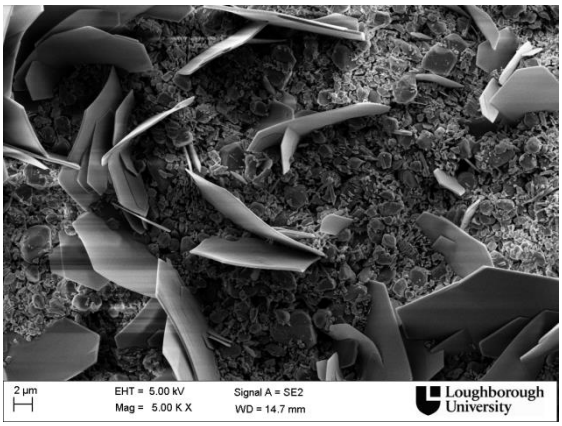

(l)

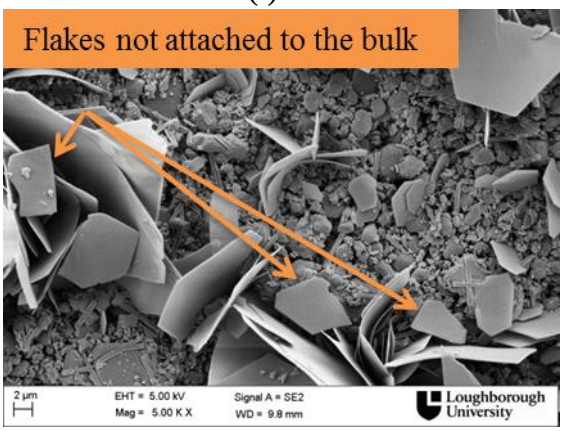

(j)

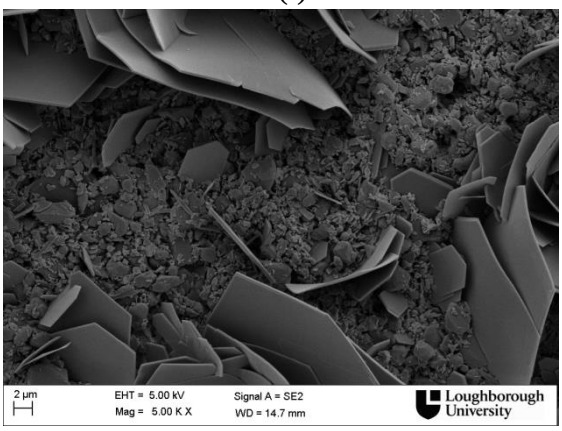

(m)

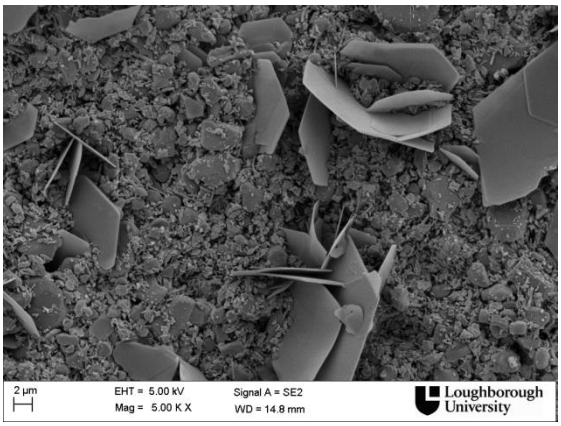

(k)

Figure 18 High magnification SEM micrographs of the LTCC samples immersed in 4M NaOH solution for (a) 0 mins, (b) 5 mins, (c) 15 mins, (d) 30 mins, (e) 50 mins, (f) 75 mins, (g) 105 mins, (h) 140 mins, (i) 180 mins, (j) 225 mins, (k) 255 mins, (l) 270 mins and (m) 24 hours

To verify above results, SEM images were taken at lower magnification to observe a larger area on the surface.

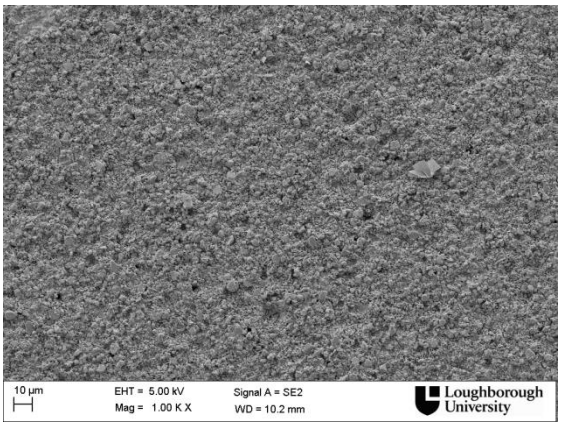
10 µm
EHT = 5.00 kV
Mag = 1.00 K X
Signal A = SE2
WD = 10.2 mm
Loughborough University

(a)

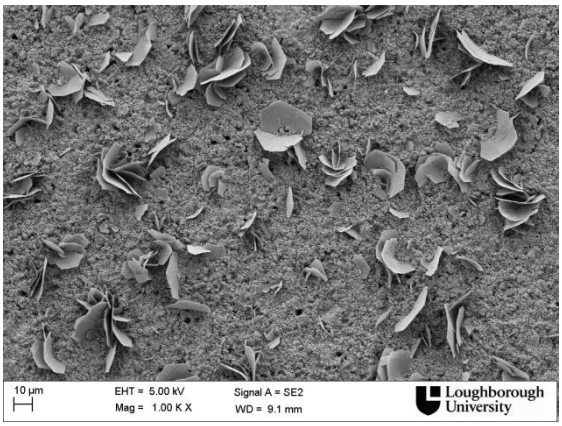
10 µm
EHT = 5.00 kV
Mag = 1.00 K X
Signal A = SE2
WD = 9.1 mm
Loughborough University

(e)

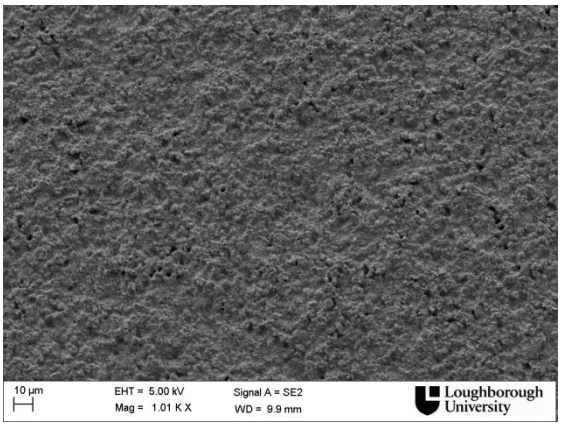
10 µm
EHT = 5.00 kV
Mag = 1.01 K X
Signal A = SE2
WD = 9.9 mm
Loughborough University

(b)

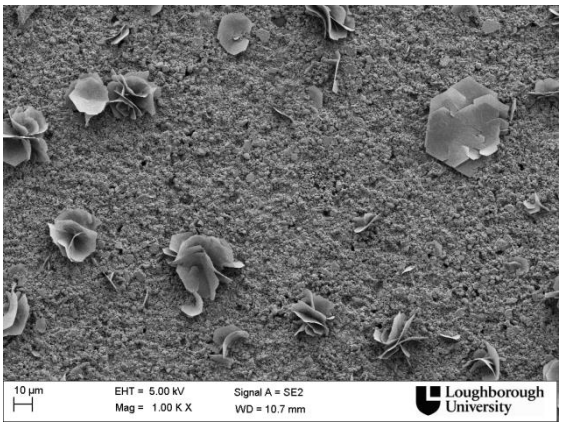
10 µm
EHT = 5.00 kV
Mag = 1.00 K X
Signal A = SE2
WD = 10.7 mm
Loughborough University

(f)

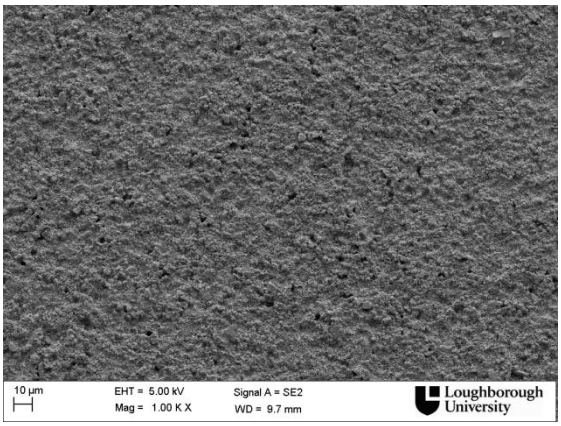
10 µm
EHT = 5.00 kV
Mag = 1.00 K X
Signal A = SE2
WD = 9.7 mm
Loughborough University

(c)

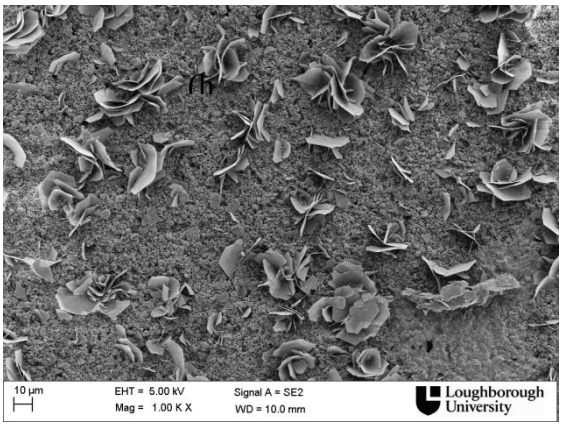
10 µm
EHT = 5.00 kV
Mag = 1.00 K X
Signal A = SE2
WD = 10.0 mm
Loughborough University

(g)

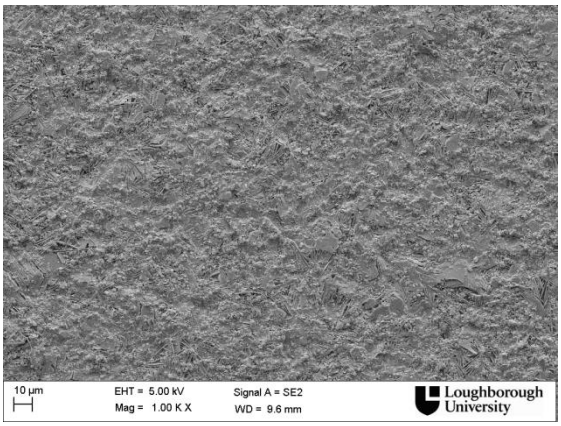
10 µm
EHT = 5.00 kV
Mag = 1.00 K X
Signal A = SE2
WD = 9.6 mm
Loughborough University

(d)

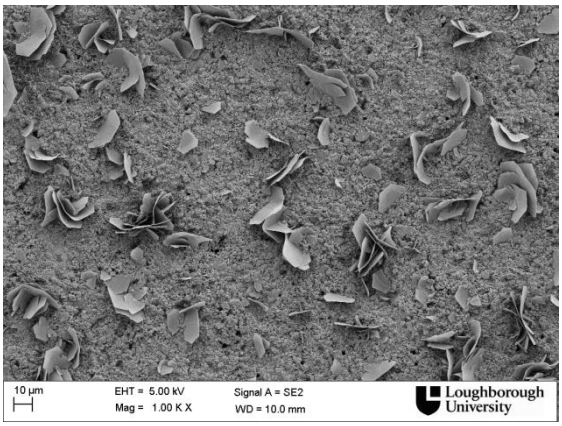
10 µm
EHT = 5.00 kV
Mag = 1.00 K X
Signal A = SE2
WD = 10.0 mm
Loughborough University

(h)

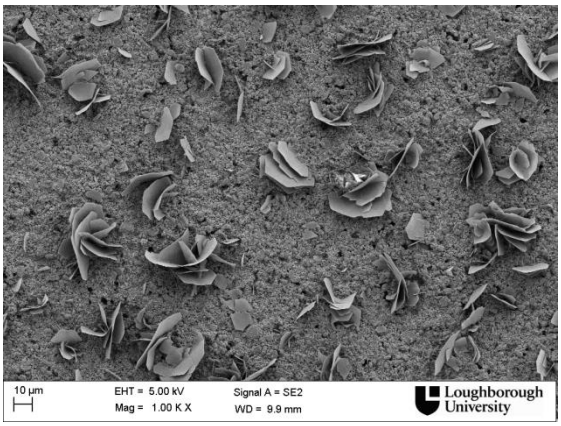

(i)

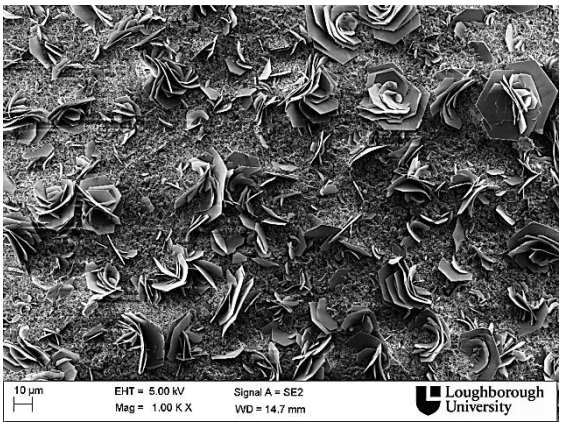

(l)

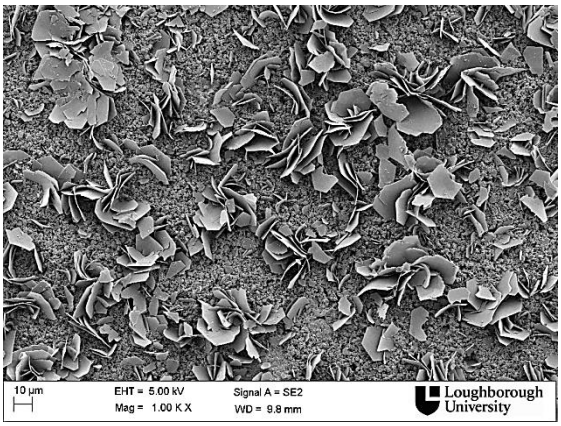

(j)

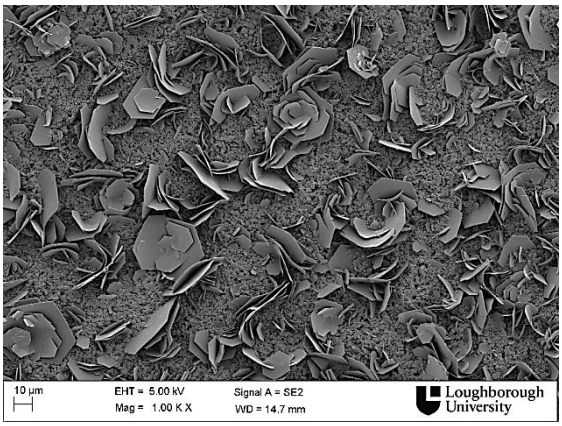

(m)

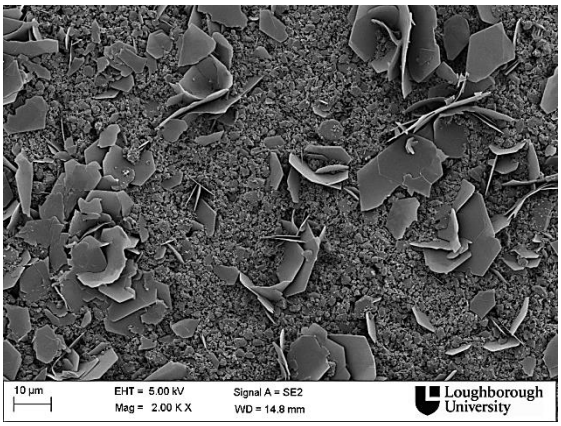

(k)

Figure 19 Low magnification SEM micrographs of the LTCC samples immersed in 4M NaOH solution for (a) 0 mins, (b) 5 mins, (c) 15 mins, (d) 30 mins, (e) 50 mins, (f) 75 mins, (g) 105 mins, (h) 140 mins, (i) 180 mins, (j) 225 mins, (k) 255 mins, (l) 270 mins and (m) 24 hours

The SEM micrographs at lower magnification (Figure 19) confirmed that the surface had started to change after 30 minutes and the flake like structures formed on the surface after 50 minutes. The coverage of these features on the surface varied. Figures 19 (e) and (f) compare the surface morphology of the sample immersed in NaOH solution for 50 minutes

and 75 minutes respectively. The coverage of the flake like structures decreased relatively in the sample immersed in NaOH solution for 75 minutes. The same variation was noticed in Figures 19 (g) and (h) and Figures 19 (j) and (k)

3.4.2 Investigation of the Etching Mechanism

From the initial experiments, it was found that the surface morphology of the LTCC substrate was changing with the NaOH pre-treatment. The SEM micrographs show a comparison of the hexagonal shaped crystal structures formed on the surface with the control sample. The immersion time as well as the concentration of NaOH affected the surface morphology. The question was whether these crystals were already dispersed in the LTCC material itself and appeared after the background surface was selectively etched away with concentrated NaOH, or were they formed due to a chemical reaction between the LTCC material and NaOH solution. Also there were other possibilities to explain the formation of these crystal structures: for example were they due to residues from the NaOH solution crystalized on the surface due to poor rinsing procedures, and another possibility was that these crystals could be formed due to the samples being exposed to moisture and air for long time periods before SEM analysis. The following analysis techniques were used to investigate the mechanisms of formation, chemical composition and the crystalline structure.

A. Optical Micrograph Study

A batch of LTCC samples were immersed in 4M NaOH solution for different time intervals at room temperature. Each sample was rinsed thoroughly and dried before the analysis. The optical micrographs of the LTCC samples were taken immediately after the drying process. This was done to find out if the flake like structures were forming on the LTCC surface due to the reaction with moisture or air while keeping these samples for a long time period.

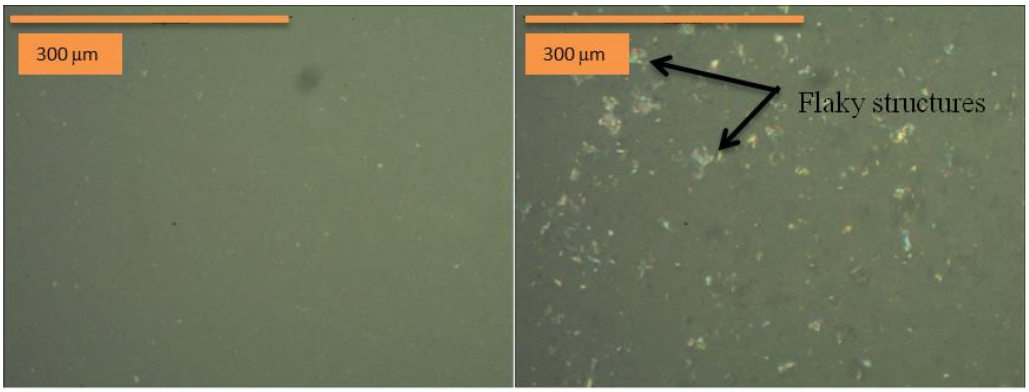

Figure 20 Optical micrographs of LTCC samples (a) control sample and (b) sample treated with 4M NaOH for 24 hours

Figure 20 shows the optical micrographs of the LTCC sample, immersed in 4M NaOH solution for 24 hours and analysed immediately after removal from the NaOH solution. The control sample showed a plain surface. Compared to the optical micrograph of the control sample, areas with shiny features could be seen on the sample treated with NaOH for 24 hours. The coverage of these features was fairly uniform on the surface. It was noticed that at higher magnification it was difficult to focus the image due to the tall and pointed features on the surface. It was very clear that the flake like structures formed while the LTCC samples were in the NaOH solution and not due to the air or moisture in the atmosphere.

B. SEM-EDX Analysis

Energy Dispersive X-ray Spectroscopy (EDX) analysis was carried out to determine the changes in elemental composition before and after exposure of LTCC to the NaOH solution.

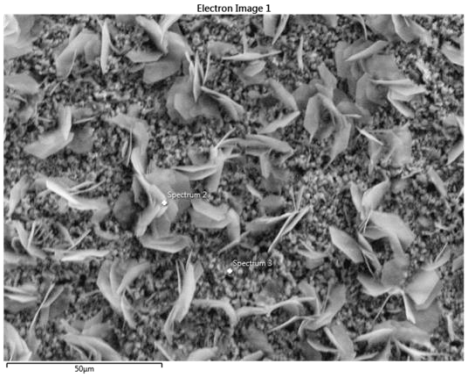

Figure 21 Area selected for EDX analysis

This system has the capability of analysing 1-10 μm depth of the surface. For the initial analysis, the complete area of the SEM image (Figure 21 as an example) was chosen, to include both flake and background surface structures. Figure 22 shows the SEM-EDX analysis of the LTCC samples. The control sample indicated the presence of aluminium, oxygen, calcium, lanthanum, boron, phosphorous and carbon as expected according to the material datasheet [82]. A small amount (0.5 wt%) of silicon was present in the control sample, however the Si peak effectively disappeared, even with 3M NaOH treatment. In general, the EDX analysis revealed a decreased elemental percentage of Al and La with increased NaOH etchant concentration. The decrease was more prominent in the samples treated with 5M NaOH for 24 hrs. It was also noted that calcium and oxygen percentages increased in the samples etched with 4M and 5M NaOH.

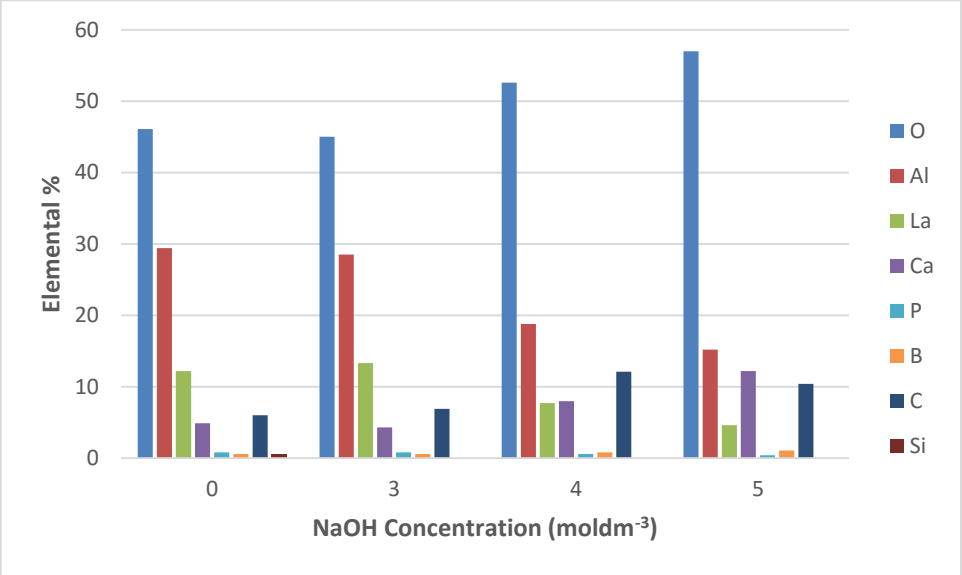

Figure 22 SEM EDX Analysis- Change in elemental % of LTCC surface with NaOH concentration (24 hours etch time)

The distribution of chemical elements of the LTCC sample etched with 4M NaOH for 24 hours was obtained using SEM-EDX elemental mapping. The image was focused on both the background surface and the flake surface as shown in Figure 23. The results were then compared to determine the change in chemical composition of the two distinct regions.

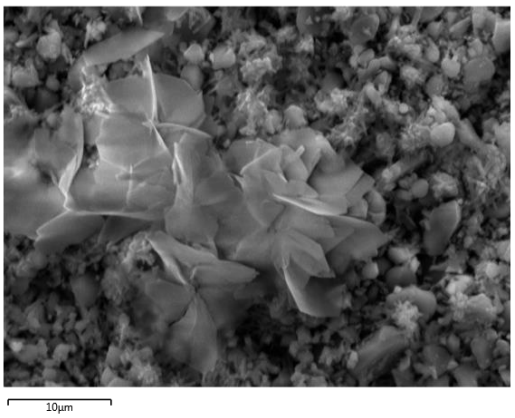

Figure 23 SEM image corresponding to elemental mapping

The elemental mapping images obtained for Al, O, La, Ca and P matched to the corresponding SEM image (Figure 23) are shown in Figure 24. Since Al and O images have the same distribution and image contrast and rarely contain other elements, it can be concluded that these areas represent aluminium oxide. It was seen that there was a clear reduction of the element distribution of lanthanum and aluminium over the flake like feature compared to the background surface. Oxygen showed fairly similar shades across the SEM image and could be due to the oxides present in both the flake like features and the background surface.

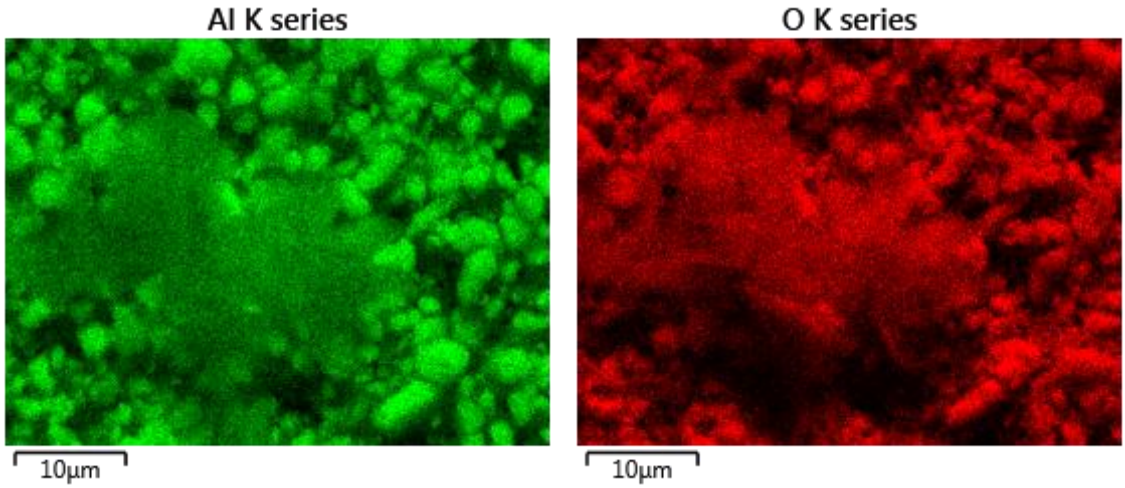

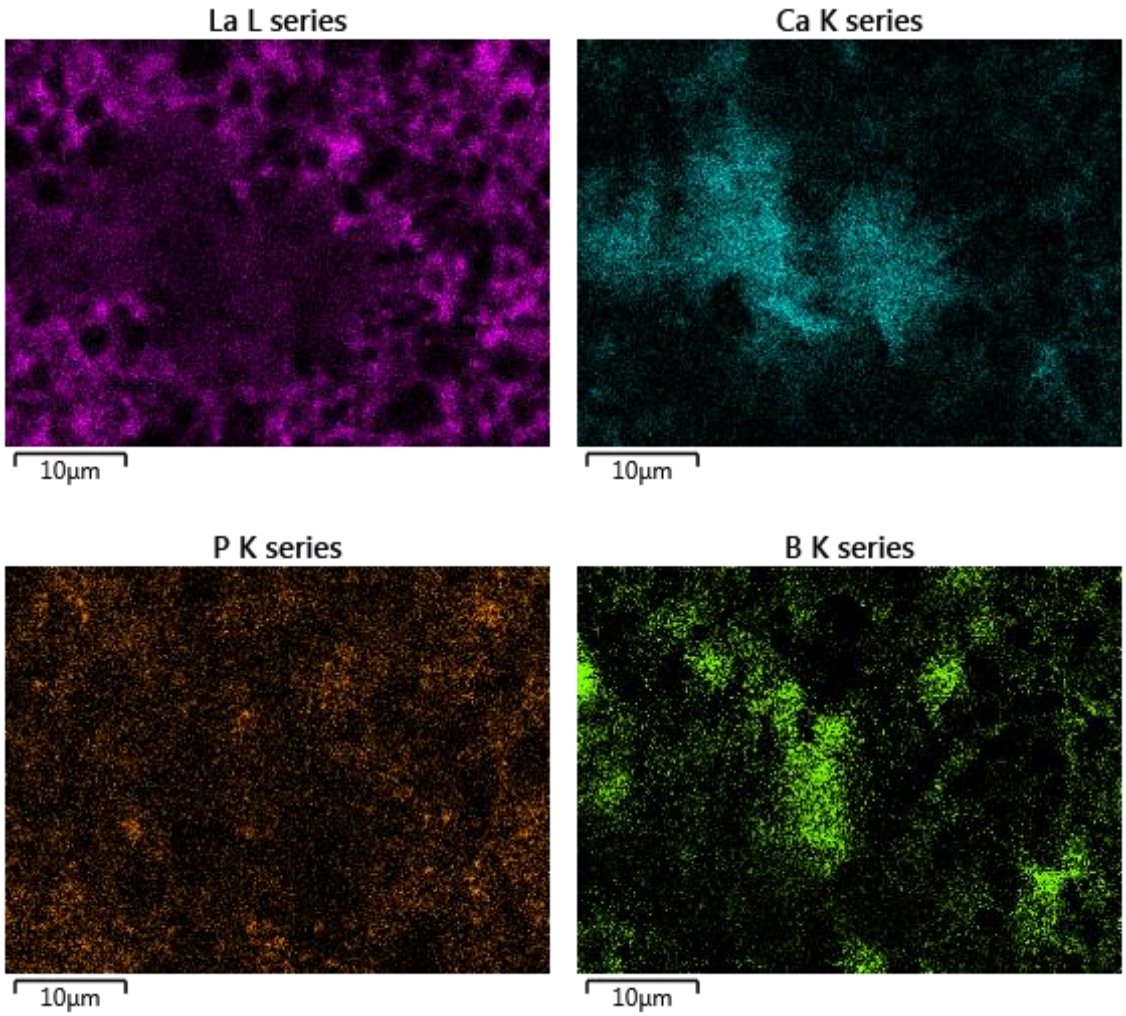

Figure 24 SEM EDX elemental mapping of the flake structure and background surface

A relatively high amount of calcium was present in the flake like feature compared to the background surface. A few bright areas could be seen in the boron map and some of these areas overlapped with the flaky structure on the corresponding SEM image. The phosphorous map showed a similar pattern to the lanthanum distribution; however it was relatively less in concentration.

C. Chemical Composition of NaOH Solution

Control NaOH (4M) and the 4 M NaOH solution which was used to treat LTCC samples were both diluted to 0.04 M and qualitatively (10% error when analysing qualitatively) analysed for their elemental composition using the ICPE-9000 system. The aim was to determine whether there were any elements present in the NaOH solution which could have been etched away from the LTCC samples. The chemical composition of the NaOH solution which was used to treat the LTCC samples was compared with the chemical

composition of the control NaOH solution. The same 4M NaOH solution used in earlier experiments were used for the analysis. Approximately ten samples had been etched in this solution and solid residues were not observed in the solution. According to the results obtained (Table 5), the elemental percentage of aluminium, boron and calcium of the NaOH solution increased compared to the control sample. It was also found that the elemental percentage of lanthanum and phosphorous remained constant.

Table 6 Comparison of chemical composition in control NaOH solution and the 4M NaOH solution which was used to treat LTCC samples

Element	Element concentration/mg/L in control NaOH Solution	Element concentration/mg/L in 4M NaOH solution used to treat LTCC
Aluminium	0.24	3.5
Boron	0.06	0.41
Calcium	0.01	0.07
Lanthanum	0.02	0.02
Phosphorous	0.17	0.17

The above observations can be compared with the EDX results obtained for the LTCC sample without any surface pre-treatments. As seen in the maps of the individual elements (Figure 26), the control sample contained aluminium, calcium, oxygen, lanthanum, boron, and phosphorous. Since aluminium and oxygen follow the same distribution and there is an absence of lanthanum and calcium on these particular areas, this leads to the conclusion that the grainy particles present on the surface are alumina particles. The rest of the area can be a single or multi-phase structure containing aluminium, lanthanum, calcium, boron, phosphorous and oxygen.

Since the NaOH solution contains aluminium, calcium and boron it can be concluded that some of the LTCC material dissolved in the NaOH solution. Absence of lanthanum and phosphorous in the NaOH solution, might be due to the selective etching of the material. Another possible explanation for the absence of these elements in the NaOH is that the parts which contain these elements could possibly drop to the bottom of the solution without dissolving in the NaOH solution.

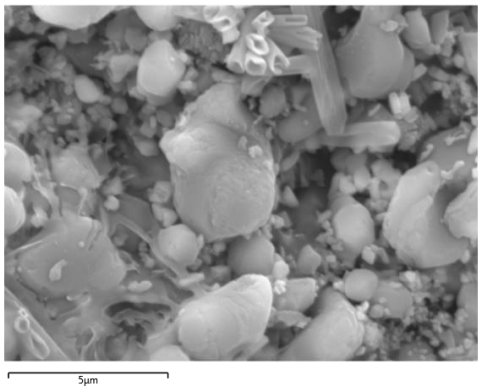

Figure 25 SEM image of the cleaned untreated sample corresponding to elemental mapping

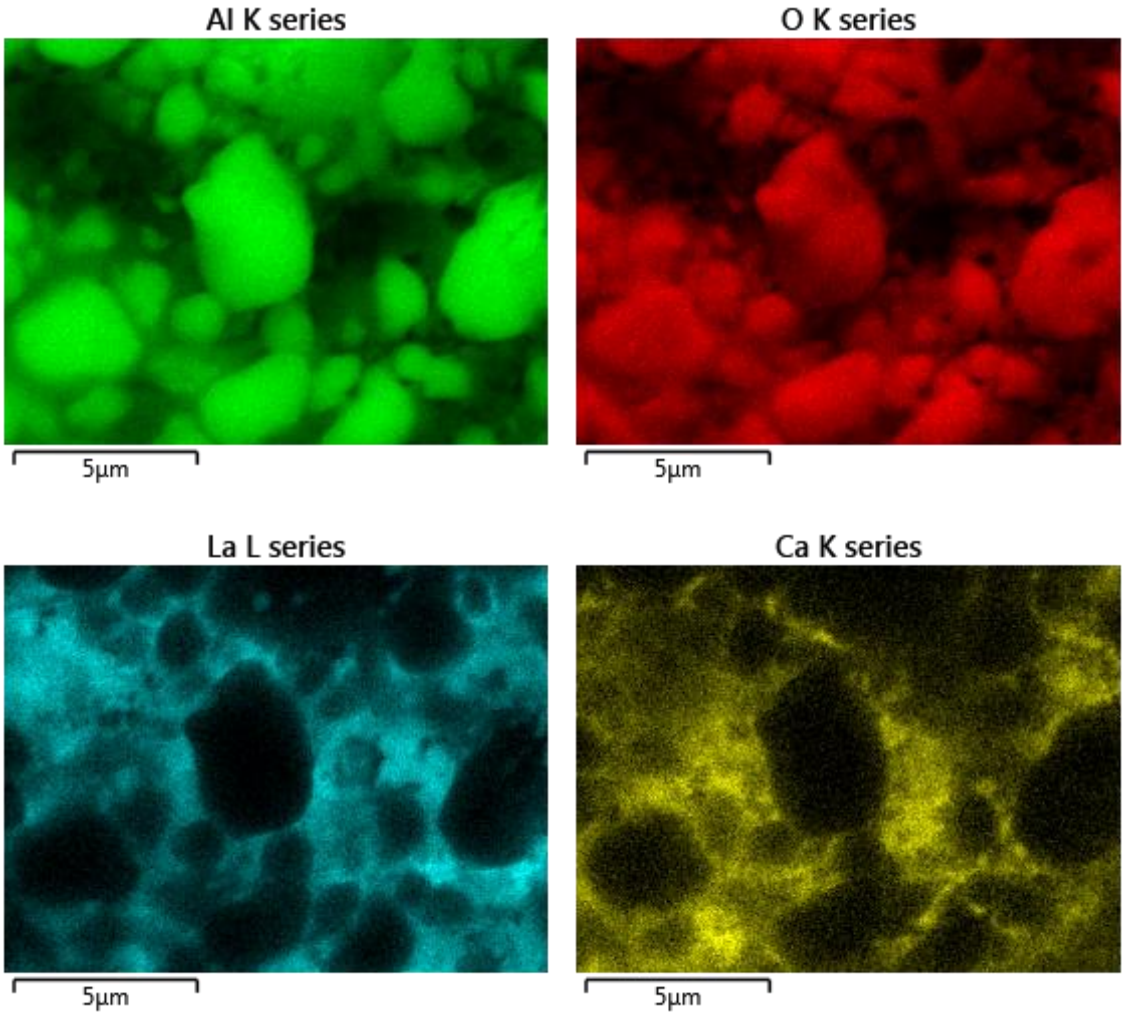

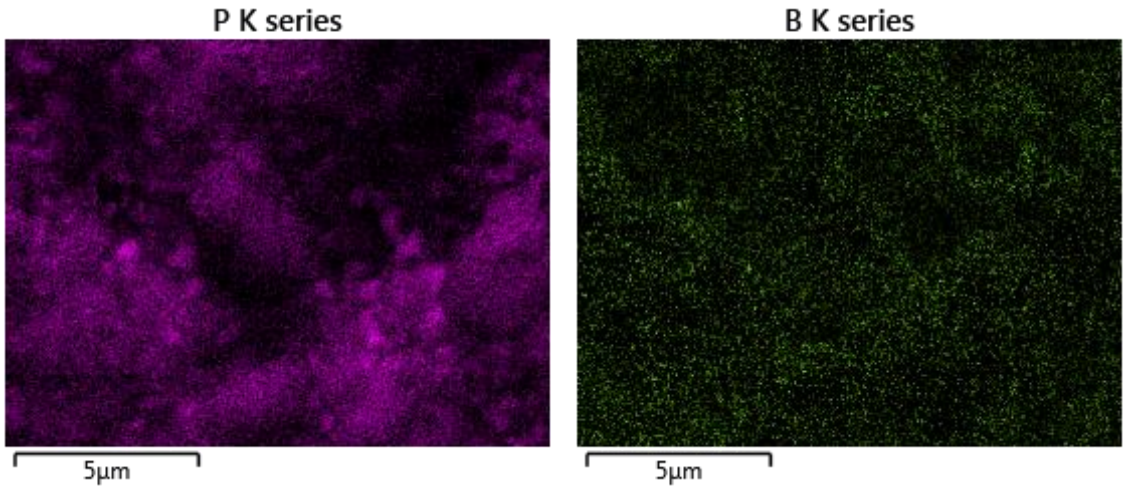

Figure 26 SEM EDX elemental mapping of the untreated LTCC surface

D. XPS Analysis

XPS is a surface sensitive analysis method and only analyses the top 5-10 nm of the material. Figure 27 (a)-(g) presents XPS scans of individual elements of the control LTCC sample and Figure 27 (1)-(6) presents the XPS scans of individual elements of the LTCC sample treated with 4M NaOH for 24 hours. The size of the surface area analysed for the control sample was 400 µm while the analysis area of the sample etched with NaOH was reduced to 30 µm: the aim was to focus the beam on a flake like structure. A flake like feature was identified on the surface using the optical camera attached to the system and analysis of this was carried out. However, as the optical image was not very clear, possibly due to the reflection from the LTCC material this analysed area may have included some additional components other than the flake.

According to the XPS scans of the control sample, the chemical elements aluminium, calcium, lanthanum, carbon, oxygen and phosphorous were present on the surface. The XPS scan of the LTCC sample treated with 4M NaOH also shows the presence of aluminium, calcium, lanthanum, carbon and oxygen with the addition of magnesium. The chemical elements aluminium, calcium, lanthanum, carbon and oxygen are therefore common in both samples. The binding energies of aluminium, lanthanum and oxygen were observed at the same position in the spectra. However, it is clearly shown in the overlapped scans of calcium and carbon in Figure 28, that the position of the binding energies of the calcium (Figure 28 (a)) peaks changed and the carbon (Figure 28 (b)) slightly changed. A stronger peak at 289 eV appeared in the carbon scan (green line indicates the etched sample

and red line indicates the control sample) that is indicative of carbonate species. The calcium peak at 347 eV in the etched sample may suggest the presence of $CaCO_3$ [83]. A magnesium peak at 1304.27 eV appeared in the XPS scan of the sample treated with NaOH. It was also noticed that two peaks at 133.35 eV and 1072.06 eV that are responsible for phosphorous 2p and sodium 1s disappeared in the XPS spectrum of the sample treated with NaOH.

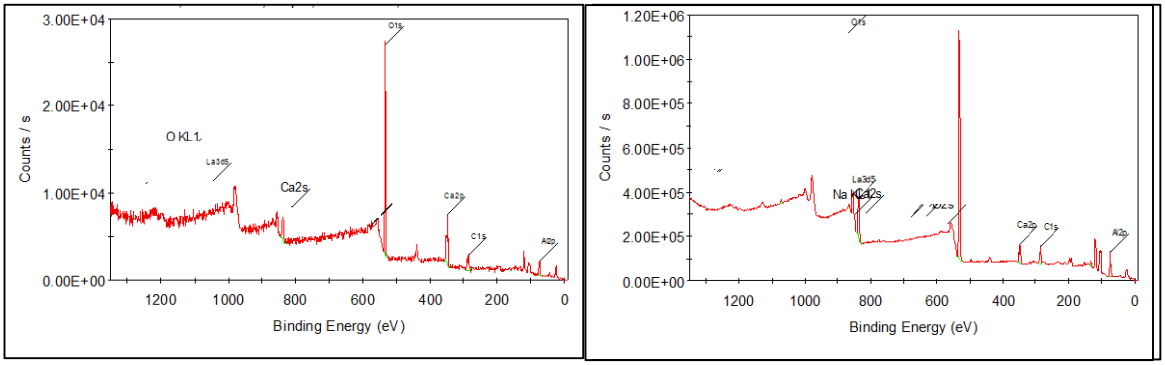

(a) (1)

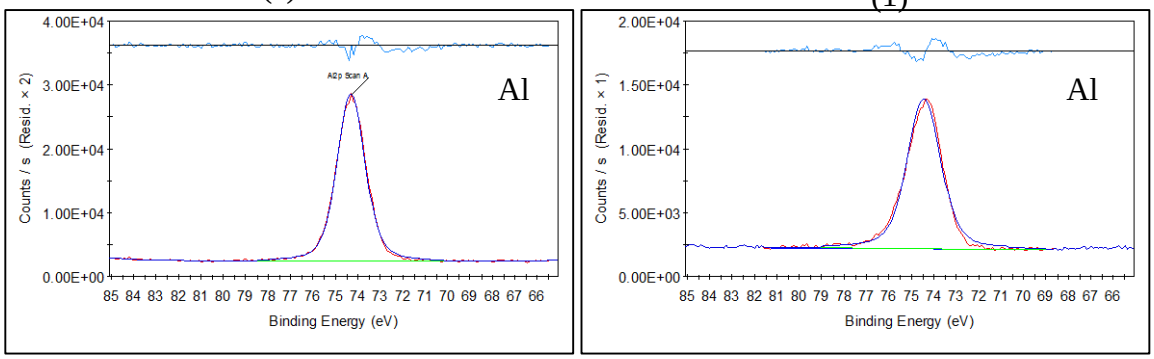

(b) (2)

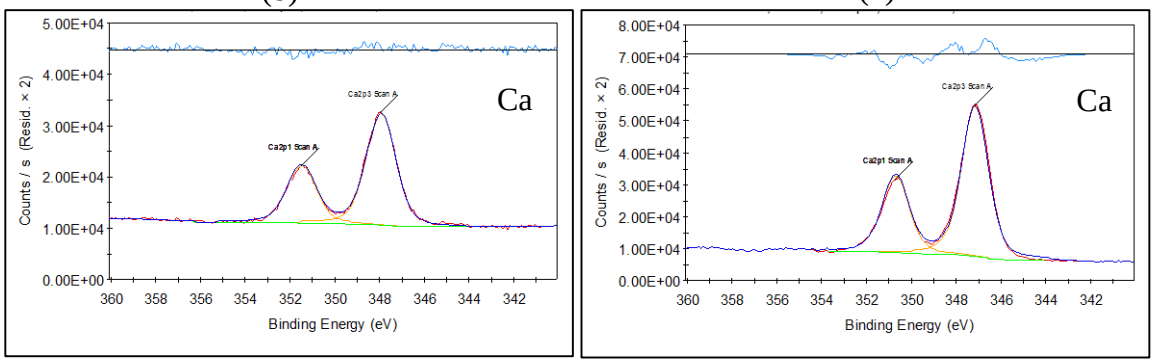

(c) (3)

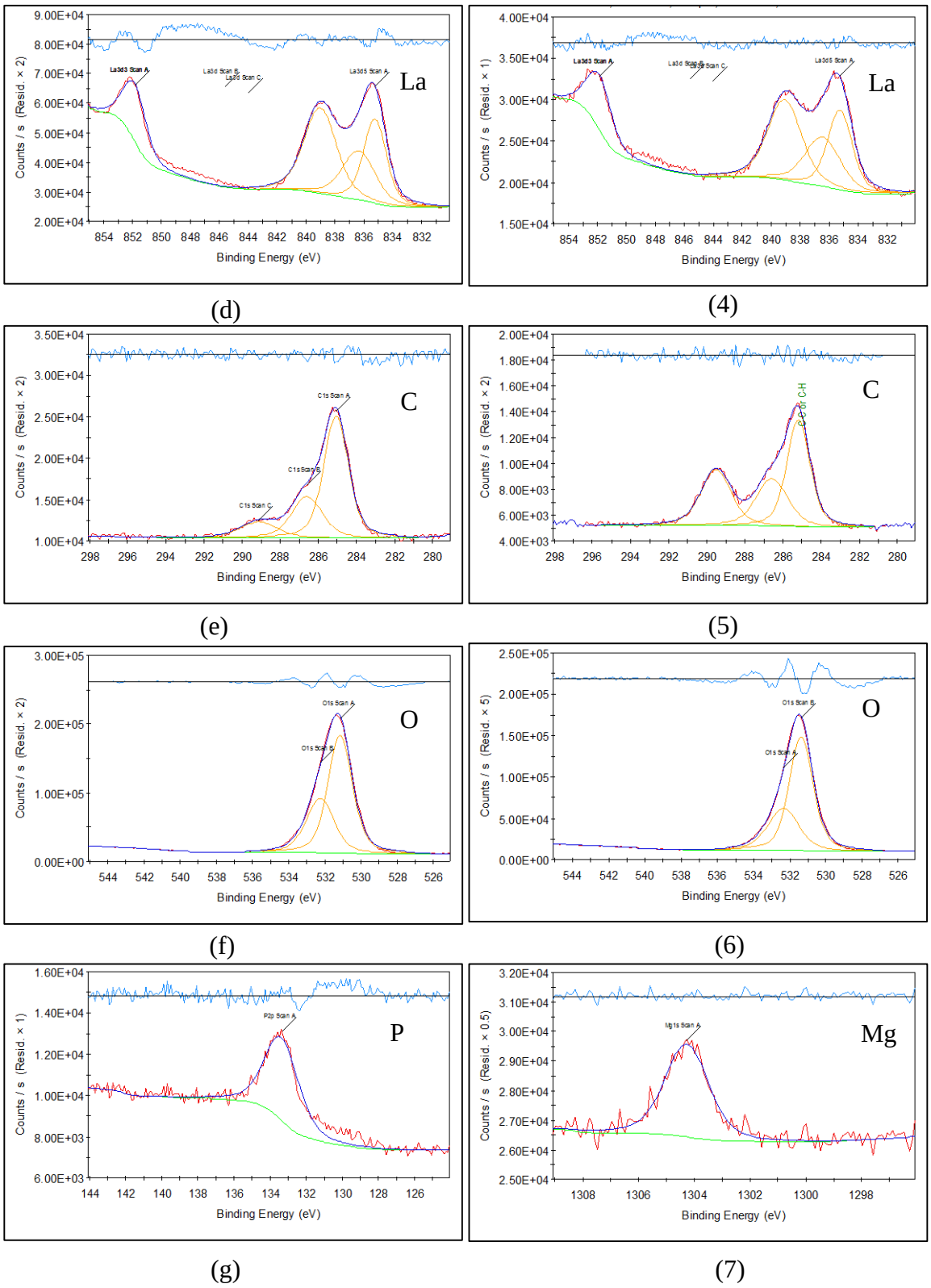

Figure 27 XPS Spectra. Control sample: (a) survey scan, (b) Al2p, (c) Ca2p, (d) La3d, (e) C1s, (f) O1s and (g) P2p. Sample etched with 4M NaOH for 24 hrs: (1) survey scan, (2) Al2p, (3) Ca2p, (4) La3d, (5) C1s, (6) O1s and (7) Mg1s.

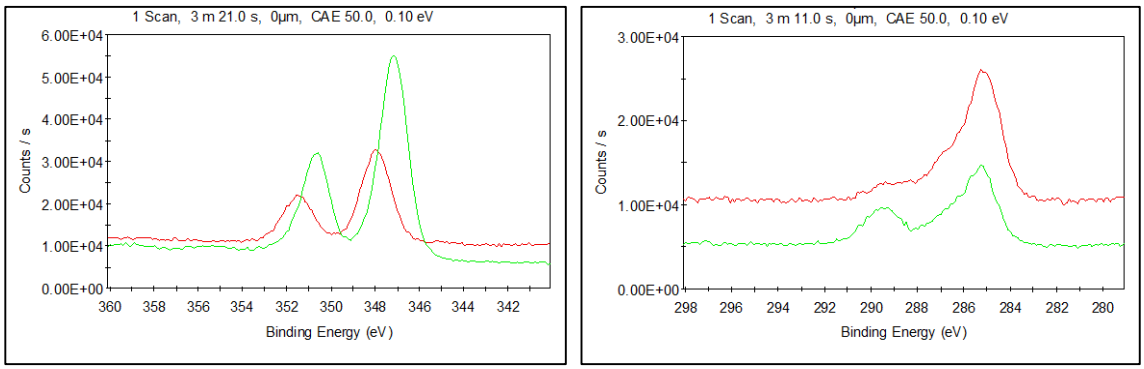

Figure 28 Overlapped scans of (a) Calcium (b) Carbon (green line - etched sample and red line - control sample)

Table 7 Atomic % of control LTCC sample and sample etched with 4M NaOH obtained from XPS

	Atomic %	
Chemical Element	Control	Sample etched with 4M NaOH
Al	22.34	22.78
Ca	3.54	9.1
La 3d5	2.21	1.03
O 1s	56.47	54.53
C 1s	12.42	11.86
Na 1s	0.59	-
P 2p	2.43	-
Mg 1s	-	0.71

Table 6 shows the change in atomic percentage of the LTCC sample with NaOH treatment. The total atomic percentage of calcium relatively increased in the sample treated with NaOH. On the other hand, there was a decrement in the total atomic percentage of lanthanum and there was no Phosphorous observed in the samples treated with NaOH. The total percentage of oxygen and aluminium remained approximately constant.

E. LTCC Cross Section Analysis

A cross section of the LTCC substrate was encapsulated into a compression mounting resin and grinding and polishing of the mounted specimen was carried out as described in section 2.4.4. The cross section of the specimen was then analysed using an optical microscope.

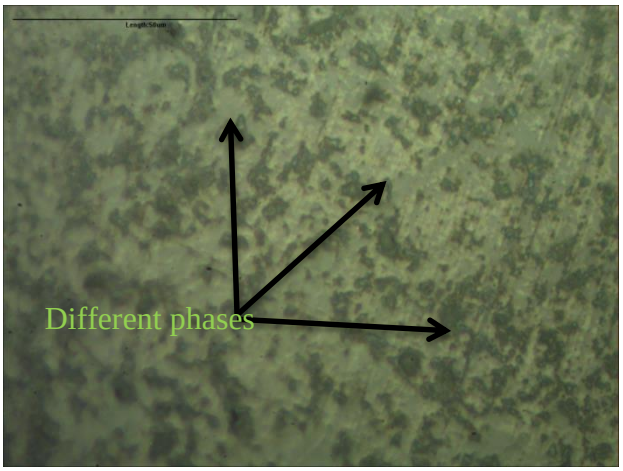

Figure 29 Optical micrograph of cross section of fired LTCC

As seen in Figure 29, three different features with different colours were identified within the optical micrographs. These could be responsible for different types of crystalline phases present in the LTCC material.

Another sample was snapped and mounted on an Al stub without polishing and the cross section was analysed using SEM. SEM micrographs of the cross section were taken at top and middle sections of the sample. Some flake like structures were found located in the middle section of the cross section. The cross section of the top surface showed a relatively dense material phase compared to the middle section. The middle layer of the cross section contained some pits as seen in the SEM micrograph (Figure 30 (c)).

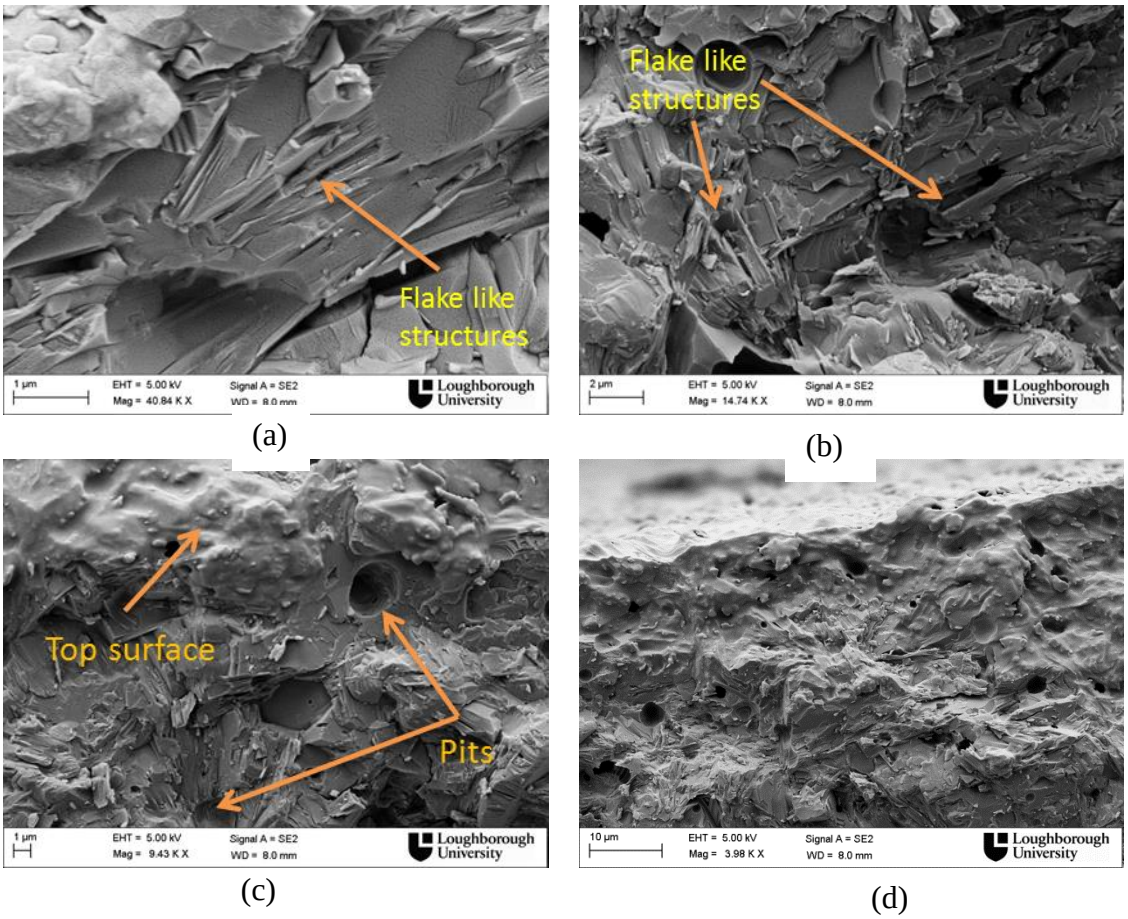

Figure 30 SEM images of LTCC cross section (a) and (b) middle region (c) and (d) top region

F. XRD Analysis

XRD analysis was carried out to investigate the different phases present in the LTCC material after the firing process. X-Ray diffraction patterns for the solid state LTCC were obtained using the D2 Phaser XRD system. The XRD spectrum is shown in Figure 31 The results were analysed using the database "The International Centre for Diffraction Data (ICDD) Powder Diffraction File (PDF)", which is part of the STOE WinXPow Software suite. The XRD spectrum showed sharp peaks confirming that the LTCC material consisted of a large number of different types of crystalline phases. The XRD peaks were overlapped in many 2 Theta positions. At this stage, three different crystalline phases were identified: corundum (Al_2O_3) (PDF card number 46-1212), calcium aluminium borate ($CaAl_2B_2O_7$) (PDF card number 19-205) and lanthanum borate ($LaBO_3$) (PDF card number 12-762).

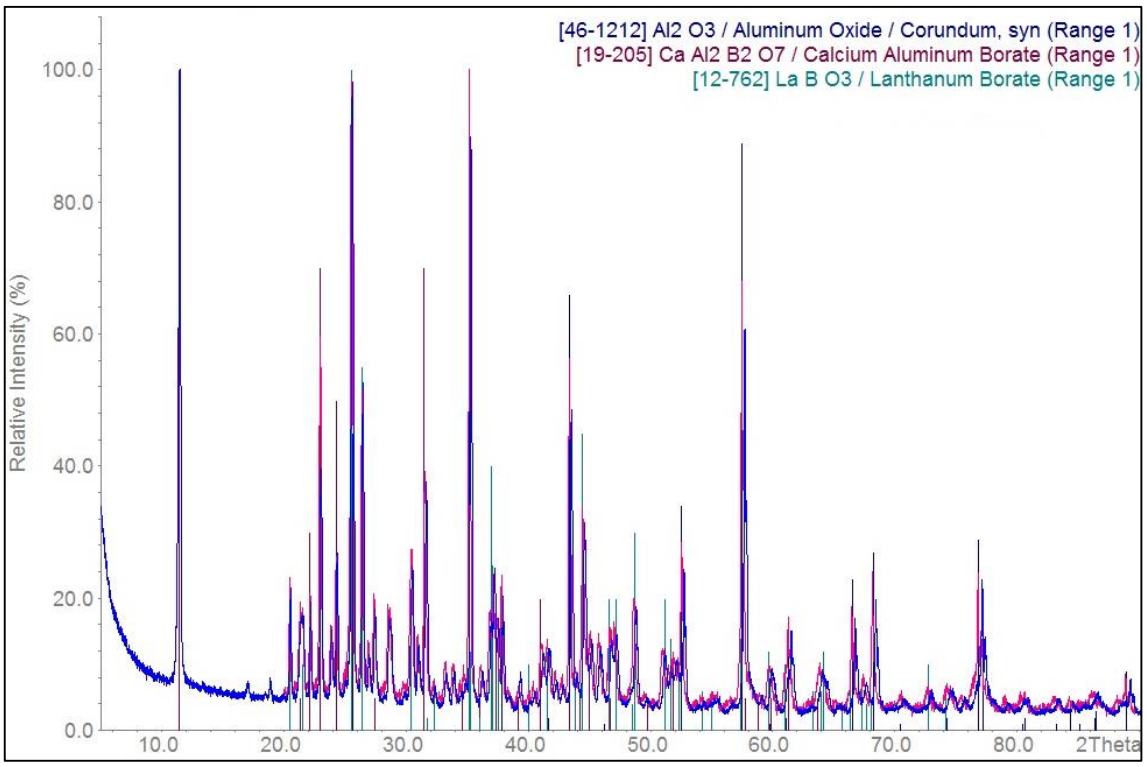

Figure 31 XRD spectrum of fired LTCC

Nair et al. studied the crystal behaviour of the fired LTCC 9k7 using X-ray diffraction [84]. However, this study did not provide any chemical compositions of the crystalline structures. Their X-ray diffraction results for LTCC 9k7 fired tape surface after the initial firing at the 26.5 hour firing profile and for the tapes refired an additional six times at 850 ^{0}C for 30 minutes were presented. Five different crystal species were identified: amorphous remanant glass, two types of crystals derived from partial crystallisation of the glass and another two types of crystals derived from the interaction of the filler with the glass and a ceramic crystalline structure. This study also showed that no further increase in the amount of crystal formation occurs with refires.

G. Weight Loss Measurements

From the previous analysis techniques, it was hypothesised that material was being removed from the LTCC surface when treated with NaOH solution. To confirm this, weight measurements were carried out on etched LTCC samples. The initial weight of the cleaned LTCC samples was measured using a KERN ABS220-4 electronic balance. These samples were then placed in a vacuum oven for approximately one hour at 80 ^{0}C. The weights of the samples were measured again and compared with the initial results and the same

procedure was carried out until the weight reached a constant value. This was done to get the weight of the LTCC samples without any moisture content. Samples were then immersed in 4M NaOH solution for different time periods. These samples were then rinsed with deionized water and dried with a specimen drier. The samples were then dried in the vacuum oven at 80 ^{0}C and the final constant weights of the etched samples were also measured.

In this experiment, the material removal rate (*R*) was then calculated using the following equations and presented in Table (7).

$$h = \frac{\Delta w}{2dA} \qquad 3.1$$

$$R = \frac{\Delta w}{2dAt} \qquad 2.3$$

Where, *h* is the change in thickness from one surface, Δw is the weight loss, *d* is the density of fired LTCC 9k7 (3.1 gcm^{-3}), *A* is the area of the sample and *t* is the etch time.

Table 8 Material removal rate of LTCC etched with 4M NaOH

Immersion time / minutes	**Sample starting Weight/ g**	**Weight loss/ g**	**Thickness of the etched material /nm**	**Etch rate/ nm/hour**
30	0.0942	0.0001	120	487
60	0.0969	0.0002	240	487
120	0.0976	0.0002	240	243
240	0.0983	0.0003	365	182
360	0.0961	0.0004	488	162
1440 (24 hrs)	0.0944	0.0041	5 μm	208

The resolution of the balance is 0.0001 g and the fourth decimal place of the first five readings of the table may therefore not contribute towards any significant conclusions. However, the weight loss increased with the etching time and this result was more obvious in the sample treated for 24 hours. The weight measurement results confirm that material was removed from the surface with the NaOH treatment. The etch rate appears to have higher values for the first one hour period and decreases over the next five hours, showing that the top layer of the LTCC samples was easier to etch away.

3.5 Discussion

It has been found that concentrated NaOH can be used as a chemical etchant in order to change the surface microstructure of fired LTCC. The microstructure of the LTCC surface was found to vary with the concentration of NaOH and sample immersion time in the NaOH solution. The most noticeable feature was the appearance of flake structures after 50 minutes in 4M NaOH solution. A number of analysis techniques were used to find out whether these features were already dispersed in the LTCC material itself and appeared after the background surface was selectively etched away with concentrated NaOH or if they were formed due to a chemical reaction between the LTCC material and NaOH solution. An initial consideration was that these crystals could be formed due to air and moisture in the atmosphere when stored for long periods. However, after considering the optical micrographs of the samples analysed immediately after they were taken out from the NaOH solution, it was very clear that the flake like structures formed while the LTCC samples were in the NaOH solution and not due to the air or moisture in the atmosphere.

The optical micrograph of the cross section of polished LTCC and the initial XRD analysis confirmed that the LTCC material consists of different types of crystalline phases. The SEM images of the surface of LTCC without any surface treatment showed loosely bound grainy particles and according to the EDX results these grainy particles may be alumina which was also seen as one of the structures in XRD. The SEM images of the unpolished cross section of the LTCC sample showed a similar feature that could be a flake like structure and this was located in the middle layer of the material. It was also found that the top surface consisted of a relatively dense material phase. XPS and SEM-EDX analysis was carried out to investigate the change in chemical composition of the LTCC surface after NaOH treatment. According to the XPS study only calcium and carbon showed small changes in peaks. This indicates that the chemical state of the other elements remains unchanged suggesting no new crystals formed on the surface due to a chemical reaction between NaOH solution and the LTCC material. Both XPS and EDX analysis confirmed an increase in calcium and oxygen percentage on the LTCC surface when treated with NaOH. On the other hand, elemental distribution of the LTCC treated with NaOH showed an increase in calcium, boron and oxygen percentages in the flake like surface while the background surface contained a high amount of aluminium, lanthanum, oxygen and phosphorous.

The model in (Figure 32) is proposed at this stage for the microstructure of the fired LTCC material according to the above observations.

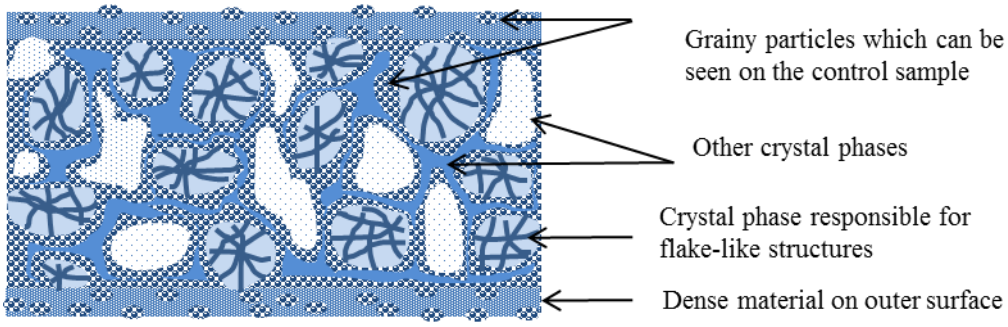

Figure 32 Model of the fired LTCC microstructure

This material model suggests that the flake like structures are already immersed in the LTCC material and concentrated NaOH has the ability to selectively etch away the background surface. Weight reduction of the LTCC samples treated with NaOH compared to the control sample and the presence of Aluminium, Boron and Calcium in the NaOH solution which was used to treat LTCC samples further support the above conclusion. Figure 33 shows the schematic diagram of the possible etching process of the LTCC when immersed in NaOH.

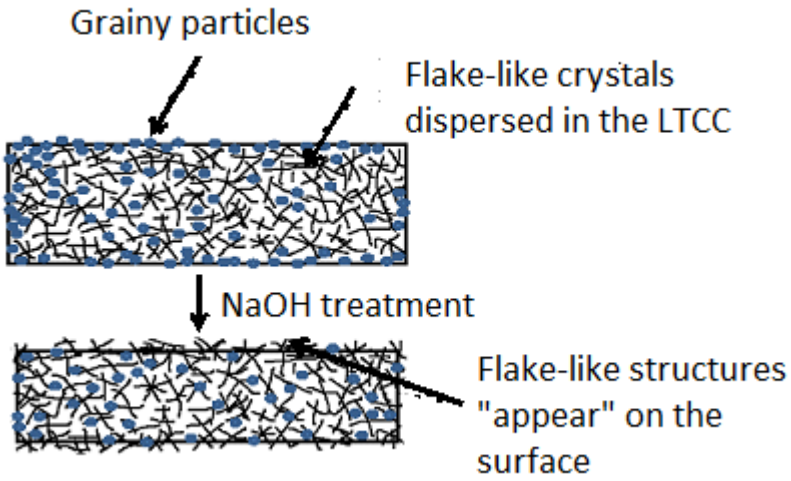

Figure 33 Schematic diagram of the etching process

3.6 Conclusions

In this study, different concentrations of NaOH were used to modify the LTCC substrate surface for later use in the adhesion of electroless Cu deposits. With this approach, a different surface morphology was observed when using different concentrations of NaOH. The sample immersion time also affected the surface morphology of the LTCC. Flake like features appeared on the LTCC surface after the NaOH pre-treatment and a series of surface analysis and chemical analysis techniques were carried out to investigate the etching mechanism and the chemical composition of the flake like structures. A material model was proposed for fired LTCC according to the results obtained and suggested that these flake like features are already dispersed in the fired LTCC material. These then "appear" on the surface once some of the background surface is selectively etched away. The change in surface roughness of the LTCC surface with the NaOH pre-treatment and the effect of change in surface morphology on adhesion improvement will be presented in the later chapters.

Chapter 4 Effect of NaOH Pre-treatment on Surface Roughness of LTCC

4.1 Introduction

As mentioned in the previous chapter, surface roughness of the substrate plays a vital role in adhesion improvement. Some of the widely used methods in order to create rougher surfaces include chemical treatments, mechanical abrasion and plasma treatments. In this research a chemical treatment method using NaOH was employed to change the surface morphology of the fired LTCC. It was noted that a flake like structure appeared on the LTCC surface with the NaOH treatment. It was necessary to investigate the effect of these features on the change in surface roughness of fired LTCC and this chapter therefore presents data for the change in surface roughness of fired LTCC once treated with concentrated NaOH. It also discusses the characterization of the surface roughness of the treated LTCC surface using traditional profile parameters such as Ra and areal surface texture parameters which may give a much better representation of the surface morphology.

4.2 Literature Survey

4.2.1 Classification of Surfaces

The relationship between surface topography and the functionality of the surface is vital for many engineering surfaces. Surfaces are usually manufactured to obey some functional properties depending on the application. These functional properties include wear, sealing and paintability etc. Hence, characterization of surface texture is important when designing surfaces for functionality [85].

In 2001, Stout and Blunt [86] presented a hierarchy of surface classification. According to their classification, surfaces can be divided into two main categories, i.e. engineered and non-engineered surfaces. This is further divided into sub-categories and illustrated in Figure 34.

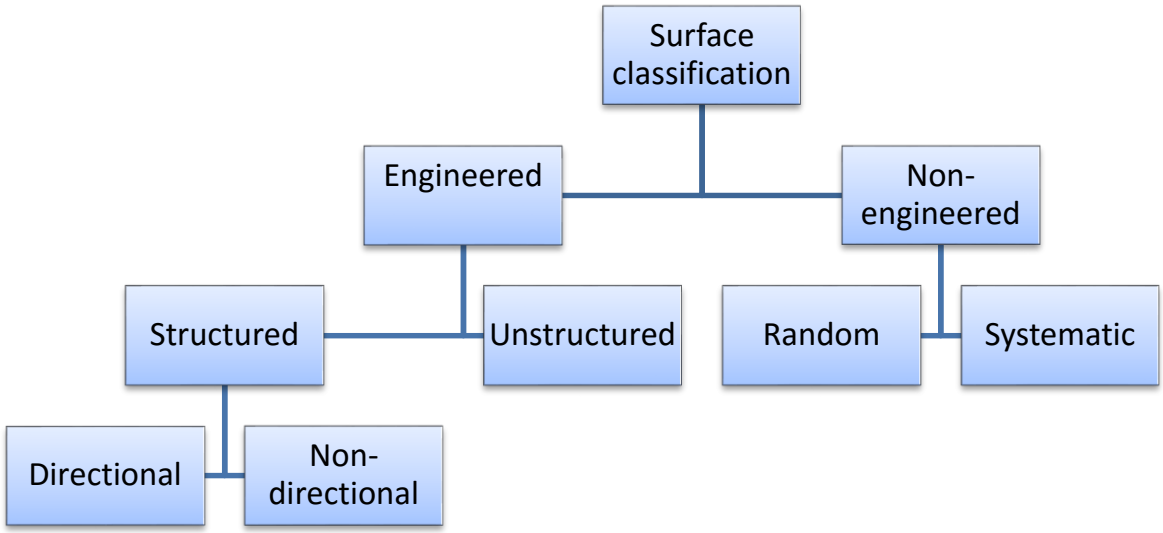

Figure 34 Classification of surfaces [86]

Engineered surfaces are obtained by altering the surface for specific functional performance, whereas non-engineered surfaces are produced as a result of the manufacturing process. Structured surfaces are defined as surfaces with a high aspect ratio of geometric features. Directional surfaces have a specific directional pattern and the non-directional surfaces have a pattern without any specific directionality. Unstructured surfaces are manufactured by partly controlled manufacturing processes. Random surfaces are obtained by removing systematic features, whereas systematic surfaces contain a pattern usually as a consequence of the production process [86]. The measuring parameters which describe the surface texture should be selected according to the functionality and the type of surface. In this case, it is important to identify the functionality and the type of the surface being measured. The ceramic surface studied in this research belongs to the engineered surface category as the final surface is due to an alteration of the surface using a chemical etching process. Since it does not convey a deterministic pattern, it can be further categorised into an unstructured surface.

4.2.2 Surface Texture Measurement Methods: 2-D vs 3-D

Surface roughness is one element of the surface texture and is usually measured using a contacting stylus or a non-contacting optical probe. In a stylus instrument, a stylus tip contacts and is dragged across the sample surface and the vertical movement of the stylus tip is measured and converted to an electrical signal by a transducer unit [87]. The size and the shape of the stylus tip and the force being used on the stylus directly affect the measured surface texture results. For example, depending on the size of the stylus tip, it may not fully penetrate into the narrow valleys of the test surface. Also, a stylus tip may never identify a re-entrant feature on the surface leading to poor representation of the surface texture [88]. Zahwi and co-workers also reported that the force applied on the stylus tip can create a scratch on the test surface and affect the surface texture results [89].

Stylus instruments that can be used to measure vertical and horizontal axes are reported in the literature [90], however, these instruments are time consuming and costly. Optical techniques on the other hand have drawn much attention when measuring surface texture in terms of getting more accurate results. Optical techniques such as interferometry [91], scattering [92] and autofocus [93] can be used as an alternative to achieve relatively faster results when measuring 3-D surface texture [94]. Leach and co-workers reported a comparison of the stylus and optical methods for 2-D surface textures. In this study, they found that the results obtained from both methods did not agree. Further, they also found that the results were varied when obtained using the same measurement technique, but with different instruments. However, proper calibration of instruments according to the given measurement type and surface can give confidence in using these techniques [95].

A good representation of the 2-D surface texture data can only be obtained when the surface is homogeneous. In the case of heterogeneous surfaces, statistical representation of a 2-D profile can be very poor as it only provides the topographic information along one direction where the 2-D profile is taken. For non-homogeneous surfaces, 3-D surface texture gives more detailed information. The 3-D surface texture represents the real surface with significant surface functionality and it gives an opportunity to derive parameters relating to surface area leading to the much better representation of statistical significance and repeatability [96].

4.2.3 2-D and 3-D Surface Texture Parameters

Coherence Scanning Interferometry (CSI) instruments normally gather a raw set of quantified numerical data which represents the topography of the test surface. The CSI software can then be used to convert these data into a graphical representation and numerical quantifiers such as surface texture parameters. Depending on the user defined data, 2-D or 3-D surface texture parameters can be obtained [97]. Areal surface texture parameters can be divided into two sub-categories i.e. S parameters and V parameters.

Once the surface has been measured, the data can be presented as 2-D or 3-D surface texture parameters. In this study, only Ra (2-D parameter) and V parameters which have been specially developed to describe the material volume and the void volume of the surface were selected. Definitions of those parameters and some of the terms that describe Ra and V parameters are presented in the following section [98].

Ordinate value (Z(x))

This is the height of the assessed profile at any position X. The height is regarded as negative if the ordinate lies below the x-axis and positive otherwise (Figure 35).

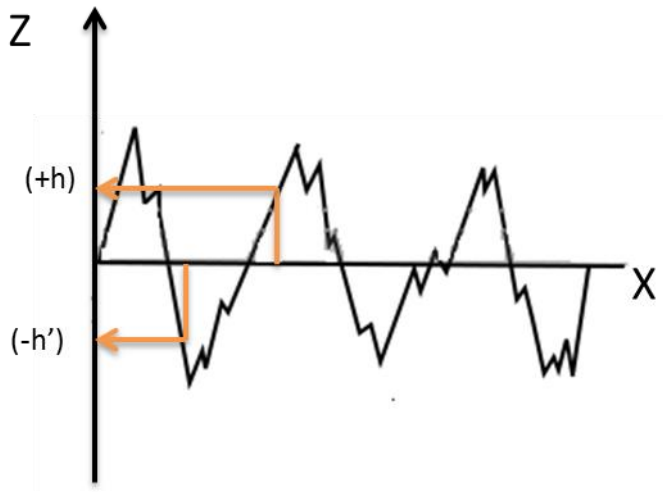

Figure 35 An example of a 2-D profile of a surface

Ra- Arithmetical Mean of the Assessed Profile

Ra is usually defined as the arithmetic mean of the absolute ordinate values Z(x) within the sampling length (*l*).

$$Ra = \frac{1}{l}\int_0^l |Z(x)|\, dx \quad 4.1$$

The Ra value is the most common surface texture parameter considered, however, it does not provide any information about any of the irregularities on the sample surface. As it takes the mean of the absolute ordinate values of a surface profile, it is possible to acquire similar Ra values for surfaces containing very different profiles [99].

F-operation, S–Filter and L-Filter

Once the surface is measured, the surface texture software usually removes forms (geometrical form such as sphere or cylinder) from the primary surface prior to the filtering process and this is called an F-operation. Filtering is a significant part in surface texture analysis. Usually it is a way of rejecting data considered irrelevant. Filters avoid signals according to a user defined scale in the x-axis in terms of wavelength. An S-filter is defined as a surface filter which removes small scale lateral components from the surface resulting in the primary surface. For example by applying an S-filter, measurement noise or functionally irrelevant small features can be removed from the sample surface [100]. A surface filter which removes large scale lateral components from the primary surface is called an L-filter. For example when the roughness profile of the surface is the factor of interest an L-filter can be applied to the measured surface to remove the waviness profile from the surface.

S-F Surface and S-L Surface

The surface derived from the primary surface after removing the form using an F–operation and S-filtration, is called an S-F surface while the surface derived from the S-F surface by removing the large scale components using an L filter is called the S-L surface. The surface (S-F or S-L) derived after filtration is known as the Scale Limited Surface.

4.2.4 Surface Texture Volume Parameters

Areal material ratio and the inverse areal material ratio of the scale limited surface are two terms that are required when explaining the surface texture volume parameters. These terms are defined in the following section.

Areal Material Ratio of the Scale Limited Surface (Smr (c))

Ratio of the area of the material (A+B+C+D) at a specific height c to the evaluation area L (Figure 36). Evaluation area is defined as the portion of the scale limited surface for specifying the area under evaluation.

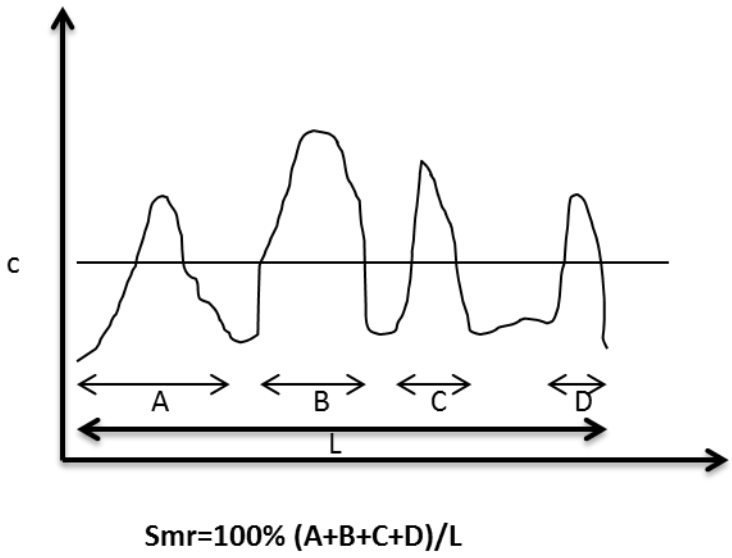

Figure 36 Schematic representation of the Areal Material Ratio of the Scale Limited Surface

Areal Material Ratio Curve

The areal material ratio of the scale limited surface is defined as the ratio of the area of the material at a specified height to the evaluation area and the areal material ratio curve is shown in Figure 37. When calculating volume parameters defined below, the default value for p and q was 10 % and 80 % respectively.

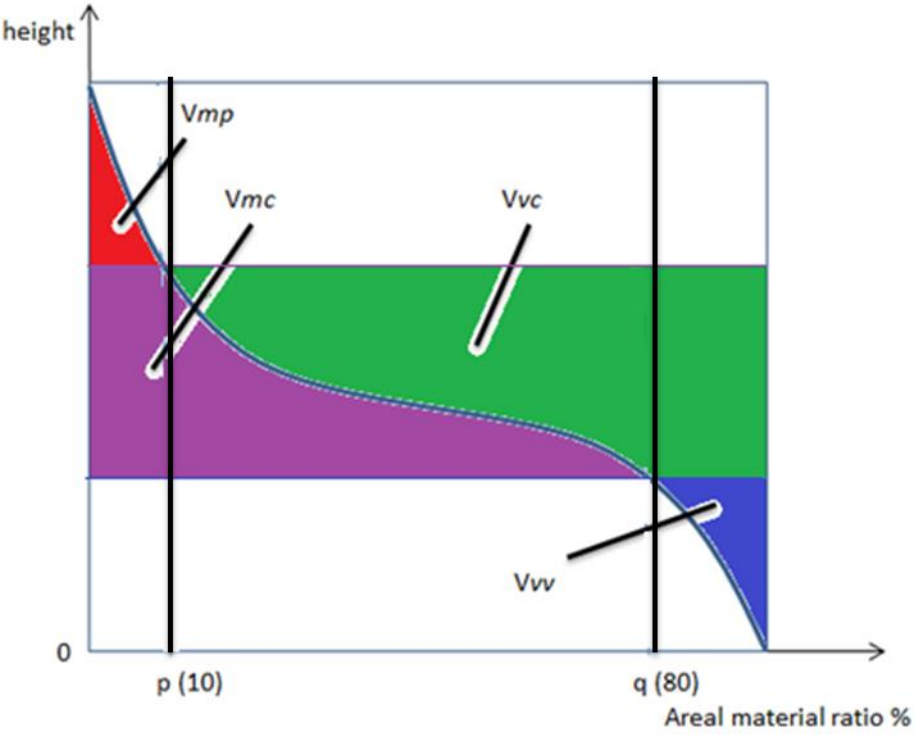

Figure 37 Areal material ratio curve

Inverse Areal Material Ratio of the Scale Limited Surface (Smc (mr))

This is the height h at which a given areal material ratio (mr) is satisfied (Figure 38).

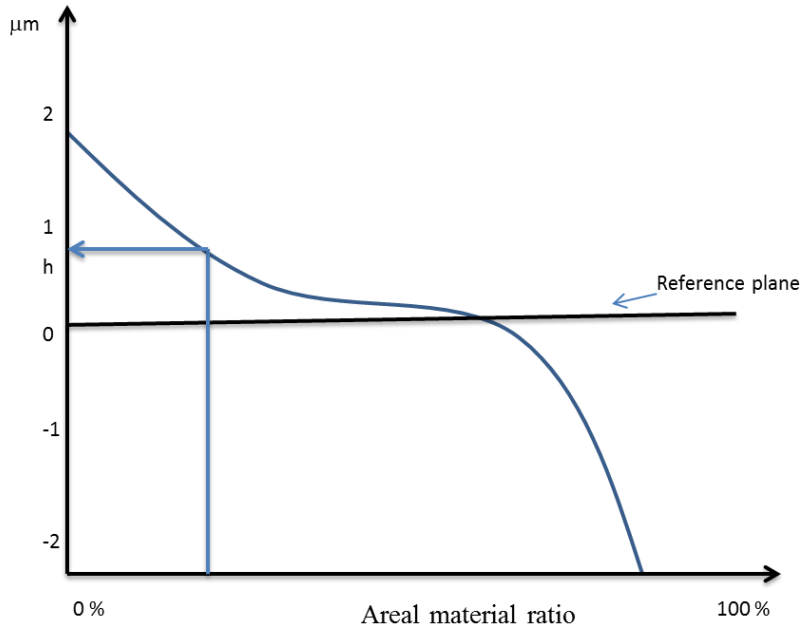

Figure 38 Schematic representation of the Inverse Areal Material Ratio of the Scale Limited Surface (Smc (mr))

V parameters have been developed based on three zones of the surface i.e. peak zone (red area of the areal material ratio curve), core zone (green area of the areal material ratio curve) and the valley zone (blue area of the areal material ratio curve) and their definition, units and mathematical representation are listed in Table 8.

Table 9 Definitions and mathematical derivation of V parameters [98].

Parameter	Definition	Units	Mathematical Formula
V*v*	Void volume	ml m^{-2}	$\frac{k}{100\%}\int_{p}^{100\%}[Smc(p)-Smc(q)]\mathrm{d}q$
V*vv*	Dale void volume of the scale limited surface	ml m^{-2}	V*vv* =V*v* (p)
V*vc*	Core void volume of the scale limited surface	ml m^{-2}	V*vc* =V*v*(p) –V*v*(q)
V*m*	Material volume	ml m^{-2}	$\frac{k}{100\%}\int_{0}^{p}[Smc(q)-Sdc(p)]\mathrm{d}q$
V*mp*	Material volume of the scale limited surface	ml m^{-2}	V*mp* = V*m* (p)
V*mc*	Core material volume of the scale limited surface	ml m^{-2}	V*mc* = V*m* (q) – V*m* (p)

Vv is defined as the voids per unit area at a given material ratio calculated from the areal material ratio curve. In other words, the volume of the space bounded by the surface texture from a plane at a height corresponding to a chosen material ratio value to the lowest valley [98], [63]. For example, if the Vv(mr) = A ml m^{-2}, it indicates that an A µm thick film over the measurement area would provide the same volume of fluid as needed to fill the measured surface from a height corresponding to a material ratio % to the lowest valley. Vmp (p) is the peak material ratio volume of the scale limited surface. This means the volume of the material comprising the surface from the height corresponding to a material ratio level p to the highest peak [98], [63]. Surfaces with large peaks are responsible for larger Vmp values and this indicates good bearing properties of the surface. Vvv is the dale void volume of the scale limited surface. Larger Vvv values indicate good fluid retention capability in the valley zone [98], [63]. Vm (Material Volume) is the volume of material

comprising the surface from the height corresponding to mr to the highest peak of the surface [101]. Vmc is defined as the core material volume of the scale limited surface. In other words, Vmc is the volume of material comprising the texture between heights corresponding to the material ratio values p and q. The surface with extreme valleys are responsible for large Vmc values and this value further indicates how much material is available for load support once the top levels of a surface are worn away [98],[63]. Vvc (p,q) is the core void volume of the scale limited surface and it is the difference between void volume between p and q material ratios. This also refers to the volume of the space bounded by the texture at heights related to the 10% and 80% range of the material ratio. Larger Vvc values indicate more fluid retention [98], [63].

4.2.5 Surface Texture Measurement of Unstructured Surfaces

The development of areal parameters started within the last three decades and the research is still being carried out to investigate the relationship between the functionality of the test surface and the surface texture parameters. The user has the challenge to select the most suitable areal parameters which describe the functionality of the surface [97]. Little research was found in the literature that has being carried out to find the relationship between surface texture parameters and the functionality of the surface.

Ann Wennerberg used 3-D texture parameters obtained using measurement equipment based on the confocal principle. In this study, the relationship between surface roughness and firmer bone implant fixation was investigated. The roughness of the implants was formed by a blasting technique and the surface texture S-parameters were used to describe the implant surface [102]. Another study carried out by the same research group compared the confocal laser scanning and stylus techniques when measuring 3-D topography of two different surfaces [103]. The surfaces used there included a titanium disc blasted with 25 μm particles and a complex surface structure with superimposed cylindrical shape that had a plateau horned surface. This study showed there was a good agreement between both measurement techniques. It also found that soft materials are best tested with a laser scanning technique, while hard materials are best evaluated with a stylus method. Their finding showed S-parameters were not suitable for describing the blasted surface due to the lack of an S-shaped material ratio curve.

A recent study [63] has been carried out to find the relationship between the adhesion strength of electroless copper deposits to roughened glass substrates and areal surface parameters. Both random and structured surfaces were created on a glass surface using excimer laser machining. In that study, height parameters, spatial parameters, hybrid parameters and volume parameters were correlated with the critical load at the copper failure point of the scratch test. A number of areal parameters which showed a strong relationship with critical load were identified. A set of areal parameters were recommended with a value range for predicting copper plating adhesion to glass. However, the recommended parameter range values were only valid for a structured glass surface. This work suggested that some of the height, hybrid, and volume parameters (Sq, Sdq, Sdr, Sxp, Vv, Vmc, and Vvc) can be used to describe the glass surface texture in order to relate to electroless copper adhesion.

4.3 Research Methodology and Experimental procedures

Surface roughness measurements have been conventionally carried out using 2-D surface texture parameters and, in the field of signal processing, the skin depth value of a conductor line is usually compared with 2-D surface roughness values [104]–[106]. For this reason, the surface roughness of LTCC test samples were initially analysed using Ra values. However, from the initial results presented below, it was found that the Ra value did not represent the surface morphology of the test surface effectively. In this case, a set of areal parameters were used to analyse the LTCC samples in order to achieve a better representation of the LTCC surface in order to correlate with the morphology observed with the SEM images. Based on the literature discussed above, it is clear that little or no compelling evidence is available to link any specific surface parameters to the function of the surface. Therefore, only V-parameters which have been specially developed to describe the material volume (Vmp, Vmc) and the void volume (Vv, Vvv, Vvc) of the surface were selected to study the surface texture of the LTCC surface treated with NaOH.

4.3.1 Experimental

The roughness measurements in this study were carried out using a Zygo NewView 5000 coherence scanning interferometer. This system has capability to measure and image 3-D microstructure and topography of surfaces using white light interferometry. This technique

uses the superposition property of light waves, i.e. two or more waves which are the same frequency and phase will add constructively and the waves that are out of phase by 180^0 will cancel each other. In a white light interferometer, the light from the microscope is split into two parts using a beam splitter. One part of this light hits an internal reference plane and the other part strikes the surface to be tested. Then the reflected light from both surfaces are collected on an observation screen and this results in an interference pattern. This gives dark and light areas usually called fringes. The same test samples prepared in section 3.3.2 and 3.3.3 A. were analysed for their surface texture using a Zygo NewView 5000 Coherence Scanning Interferometer. The surface roughness measurements were processed and analysed using the TalyMap Platinum v5.1 surface texture processing software. Filtering is important in surface texture data processing to remove unwanted noise, spikes or functionally irrelevant small or large scale lateral components [97]. Microroughness which is usually due to instrument or environmental noise was filtered using a 2.5 μm cut-off wavelength. A 2.5 mm cut-off wavelength Gaussian filter was applied to remove any form or waviness of the sample surface. The same filtering was applied in each and every data processing to maintain the consistency of the analysis. The initial test samples were analysed only using Ra parameters and the later samples were analysed using Ra and areal parameters for comparison.

4.4 Results and Discussion

4.4.1 Effect of NaOH Concentration on LTCC Surface Roughness

The first batch of LTCC samples were immersed in 3M, 4M, and 5M NaOH solution and were kept at room temperature for 24 hours, while other LTCC samples were immersed in 6M and 7M NaOH at room temperature for 7.5 hours as described earlier. The Ra was measured in three locations on the sample surface as shown schematically in Figure 39 using a Zygo NewView 5000; the data points in the graph (Figure 40) show the average of the three values obtained, while the error bars indicate the maximum and minimum of the three Ra values.

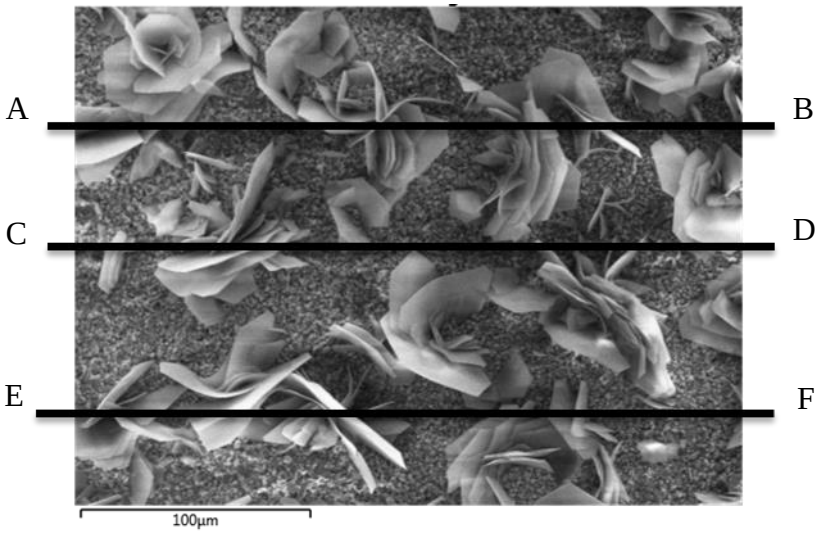

Figure 39 2-D Surface profiles taken in 3 different locations

Figure 40 illustrates the increase of surface roughness values (Ra) with the NaOH concentration. In some cases there were very large differences between the maximum and minimum Ra from the same surface which is thought to be due to the random selection of the measured line (A-B, C-D or E-F in Figure 39) that may or may not have included the flake like structures. In this situation areal surface profile measurements may be more appropriate [107] to include all features and this was studied in later experiments. Considering the average Ra values, the surface roughness of the samples increased with the NaOH concentration as well as the immersion time. High surface roughness values (Ra) were observed for samples etched for longer times in less concentrated solutions. One unanticipated finding was that the samples etched with 4M NaOH had similar Ra values to the samples etched with 5M NaOH, although rougher (flakier) surfaces were observed in the SEM micrographs (Figure 17 c and d) in Chapter 3. This rather contradictory result may be due to the poor representation of the 2-D profile data when calculating Ra values as described above.

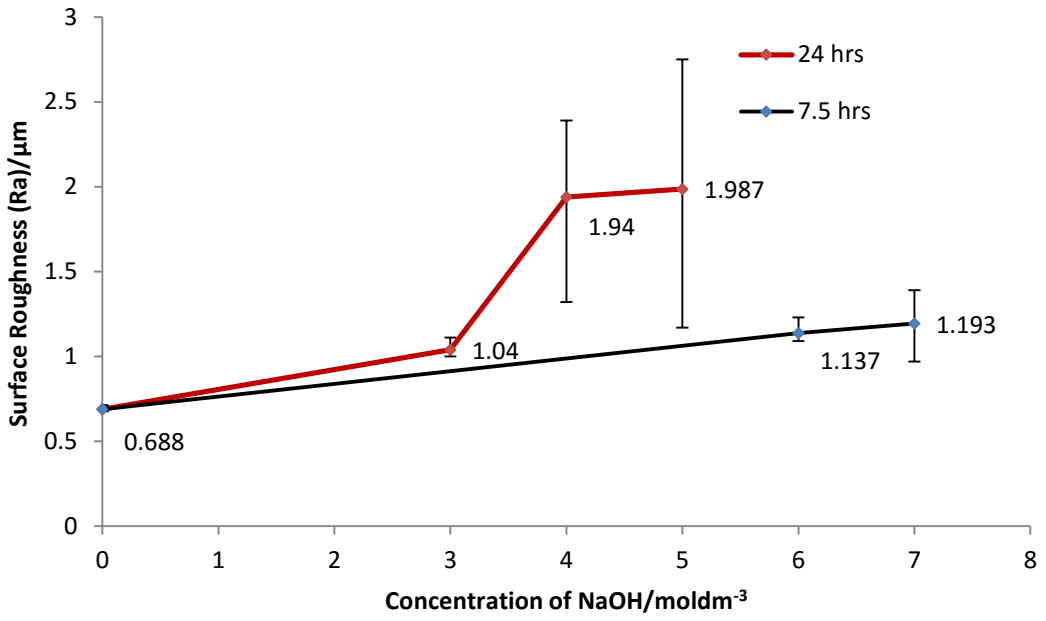

Figure 40 Variation of surface roughness as a function of NaOH concentration and immersion time

4.4.2 Effect of Immersion Time

The correlation between surface roughness parameters and the sample immersion time in the NaOH solution was also investigated. A particular concentration of NaOH (4M) was selected and LTCC samples were immersed in this solution for different time intervals. Again, scanning white light interferometry (Zygo NewView 5000 instrument) was used to image and measure the micro structure and topography of surfaces. Both Ra values and areal V- parameters were analysed for comparison reasons. The measurements were taken on three different areas (each approx. 500 µm x 600 µm) of the sample and an average value was calculated. The correlation between surface morphology and roughness parameters were also investigated. For comparison reasons, the analysis was carried out using the same samples used to obtain the SEM micrographs in section 3.5.1.B.

In general, all the parameters measured for the samples (Figure 41) have a fluctuation of surface roughness with immersion time. The average Ra values again show large differences between maximum and minimum values (Figure 42 (a)). After 5 minutes of immersion time, there is a small decrease in all the parameters. It was also noted that all the parameters have their peak values in the range of 75 minutes to 105 minutes and at 225 minutes. The variation of Vv, Vmc and Vvc show a very similar pattern of fluctuation. Vvv

suddenly drops at 15 minutes showing different variation to the other parameters. The error bars of each graph represent the maximum and minimum values of each parameter used. The error bars of the graph which represents the change in average Vmp against immersion time has relatively large values at two points. The rest of the graphs have relatively smaller error bars representing the lower variability of these surface parameters.

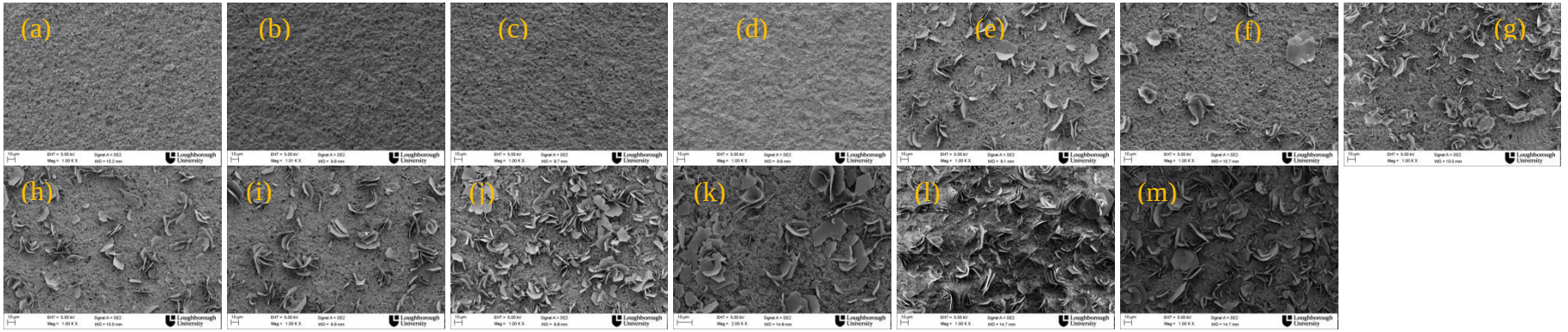

Figure 41 SEM micrographs of the LTCC samples immersed in NaOH solution for (a) 0 mins, (b) 5 mins, (c) 15 mins, (d) 30 mins, (e) 50 mins, (f) 75 mins, (g) 105 mins, (h) 140 mins, (i) 180 mins, (j) 225 mins, (k) 255 mins, (l) 270 mins and(m) 24 hours (these are the same as Figure 19 and are repeated here for convenience)

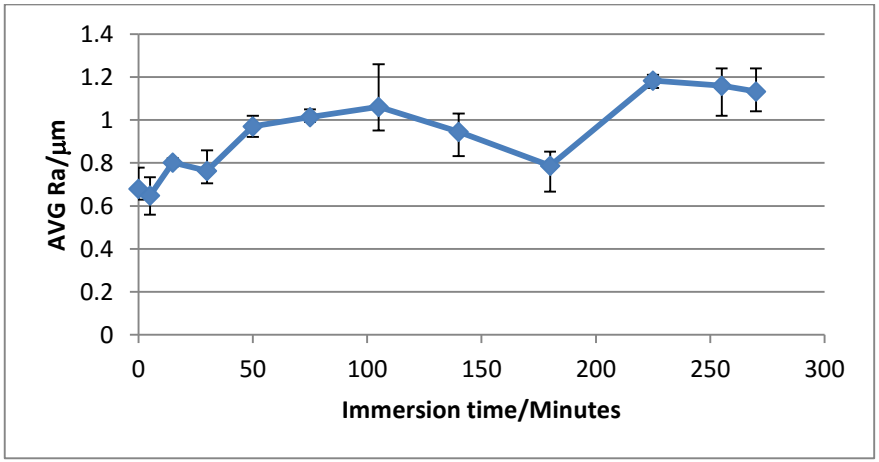

(a)

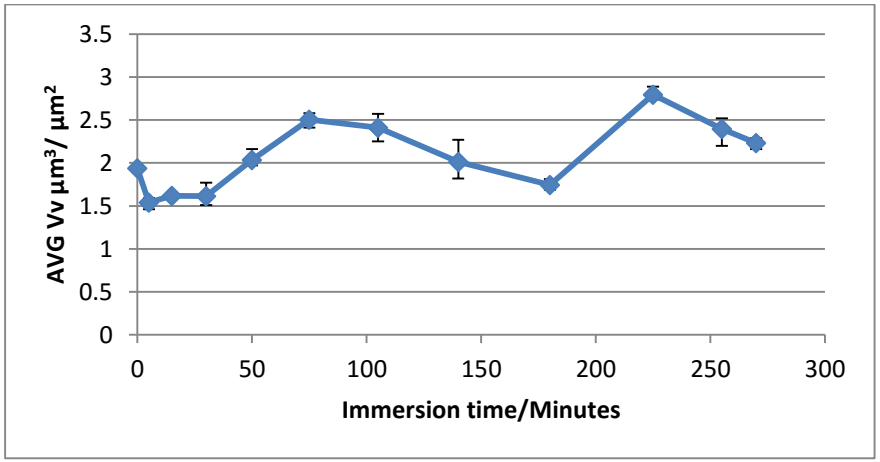

(b)

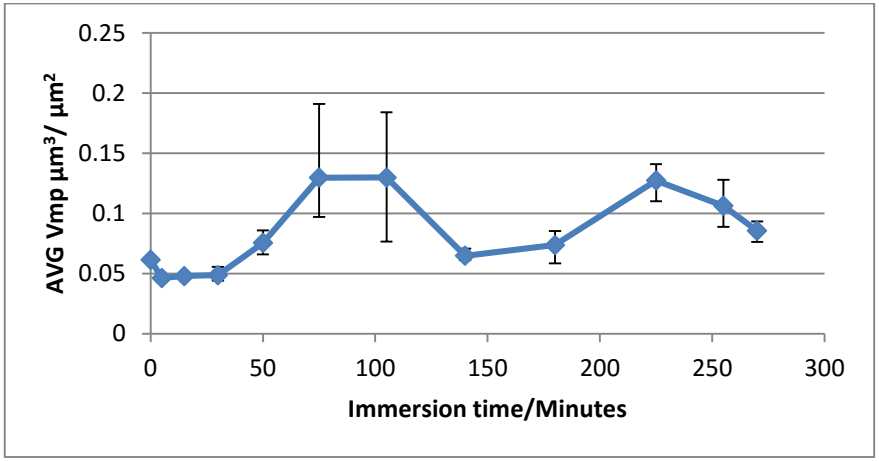

(c)

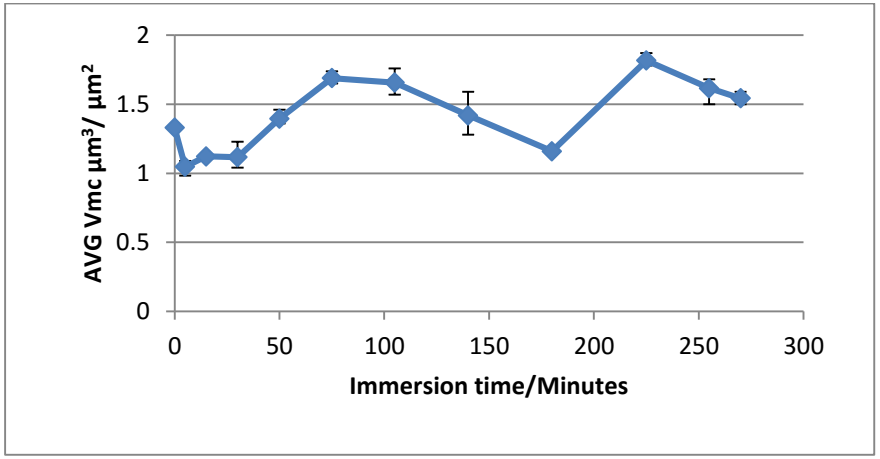

(d)

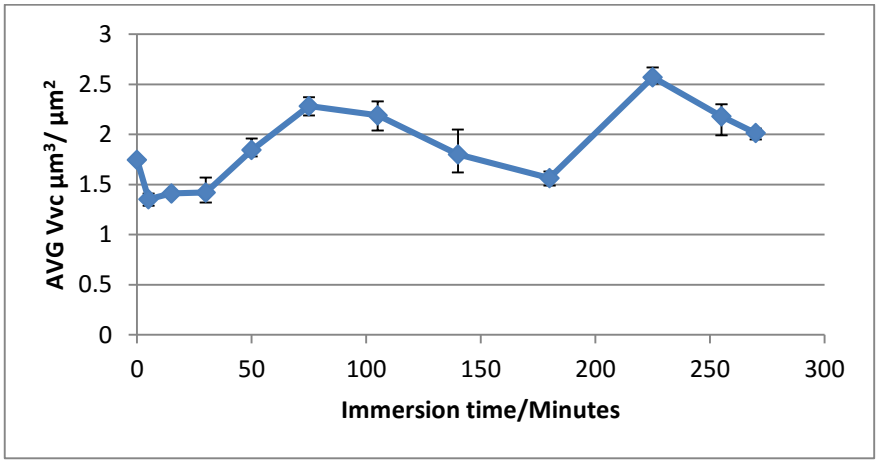

(e)

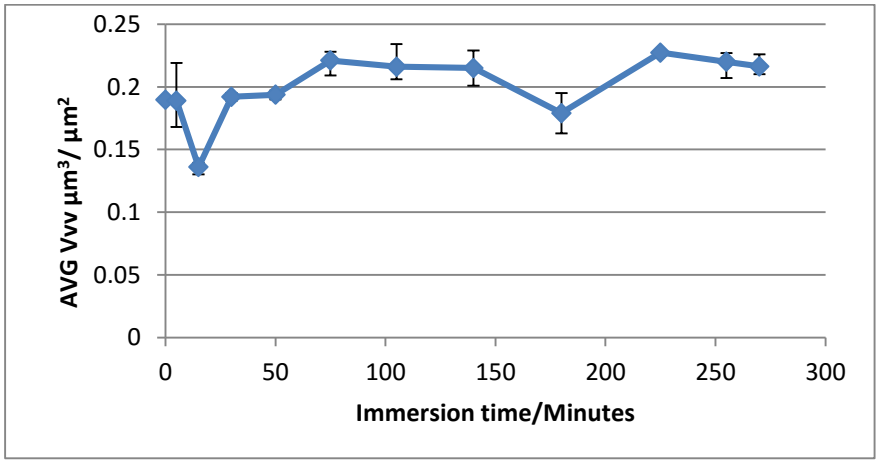

(f)

Figure 42 Variation of average (a) Ra (b) Vv (c) Vmp (d) Vmc (e) Vvc (f) Vvv as a function of immersion time

When compared with the SEM images of the surface, the average Vv values showed contradictory results at some points. The higher average Vv at 50 minutes of immersion time compared to that at 30 minutes is presumably due to the formation of flake like structures on the surface (Figure 41 (d) and (e)). The decrease in the coverage of these flake like structures and taller features could be responsible for the increase in average Vv value at 75 minutes of immersion time (Figure 41 (f)). The average Vv value at 105 minutes showed a lower value compared to the point where the immersion time was 75 minutes and this could be ascribed to the increase in coverage of the flake like features in the SEM image (Figure 41 (g)). The next two SEM images (Figures 41 (h) and (i)) of the samples immersed in NaOH solution for 140 minutes and 180 minutes respectively showed relatively low surface coverage of flake like structures and therefore higher average Vv values were expected. However, these two samples showed relatively low average Vv values compared to the average Vv value of the sample immersed in NaOH solution for 105 minutes. One possible reason for this could be that these particular surfaces have a lower reference plane due to shorter flake like structures. The sample immersed in NaOH solution for 225 minutes has the highest average Vv value. This surface consisted of a high coverage of flake like structures and therefore lower average Vv values were expected. This contradictory result might be due to the taller surface features.

The average Vmp values are relatively higher for the samples immersed in NaOH solution for 75, 105 and 225 minutes and relatively lower for the samples immersed in NaOH solution for 140 and 180 minutes.

The higher average Vmc values at 105 and 225 minutes of immersion time could be explained by the SEM images (Figures 41 (g) and (j)). The flakes formed on these surfaces with broader material cores might be responsible for these higher values. The relatively high average Vmc value at 75 minutes of immersion time did not correlate with the SEM image (Figures 41 (f)). The SEM image showed relatively large features on the surface compared to the background surface and observed low coverage of these features. When considering the scale limited surface the peaks responsible for these features could be cancelled and the Vmc values may be calculated considering the background surface only.

Relatively higher average Vvc values were obtained at 75, 105 and 225 minutes of immersion time. The high Vvc values at 105 and 225 minutes of immersion time might be due to the broader material cores (Figures 41 (g) (j)). The low surface coverage of the flake like features (Figure 41 (f)) could be responsible for the high Vvc value at 75 minutes of immersion time.

The Vvv did not show remarkable fluctuation with sample immersion time in the NaOH solution apart from the points at 15 and 180 minutes of immersion time. The one possible reason for this could be the minimal change in surface morphology of the background surface. The lower average Vvv values at these two points might be due to the relatively smoother background surface of the samples.

4.5 Discussion

In this study, the surface texture volume parameters were correlated with the surface morphology of the samples treated with 4M NaOH solution. However, at some points a correlation between surface morphology and the surface texture was not observed. Figure 43 (a) and Figure 44 (a) show the SEM micrographs of the sample treated with 4M NaOH for 75 and 225 minutes respectively and Figure 43 (b) and Figure 44 (b) show the 3-D profiles of the corresponding samples.

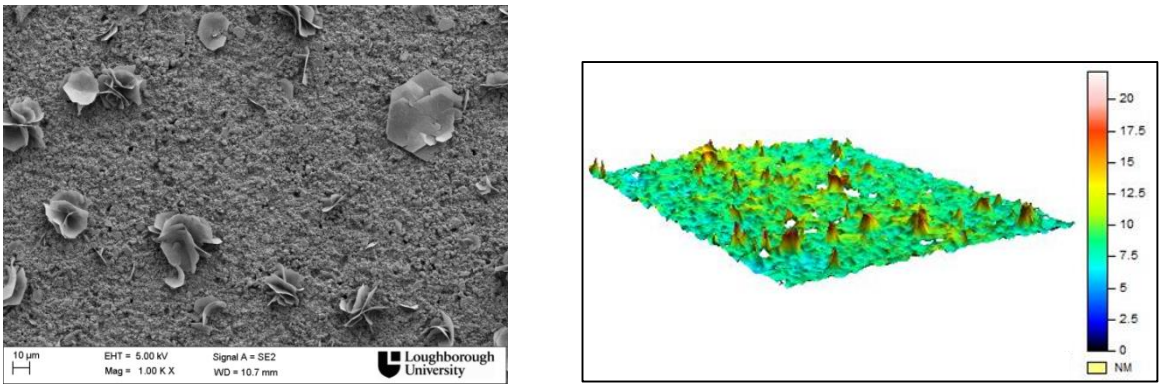

(a) (b)

Figure 43 Surface morphology of LTCC sample treated with 4M NaOH for 75 minutes (a) SEM micrograph and (b) 3-D profile

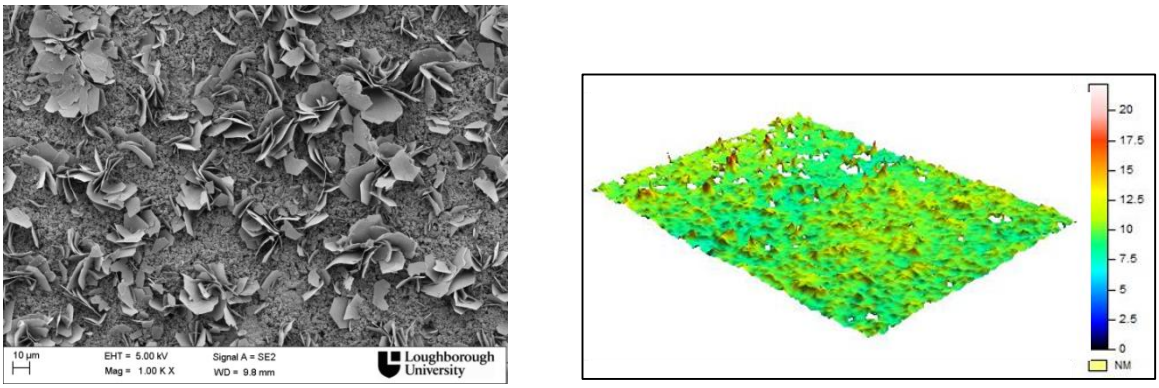

(a) (b)

Figure 44 Surface morphology of LTCC sample treated with 4M NaOH for 225 minutes (a) SEM micrograph and (b) 3-D profile

When compared with the 3D profiles of the two samples, the sample immersed in NaOH solution for 75 minutes showed relatively higher peaks (Figure 43 (b)). However, when comparing the SEM images of the two samples (Figure 43 (a) and 44 (a)) the height of the flake like structures did not show much difference. This rather contradictory result might be due to some of the errors of the Coherence Scanning Interferometry (CSI) instrument. Some missing data points were observed in both 3-D profiles and could be correlated with large surface gradients on the surface. It was obvious from the SEM images (Figure 43 (a) and 44 (a)) that these surfaces did not convey a well defined or well structured surface. As a result of the chemical etching process, these surfaces showed random features on the surface. These re-entrant features (Figure 45) might not be measured accurately and lead to poor representation of the surface. Another possible reason for unexpected results could be that the LTCC material itself is composed of different phases and this might lead to a different phase change on reflection.

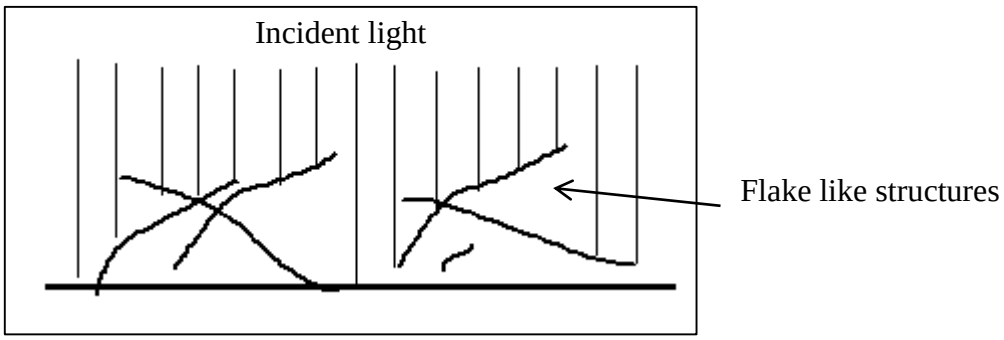

Figure 45 Re-entrant features effect

4.6 Conclusions

The work presented in this chapter has focused on the investigation of the change in LTCC surface roughness with NaOH pre-treatment in terms of immersion time and NaOH concentration. Both Ra and surface texture volume parameters (Vv, Vvv, Vvc, Vmc, Vmp) were used to analyse surface roughness of NaOH treated LTCC. It has been found that Ra values show poor representation of the LTCC surface roughness when compared with the surface morphology analysed by SEM. The variation of volume parameters with the immersion time in 4M NaOH characterised the surface morphology of the LTCC surface to some extent, but the explanation was difficult at some points. However, except for Vmp, volume parameters gave relatively smaller error bars compared to Ra values showing lower variability and suggesting more representation of the LTCC surface.

Chapter 5 Characterization of Deposited Copper on LTCC Substrate

5.1 Introduction

Metal films are essential components in the electronics industry and the reliability of these films is crucial in the service life of electronic devices. Of particular importance, interfacial adhesion plays a vital role in the reliability of metal films on substrates. However, the level of adhesion required depends greatly on the practical application. For example, metal films in electronic devices that are operating in harsh environments such as automobile and aerospace require better adhesion strength than that of devices in consumer electronics. On the other hand, surface roughness and thickness of the conductor affects the performance of the electronic devices, especially when operating at high frequencies. Conductor surfaces ideally require low surface roughness for better signal propagation at high frequencies. This chapter therefore reports an investigation of the surface roughness and interfacial adhesion between deposited copper and NaOH treated LTCC substrates. The chapter begins by reviewing the methods of determining the film adhesion and the effect of surface roughness on high frequency performance.

5.2 Literature Survey

5.2.1 Test Methods for Metal Film Adhesion

The common test procedures for measuring metal film adhesion strength include scratch, pull, peel, scotch tape, blister and indentation tests, however, the type of test that can be

used varies depending on the strength of the adhesive bond and the level of detail of the results to be obtained. For example, scotch tape tests can be used where the tests require only qualitative results and scratch and indentation tests can be used where a quantitative result is needed [108]. The tests that can be applied to measure the adhesion strength of electroless copper deposits on substrates have been widely reviewed elsewhere [63],[16]. Tape peel test and scratch test were selected to measure the interfacial adhesion strength between electroless copper and LTCC substrate based on ease of use and sample preparation. Furthermore by using both tests, this provided an opportunity to evaluate the test results quantitatively and qualitatively.

A. Tape Peel Test

The tape peel test was first reported by John Strong in 1931 and the adhesion strength of aluminium films on glass was tested using scotch tape [109]. As described in section 2.4.5, in the tape peel test, the adhesive tape is pressed on to the test surface and peeled off rapidly. This is a qualitative method of determining adhesion strength and the experiment normally gives a "pass" or "no pass" result. Three possibilities that could happen in this test are complete removal of the film from the substrate, partial removal of the film from the substrate or the film is not removed from the surface [110]. Marlene and co-workers [111] used the Scotch tape test in order to investigate the interfacial adhesion between electroless nickel and plasma processed glass substrates. The glass substrates were first treated with plasma-polymerization and grafting processes using allylamine or acetonitrile prior to the electroless deposition process. A test value (TV) = 5 was assigned for the samples which did not show any metal removal in the tape test. The optimum thickness for the Ni films (3.9 μm for allylamine treated samples and 0.6 μm for acetonitrile treated samples) were reported based on TV=5 as these films adhered to the glass surface without any metal removal in the scotch tape test. The same research group evaluated adhesion of palladium free electroless copper on different polymer substrates using a Scotch tape test [112]. In this study, copper (II) organic precursor film was deposited on polymer substrates by spraying and spin coating of copper acetate in ethanol solution. The deposited copper (II) was reduced either using a $NaBH_4$ solution; by heating at 270 ^{0}C under nitrogen flow; by plasma in an Ar atmosphere; or by UV irradiation under vacuum. The scotch tape test

results were used to classify the influence of different treatments such as chemical, thermal, photonic and plasma techniques based on adhesion levels of films obtained under various conditions. For 15 minutes plating time all methods gave TV=5 for all substrates however, when the plating time was increased to 30 minutes only a few substrates gave TV=5 result. On many other occasions the Scotch tape test has been carried out in order to evaluate the qualitative interfacial adhesion between metal films and substrates [112]–[115].

B. Scratch Test

The scratch test is a common quantitative test method for adhesion measurement of metal film coatings. A diamond stylus is drawn across the coated surface under an increasing load until some well-defined failure occurs at a load which is called the critical load (Figure 46) [116].

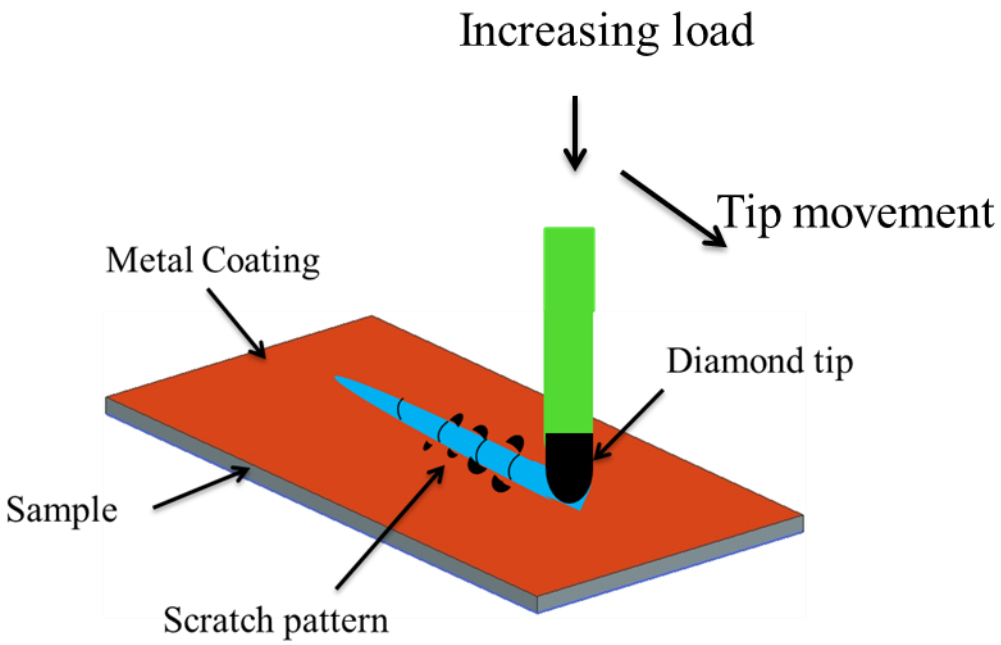

Figure 46 Schematic diagram of the scratch test

A scratch test was first reported in 1950 by O.S. Heavens [117]. He studied the influence of chromium on the adhesion strength of vacuum evaporated silver and aluminium on glass. He used a 0.03 mm radius stylus tip to drag across the surface. The load on the stylus was gradually increased until the film was removed completely. This method was used to find the optimum thickness of chromium which produced an improvement in adhesion. In 1959,

this method was reviewed by Benjamin and co-workers [118] and suggested that the critical load which was applied to remove the film from the substrate was not the only factor that measured the adhesion of the film. They also suggested other factors such as the hardness of the film and the substrate, and film thickness. This research group studied the other factors that may influence the results of the scratch test suggested by Heavens. They suggested that a shearing force can occur on the substrate film interface due to the plastic deformation caused by indentation. They derived an equation to calculate the shear force that depends on the critical load, the radius of the tip, the radius of the circle of contact and the indentation hardness of the substrate material. They also suggested that the adhesion of metal films can be measured as the shear force. They used the same scratch test apparatus used by Heavens to measure the adhesion of silver films on various substrates and adhesion and hardness of various metals on glass. According to their experimental results, they concluded that measurements of adhesion may be made by using the vertical load when comparing different metal films on the same substrate. However, shear force should be taken into account when comparing the adhesion of metal films on different substrates.

The identification of the exact coating failure point can be difficult in scratch testing. The failure point can be identified using microscope observation, acoustic emission and measuring penetration depth [119]. Many failure modes were identified and reported in the literature [120]–[122]. However, to identify the substrate coating adhesion, only the adhesion related failure modes should be considered. S.J. Bull identified buckling, wedge spallation and recovery spallation as the adhesion related failure modes [116]. The recent scratch testing methods usually correlate the scratch patterns with acoustic emission and friction forces to derive the critical load. Figure 47 shows the various damage patterns which may occur during the scratch test that can be responsible for acoustic emission and friction forces [123].

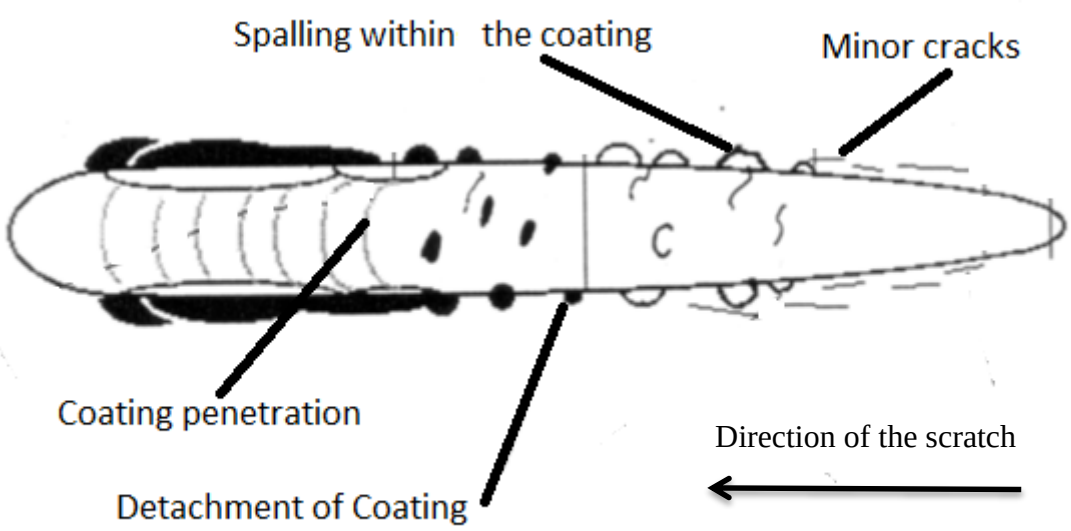

Figure 47 Damage patterns that may be observed in a scratch test [123]

5.2.2 Effect of Surface Roughness on High Frequency Applications

Roughness and the thickness of the metal surface are two parameters that affect the performance of the microwave frequency components. The term "skin depth" (δ) is a measure of how deep the conduction takes place from the surface of a conductor [124] and can be calculated using the following equation.

$$\boldsymbol{\delta} = \sqrt{\frac{\rho}{\pi f \boldsymbol{\mu}_0 \boldsymbol{\mu}_R}} \quad \ldots\ldots\ldots\ldots \text{5.1}$$

ρ - Resistivity of the metal

f - Frequency

$\boldsymbol{\mu}_0$ – Permeability of free space

$\boldsymbol{\mu}_R$ – Relative permeability

Skin depth is a function of applied frequency and varies with the type of metal. As frequency increases, the skin depth value decreases and as a rule of thumb, the thickness of the metal layer should be 5-7 times that of the skin depth of the particular metal for good

signal propagation. At micro and millimetre wavelengths, the signal only propagates on the skin of the conductor and does not penetrate deeper in to the metal. This is due to inductance created by the conductor at high frequencies [125]. The required thickness of the layer in a particular metal can be clearly defined in terms of applied frequency. For example the skin depth for copper at 10 GHz is 0.65 µm.

Surface roughness of the conductor has a considerable impact on signal propagation. At high frequencies when skin depth becomes a few microns, surface roughness values should be less than that of the skin depth values. Figure 48 shows a cylindrical conductor with radius (r), skin depth (δ) and surface roughness (R). For good signal propagation R should be less than δ.

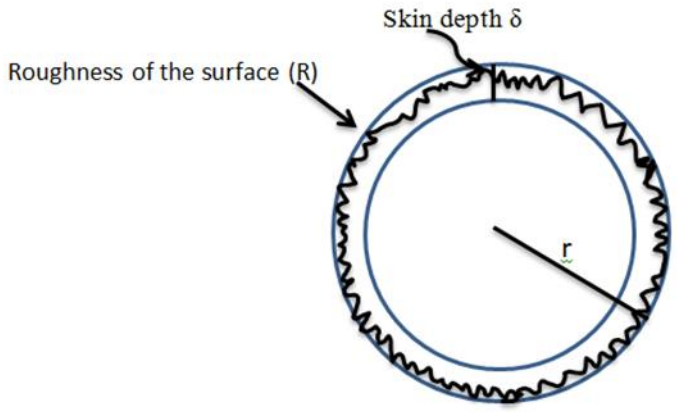

Figure 48 Cylindrical conductor showing relationship of skin depth, radius and roughness

The relationship between conductor roughness and signal loss in high frequency applications have been studied in the literature. A study was carried out to find the effect of copper surface roughness on measured signal loss and dissipation factor values of PCB laminate [106]. The total loss (conductor loss and dielectric loss) was measured on test samples with different surface roughness values using a vector network analyser at 3 different frequencies i.e. 3 GHz, 5 GHz and 10 GHz. At 10 GHz, 50 % difference in total loss was observed between the material which had lowest roughness (electrodeposited foil Ra = 1.5-2 µm) and the material which had highest roughness (standard foil Ra = 7-8 µm). The measured total loss showed increased values for rougher surfaces. The increase in total loss was also higher at 10 GHz.

5.3 Methodology and Experimental Procedure

The NaOH pre-treatment described in Chapter 3 clearly affected the surface morphology as well as the surface roughness of the fired LTCC. Adhesion tests including tape peel test as described in section 2.4.5 and scratch tests were carried out to investigate the effect of NaOH pre-treatment on the interfacial adhesion strength between electroless copper and LTCC substrates. Furthermore, the failure mode was investigated by analysing the surfaces of the LTCC samples and the tape which was used in the tape test using XPS.

The surface roughness of the deposited copper was measured using a Zygo NewView 5000 Coherence Scanning Interferometer. In this case only the Ra parameter was considered in the characterisation of the electroless copper deposits in terms of surface roughness, as the performance of signal propagation can be compared with the Ra parameter as described in section 5.2.2.

5.3.1 Experimental

A. Sample Preparation for Tape Peel Test and Scratch Test

The fired LTCC samples were cleaned and pre-treated with different concentrations of NaOH prior to the electroless copper deposition. Sample cleaning was carried out according to the procedure described in section 2.4.2 A. One batch of samples were then immersed in 3M, 4M and 5M NaOH solution for 24 hours and the other batch of samples were immersed in 6M and 7M NaOH solution for 7.5 hours. Electroless copper was then deposited on these samples for one hour at 30 ^{0}C leading to a thickness of approx. 3 μm. The procedures described in section 2.4.2 and 2.4.3 were followed for the electroless bath preparation.

B. Tape Peel Test

Interfacial adhesion of the electroless copper and NaOH treated LTCC substrate was measured qualitatively using a tape peel test as described in section 2.4.5.

D. Scratch Test

Adhesion strength of the Cu coatings was quantitatively measured using a scratch test system ST 3001 based at the National Physical Laboratory. A diamond indenter tip with an approximate tip radius of 200 µm and cone angle 120^0 was used to create scratches on the substrate surface. Figure 46 shows the schematic representation of the scratch test. The start load was set and increased stepwise to a maximum load until coating failure occurred. The initial load was varied in each sample as in some cases substrate cracking occurred during the test. Scratch testing parameters were set including scratch speed - 5 mm/minute, and the loading rate was varied between 10 N/min and 2 N/min. The scratches were then analysed using optical micrographs. Frictional force and acoustic emission were also taken into account when analysing results.

5.4 Results and Discussion

5.4.1 Tape Test

The tape test was carried out to determine the adhesion strength between the samples treated with different concentrations of NaOH solution and the copper deposits. Figure 49 illustrates the correlation between adhesion and concentration of NaOH solution. The results showed that copper was not completely removed from the samples showing some adhesion improvement compared to the untreated substrate (Figure 15). Only a small amount of copper was removed from the sample treated with 4M NaOH for 24 hours. The sample treated with 7M NaOH also showed relatively good adhesion compared to the untreated sample presented in section 2.5.5 (Figure 15). It was also noticed that the locations where the copper was removed from the samples treated with 3M NaOH appeared a dark colour. This was different from the colour of the bare LTCC surface and may be due to some traces of the electroless copper left behind after the peel test. The colour of these areas on the sample treated with 5M and 6 M NaOH was relatively lighter. This suggests that a thinner layer of copper was left behind on the samples treated with 5M and 6M NaOH. Only traces of copper were observed on the tape which was used to test the LTCC

sample treated with 4 M NaOH. Relatively small patches were removed from the surface of the sample treated with 7 M NaOH.

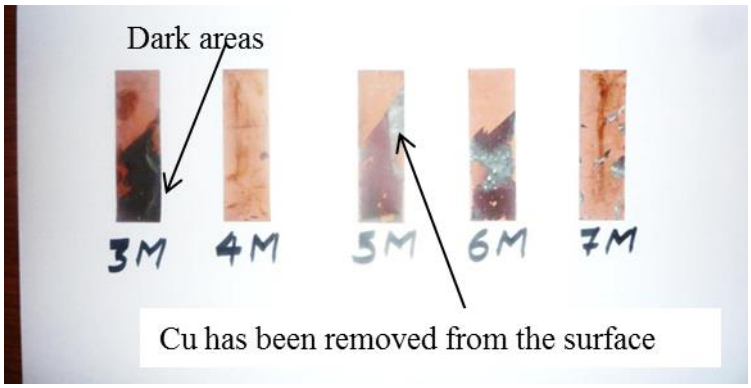

Figure 49 The image of Cu deposited on LTCC samples taken after the tape peel test

The dark areas which can be seen on the LTCC surface after the tape peel test are thought to be the copper nano particles deposited at the very first stage of the electroless copper plating process. The stepwise deposition process was studied and is presented later in the chapter. The dark colour of the copper deposits may be due to the absorption of visible light by the oscillation of valence conduction electrons present in the copper nano particles, a process called surface plasmon resonance [126].

To study the above observation further, an LTCC sample after the peel test was analysed using XPS. The tape test was carried out on a new LTCC sample which was treated with 5M NaOH. Three areas including a dark area, relatively lighter area and the area where copper still remained (referred to as shiny) on the LTCC surface were analysed (Figure 50).

Figure 50 XPS analysis on three different areas

A summary of the elements present in the survey scans of all three areas, their binding energies and atomic percentage is presented in Table 9. The survey scan of the shiny area showed copper, oxygen, chlorine, and carbon while the dark area and the light area showed copper, oxygen, chlorine, carbon, tin, lanthanum, nitrogen, sodium and phosphorous. The presence of lanthanum, phosphorous, aluminium, a portion of oxygen and carbon shown in Table 9 is attributed to the chemical content present in the LTCC surface. Ca (0.48 At %) was also present in the light area analysed. A very small percentage of nitrogen and sodium was also present and this could be due to contamination.

Copper was present in all three areas with the atomic percentage of shiny, dark and light areas as 5.42 %, 4.88 % and 4.68% respectively. The high resolution spectrum of the copper was obtained in the binding energy range of 925 eV-965 eV for all 3 areas (Figure 51). The binding energy of the peaks fitted to the high resolution spectra at 932 eV, 934 eV and 943 eV revealed the presence of Cu(0), Cu(I) and Cu(II). The strong peak located at 932 eV was identified as due to Cu(0) and Cu(I) (these two species have very similar binding energy) and the minor peak located at 934 eV is thought to be due to Cu(II). The satellite peak located at 943 eV also confirmed the presence of Cu(II). The oxygen peak at 545 eV also suggests that the copper is in the form of CuO or Cu_2O. The XPS analysis of the dark and the light area showed a tin 3d doublet peak at 486 eV and 495 eV which may correspond to SnO_2. The presence of Sn on the surface is possibly due to the catalyst treatment. The atomic percentage of tin was less than 0.1 % in both areas.

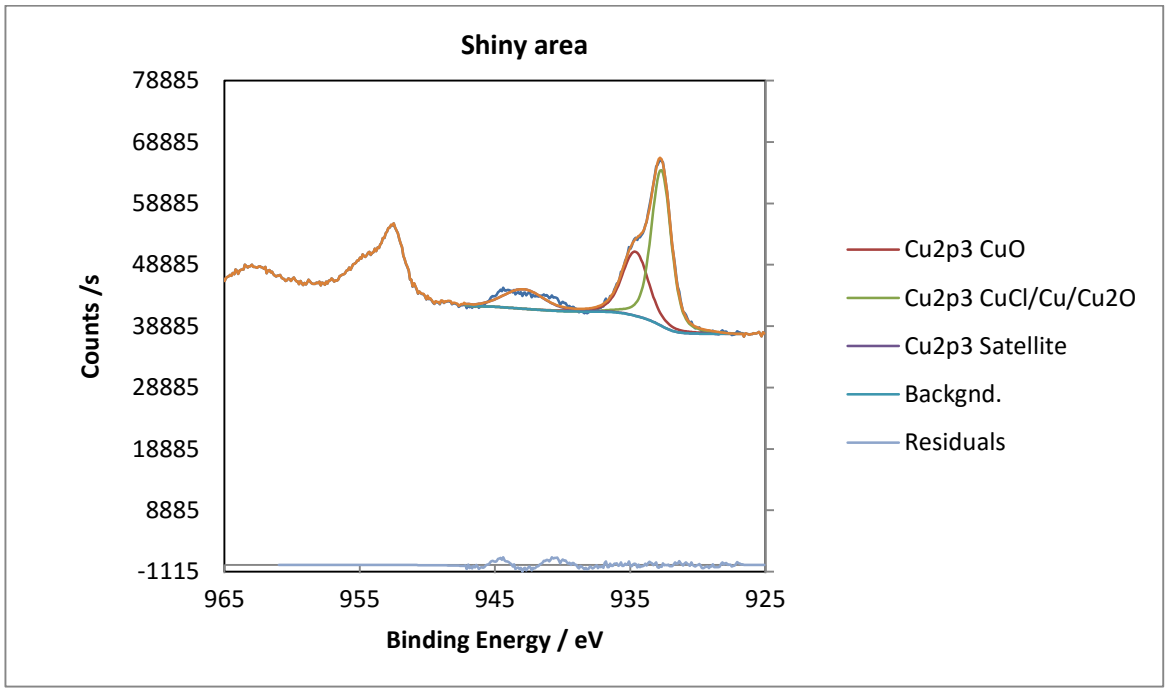
Shiny area
78885
68885
58885
48885
38885
28885
18885
8885
-1115
Counts /s
965
955
945
935
925
Binding Energy / eV
Cu2p3 CuO
Cu2p3 CuCl/Cu/Cu2O
Cu2p3 Satellite
Backgnd.
Residuals

(a)

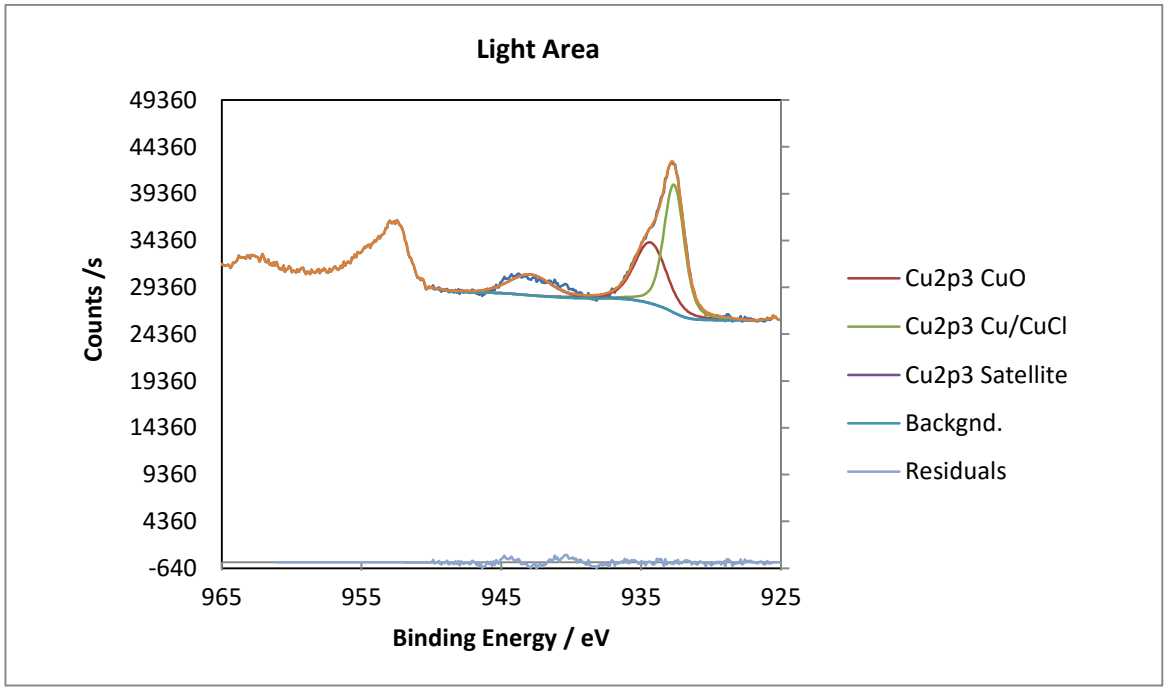
Light Area
49360
44360
39360
34360
29360
24360
19360
14360
9360
4360
-640
Counts /s
965
955
945
935
925
Binding Energy / eV
Cu2p3 CuO
Cu2p3 Cu/CuCl
Cu2p3 Satellite
Backgnd.
Residuals

(b)

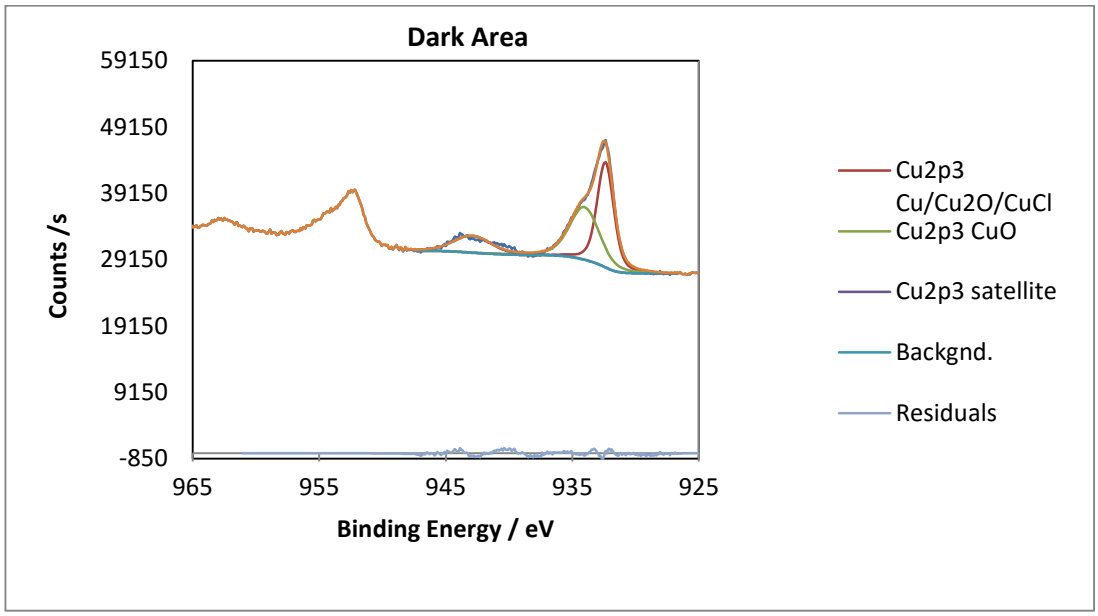

(c)

Figure 51 Copper XPS peaks of the three different areas (a) shiny area, (b) light area and (c) dark area

Table 10 Surface compositions and binding energies of three different areas of the LTCC surface after peel test

Elements	**Shiny**		**Dark**		**Light**	
	Binding Energy/eV	Atomic %	Binding Energy/eV	Atomic %	Binding Energy/eV	Atomic %
Cu2p3	934.6	5.4	933.9	4.9	934.4	4.7
Sn	-	-	486.5	0.1	486.9	0.1
O1s	532	19.6	531.2	40.6	531.3	41.3
Al2s	-	-	118.9	13.5	119.8	11.4
Cl2p	198.7	0.7	-	-	-	-
C1s	285.2	63.8	285.2	31.7	285.5	32.2
La3d5	-	-	836.1	2.4	836.1	2.5
P2p	-	-	133.1	3.5	134.1	3.9
N		8.7	400.2	2.1	400.4	2.1
Na		1.9	1071.2	1.2	1071.9	1.5
Ca2p	-	-	-	-	347.4	0.4

5.4.2 Copper Failure Analysis on Untreated LTCC

XPS analysis was also carried out on the untreated LTCC surface after the Sn/Pd catalyst activation and the LTCC substrate after the delamination. The surface of the tape which held the delaminated copper film after the tape test was also analysed using XPS.

Figure 52 (A) shows the survey scan of the LTCC sample first cleaned with Decon solution for 24 hours and then treated with catalyst for 2 minutes. The main elements present in the sample were La, O, Sn, Ca, C, B and Al. Among those, La, O, Ca, B and Al were attributed to the elements present in the LTCC sample. For the sample treated with Sn/Pd catalyst solution, it was expected that a Pd 3d peak 335-336.7 eV would be seen. However, Pd did not appear in the survey spectrum (Figure 52 (A)). Even with the high resolution spectrum the Pd signal could not be clearly seen (Figure 52 (B)). One possible reason for this could be the low adsorption of palladium on the LTCC surface within 2 minutes of immersion time. However, a Sn 3d peak (487.09 eV) was clearly seen in the survey spectrum (Figure 52 (A)): the atomic percentage of Sn was 1.69 %. Another LTCC sample was immersed in catalyst solution for 10 minutes after the cleaning step as described earlier and the XPS analysis was carried out for comparison. The Sn peak was present in the survey scan as expected: the atomic percentage increased to 2.21 %. It was not possible to detect a Pd peak in the survey scan again, however the Pd doublet in the region of 334-344 eV was present in the high resolution spectrum. It can be concluded that Sn and Pd adsorption had increased with the catalyst immersion time. A sodium signal at 1071.86 eV was also present in the survey spectrum and this could be due to material left behind from the cleaning process.

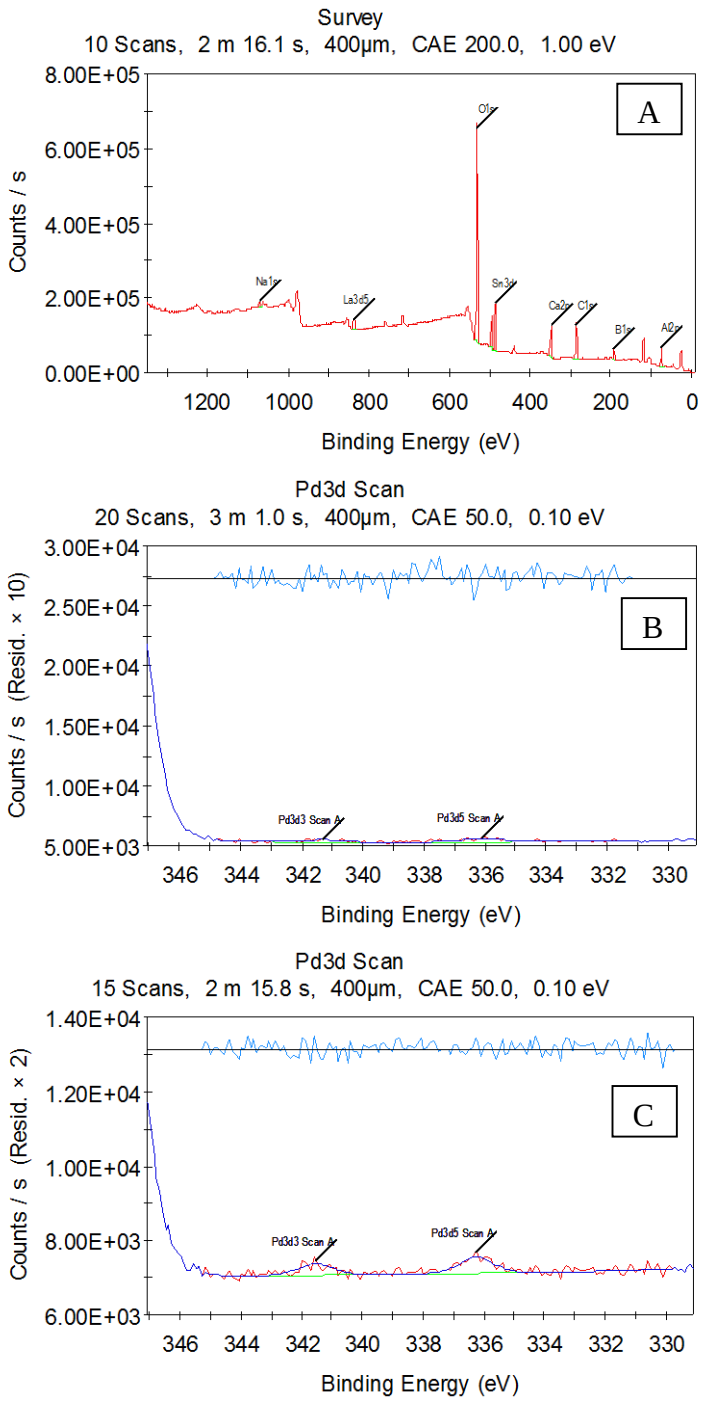

Figure 52 (A) XPS survey scan (B) high resolution Pd scan for LTCC sample immersed in Sn/Pd catalyst solution for 2 minutes (C) high resolution Pd scan for LTCC sample immersed in Sn/Pd catalyst solution for 10 minutes

The XPS survey spectrum of the LTCC sample after the tape test is shown in Figure 53 (A). Compared to the chemical elements present in the LTCC surface activated with Sn/Pd

catalyst, the spectrum showed the disappearance of the Sn 3d peak. As expected, a Pd peak was not present even in the high resolution spectrum (Figure 53 (C). This is probably due to the removal of the Sn in the electroless bath. As expected, a tiny amount of Cu was present on the surface, however the atomic percentage of Cu was only 0.67%.

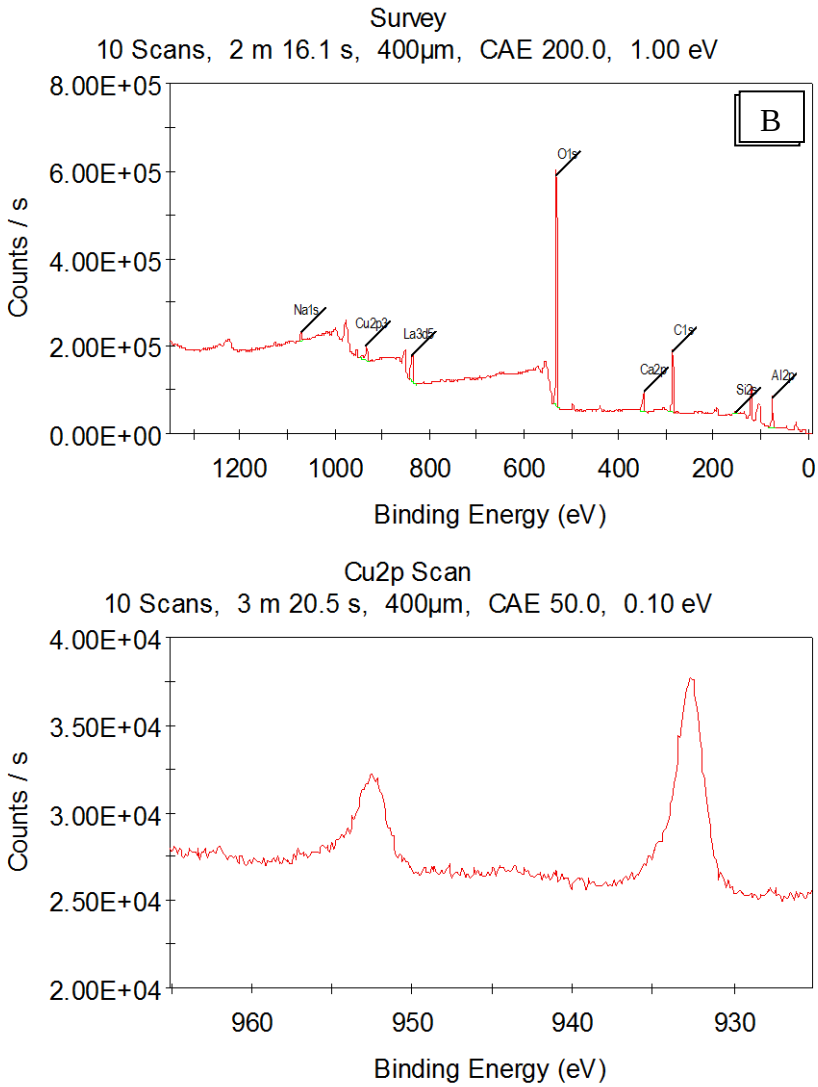

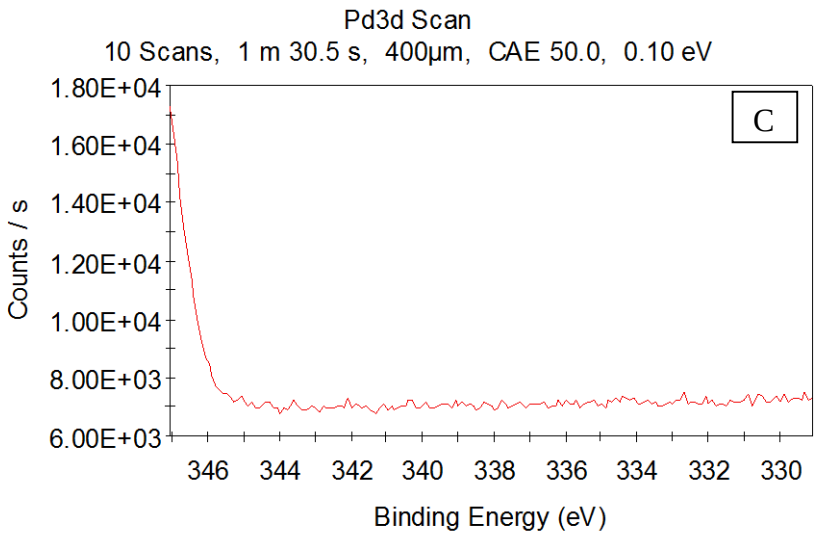

Figure 53 (A) XPS survey scan, (B) high resolution Cu scan and (C) high resolution Pd scan for the LTCC surface after the tape test

To find the adhesion failure, the tape which was used in the tape test was also analysed for its chemical composition. The XPS survey spectrum (Figure 54 (A)) showed a high percentage (12.53 %) of Cu on the surface of the tape. The features of the Cu2p signal in the high resolution spectrum showed the presence of copper metal in addition to oxidised Cu. The weak satellite in between the two intense peaks (Figure 54 (B)) indicates the presence of copper oxide. Both Pd and Sn were not detected with the XPS analysis on the surface of the tape. Previous research suggested that the failure of electroless copper and glass occurs [16] at the catalyst/copper interface. In that study, they reported the presence of Pd and Sn on the surface of the delaminated glass, but not on the surface of delaminated copper on the adhesive tape confirming the copper failure at the catalyst copper interface. Unfortunately, the absence of Sn and Pd both on the tape and delaminated surface in the present study resulted in difficulty in drawing any further conclusion regarding the location of the adhesion failure in the electroless copper / LTCC system.

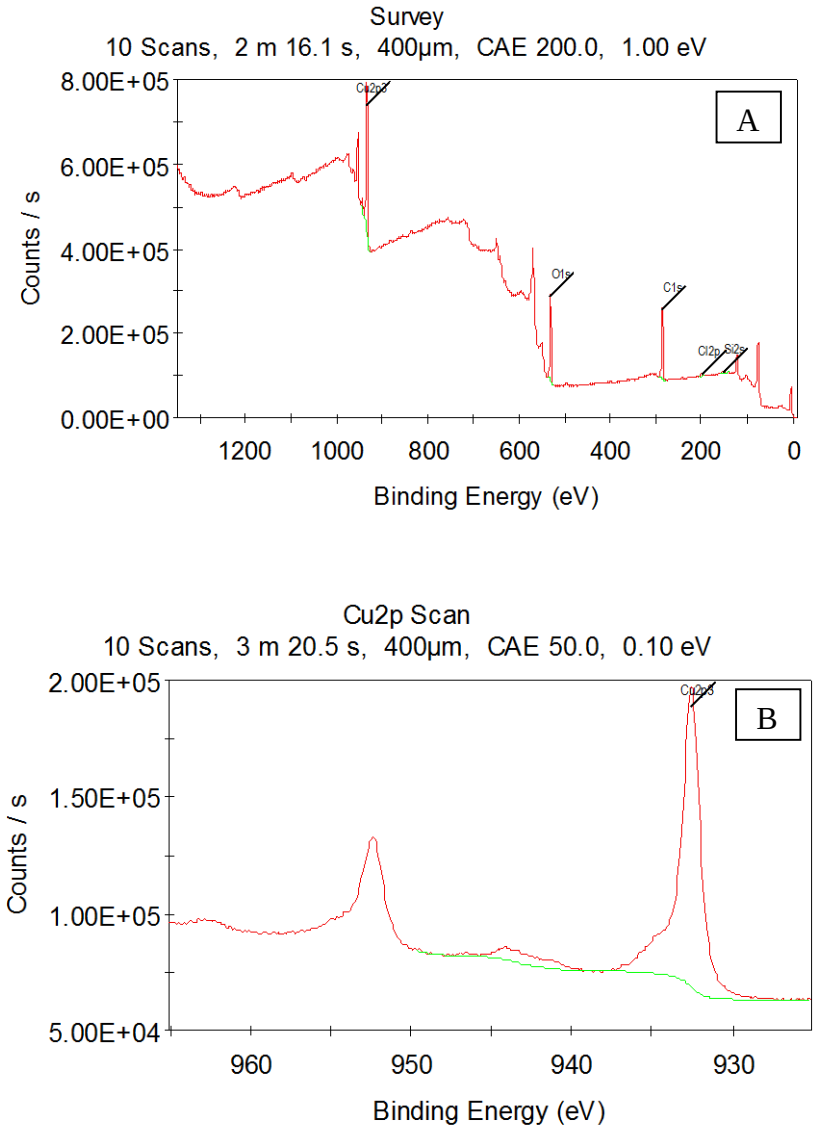

Figure 54 (A) XPS survey scan, (B) high resolution Pd scan and (C) high resolution Cu scan for delaminated Cu film on the tape

5.4.3 Scratch Test

Scratch testing was carried out as a quantitative measurement to determine the adhesion strength between the Cu deposit and the LTCC substrate. A batch of LTCC samples treated with a series of NaOH solutions with different concentrations and plated with Cu for 60 minutes at 30 ^{0}C were analysed using a scratch tester. Figure 55 shows an example of the scratches made on electroless copper deposited on LTCC. Initially the scratch appears

bright where the surface is removed, then the failure of the coating occurs and in this case, substrate cracking occurred with the increasing load.

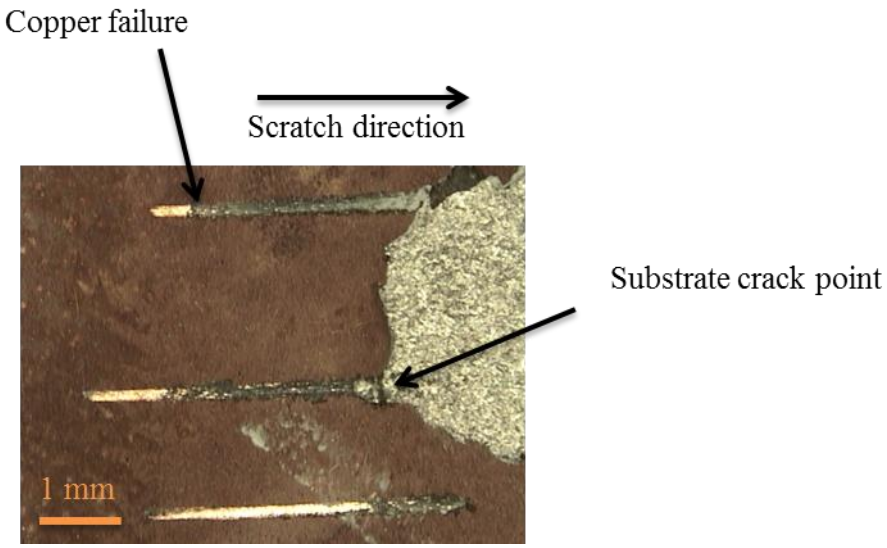

Figure 55 Scratches made on electroless copper deposited on LTCC sample

As the rate of increase of load per minute was known by determining the length of the scratch before failure the critical load could be determined. The Cu failure point was defined as the location where the substrate was visually seen under the optical microscope. The optical micrographs such as those shown in Figure 55 of the scratches were initially analysed to find the failure point. However, scaling from these optical micrograph images was not clear enough to find the exact Cu failure point. Instead, an SIP Universal optical measurement machine was used with a magnification factor of 12.5. This instrument allowed measurement along the scratch by moving the stage manually, while inspecting the scratch through an eyepiece and provided a digital readout relative to the start position.

The initial load of the scratch tester was set to 15 N for the sample treated with 1M NaOH and increased stepwise. The load rate was 10 N/minute. The microscope analysis showed that Cu failure happened at the start point of the scratch and the substrate cracked after 2.5 mm with a load of 20 N (Figure 56). As the substrate crack occurred at 20 N, the initial load was lowered down to 10 N and applied on the LTCC samples treated with 2M and 3M

NaOH. The load rate was maintained at 10 N/minute. The visual measurements emphasised that the Cu failure also started at the very beginning in both samples.

The initial load was further lowered down to 1N for the samples treated with 4M, 5M, 6M and 7M NaOH. The load rate was 10 N/minute for the 4M sample and for the rest of the samples the load rate was 2 N/minute.

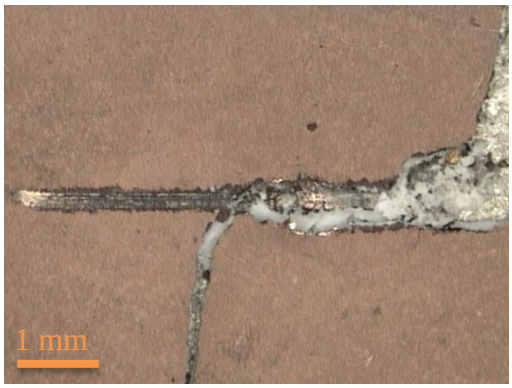

Figure 56 Scratch created on LTCC sample treated with 1M NaOH

The Cu failure could be identified with scratches on the samples treated with 4M, 5M, 6M and 7M NaOH by analysing the samples with the SIP Universal optical measurement machine and, at the failure point, the critical loads were identified as 8.1 N, 1.6 N, 2.3 N, and 1.5 N respectively. The acoustic emission and frictional force obtained from the ST 3001 was also plotted against the scratch path to correlate to the failures observed under the microscope and presented later in the chapter. The LTCC sample treated with 4M NaOH showed a relatively higher critical load compared to the samples treated with 5M, 6M and 7M NaOH and this agreed with the tape test results.

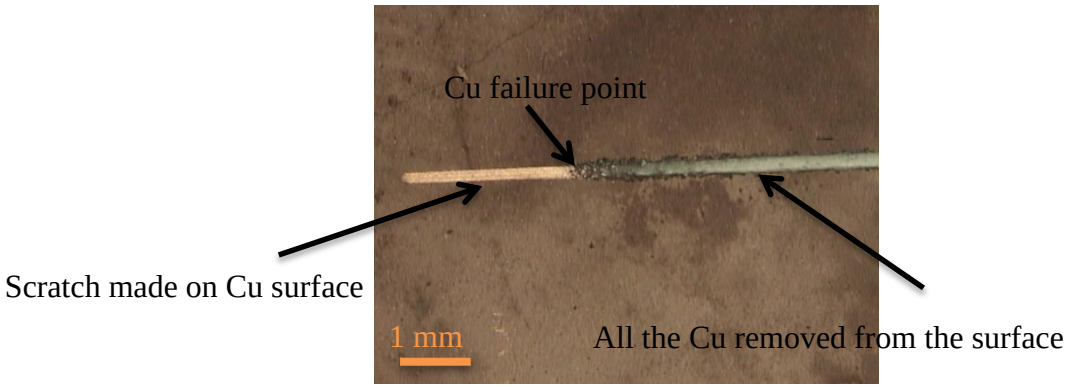

Figure 57 Scratch created on LTCC sample treated with 7M NaOH

The fluctuations of the frictional force and acoustic emission along the scratch path should also provide the position of the failure point. The load was plotted against the frictional force and the acoustic emission for samples treated with 4M, 5M, 6M and 7M NaOH. Figure 58 shows an example of the graphical representation of the frictional force and the acoustic emission along the scratch path.

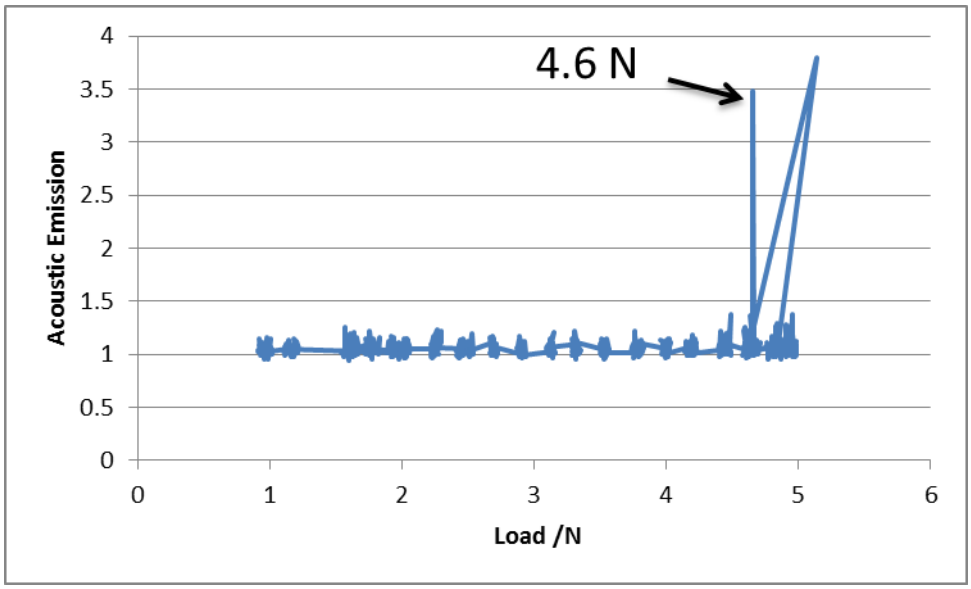

(a)

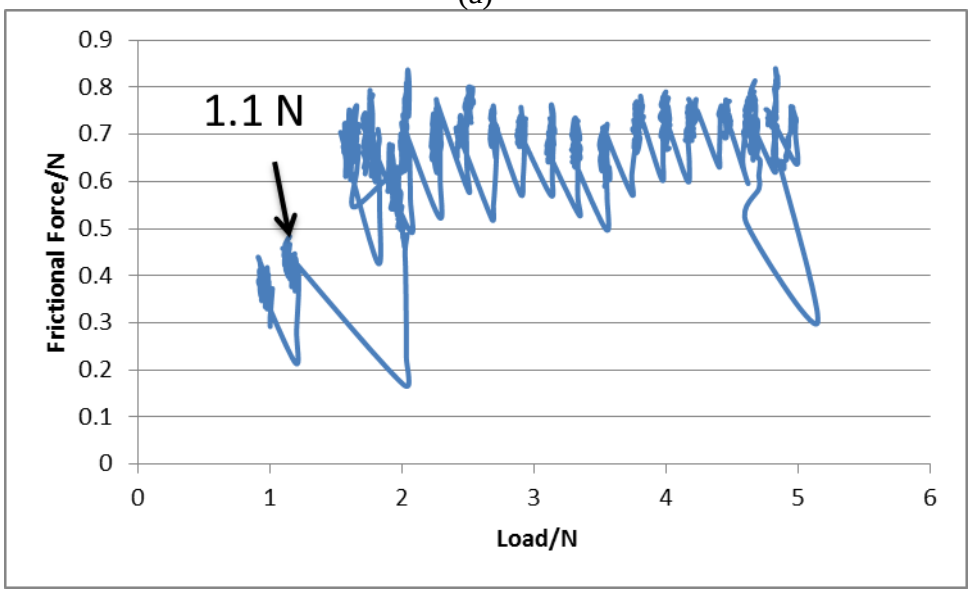

(b)

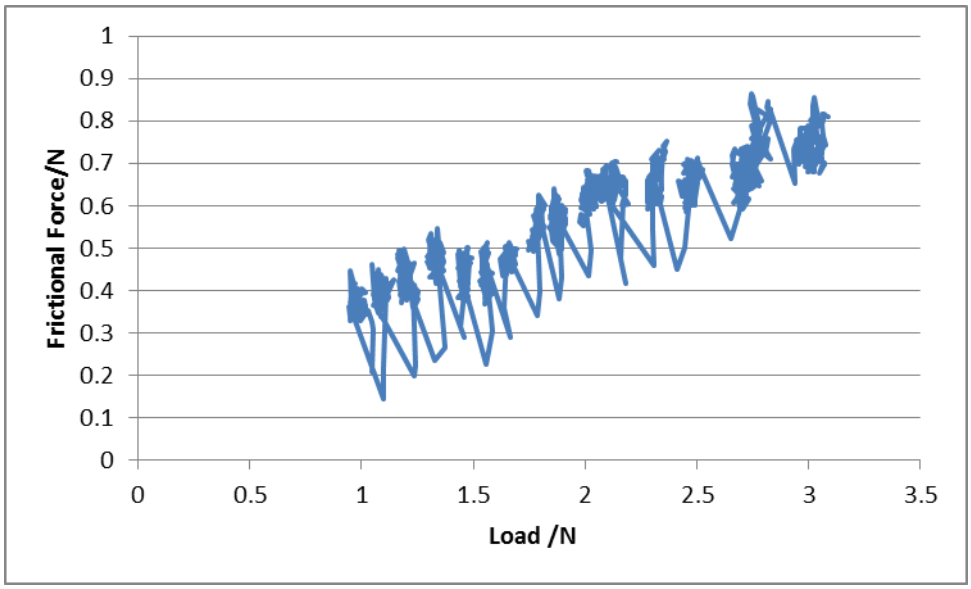

(c)

Figure 58 Graphical representation (a) load vs acoustic emission, (b) load vs frictional force of sample treated with 5M NaOH and (c) load vs frictional force of sample treated with 6M NaOH

Figures 58 (a) and (b) show the graphical representation of applied load vs acoustic emission and applied load vs frictional force respectively of the LTCC sample treated with 5M NaOH. The critical loads obtained according to the change in acoustic emission and the frictional force were 4.6 N and 1.1 N respectively. A large difference between critical load values for the same sample resulted in difficulty in identifying the copper failure point. Figure 58 (c) shows the graph of applied load vs frictional force for the LTCC sample treated with 6M NaOH. Again, the load vs frictional force graph did not indicate an abrupt change in the slope leading to poor identification of the failure point. Table 10 summarizes the copper failure point values identified with the microscopic examination and graphical representations.

Table 11 Summary of scratch test results (scratch speed 5 mm/minute)

Concent-ration of NaOH	**Initial load/ N**	**Load rate/ N/minute**	**Substrate crack point/mm**	**Load at Cu failure point/N**	**Load at substrate crack point/N**	**Critical load identified with**	
						Acoustic emission	Frictional force/N
1M	15	10	2.5	-	20.3	-	-
2M	10	10	7.6	-	25.0	-	-
3M	10	10	No crack	-	-	-	-
4M	1	10	No crack	8.1	-	11.0 N	12.2
5M	1	2	No crack	1.6	-	4.6 N	1.1
6M	1	2	No crack	2.3	-	2.1 N	Difficult to identify
7M	1	2		1.5	-	1.1 N	1.1

In some samples (1M and 2M), substrate cracks were observed before the Cu failure point. The loading parameters were varied due to substrate cracking, however, it was assumed that in cases where cracking did not occur the loading parameters did not affect the critical load. The copper failure was observed at the initial point of the scratch for LTCC samples treated with 2M and 3M NaOH. The copper failure point was identifiable for the LTCC samples treated with 4M, 5M, 6M and 7M NaOH. The sample treated with 4M NaOH showed a change in slope of the graphical representation around 11-12 N, however the visual data from the scratch indicated a different critical load (8.1 N) at the failure point. The visual examination and graphical data also gave contradictory results for the LTCC sample treated with 5M NaOH showing 3 N difference. Critical load values obtained from microscope evaluation and the critical load vs acoustic emission graph for the sample treated with 6M NaOH were 2.1 N and 2.3 N respectively and showed fairly close values. However, the frictional force did not give any clear result. The visual observation of the

scratch on the sample treated with 7M NaOH and the graphical representation showed similar critical load values.

5.4.4 Surface Roughness of Deposited Copper

In order to study the surface roughness of the deposited copper on LTCC samples treated with different concentrations of NaOH solution, the Ra parameters were obtained using a Zygo NewView 5000 Coherence Scanning Interferometer. Figure 59 shows the variation of average Ra values with the concentration of NaOH solution. Average Ra values were calculated by taking the Ra values from three places on the surface. The length of the line where the 2-D profile was taken was approximately 650 μm. The error bars indicate the difference between the minimum and the maximum Ra value of the surface. The LTCC samples treated with 3M, 4M and 5M NaOH were immersed in the solution for 24 hours and the samples treated with 6M and 7M NaOH were immersed for 7.5 hours. The surface roughness of copper deposited on untreated LTCC samples showed an average Ra value of 0.83 μm which is slightly higher than the Ra value of the plain LTCC sample (~0.65 μm as mentioned in section 2.5.1).

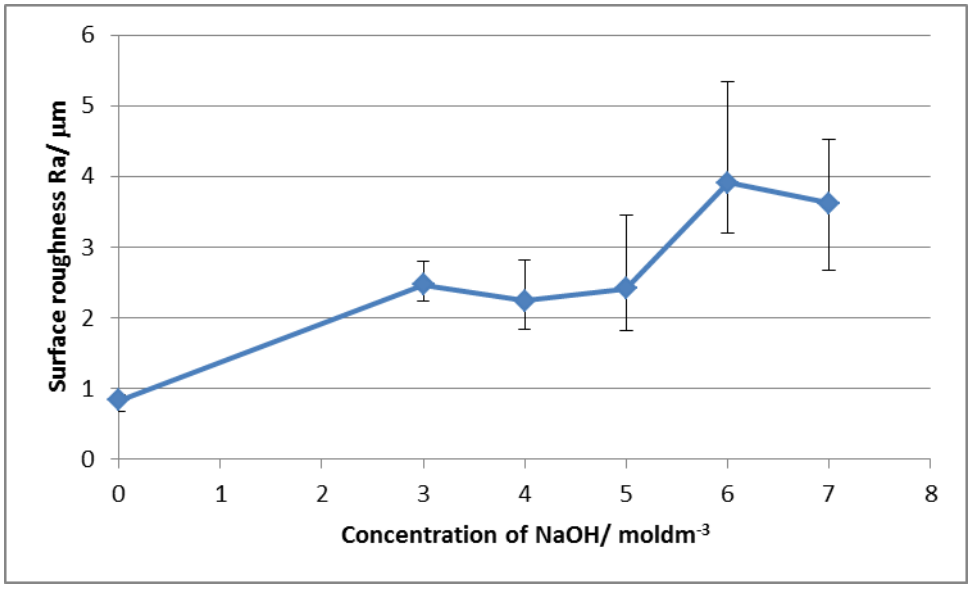

Figure 59 Surface roughness of copper deposits

The Ra values of the copper deposits showed a dramatic increase for the LTCC samples treated with NaOH. This observation is expected as the NaOH treated LTCC surface

showed relatively higher roughness (Ra) values compared to the corresponding untreated surface. Large error bars could be seen at some points in the graph. This again highlights the poor representation of 2-D surface roughness data as described in the previous chapter. A possible reason for higher values of Ra could be the different growth mechanism of the electroless copper on the treated LTCC substrate: it was shown in Chapter 3, that the NaOH treated LTCC surface showed changes in morphology and microstructure. It has been discussed in several studies in the literature that the growth mechanism and the microstructure of electroless copper depends on the type of substrate surface. Nakahara and co-workers reported that the nucleation and growth patterns of electroless copper depend greatly on the substrate due to different mechanisms of catalyst absorption [66]. Figure 60 shows the surface topography of the electroless deposits on both the treated and untreated LTCC surface. The treated surface showed a relatively large grainy structure compared to the untreated surface (Figure 60 (b)). Kim and co-workers [127] also studied the microstructure of electroless copper on different substrates. The substrates included epoxy, evaporated copper film, evaporated gold film, and mirror-finished polycrystalline and single crystals of copper. They showed that rougher electroless deposits occurred due to the original roughness of the substrate. They also reported that different crystallographic structures on the substrate surfaces were more favourable to electroless copper growth than others leading to different growth rates on different substrate surface structures. Hence, one possible reason for the observed larger electroless copper grains on the treated LTCC may be due to higher electroless copper deposition rates.

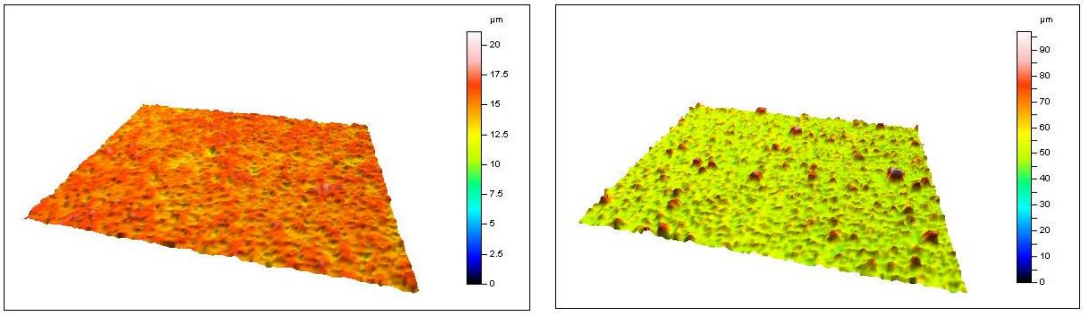

Figure 60 (a) Copper deposit on untreated surface (b) on 7M treated NaOH

5.4.5 Role of Flake-like Structures on Electroless Cu Deposits

The electroless copper deposits on NaOH treated samples showed a very rough surface and the large nodules noted in Figure 60 (b) were not evenly distributed on the surface. Another possible reason for these nodule structures was thought to be that the flake like structure that appeared on the NaOH treated LTCC surface, as presented in Chapter 3, could have been mostly responsible for the Cu surface roughness. If the electroless copper started to grow on the flake like structures and followed the surface morphology of the NaOH treated LTCC surface, it could lead to a rough surface. The grain growth behaviour of the copper deposits on NaOH treated LTCC was hence investigated.

A. The Observations of Grain Growth Behaviours in Copper Deposits

Figure 61 illustrates the microstructure of the electroless copper deposits at different stages of the deposition process. The samples were treated with 4M NaOH before the deposition process and the same procedures were followed for the copper plating process as described in section 2.4.2. However, samples were removed after only short periods of time in the plating bath and rinsed in order to determine how the plating process developed over the time. The very initial stage of the electroless deposition process is presented in Figure 61 (a) and (b) which corresponds to 30 seconds and one minute of plating time respectively. Nano metre scale individual copper particles which are in white contrast in Figure 61 (e) against the grey background are deposited on the catalytic sites of the surface after one minute of plating time.

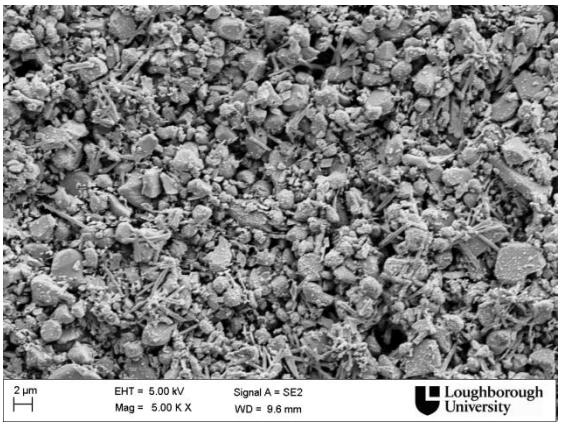

(a)

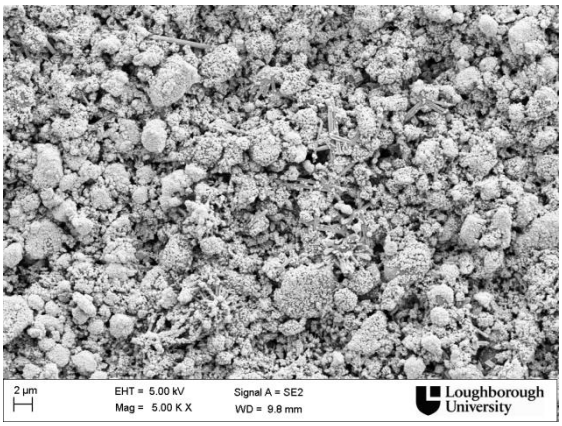

(b)

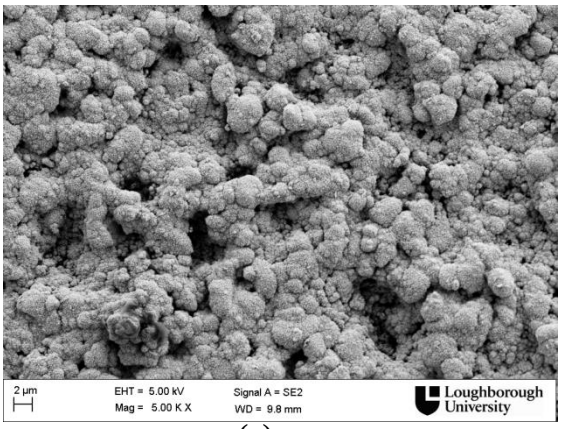

(c)

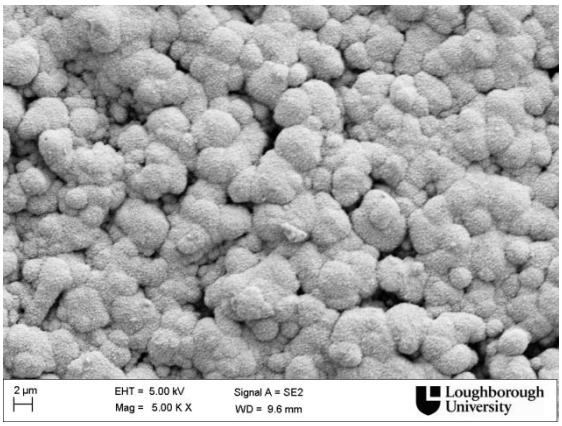

(d)

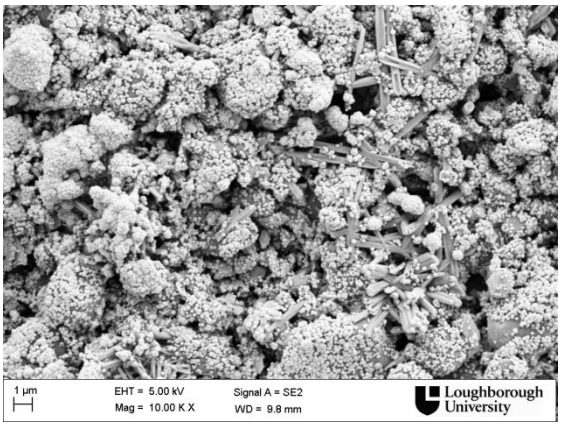

(e)

Figure 61 SEM images of the electroless copper after (a) 30 seconds (b) 1 minute (c) 15 minutes (d) 1 hour and (e) magnified image of (b)

As the process continues these individual copper nanoparticles combine to form agregates (Figure 61 (c)). The size of these agregates became larger (Figure 61(d)) as the plating time was increased to one hour. A continuous copper deposit covering the LTCC could be seen after one hour of plating time. Similar observations for electroless copper growth on a carbon substrate were reported by Sard [65]. It was noticed that throughout the copper plating process, the flake like structures were not observed on the LTCC surface. The disappearence of the flake like structures even in the very early stage of the copper plating process suggested the disapearence of these features in a previous step of the plating process.

To observe the effect of the different plating steps on the flake like structures, the LTCC samples treated with 4M NaOH solution for 24 hours were immersed in pre-dip solution for 2 minutes and then catalyst solution for 2 minutes. The SEM micrographs (Figure 62

(b) and (c)) of these samples were then analysed for their surface morphology. The SEM images show that the flake like crystals disappeared from the samples immersed in the pre-dip solution and catalyst solution which are both fairly acidic. It can be suggested that these crystals are soluble in the acidic media. This can be further supported by the observations reported by Bittner et al [23]. Their study suggested that acid etching preferentially removed one of the crystalline phases from the ceramic body.

The samples immersed in the pre-dip and catalyst solutions were further dipped in 4M NaOH solution to investigate the reappearance of the flake like structures. SEM images showed that the surface morphology of the samples changed after 3 minutes of immersion in NaOH. A porous surface was observed (Figure 62 (e)) and the grainy particles which can be seen on the samples treated with pre-dip and catalyst solution disappeared from the surface. However, these grainy particles started to reappear on the sample surface when samples were exposed to a further 10 minutes in the NaOH solution (Figure 62 (f)). The flake like features reappeared on the LTCC surface after 15 minutes of immersion time (Figure 62 (g)). The time taken for reappearance of the flake like structures was much less than the time taken for the first flake like features to appear on the fresh LTCC surface which was 50 minutes. The SEM micrographs of the LTCC cross section as shown in chapter 3 showed a very dense top layer. It can be suggested that after this hard top layer has been removed by the first immersion in the NaOH solution, the second etching step takes much less time for reappearance of the flake like structure.

The surface roughness of the samples treated with pre-dip and the catalyst solutions was found to be relatively high (Ra=1.176 μm and 1.21 μm respectively) compared to the control sample (Ra=0.65 μm), but lower than the average Ra value (1.94 μm) obtained for the LTCC sample treated with 4M NaOH before the catalyst treatment. Hence it would appear that when treated with NaOH there is a change in the background surface of the LTCC in addition to the formation of flake like structures. These higher surface roughness values are likely to be responsible for the adhesion improvement discussed earlier in this chapter.

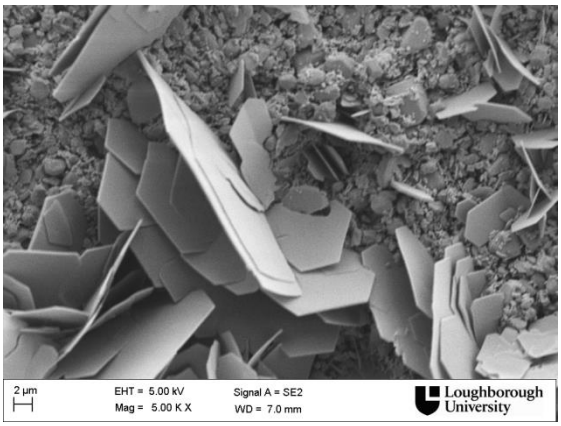
2 µm
EHT = 5.00 kV
Mag = 5.00 K X
Signal A = SE2
WD = 7.0 mm
Loughborough University

(a)

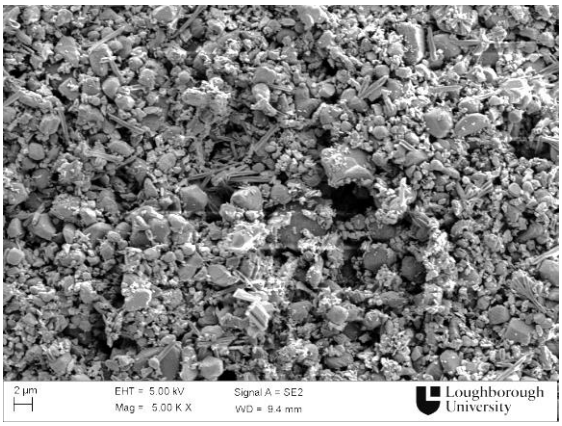
2 µm
EHT = 5.00 kV
Mag = 5.00 K X
Signal A = SE2
WD = 9.4 mm
Loughborough University

(b)

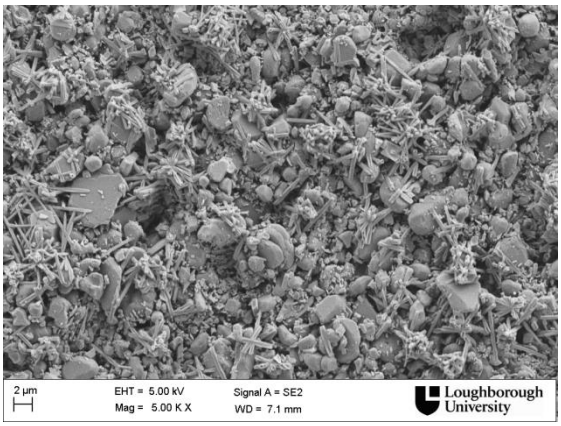
2 µm
EHT = 5.00 kV
Mag = 5.00 K X
Signal A = SE2
WD = 7.1 mm
Loughborough University

(c)

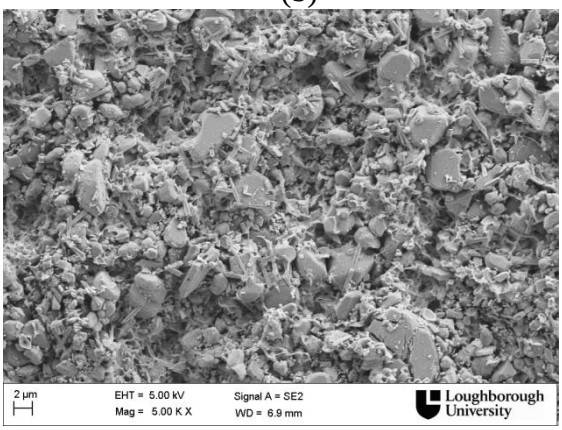
2 µm
EHT = 5.00 kV
Mag = 5.00 K X
Signal A = SE2
WD = 6.9 mm
Loughborough University

(d)

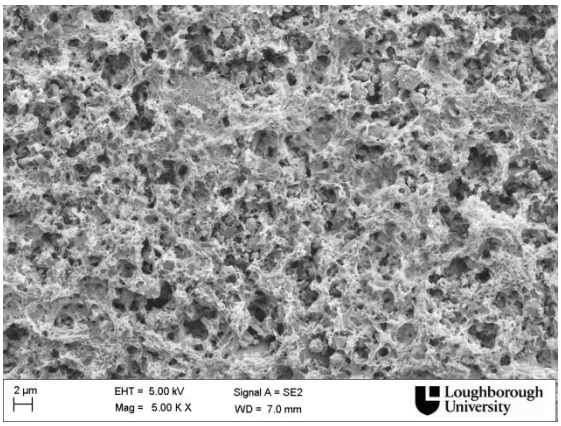
2 µm
EHT = 5.00 kV
Mag = 5.00 K X
Signal A = SE2
WD = 7.0 mm
Loughborough University

(e)

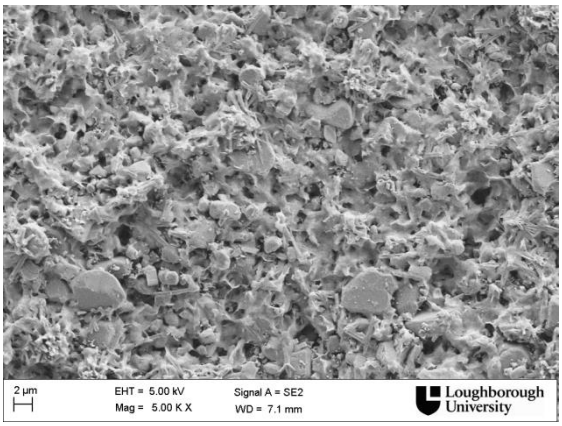
2 µm
EHT = 5.00 kV
Mag = 5.00 K X
Signal A = SE2
WD = 7.1 mm
Loughborough University

(f)

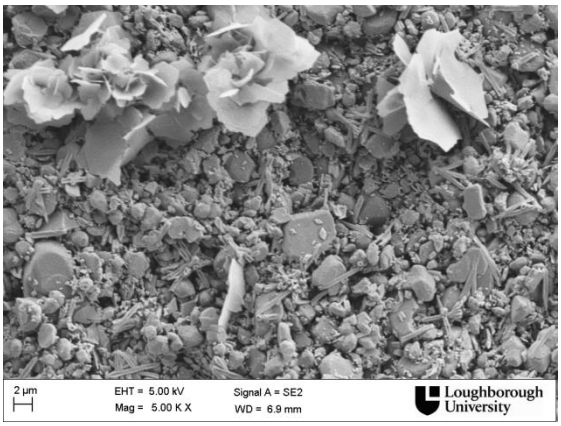

(g)

Figure 62 SEM micrographs of (a) Control Sample; NaOH treated LTCC samples after immersion in (b) Pre-dip solution, (c) Pre-dip and catalyst solution, (d) 1 minute in NaOH solution, (e) 3 minutes in NaOH solution, (f) 10 minutes in NaOH solution and (g) 15 minutes in NaOH solution

5.6 Conclusions

Adhesion tests including tape test and scratch test were carried out to find the interfacial adhesion between electroless copper and NaOH treated fired LTCC. The effect of NaOH concentration on adhesion was mainly considered. Both tape test and scratch test showed adhesion improvement in NaOH treated LTCC samples compared to untreated LTCC. According to the peel test, the 4M NaOH treated sample showed relatively better adhesion. The other LTCC samples also showed some traces of copper attached to the surface after the tape test which could not be observed in the untreated LTCC sample. Due to sample cracking, the critical loads of the scratch testing were only obtained for LTCC samples treated with 4M, 5M, 6M, and 7M NaOH and the critical load values were 8.1 N, 1.6 N, 2.3 N and 1.5 N respectively again indicating 4M as the preferred NaOH concentration.

Chapter 6 Excimer Laser Machining of Fired LTCC

6.1 Introduction

The microelectronics industry requires the size reduction of radio frequency components with the aim of system miniaturisation and low cost. With its multilayer technology, Low Temperature Co-fired Ceramic is a promising candidate among other electronic substrates when achieving system miniaturisation. LTCC has been established as a multilayer technology and the state of the art of this technology provides channel structures and cavities inside the ceramic body [128]. These cavity structures and microchannels become very attractive when improving the functionality of miniaturised electronic devices [21]. Usually these structures are built using laser machining of green state LTCC and stacking of these sheets followed by the firing process. However, to prevent the deformation of cavities and channels, careful alignment of the green tapes is needed due to shrinkage of the LTCC when sintering. Laser machining of fired state LTCC could be a possible solution to form cavities and microchannel structures. In particular, excimer laser machining could be ideal to machine microchannel structures that require low surface roughness for high frequency applications.

LTCC technology also allows the fabrication of planar circuitry and passive components in between layers and these are usually realized on green state LTCC using the screen printing process. However, when considering small feature sizes, thick film technology has its own limitations due to the shrinkage properties of the metal paste as well as the green tapes. For example, X and Y shrinkage of the green tape and the capabilities of the screen printing process affect the widths and spacing between printed conductor lines which are key factors for microwave performance of the passive components such as capacitors. The non-

uniformity of the tape shrinkage can also affect the shape of the printed metal lines [129]. As a solution, thin film technologies can be applied on fired LTCC for structuring microwave and millimetre wave components. Among the thin film technologies available for electronic manufacturing, there is an opportunity to use electroless plating techniques in the process of fabricating passive components on fired LTCC.

The objective of the research presented in this chapter was to investigate excimer laser machining techniques on fired state LTCC tapes in order to create open microchannel structures. Selective metallisation of these channels using electroless copper plating and optimization of these processes to achieve low roughness metal deposits for high frequency applications was also carried out. The possible applications include substrate integrated waveguide structures and RF MEMS components which are operating in the microwave and millimetre wave regions of the electromagnetic spectrum. In addition, this chapter also describes the formation of conductor patterns on fired LTCC as an alternative to the conventional thick film technology used prior to the firing process. The mask projection technique of the excimer laser system combined with electroless copper plating was used to achieve the required patterns on fired LTCC. The patterns including a complete circuit layout and planar passive components are presented in this chapter.

6.2 Literature Survey

6.2.1 LTCC Cavities and Channel Structures

As mentioned in the introduction of the thesis, LTCC multilayer technology allows realization of cavities and micro channels inside the ceramic body. These structures are used as cooling systems [130], waveguides [131] microfluidic systems [132] and cavities that accommodate RF-MEMS components [133]. The conventional way of creating cavities in the ceramic body is through the formation of apertures in the single green tapes, aligning and stacking of green tapes, filling of cavities with sacrificial materials, lamination of green tapes by thermocompression and sintering of the laminate [134]. Laser micromachining has been widely used to create cavities in green tapes. A modified tape

processing procedure was reported in the literature [135] in terms of fabrication of parallel closely-spaced channels. In that study, a diode pumped Nd:YAG laser was used to micromachine the LTCC green tapes. The micromachining process was optimized using different laser parameters. Smoother cutting edges and more rectangular-like shapes were achieved by using repeated laser pulses with less laser power. The lamination of green tapes was carried out in different pressure conditions and different lamination time periods to find the optimum conditions. However, the embedded channels experienced delamination, distortion, sagging and even crack formation during unconstrained firing. Adhesive assisted lamination was also investigated using different types of pressure sensitive adhesives at reduced lamination pressures. A defect-free channel structure was achieved by spin coating hydroxyethylcellulose in between the layers before the lamination process. Filling of hydroxyethylcellulose as sacrificial material into the channel structures was found to be a promising method when achieving defect free embedded channel structures. However, the standard lamination pressure and the firing profile were altered to obtain optimum conditions. Mechanical punching [136] was also reported as a successful method of creating channel structures in glass ceramic green sheet. Overlap punching was carried out using a single punching tool to form 600 μm long channel structures. Mechanical punching is widely used for the formation of via holes in green tapes with diameters down to 50 μm [38], [137].

Hot embossing of green ceramic tapes is another way of creating channel structures. Embossing dies with a meander structure for microfluidic applications and patterns to create circular and rectangular cavities were used [138]. The LTCC green tapes were embossed by applying a force of 60 kN at 130 ^{0}C which was set above the glass transition temperature of the binder contained in the green tapes. Cavities with 225 μm depth profiles were obtained in the green tapes. The depth of the final cavities was 110 μm due to 50% z-direction shrinkage during the firing process. Another study was carried out to create channel structures with different channel and line widths using hot embossing [139]. In this study, the channels were created with an applied force of 20 kN at different temperatures. The depth of the channels was increased with the embossing temperature and after the firing process, 20–22% vertical shrinkage and 10 and 13% horizontal shrinkage was observed. The channels with 100 μm width showed 21 μm average depth with 20 kN force at 85 ^{0}C.

One of the associated problems in the process of creating 3-D structures in green LTCC tape is the deformation of cavities and channel structures and sagging of suspended structures. Different types of sacrificial material have been used to prevent the deformation and sagging. Microchannels created using carbon-black paste and cetyl alcohol [140] [141] as a sacrificial layer and mineral sacrificial layers [142] have been reported in the literature.

Espinoza-Vallejos and co-workers studied a photolithographic technique which can be used for meso-scale 3-D structuring of LTCC without sacrificial layers [143]. Partially sintered LTCC was used in this study due to ease of chemical etching. Dry resist lamination was carried out on partially sintered LTCC at temperatures between 90 ^{0}C - 130 ^{0}C. Required patterns were then formed on the LTCC using UV exposure (40-100 mJ/cm^2) followed by developing in sodium carbonate solution. Two systems including HF: Ammonium Fluoride (1:4) at 90 ^{0}C and HF: H_2O (1:6) at 60 ^{0}C were used for etching. The process was used to develop an electrophoretic channel and a low resistance coil that was needed in order to achieve electromagnetic actuators. The depth of the channels for each application was 70 μm and 114 μm respectively after the final firing process.

6.2.2 Laser Machining of Ceramics

Laser machining of ceramic is an important aspect for many structural, tribological, optical and electronic applications and becomes an ideal tool when realizing smaller and high precision components [144]. Many studies have been reported in the literature about laser machining of ceramics.

A study comparing machining strategies for ceramic using Nd:YAG (wavelength 355 nm) and excimer laser (wavelength 248 nm) was reported by Tonshof et al. [145]. Straight and spiral cuts were made on an AlN substrate (thickness 250 μm) with different cutting speeds. The Nd:YAG laser was operated at the maximum pulse energy of 3 mJ at a frequency of 1 kHz with a 5 mm/min feedrate. The excimer laser was operated at an energy density of 20 J/cm^2 and a pulse repetition rate of 200 Hz. The results showed both lasers could cut through the AlN substrate but the Nd:YAG laser provided a shorter processing time.

Another study revealed the microstructural changes induced by an excimer laser (KrF, 248 nm) on alumina and silicon carbide. In this study, the materials were treated with different

parameters such as laser fluence, energy, number of pulses, sample speed, atmosphere, spot size and beam angle. The microstructure and chemistry of the treated area was analysed using SEM and removed material was also investigated. The key findings of the study were: oxidation of silicon carbide when treated in atmospheric conditions; at low fluences, both ceramics showed melting and resolidification, while at high fluences, material was removed by vaporization; the ablation depth was higher in alumina when compared to silicon carbide and linear with increasing pulse number [144].

Jaroslaw Kita and co-workers used laser technology to fabricate 3-D structures and elements on both fired and unfired LTCC. In this study, vias with diameters 50 µm, 100 µm, 200 µm and 400 µm were machined on the fired LTCC using an Nd:YAG laser (wavelength 1064 nm). The results showed that laser power was too low and could only scribe the substrate. Small vias produced with high laser power or slow cutting speed showed poor machining quality [146].

In summary, it appears that the Nd:YAG laser removes material through melting or vaporisation, when the material is heated from solid to liquid and gaseous state. In contrast, the high energy photons from the excimer laser reduce the interaction time between the irradiated surface and the bulk material and hence minimize the heat affected zone resulting in high precision machining compared to the Nd:YAG lasers [147]. Both the excimer and the Nd:YAG laser have been employed for machining of ceramic materials, but only the latter appears to have been used for fired LTCC and the laser parameters played a vital role in the machining quality, mechanisms and the efficiency.

6.2.3 Metal Patterning on LTCC

The research on other metallisation techniques, which were used to metallise fired LTCC is described in Chapter 1. The following section describes the work that has been done in the literature to form metal patterns on LTCC. When moving towards higher frequencies, fine printing resolution and reliability is a major concern of millimetre wave circuits [148]. Deviating from the conventional screen-printing process, several thin film and thick film metallisation techniques have been employed for the formation of conductor patterns on both fired and unfired LTCC over the years. Van Tassel and Randall [149] studied

electrophoretic deposition (EPD) on green LTCC to create conductor patterns. In this study, feature widths down to 2 μm of conductive platinum patterns were formed using conventional photolithography followed by a sputtering process. Silver and barium titanate, which were dispersed in organic solvents, were then used in the EPD process to create conductor lines. They achieved conductor traces with widths of 15 μm for the silver and 5 μm for barium titanate. The lateral growth and the ramified growth of the particles however limited the line spacing to 8 μm.

J. Müller and co-workers [150] used four different metallisation techniques to pattern conductors on both fired and un-fired LTCC tapes. Commercially available photosensitive gold paste was used in their study to screen print on green LTCC and the pattern was formed using UV exposure through a negative photomask followed by spray development and then the firing process. The line width was 30 μm, the space resolution was limited to 50 μm. Gold thick film etching using a positive photoresist and thin film deposition using sputtering, and electroplating procedures were also demonstrated. The line resolution for gold thick film etching was 30 μm, however, for thin film deposition it was 10 μm. Their study showed that thin film technologies on fired LTCC allowed better resolution, but higher DC resistance, leading to higher insertion losses. Hildebrandt and Wolter [151] reported thin film structuring on sintered LTCC using lift-off patterning and semi-additive patterning. In the lift off patterning process, the substrate, which was covered in spin coated liquid resist, was exposed to UV light through a glass mask to produce the pattern. The resist was developed and stripped and platinum was deposited on the bare substrate. The major drawback of the process was the limited film thickness leading to large sheet resistance. As a solution, they deposited copper galvanically onto a thin seed layer of titanium and copper followed by nickel and gold electroplating. The pattern was formed on sputtered titanium and copper using photolithography. Minimum line/spacing was 60/25 μm for the semi-additive patterning.

6.2.4 Embedded Passive Components in LTCC

Advances in LTCC multilayer technology provide for the integration of passive components in to the ceramic body. This allows the elimination of the solder joints and

wiring in the circuitry, leading to device miniaturisation and reduction of parasitic inductance. Integral passives also benefit from better electrical behaviour, reduced size and cost [152]. The performance of the planar passive components depends on several parameters. For inductors, it depends on the width of the conductor path and spacing, number of turns and structure size. For capacitors, it depends on the width of the fingers, their spacing and the structure size [153].

Markku et al. demonstrated planar inductors on an LTCC substrate using gravure-offset printing [154]. Silver conductive paste was used in the printing process and the size of the coil was 2.5 x 2.5 mm^2. The particle size of the printing ink limits the line width/space and in this case, it was limited to 60-175 μm. Square and circular shaped spiral inductors were fabricated with 11-15 μm of coil thickness. They found that printing of circular spirals were rather difficult resulting in wider line widths and a higher non-uniformity of the conductor lines leading to lower inductance values compared to the square spirals. A self-shielding toroid inductor with inside and outside radius of the toroid approximately 1.37 mm and 2.65 mm respectively and capacitors with a dielectric thickness of 35 μm and 96 μm were reported [155]. These components were embedded in LTCC, however the method of metallisation of these components was not clearly reported.

The fractal approach for capacitor design is promising for use in lateral flux capacitors. However, conventional lithography limits the fabrication of these structures due to the complexity of such designs [156]. Plated recesses on the other hand, are a possibility to enhance performance of a capacitor that is effectively a 2.5D structure: these structures provide high edge capacitance. With further process modification, the plated recesses can also be filled with metal conductors to reduce the associated ohmic losses [129].

6.3 Research Methodology

Laser machining of green state ceramic has been widely used when designing cavities and channel structures. Established metallisation techniques are usually based on green state LTCC. A number of techniques have been reported for selective metallisation of electronic substrates such as photoimageable inks, inkjet deposition, thermal spray and direct laser

machining of gold or platinum coated unfired tapes [26]. However, the shrinkage properties of LTCC can cause deformation problems to the fine conductor lines when firing the green tape. In addition, cavities and channel structures can also cause deformation problems when firing. If the conductor lines can be patterned on fired LTCC, the above problems can be prevented.

The excimer laser machining of fired LTCC has not been examined before and this was therefore chosen. However, as with other ceramics it is expected that the thermal conductivity of LTCC which is relatively low in the order of 2–5 $Wm^{-1}K^{-1}$ [157] will play a part. This property of the LTCC material is likely to enhance the temperature of the surface where the laser is incident as the heat will not be conducted away quickly, therefore exceeding the boiling point causing rapid vaporisation and subsequent material removal by thermal ablation [158]. In addition, the high energy of the excimer laser is sufficient to break many of ceramic bonds leading to photochemical ablation [144].

The initial part of the work presented in this chapter was selective metallisation of the walls and base of LTCC open micro channel structures. The following objectives were individually addressed,

- The KrF excimer laser machining of fired LTCC was investigated. Single tracks were machined on fired LTCC using a square mask and machined tracks were characterized for their depth and roughness using white light interferometry.
- The process was then optimised to achieve uniform and smooth surface conditions using different laser parameters such as repetition rate, feedrate and number of passes of the laser beam.
- Selective copper deposition onto machined tracks was then investigated. The key challenge was to catalytically activate the surface with Sn/Pd catalyst only on the machined paths. A photoresist process was used to overcome the problem for which the process steps are shown schematically in Figure 63. Dry film photoresist was applied on the fired LTCC before the excimer laser machining process in order to create channels and required patterns. When the machined samples were immersed in the catalyst solution, only the machined parts of the LTCC surface would be exposed to catalyst solution leading to selective activation. After removing the

photoresist, electroless copper could be selectively deposited only on the catalytically active LTCC surface.

- The characterisation of selectively deposited copper tracks was carried out. This included the depth of machined tracks after the copper deposition process, roughness profiles, and electrical resistivity of deposited copper. Correlation between laser parameters and characteristics of machined lines was also considered.

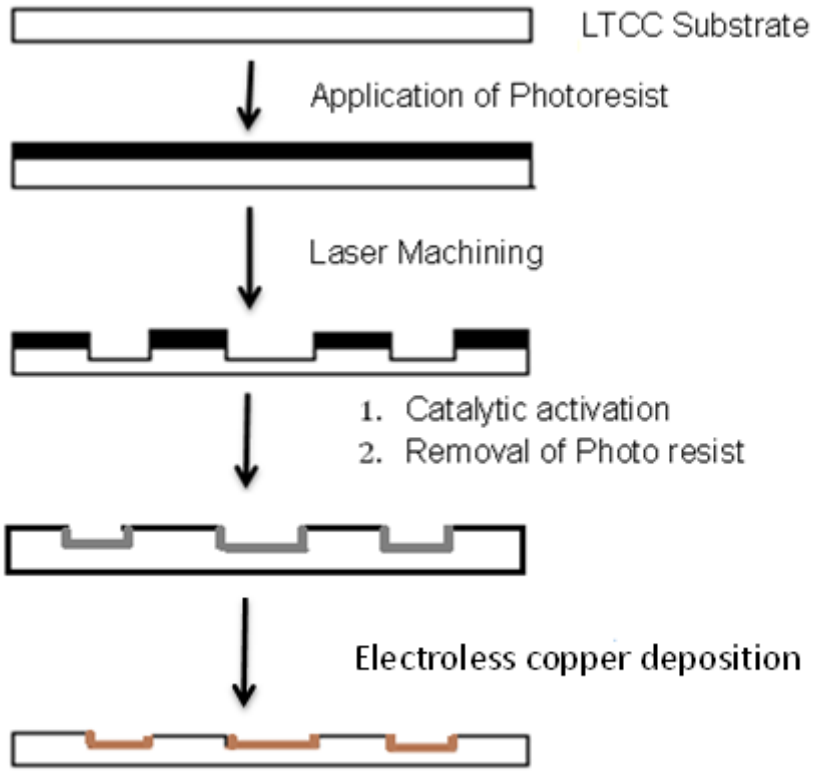

Figure 63 Schematic diagram of the selective electroless copper deposition

The next part of the study was aimed at fabricating planar passive components and circuit patterns on fired LTCC using the techniques described above. Based on the literature review, there are several possibilities that can be used to pattern metal deposits on both fired and unfired LTCC tapes. The resolution of line/space is still a crucial issue along with the edge quality of the deposited metal. The combination of photolithography, mask projection of the excimer laser, along with the electroless copper plating process can be applied to realize passive components on fired LTCC.

This chapter also describes the realisation of a resonator on fired LTCC. In this design, fabrication of an inductor on one side of the LTCC and a capacitor on the other side of the LTCC, which are electrically connected with two metalised via holes, are illustrated in Figure 64.

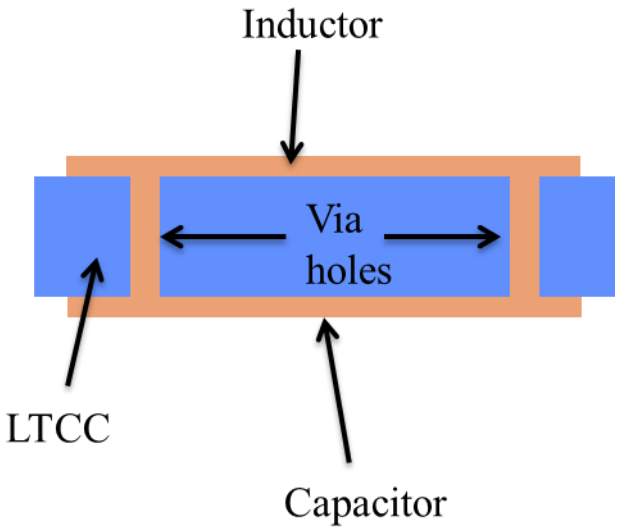

Figure 64 Schematic diagram of resonator design

6.3.1 Excimer Laser Machining

The term Excimer is generated from the words excited dimer. In this case, a dimer is a molecule formed from rare gas (argon, krypton, xenon) and halogen (fluorine, chlorine, bromine) atoms. The output wavelength of the excimer lasers varies from 193 nm to 351 nm in the electromagnetic spectrum depending on the rare gas and the halogen used to produce the laser beam (ArF- 193 nm, KrCl- 223 nm, KrF- 248 nm, XeCl- 308 nm XeF- 351 nm) [159].

Once the Excimer laser beam is incident on the surface, it can be absorbed, reflected, scattered and transmitted by the material. The machining process takes place due to removal of material by melting, dissociation or decomposition of chemical bonds, evaporation and expulsion [158]. So the efficiency of the laser machining process depends on the thermal, chemical and optical properties of the material rather than the mechanical properties [147].

A. Excimer Laser System

The Lambda Physik Lasertechnik LPX200 system used in this research uses Krypton (Kr) and Fluorine (F_2) as the laser gas mixture. A high voltage discharge between the electrodes in the laser tube provides the energy required to excite the rare gas molecules, in this case, Kr. The excited rare gas molecules are highly reactive and react with the fluoride molecules in the gas mixture to form excited KrF molecules. The binding energy for this attraction with the internuclear separation is shown in Figure 65.

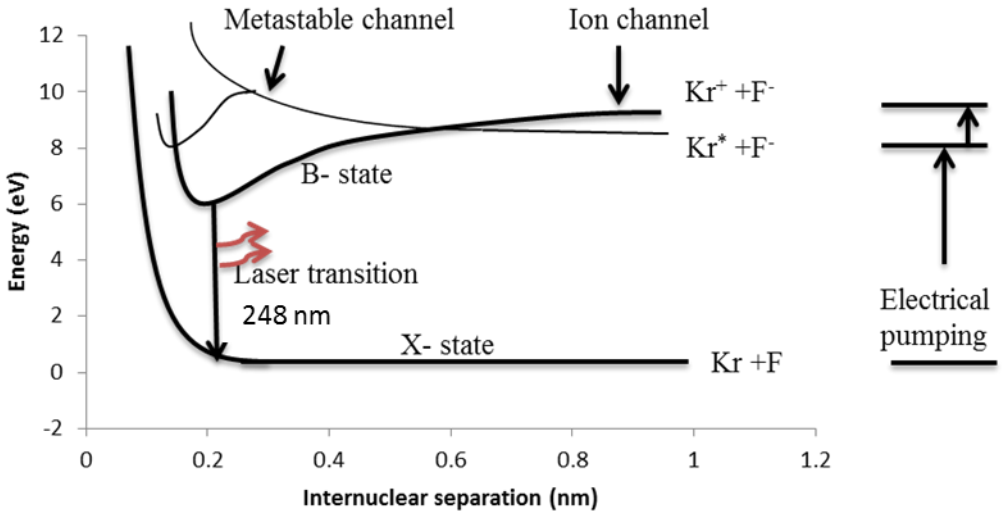

Figure 65 Variation of binding energy with the internuclear separation of KrF [160]

At some point the number of excited molecules exceeds the number of ground state molecules, a process known as population inversion. The molecules that are in the excited state have high energy and hence are unstable. Once triggered, the excited molecules emit photons in the UV range and in the case of KrF this is at 248 nm wavelength [160]. Once the laser beam is generated it goes through a beam delivery system which consists of attenuator, beam homogenizer, beam expanding and shaping optics and mask before it reaches the work piece. The positions of work piece, mask and attenuator are computer controlled and a schematic view of the excimer laser components is shown in Figure 66.

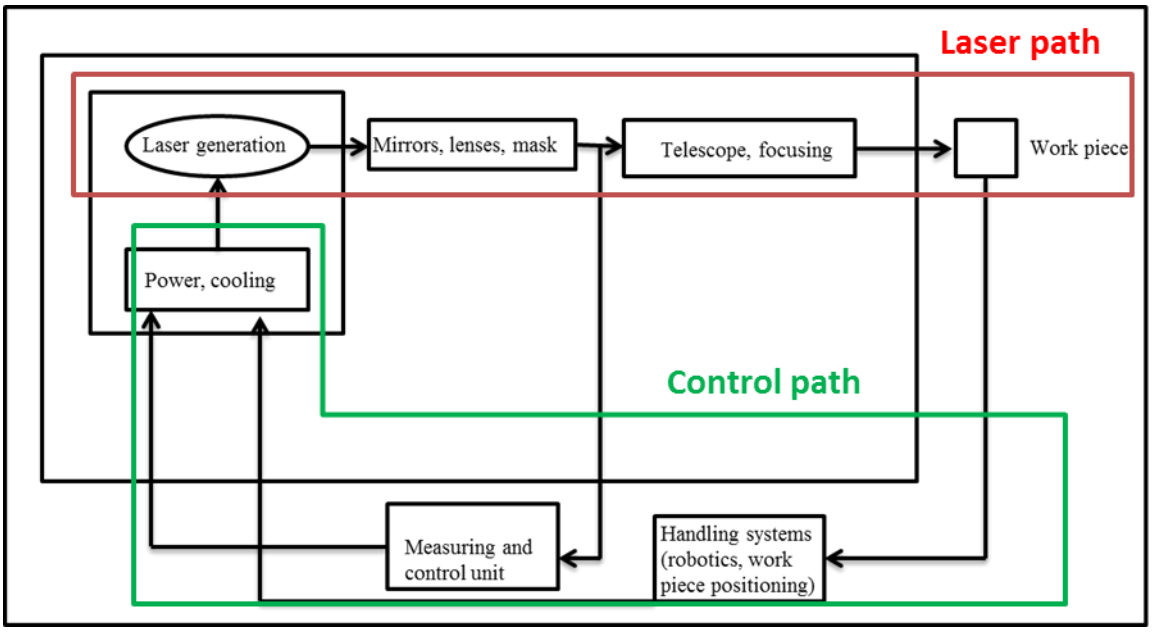

Figure 66 Excimer laser components

The main advantage of this technique is the application of a mask projection technique to achieve micron level features with very fine edge quality. The excimer laser system uses a mask as shown in Figure 67. The mask defines the shape and the size of the machined feature on the sample. These masks are usually made with thin metal sheets. The de-magnifying projection optics of this particular system allows the size of the final machined features to be reduced by 10 times of the size of the mask.

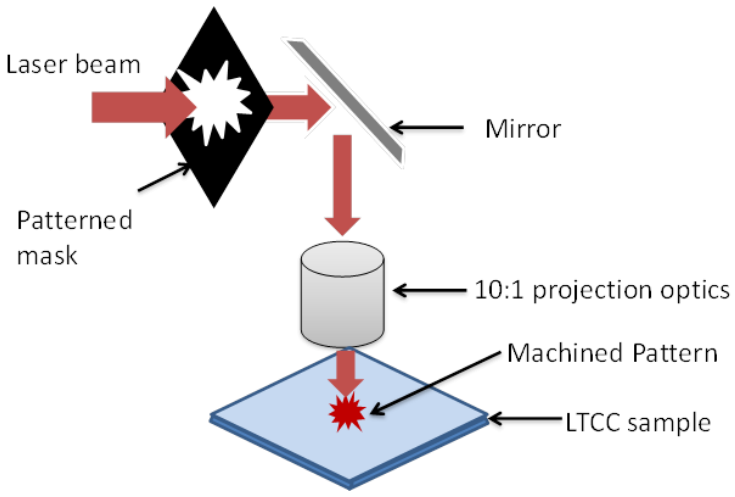

Figure 67 Schematic illustration of mask projection technique of the excimer laser

6.4. Experimental

6.4.1. LTCC Sample Preparation

Double layer fired LTCC (DuPont 9K7) was used in the experiments and was laminated and fired according to the manufacturer's instructions by the University of Leeds. Samples were soaked in a 10 vol % Decon 90 solution in de-ionized water for 24 hours at room temperature to clean the surface. These were then rinsed with de-ionized water and dried. A dry film photoresist (Ordyl Alpha 440T, ~40 μm thick) was then applied on both sides of the LTCC samples using an Albyco photopro 33 laminator operating at 110 ^{0}C. The samples were then exposed to UV light to harden the resist for 8 seconds and the protective plastic layer on the resist was removed before machining.

6.4.2 Laser Machining Process

A Lambda Physik Lasertechnik LPX200 KrF pulsed excimer laser system operating at 248 nm wavelength with pulse energy of 250 mJ/pulse and pulse duration of 20 ns was used to machine the patterns. Laser parameters: pulse repetition rate, feedrate and number of passes of the laser beam were varied when machining different tracks to find the optimum conditions. As described earlier, the process uses a mask projection technique to shape the beam which is then followed by 10:1 reduction optics that reduces it to the final feature size at the sample surface. The beam focal point was determined for each sample by moving the sample vertically to achieve the best machining with maximum depth and sharp edge quality. Different masks were then used to create different patterns for electroless plating as described in later sections. The masks used in the first experiments were prepared using ~250 μm thick brass sheet. The patterns were designed using AutoCAD software and transferred to the brass sheet using photolithography and a chemical etching process. In the later experiments more detailed patterns were created by a collaborator at Imperial College on brass sheet using laser machining, in this case thinner brass sheet (~120 μm) was used due to the ease of laser cutting. An example of a chemically etched mask is shown in Figure 68.

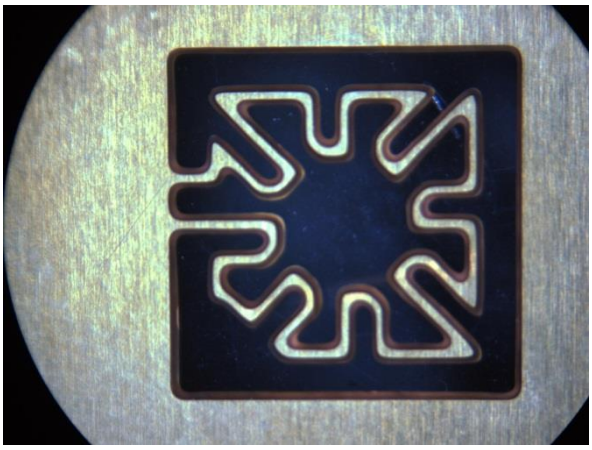

Figure 68 Example of a brass mask (approximately 10 mm x 10 mm)

6.4.3 Electroless Plating Process

After machining, the LTCC surface was still covered in resist except where the patterns were formed. To activate the LTCC surface, the samples were immersed in pre-dip and Sn/Pd catalyst for 2 minutes and then rinsed thoroughly with deionized water. The dry film photoresist was then removed from the specimens by dipping the samples in acetone (99 % Fisher Scientific). After removal of the photoresist, the samples were rinsed with deionized water and then electroless copper plated for one hour using the same electroless bath described in section 2.3.4. Then the LTCC samples were rinsed with deionized water and dried. Figure 69 summarises both the excimer laser machining process and the plating process.

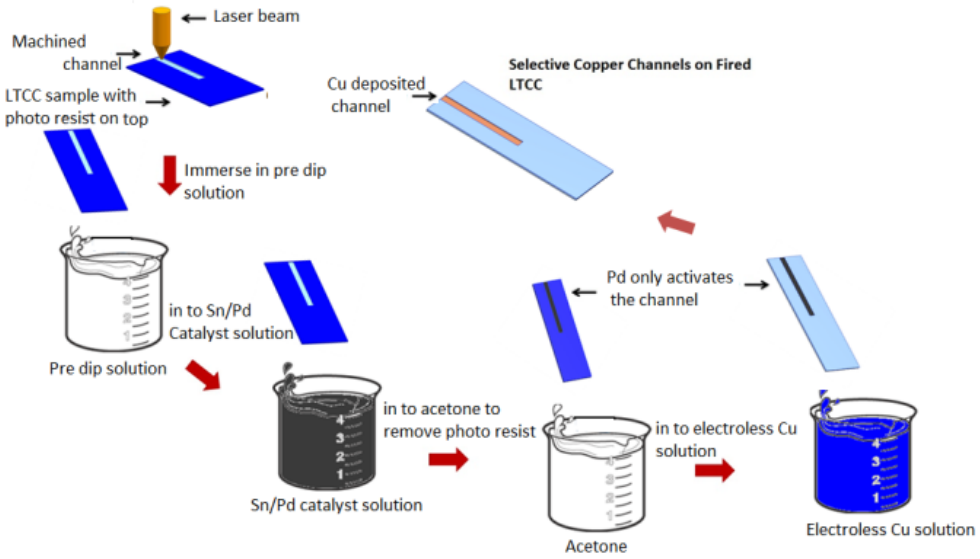

Figure 69 Process steps of the selective electroless copper deposition

6.4.4 Surface Characterization of Machined and Plated Tracks

The depth and surface roughness of machined tracks before and after copper deposition were measured using a Talysurf CSI 2000 optical measuring system. The measurements were taken with a non-contact high resolution gauge CLA 300. The measuring speed, spacing and length were set at 200 µm/s, 1 µm and 2 mm respectively. The resistance of deposited tracks was measured with the four point probe method over a length of 3 mm using a Keithley 580 microohmmeter.

6.5 Results and Discussion

6.5.1 Absorptance of LTCC in the Laser Operating Wavelength

The operating wavelength of the excimer laser used in this study is 248 nm. To examine the absorptance of this wavelength by the fired LTCC, the UV-VIS absorption spectra were obtained using a Lambda Bio 40 UV-VIS spectrophotometer. Figure 70 shows the UV-VIS spectrum of the fired LTCC sample taken between 242-349 nm wavelengths. The percentage of the total reflectance of the LTCC solid sample was measured and percentage

absorptance was calculated (% Absorptance = 100% - % reflectance) assuming that the remaining radiation was absorbed by the material. At the KrF excimer wavelength this indicated that 57.9 % of the laser radiation was absorbed by the LTCC material. The above mentioned properties of the LTCC material allow the implementation of excimer laser machining.

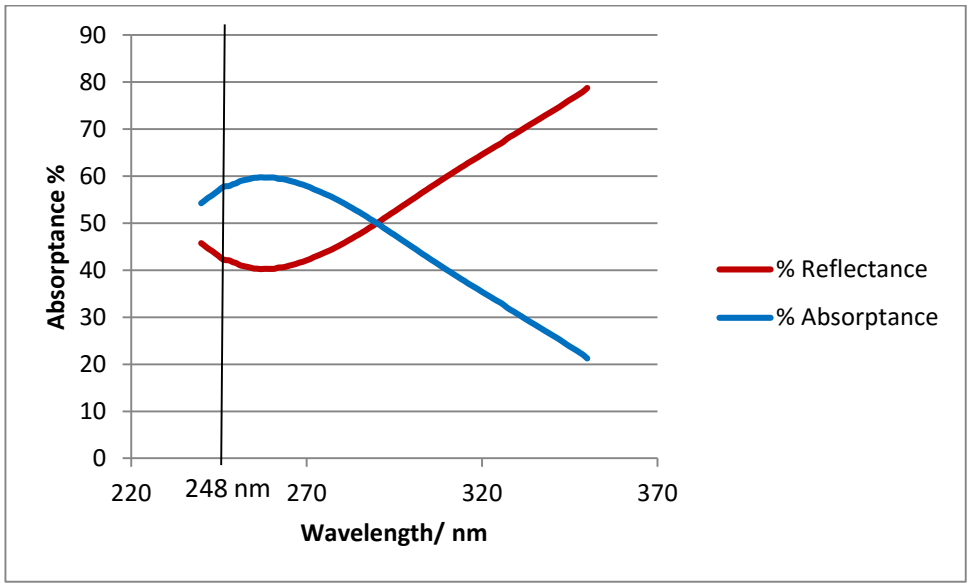

Figure 70 UV-VIS absorption spectra of LTCC

6.5.2 Calculating the Offset between the Camera and the Laser Head

The excimer laser system is computer controlled and consists of a working stage, laser head and an alignment camera. The working stage can be moved in X, Y, and Z directions. The machined features can be examined through the camera and machining can also be carried out on a particular position of the sample using the alignment camera as illustrated in Figure 71. The precise distance between the camera and the laser head should be found in order to align the camera. To do this, the working stage was first moved to the home position. Then a single feature was machined on a particular position of the sample surface. The coordinates (X, Y) of the initial machining position were recorded. Then the sample was moved to the alignment camera where the machined feature was aligned with the cross-hair of the alignment camera which could be seen in the computer monitor. The X and Y coordinates (X', Y') were then recorded.

The offset between camera and the laser head was calculated as follows,

Offset = (X'-X, Y'-Y) = ΔX, ΔY

When a feature was to be machined on a particular location of the sample, this location was first aligned with the camera and values for X'' and Y'' obtained. The new machining coordinates were then calculated by adding the ΔX and ΔY values.

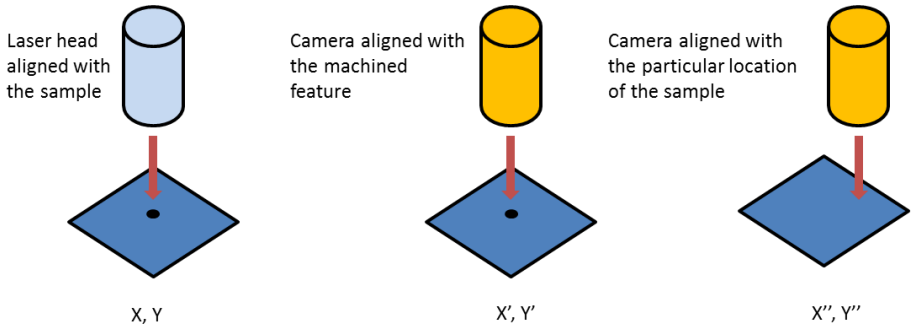

Figure 71 Illustration of calculation of offset between the camera and the laser head

6.5.3 Determination of the Laser Machining Focal Point

The maximum power per unit area of the excimer laser beam is achieved at the focal point of the laser beam. At this point the laser beam is at its smallest diameter and capable of giving maximum irradiance on the processed material [147]. The focal spot of the laser beam was determined by machining a series of tracks on a glass slide covered with permanent marker ink and for each track changing the work piece vertical position. A square mask (10 mm x 10 mm) was used to machine 10 mm long tacks. The vertical value was measured relative to the stage home position. By observing the quality and the size of the machined features, the optimum position was determined. The maximum depth of the machined tracks was measured using the Talysurf CSI 2000 optical measuring system. Three measurements were taken along the track and the mean depth was calculated. Figure 72 shows the change in mean depth against vertical position of the work piece. The mean depth came to a peak value at 6.4 mm and then started to drop back.

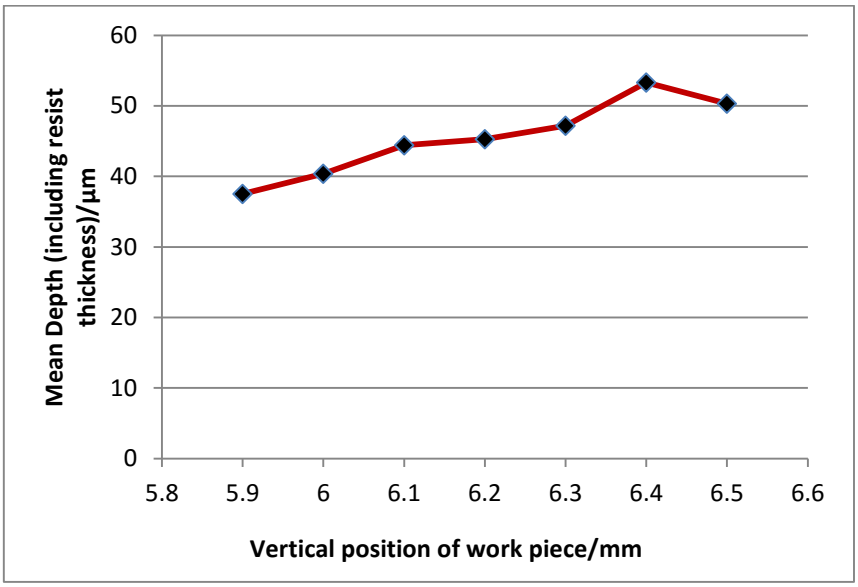

Figure 72 Change in machined depth with vertical position of the workpiece

Figure 73 shows the change in the width of the tracks with vertical position of the work piece. At 6.4 mm the width came to a minimum value. After consideration of the maximum depth and the width of the track 6.4 mm was taken as the focal point of the laser beam.

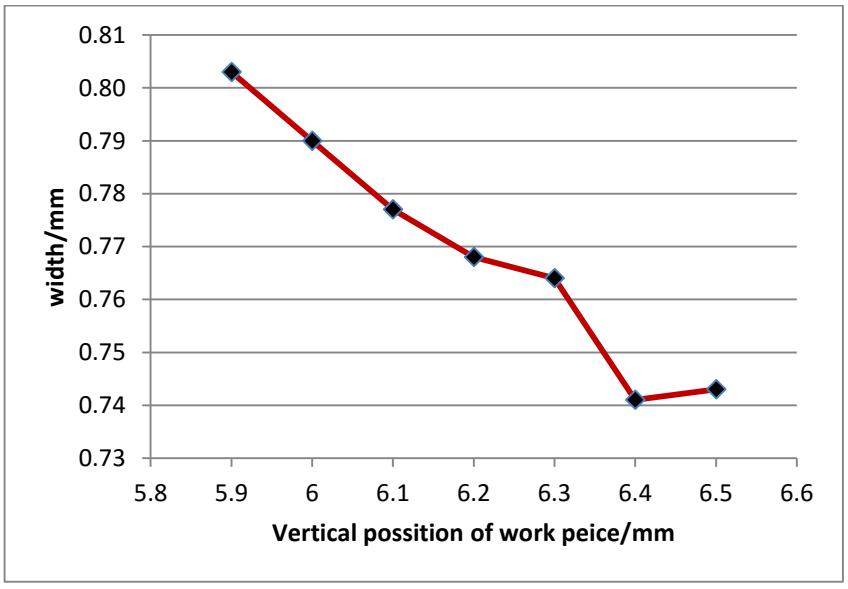

Figure 73 Change in width of the track with vertical position of the workpiece

As the vertical position recorded at the focal point of the laser beam was that of the sample stage, the actual focal position at the sample surface would depend on the sample thickness. As the test piece thickness was known, with the value obtained in the previous experiment,

it was possible to calculate the approximate focal position on other samples with known thickness. However, the focal point of the laser beam for each sample should be determined to achieve the optimum value. Kapton film is very sensitive to the excimer laser beam and a series of small machined features could be compared in terms of their edge quality and size. To find the precise focal point of the laser beam on each LTCC sample, first kapton adhesive tape film was applied and a series of circular features was machined at different vertical position of the work piece. Figure 74 shows several machined features on a Kapton film at various vertical positions around the focal point. Thermal damage caused by an unfocused beam could be clearly seen in the image. A sharp edge quality was observed on the feature machined at the focal point of the laser beam. When machining on the LTCC sample the coordinates of the vertical position of the focal point of the beam were changed by adding the thickness value of the LTCC sample and the Kapton film. Thickness of the LTCC sample was calculated by focusing the camera on both the LTCC and kapton surface and taking the difference between vertical positions.

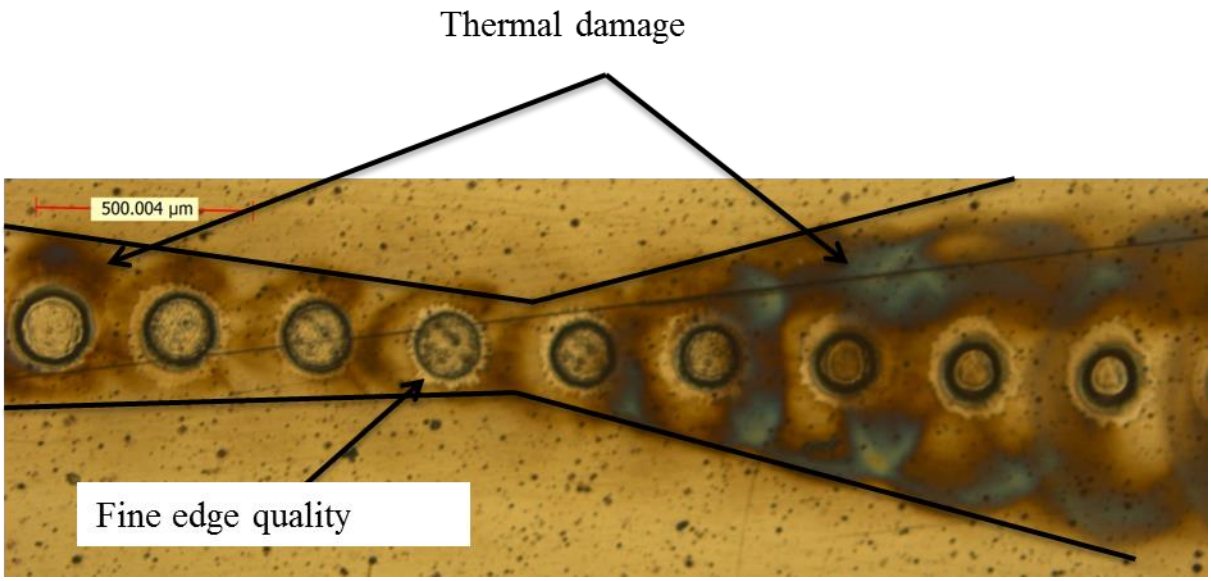

Figure 74 Features machined at various positions around the focal point

6.5.4 Effect of Laser Parameters on Efficiency of Machining

A square mask with dimensions 10 mm × 10 mm was used to form a square laser spot (approx. 1 mm x 1 mm) on the sample surface. During machining, the sample stage was

moved horizontally for 10 mm to create 10 mm long tracks. The feedrate, repetition rate and number of passes were changed to identify the optimal conditions for laser machining of the LTCC.

As an initial experiment, the laser parameters were varied according to Table 11 and machining depth and roughness (Ra) values were determined using the Talysurf CSI 2000 optical measuring system for three profiles taken across the width of the track. The pulse energy of the laser was set at 250 mJ per pulse (laser output). The number of shots per area was calculated according to Equation 6.1. The length of the laser spot was taken as 1 mm for the calculation purposes as the dimensions of the mask were 10 mm x 10 mm with a demagnification factor of 10, however, the track width was only 0.74 mm, so this may indicate in practice a lower value for the beam length.

$$Number\ of\ shots\ per\ area = \frac{R \times 60 \times N \times L}{F} \quad \ldots\ldots\ldots\ldots\ldots\ldots \quad 6.1$$

Where, L is the length of the laser beam in the direction of the beam's movement in mm

F is feedrate in mm/minute, R is the repetition rate in Hz and N is the number of passes of the laser beam.

Table 12 Change in machining depth with laser parameters

Track	No. of passes of the laser beam	Feedrate/ mm/minute	Repetition rate/ Hz	Total no. of shots per area	Maximum depth/ µm	Ra/ µm
a	10	10	5	300	8.3	1.16
b	20	10	5	600	10.6	1.86
c	20	10	10	1200	38.8	4.19
d	20	10	15	1800	68	4.68
e	20	5	5	1200	37	2.84
f	30	5	5	1800	46.9	3.45

Table 11 shows the range of parameters investigated. Total number of shots was calculated using Equation 6.1 considering total passes of the laser beam, feed rate and the repetition rate. Tracks a and b were machined with equal feed rate and repetition rate values and the number of shots per area was increased by increasing the number of passes of the laser beam on the sample. The maximum depth and the roughness increased with the number of shots per area. Tracks b, c and d were machined with the same feed rate and number of passes and the repetition rate was increased. It was found that the maximum depth and the Ra value increased with the repetition rate. Tracks c and e were machined with equal number of shots per area, but with different repetition rate and feed rate values. These two tracks had very similar maximum depth values however, the Ra values increased dramatically in the track machined with higher repetition rate. A similar relationship was observed in tracks d and f.

Further experiments were carried out to find the optimal conditions for the laser machining process using different feed rate and repetition rate values and different number of passes of the laser beam in order to achieve better electroless copper coating on machined tracks. In these experiments, the dry film photoresist (approx. thickness 40 µm) was applied on both sides of the single layer LTCC sample for subsequent electroless copper plating. Pulse repetition rate (R = 5 Hz) and number of passes of the laser beam (N = 20) were kept constant while the feed rate (F) was changed from 10 mm/minute to 2 mm/minute respectively. Depth profile measurements of the machined channels were taken before and after the copper plating process. However, in order to do this, the photoresist had to be left on the sample when measuring the depth before copper plating and the profile results and the maximum depth measurements therefore include this additional thickness. Figure 75 shows the change in maximum machined depth of the tracks with feed rate. The rate of machining decreased as the feed rate increased. The track machined with the same laser parameters (F = 10, N = 20 and R = 5 Hz) in the previous experiment (track b in table 11) showed approximately the same maximum depth when the resist thickness is taken into account.

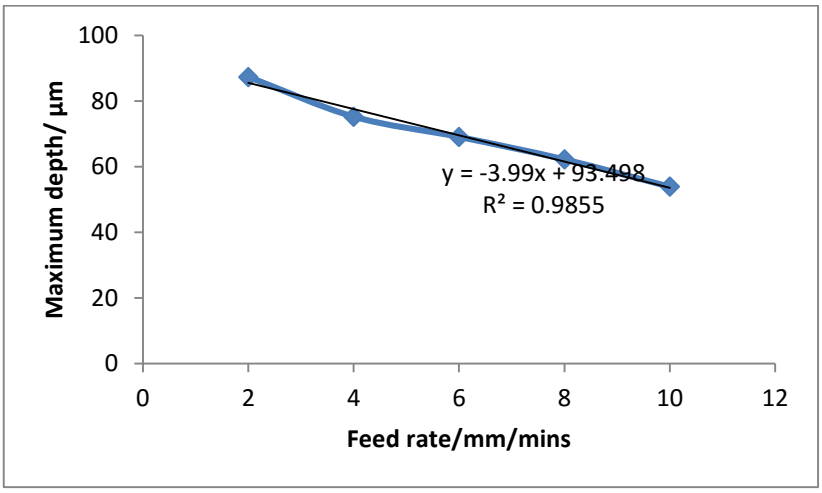

Figure 75 Variation of maximum depth with feed rate

A further set of tracks was machined using constant feed rate (5 mm/minute) and number of passes of the laser beam (20). The repetition rate was changed from 5 Hz to 15 Hz. Figure 76 shows the change in maximum depth of the machined track with repetition rate. The maximum depth showed a strong linear relationship ($R^2 = 1$) with repetition rate over the range investigated.

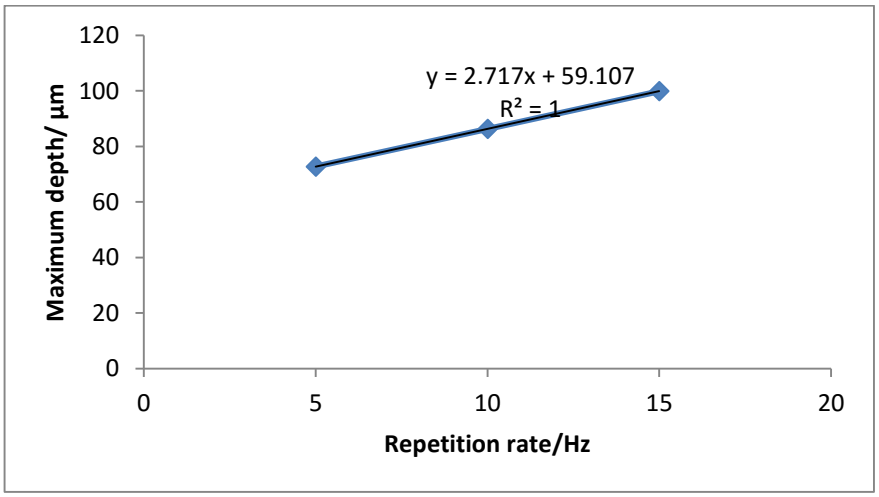

Figure 76 Variation of maximum depth with repetition rate

Tracks were also machined with constant repetition rate (5 Hz) and feed rate (2 mm/minute) and the number of passes of the laser beam was changed from 5 to 25. Figure 77 shows the change in maximum depth with the number of passes of the laser beam. Here the first three points showed a linear relationship between maximum machined depth and number of

passes of the laser beam, which might be expected as each subsequent pass removes more material. However, the slope of the curve decreased with further passes of the laser indicating a reduced rate of material removal and this could be due to loss of focus of the laser beam when machining deeper and difficulty in ejecting ablated material from a deeper trench.

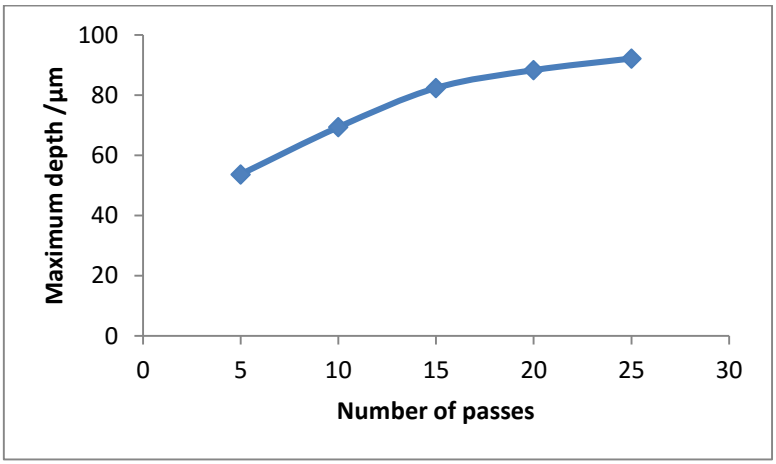

Figure 77 Variation of maximum depth with number of passes of the laser beam

Figure 78 shows the relationship between maximum depth and the number of shots per area when using different laser parameters. Even with the same number of shots per area, the repetition rate curve showed higher maximum depth of the tracks compared to the curves of the feed rate and the number of passes of the laser beam.

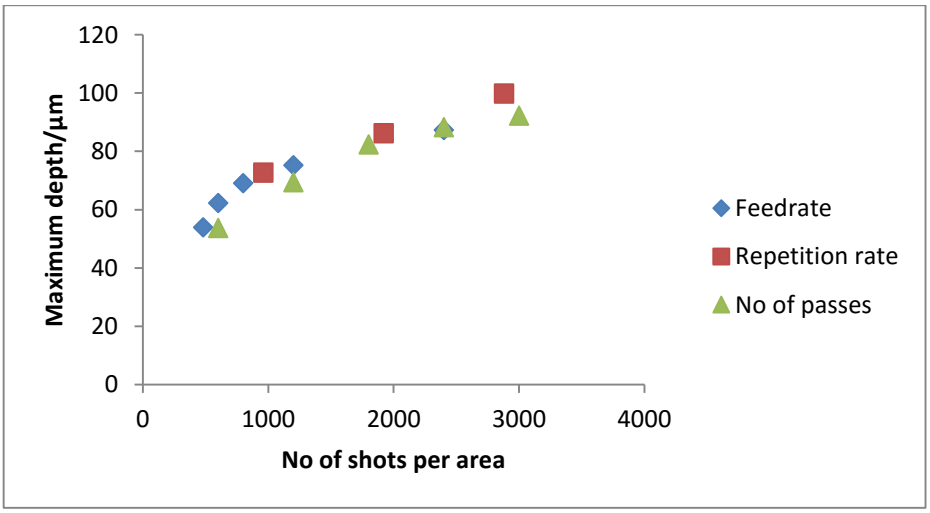

Figure 78 Variation of maximum depth with number of shots per area

6.5.5 Effect of Laser Parameters on Surface Roughness (Ra) of Machined Tracks

For all 3 parameters, the surface roughness generally increased with number of shots per area compared to the surface roughness of the control sample (Ra = 0.688 µm) and reached a plateau / or decreased a little after 2000 (Figure 79).

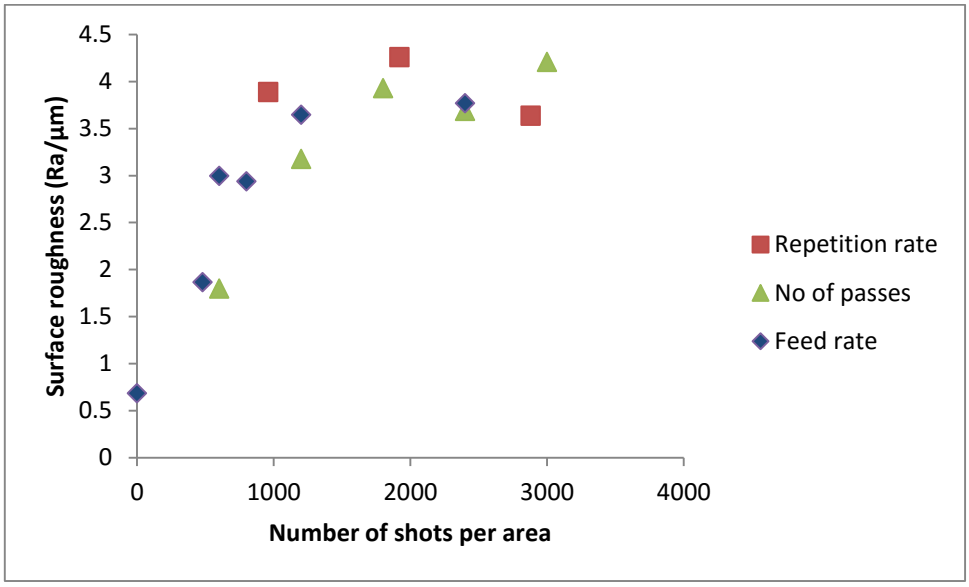

Figure 79 Variation of surface roughness with (Ra) with number of shots per area

Excimer laser machining also modifies the LTCC surface and therefore the Ra values of the excimer laser machined surface and NaOH treated surface were compared. The LTCC samples treated with 4M NaOH solution for 24 hours typically showed Ra values below 2 µm. With laser machining, this value was exceeded when the number of shots was greater than 1000.

6.5.6 Electroless Copper Plating of Machined Lines

Figure 80 shows the electroless copper deposited on two machined tracks according to the procedures described in section 2.2 and 2.4. Both tracks were machined with a feed rate of 10 mm/minute and a repetition rate of 5 Hz. The left hand track was machined with 15 passes of the laser beam and the right hand track was machined with 20 passes. Copper

deposits were successfully achieved selectively only on the walls and base of the tracks with clearly defined edges (Figure 80). The 2-D profile of the two tracks (Figure 80 (b)) shows that these tracks maintained the channel structure even after copper deposition.

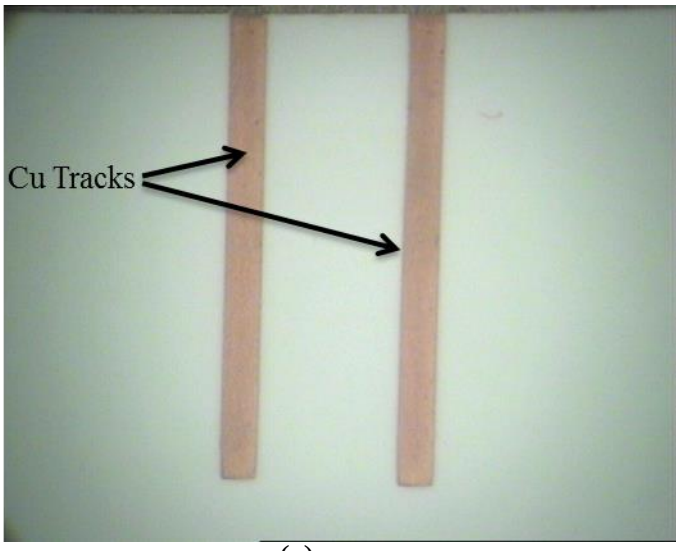

(a)

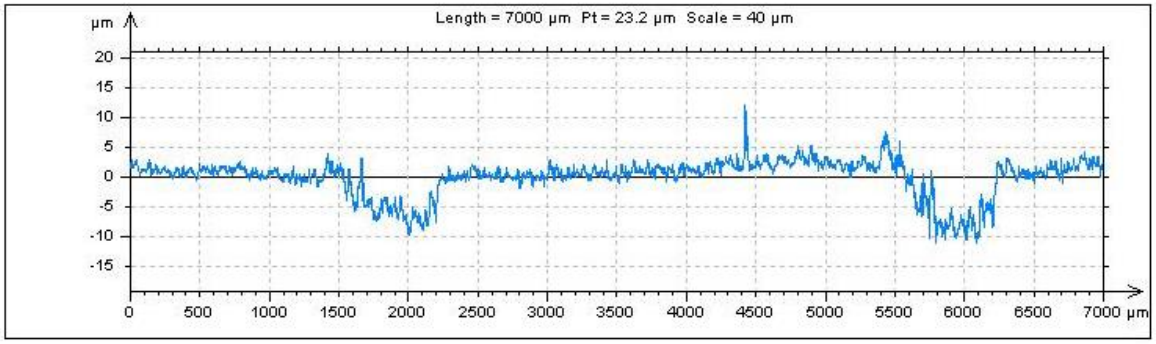

(b)

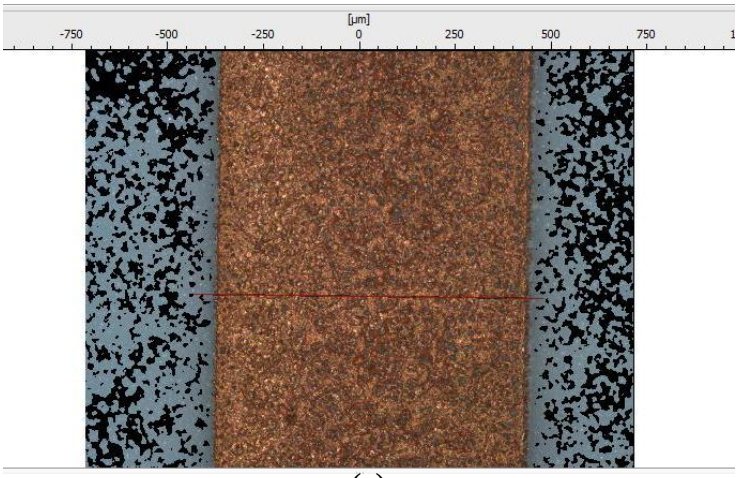

(c)

Figure 80 Electroless copper deposits on machined tracks (a) camera image, (b) 2-D profile across the two tracks and (c) optical micrograph

6.5.7 Effect of Laser Parameters on Electroless Plating and Resistance of Machined Tracks

The excimer laser machined tracks prepared using different laser parameters were subjected to subsequent electroless plating according to the process described in section 3.4.3. In this experiment, all 3 samples were plated in the same pre-dip, catalyst and electroless copper bath and for equal plating periods to ensure consistency.

All 3 samples (Figure 81) showed that the copper was only deposited on the machined path, again showing the selective copper deposition. Figure 81 (a) shows the copper deposits on tracks machined with different number of passes of the laser beam. Figure 81 (b) shows the copper deposits on tracks machined with different repetition rate. The resistance of deposited copper tracks were measured and the results are shown in Table 12. In contrast to the tracks machined with a different number of passes of the laser beam, the tracks machined with different repetition rates showed a decrease in resistance with the increase in repetition rate. It was also noticed that the resistance increased slighly with the number of passes of the laser beam. Figure 81 (c) shows the copper deposits on tracks machined with different feed rates. The tracks machined with different feed rates showed relatively large resistance values compared to the tracks machined with different repetition rate and number of passes of the laser beam. The track machined with feed rate of 10 mm/minute showed very large resistance (5 Ω) and the plating results were poor.

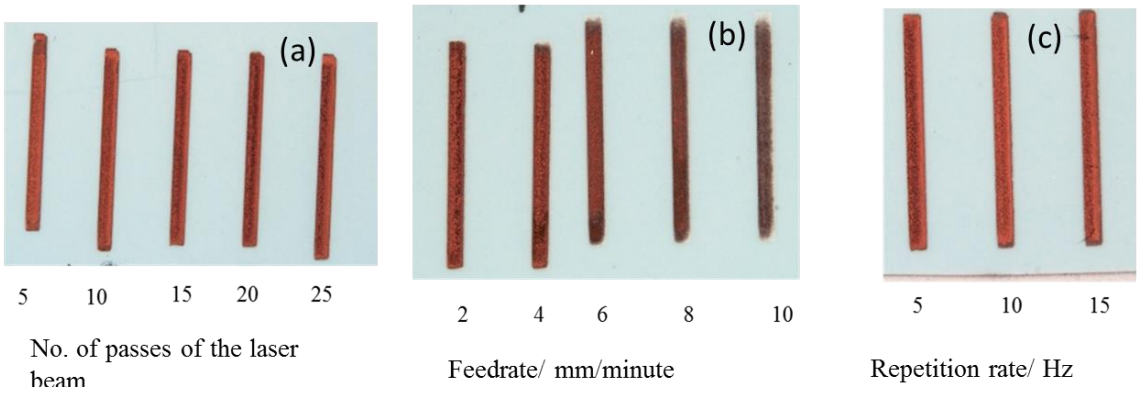

Figure 81 Electroless Cu deposits on LTCC tracks machined with (a) different number of passes of the laser beam (feed rate 2 mm/minute, repetition rate 5 Hz), (b) different feed

rate (number of passes 20, repetition rate 5 Hz) and (c) different repetition rates (number of passes 20, feed rate 5 mm/minute)

Table 13 Resistance of Cu tracks on LTCC surfaces machined with different number of passes of the beam

Number of passes	Resistance/ mΩ	Repetition Rate/ Hz	Resistance/ mΩ	Feed rate/ mm/minute	Resistance/ mΩ
5	35	5	35	2	55
10	35	10	34	4	58
15	48	15	30	6	54
20	45			8	102
25	45			10	5 Ω

The resistance values were plotted against the number of shots per area and shown in Figure 82. The last point of the feed rate series was not included in the graph as the resistance value was 5 Ω. The resistance values were different for the tracks machined with different laser parameters, but with similar number of shots per area. The lowest resistance values were observed for the tracks machined by changing the repetition rate. It was also noticed that the tracks machined with different feed rate values showed relatively larger resistance values.

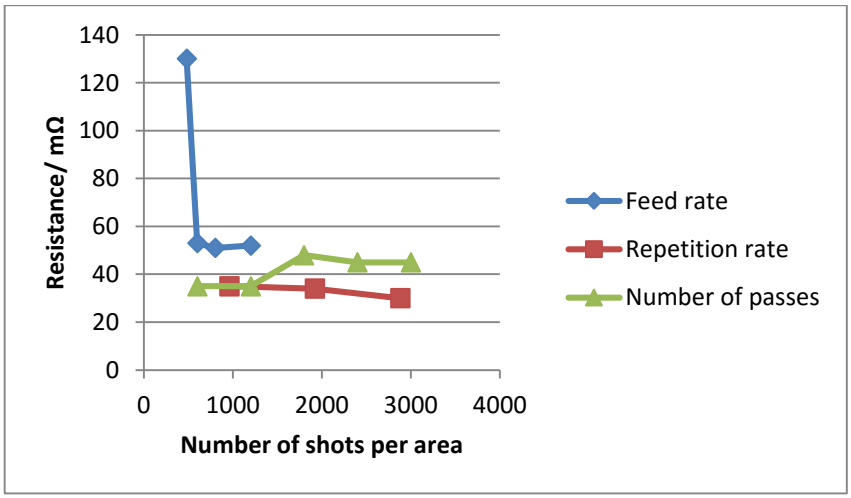

Figure 82 Plated track resistance vs number of shots per area

6.5.8 Characterization of Copper Deposits on Machined Tracks

Figures 83, 84 and 85 show the 2-D profiles of tracks machined with a feed rate of 2 mm/minute, repetition rate of 5 Hz and number of passes of 20 (3000 shots per area), a feed rate of 2 mm/minute, repetition rate of 5 Hz and number of passes of 25 (3750 shots per area) and feed rate of 5 mm/minute, repetition rate of 15 Hz and number of passes of 20 (3600 shots per area) respectively, before and after the copper plating process. These tracks represent the highest number of shots per area for each sample. The profiles of the unplated tracks were taken while the photoresist was still attached to the sample. The track in Figure 83 (a) shows vertical side walls and a curved base with some roughness. When copper was deposited on to this track (Figure 83 (b)) the track maintained its channel structure even after the copper plating process. However the width of the track decreased compared to Figure 83 (a) showing more plating on the edges of the track. The average Ra value (2.43 µm) of the plated track showed a relatively low value compared to the Ra value (3.77 µm) of the track before plating. The Ra value of the machined LTCC showed a higher value compared to the Ra values of the NaOH treated LTCC samples. The Ra value of the copper deposits on laser machined LTCC samples also showed higher Ra values compared to the copper deposits on NaOH treated LTCC samples. The maximum depth of Figure 84 (b) decreased compared to that of Figure 83 (b) and showed more copper on the track. This suggests that the plating rate increased when using a higher number of shots of the laser beam per area. It was noted that the left side of the track was machined deeper than the right side of the track and this was also observed after the copper plating process. The average Ra value (2.96 µm) of the plated track showed a relatively low value compared to the Ra value (4.21 µm) of the track before plating. The right hand side of the track in Figure 85(a) machined deeper and maintained its channel structure even after the copper plating process. In contrast to the other two tracks, the average Ra value of the plated track (4.32 µm) showed a relatively higher value compared to the Ra value of the track before plating (3.64 µm).

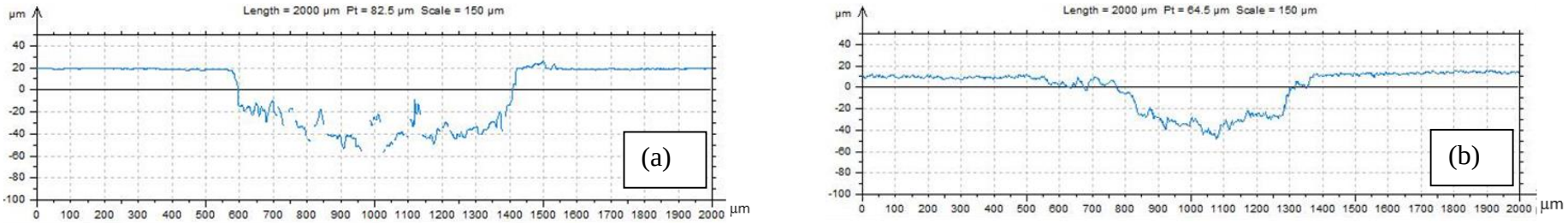

Figure 83 2-D profile of the machined track (feed rate: 2mm/minute, rep. rate: 5 Hz, number of passes: 25) (a) before and (b) after Cu deposition

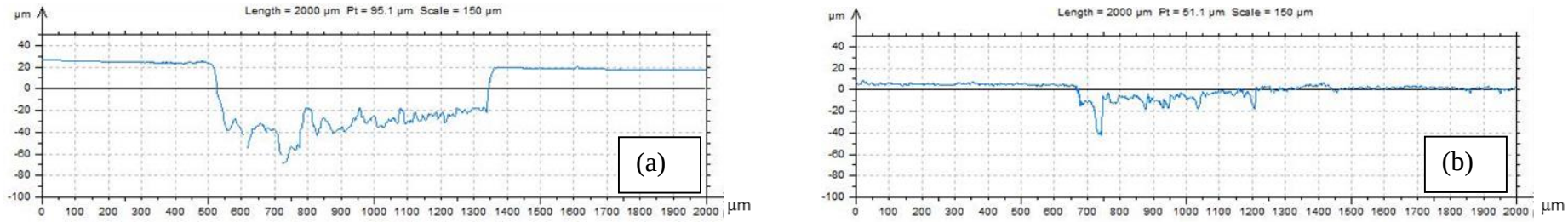

Figure 84 2-D profile of the machined track (feed rate: 5mm/minute, rep. rate: 15 Hz, number of passes: 20) (a) before and (b) after Cu deposition

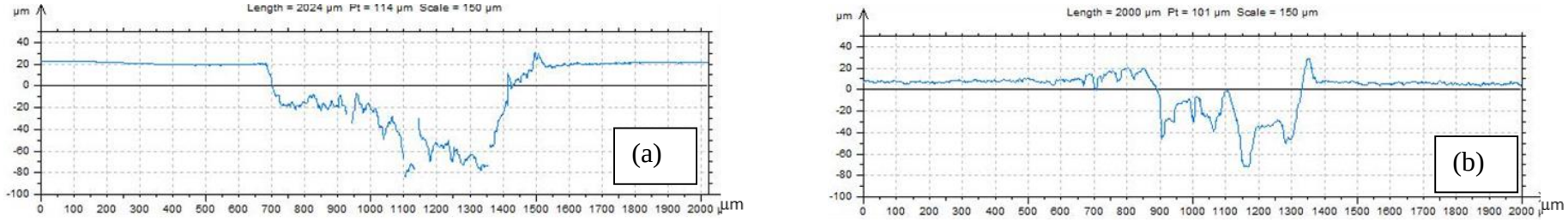

Figure 85 2-D profile of the machined track (feed rate: 5mm/minute, rep. rate: 15 Hz, number of passes: 20) (a) before and (b) after Cu deposition

The 2-D profile of the tracks demonstrated that one side of the tracks machined using different repetition rate and number of passes of the laser beam, showed relatively higher maximum depth compared to the other side of the track. The possible reason for this could be the misalignment of the laser beam with the mask or beam non-uniformity. The plating rate decreased when using relatively higher feed rate values (last track in Figure 81). The copper plated track machined using a very similar number of shots per area, but changing the number of passes of the laser beam, (first track in Figure 79), showed relatively higher plating rate. It can be suggested that poor Sn/Pd catalyst adsorption may have been responsible for the lower plating rate. The change in material removal mechanism could be a possible reason for the difference in catalyst adsorption. A higher resistance value was also observed for the last track in Figure 81 (b) which was related to the poor plating.

6.5.9 Creation of Circuit Patterns

Using the laser machining and electroless plating process a complete circuit pattern was prepared. When producing the circuit pattern, a ~2.3 mm x 2.3 mm square mask was used to give an ~230 µm x 230 µm spot at the surface. This was used to machine the conductor lines by moving the sample stage using a CNC program to form the required circuit pattern, which was machined using a repetition rate and feed rate of 20 Hz and 5 mm/min respectively and with five passes of the laser in order to increase the depth. After preparation of the tracks, a ~10 mm x 10 mm square mask was used to directly machine square connection pads for component interconnection. Figures 86 (a) and 86 (b) show the optical micrographs of a conductor pad and a conductor line respectively after electroless copper deposition. These images indicate the uniformity of the copper deposits with well-defined edges and the highly selective nature of the deposition only on the machined surface. The widths of the conductor lines showed agreement with the expected beam spot size and confirmed that the machining was done at the beam focus position. The thickness of the copper was estimated to be 3 µm according to the plating rate provided in the supplier's data sheet (0.5 µm in 10 minutes). In this particular application, the number of shots per area of the laser was kept to a minimum where it was sufficient enough to remove the photoresist and roughen the surface for better adhesion.

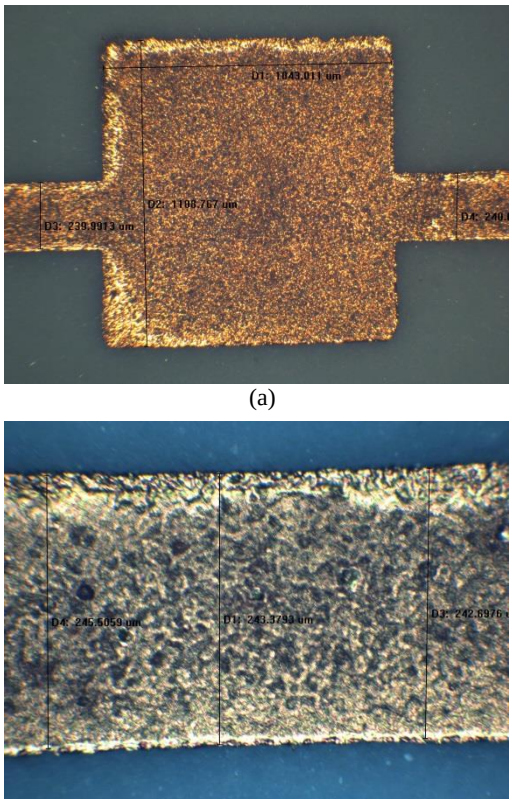

(a)

(b)

Figure 86 Optical micrographs of the copper deposits on fired LTCC (a) conductor pad (b) conductor line

Figure 87(a) shows a complete circuit pattern prepared in this way, again highlighting the selectivity of the surface activation and copper deposition. To assemble a functional device, lead free solder paste was applied using a syringe to the copper connection pads and components were manually placed. The sample was then passed through a conventional reflow oven to form a complete circuit (Figure 87(b)). The circuit was electrically tested with an input voltage of 4.5 V and the flashing LED indicated the presence of continuous and conductive copper deposits and effective solder joints.

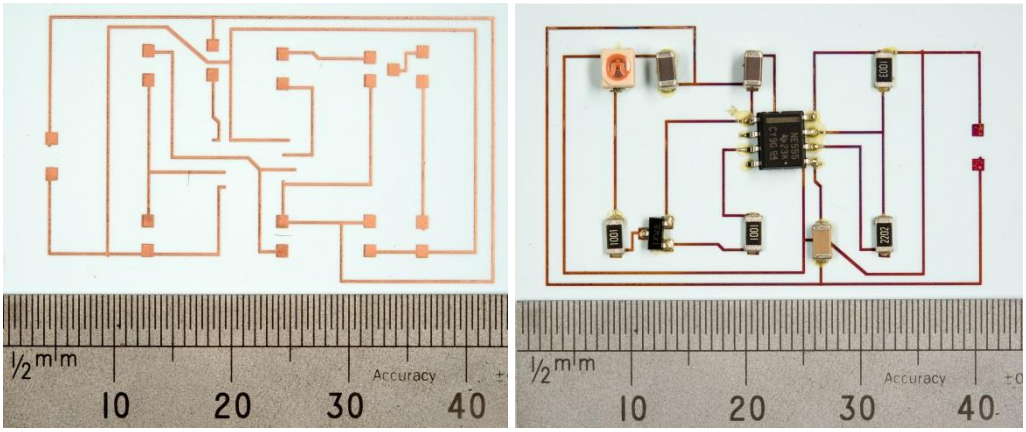

(a) (b)

Figure 87 (a) Deposited copper on circuit pattern, (b) Complete circuit after component assembly

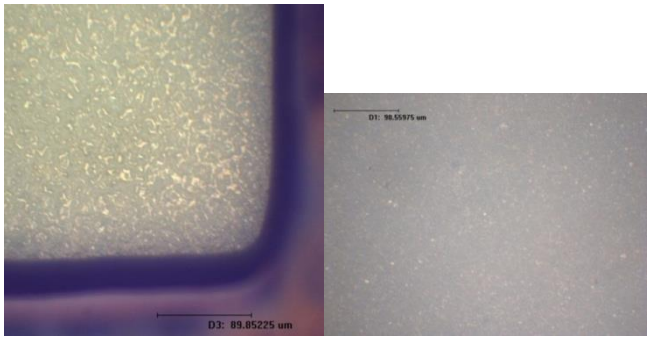

(a) (b)

Figure 88 Optical micrographs of LTCC surfaces (a) after excimer laser irradiation, (b) plain LTCC

Figure 88 (a) shows an optical micrograph of the LTCC surface with photoresist layer after excimer laser irradiation. The photoresist was cleanly machined away which is to be expected for this high energy laser source interacting with a polymer. The machining of the LTCC was significantly slower and the surface morphology of the irradiated surface showed a relatively rougher surface compared to the original plain LTCC surface (Figure 88 (b)). From the previous study, it was found that the KrF excimer laser has the capability to remove the material from the LTCC surface to create a trench. At the same time it introduces a roughness to the machined surface that can be beneficial for metal to substrate adhesion. SEM images were taken on the machined surface at several magnifications and shown in Figure 89. As the excimer laser beam hits, heating and melting occurs on the LTCC surface. At the current output energy of 250 mJ/pulse, the ablation takes place due to the melting and resolidification of the material [158]. The laser ablation was uniform over the surface and showed re-solidified lumps and the surface morphology was different from the flake like surface obtained from the NaOH pre-treatment. The magnified SEM

image (Figure 89) showed micro-cracks around the re-solidified material and this is thought to be due to the thermal stress that occurred during the machining process. It was also noticed that the material was removed more at some locations on the surface. As mentioned previously, the LTCC material consists of different phases and it is possible that some of the phases of the material are removed more readily with the excimer laser ablation.

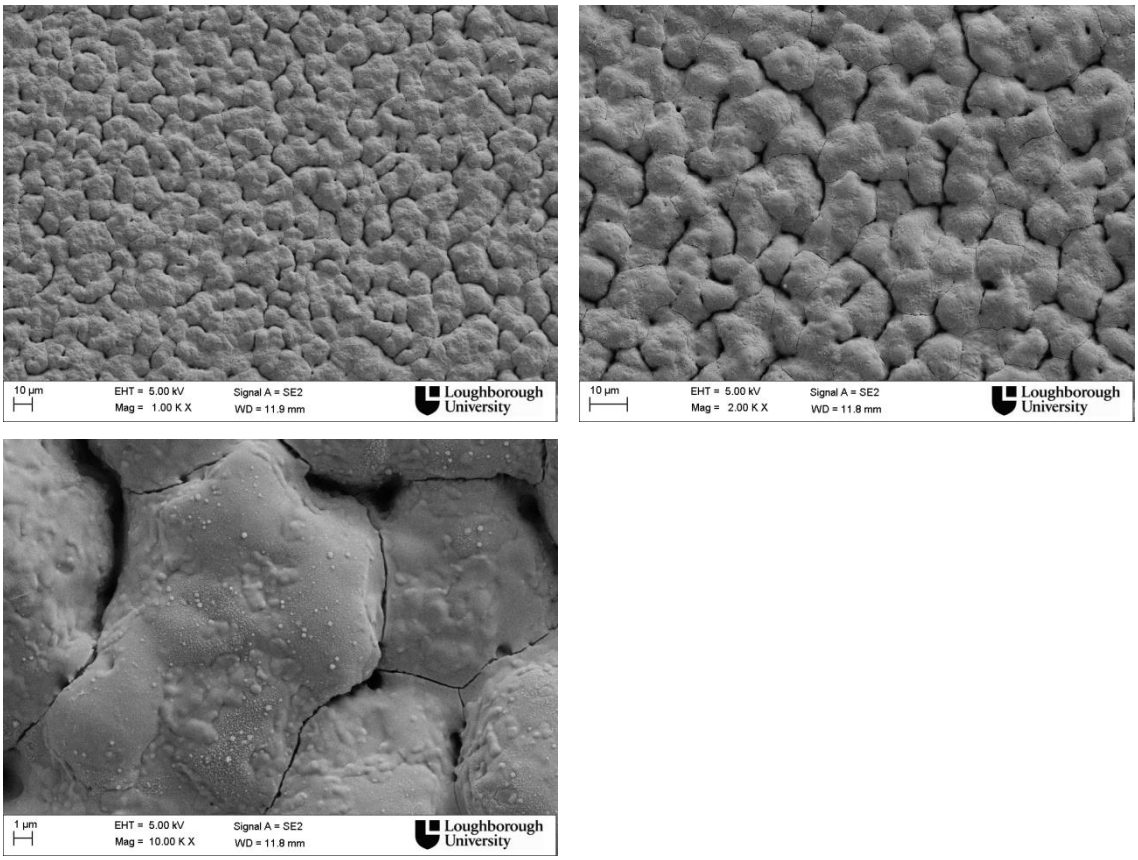

Figure 89 SEM images of the laser machined LTCC at different magnification

6.5.10 Inductor / Capacitor Fabrication

In this work, the projection technique of excimer laser machining was used to machine planar components on fired LTCC using designed masks. The great advantage of using projection optics is that it enables complex patterns to be created without the need to raster a beam spot across the surface, with associated limitations due to the spot dimensions: this enables features below 10 µm in size to be prepared. Furthermore, as the size of the final machined features is reduced by ten times from that of the mask, complex patterns can be prepared from masks that are relatively easily fabricated using standard lithographic or other micromachining techniques.

To create the inductor and capacitor designs, two masks were used. Initially, one was prepared by chemically etching a brass sheet, the second mask that was used for capacitor design was prepared by laser cutting of a brass sheet. The capacitor was designed with dimensions of 10 mm x 10 mm (Figure 90 (a)) and the radius of the inductor design was ~4.4 mm (Figure 90 (b)). These masks were then used to machine matching structures in the LTCC surface. In this case, the samples were exposed to 100 shots of the laser beam without moving the stage and using a repetition rate of 10 Hz.

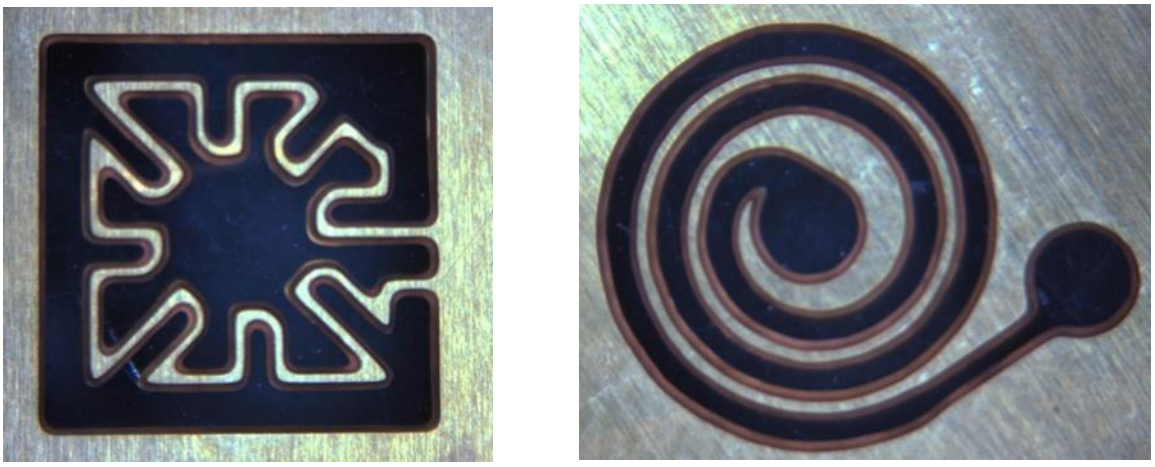

(a) (b)

Figure 90 Masks (a) capacitor and (b) inductor

Using the method described in section 6.4, several patterns of inductors and capacitors were prepared on LTCC. Figures 91 (a) and (b) show the initial structures machined into the photoresist on the LTCC surface.

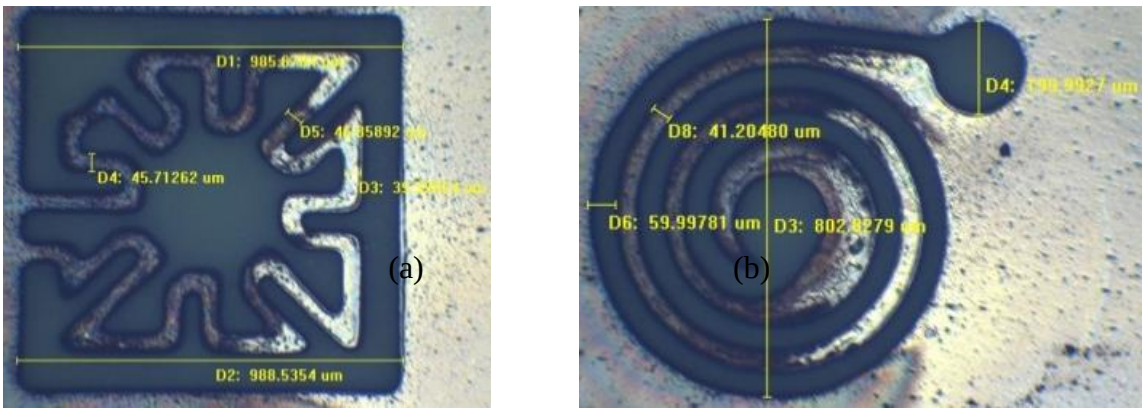

Figure 91 Optical micrographs of machined features in photoresist on LTCC (a) capacitor and (b) inductor.

These features had identical shapes to the projection masks confirming the reproducibility of the mask projection technique. As seen earlier for the circuit patterns, it was found that

the electroless copper deposition was highly selective such that the structures were accurately reproduced (Figures 92 (a), (b), (c)). The overall size of the deposited capacitor was approximately 1 mm x 1 mm and showed the expected 10:1 size reduction from the original mask. The gap between the deposits was below 60 μm and the minimum dimension of the deposits was below 50 μm.

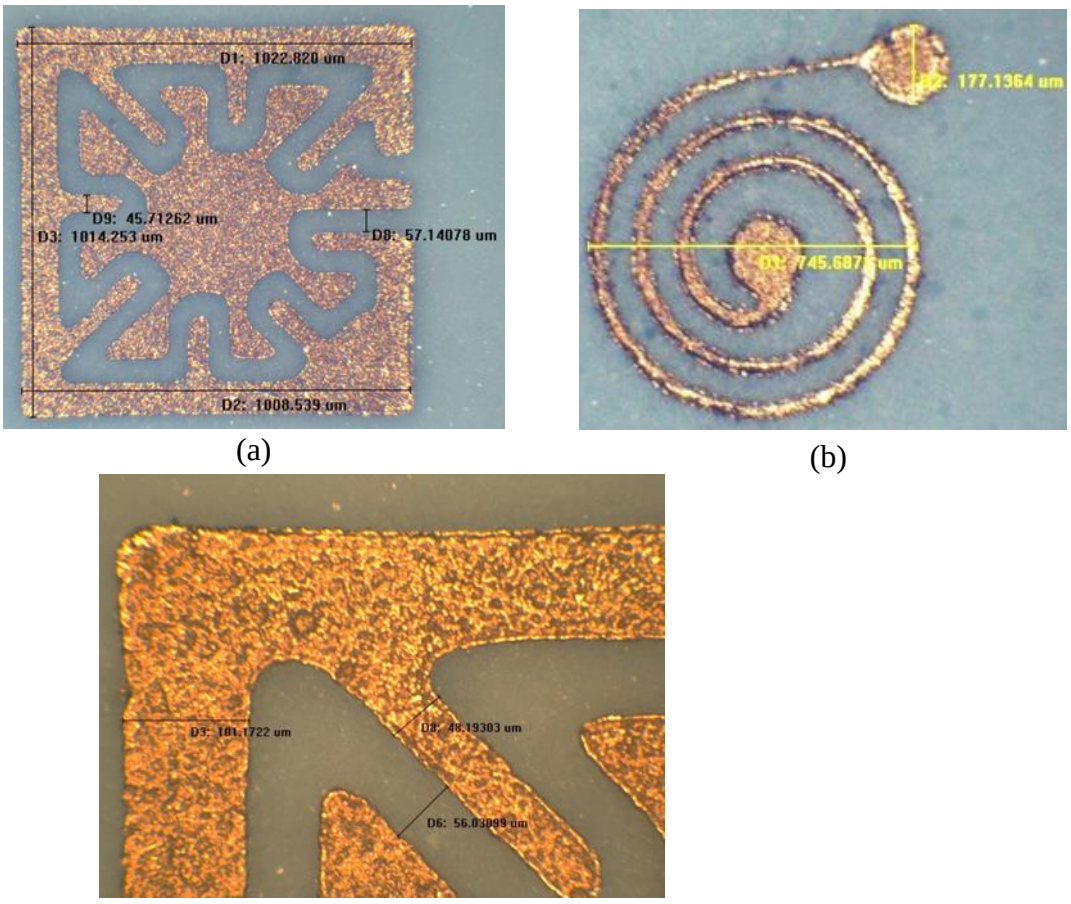

(a) (b)

(c)

Figure 92 Optical micrographs of electroless deposits on machined features (a) capacitor, (b) inductor and (c) magnified image of the capacitor

6.5.11 Resonator Design

To create a resonator structure, a capacitor and inductor had to be machined on opposite sides of the LTCC sheet and interconnected. In this approach, two micro vias were created on the green LTCC which was then laminated and fired by collaborators at Imperial College so that these vias were located in the LTCC after the lamination and firing process. A brass mask with a pseudo-fractal capacitor design was used to machine the capacitor on one side of the LTCC and a spiral inductor was machined on the other side of the LTCC sample as illustrated in Figure 93. These were also supplied by Imperial College. When machining

the features, it was essential to align the capacitor and inductor with the two micro vias which were pre-created on the LTCC sample to achieve the electrical connection.

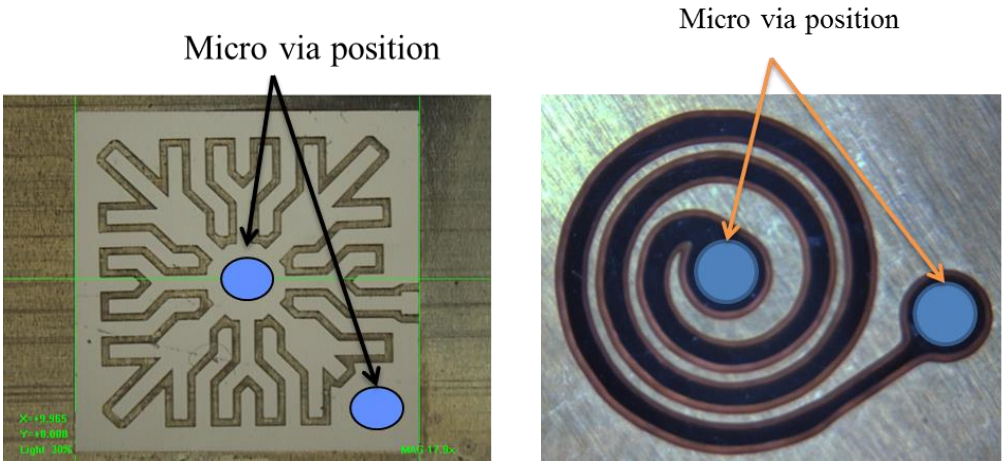

Figure 93 Micro via position on capacitor and inductor (images of masks)

To align the via holes with the machined features, the optical camera system of the excimer laser was used. In the first experiments, the via holes were marked on the photoresist layer with a pin as they could not be seen with the bright and concentrated lighting of the optical camera. This could sometimes, cause damage to the photoresist around the via holes leading to electroless copper deposition on unwanted areas. As a result the separation between metal deposits in the capacitor could be lost. To avoid this problem, it was necessary to find the via holes without damaging the photoresist. To do this, the LTCC sample which contained the via holes and covered with the photoresist was placed on a transparent acrylic block and illuminated with a different light source so that the via holes could be seen through the photoresist as illustrated in Figure 94.

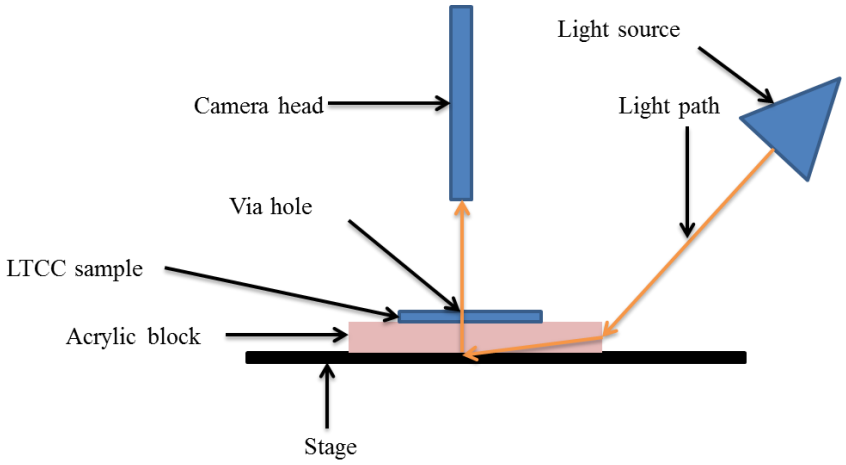

Figure 94 Lighting through via holes

The via holes were 500 μm apart as shown in Figure 95 (a). Using the alignment camera as described above, an inductor and a capacitor were machined on opposite sides of the LTCC sample. Figure 95 (b) and (c) shows the machined inductor and capacitor on the LTCC sample. The radius of the via hole was approximately 100 μm. The separation between adjacent coils in the inductor pattern was approximately 50 μm and the separation between machined parts in the capacitor pattern was approximately 20 μm after the machining process.

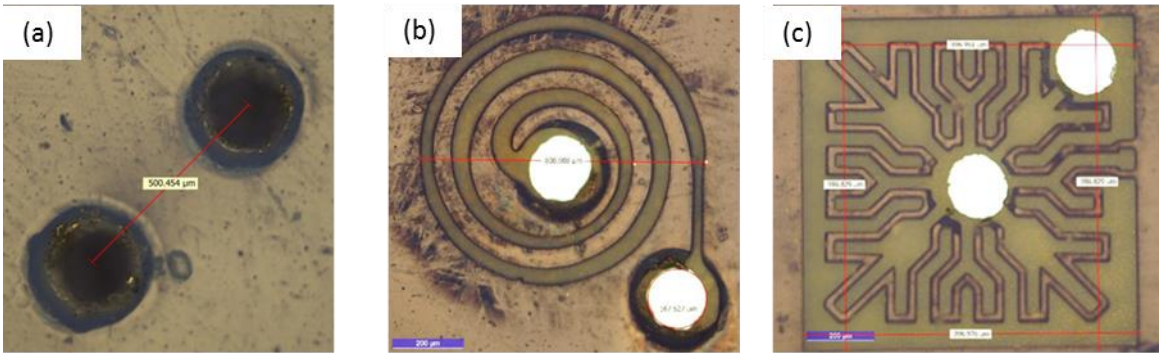

Figure 95 (a) Via holes, (b) spiral inductor aligned with via holes and (c) capacitor aligned with via holes (machined images with photoresist on top)

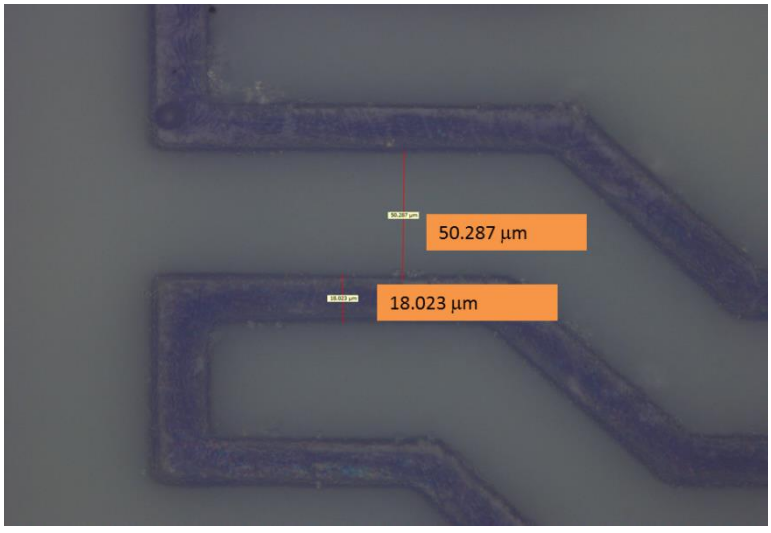

Figure 96 Magnified image of the capacitor pattern

Electroless copper was deposited on the machined features using the procedure described in section 6.4.3. With one hour plating time, it was noticed that some locations on the features were not continuously plated as expected (Figure 97). A possible reason for this

could be trapping of air bubbles on the small features even though vigorous agitation was carried out. When the plating time increased to one and a half hours, the separations between conductor lines were covered with electroless copper deposits (Figure 98). As the separation between these conductor lines was only 18 μm (Figure 96), electroless copper particles may connect to activate this area as the deposits grow. Electroless copper deposition into the via holes was tested with the use of a multimeter and the reading confirmed the electrical connection between capacitor and inductor on opposite sides of the LTCC.

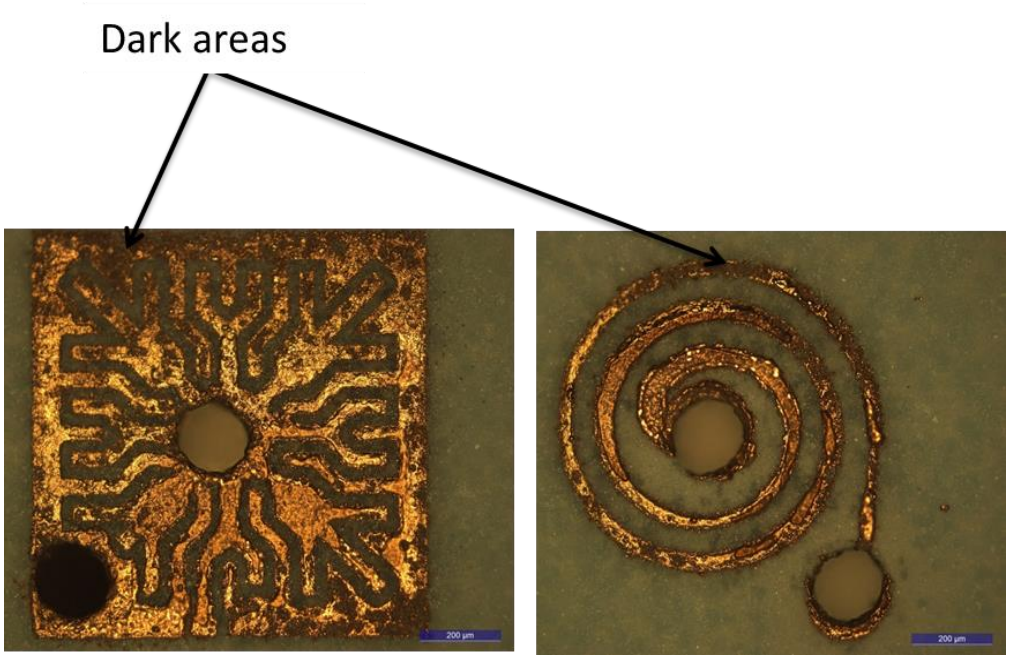

Figure 97 Electroless deposits on both sides of the resonator

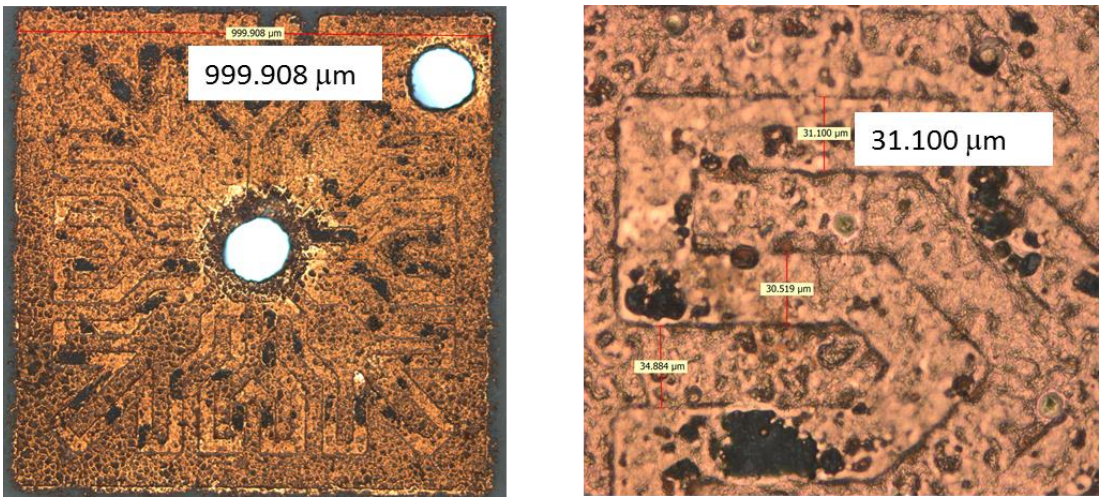

Figure 98 Electroless deposit on capacitor after 1 and a half hours

This study demonstrated the use of the mask projection technique to create complex patterns of passive components. Planar components such as capacitors and inductors were conventionally fabricated on a single substrate (Figure 97, 99 (a)). The performance of the capacitors can be improved if the capacitors are embedded in the substrate (Figure 99 (b) (c)). Future work should consider machining deeper trenches and filling them with metals to reduce the ohmic losses (Figure 99 (c)) [129].

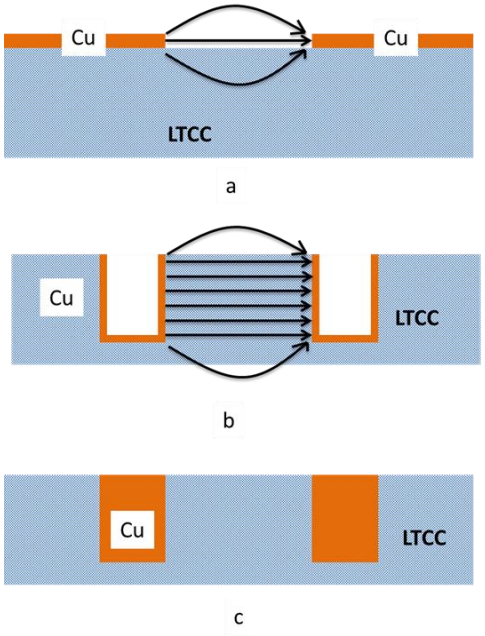

Figure 99 (a) Electric field between plates with standard printing technique, (b) Electric field between plates with plated recesses and (c) Conductor filled recesses [Image was re-drawn from ref. [129]]

6.6 Conclusion

Excimer laser machining can be employed to prepare open channel structures on fired LTCC and electroless copper can be selectively deposited on machined channel structures. It was found that the copper plating rate depends on the laser parameters used to machine the channel structures when plating in the same bath conditions. Even with a similar number of shots per area, the tracks machined with higher repetition rate showed relatively more machining depth as well as good plating conditions with low resistance values. Surface roughness of the machined channels increased with the number of shots of the laser beam per area. The mask projection technique of the excimer laser system combined with electroless plating was used to deposit copper selectively onto fired LTCC. A complete

working circuit and passive components including a capacitor and an inductor were fabricated on fired LTCC.

Chapter 7 Metallisation of Closed Channel Structures

7.1 Introduction

As described in chapter 1, SoS is an emerging system technology where the device miniaturisation is achieved by integrating system components into and onto the substrate (Figure 100). Advances in LTCC multilayer system technology allow the integration of the system components to achieve further miniaturisation of the complete system. One important aspect of the SoS concept is Substrate Integrated Waveguides (SIW). Integration of SIWs into the ceramic body requires metallisation of cavity and channel structures (Figure 100). As described earlier (section 1.4), the conventional screen printing process for green LTCC restricts the metallisation of the walls of the cavity structures, hence opening a new research window to explore other techniques that can be used to metalize the internal walls of the cavities that are embedded in the LTCC body. The electroless plating process was therefore investigated as a potential method to deposit thin metal films inside the closed channel structures using continuous fluid flow mechanisms.

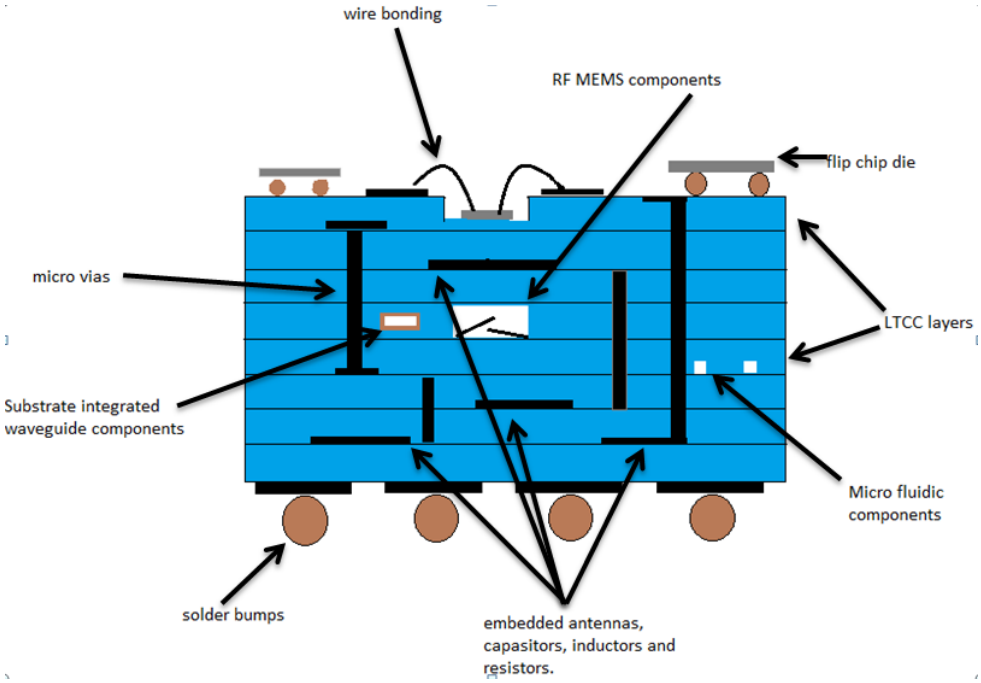

Figure 100 System on substrate concept

This chapter presents the research to develop methods for electroless copper deposition onto the internal walls of closed channel structures. The technique was first implemented on glass capilaries to research and develop a transferrable process which could then be used to metalise the closed channel structures created in fired LTCC.

7.2 Literature Review

7.2.1 Substrate Integrated Waveguide (SIW)

In conventional transmission lines, the signal propagates from one point to another by conductance. Thus, the possible signal losses are conduction loss, radiation loss and dielectric loss [161].

- Conduction loss- as current flows through a conductor some of the energy is lost due to the resistance of the conductor
- Dielectric loss- due to the loss tangent of the dielectric material
- Radiation loss- due to possible leakage of electromagnetic waves

However, at high frequencies, transmission lines can be replaced by waveguide components to limit transmission and radiation losses [162]. Since the signal propagation in the waveguide is due to reflection and not due to conduction, the transmission losses are at a minimum, especially in the high frequency region. In general, a waveguide is a hollow

conductor in which an electromagnetic wave travels by reflection [163]. Waveguides have different physical shapes depending on the operating wavelength. The types of waveguide include coaxial cable, rectangular metal pipe, microstripline, coplanar waveguide and optical fibre [164]. When frequency increases, the transmission losses limit the application of planar structures such as microstripline or coplanar waveguides. Non-planar waveguide structures are known to have the best transmission characteristics as they produce no electromagnetic radiation [165]

At microwave and millimetre wave frequencies, the transmission losses can be reduced by integrating the whole waveguide component into the substrate material. With multilayer technology, non-planar waveguide structures, such as rectangular waveguides, can be fully integrated into a 3-D system [3] and known as Substrate Integrated Waveguides (SIW). The substrate integrated waveguide is a particular feature in SoS approaches as it can be integrated into the system as a planar structure. There are two types of substrate integrated waveguides that can be found in the literature. First, dielectric filled waveguides (Figure 101) which are fabricated by two rows of vias filled with a conductive material in a dielectric substrate and electrically connected by two parallel metal plates [166]. In this type, at high frequencies there will be a significant transmission loss from these metal vias.

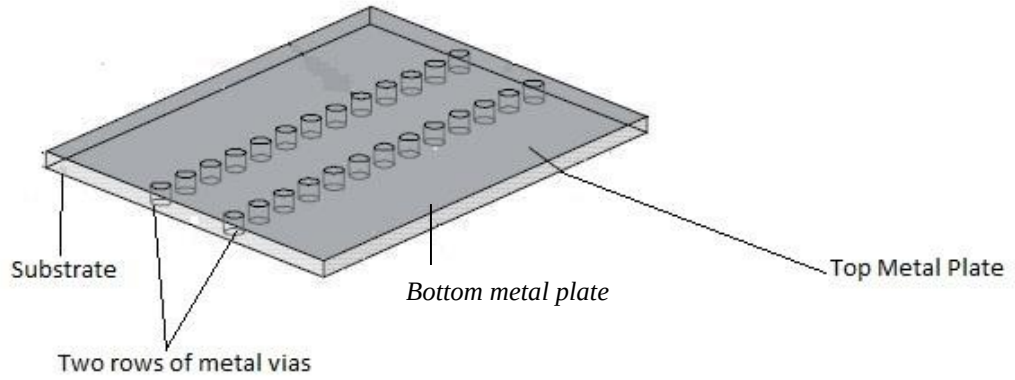

Figure 101 Conventional substrate integrated waveguide [166]

The second type is an air filled substrate integrated wave guide (Figure 102) where the side walls of the microchannel created inside the substrate are metallised with a uniform layer of metal [167]. This type of SIW is a very similar structure to a conventional rectangular waveguide. The best way of minimising dielectric loss is to use air as the dielectric material. The conductor losses and the radiation losses are also reduced by using metallic side walls compared to the metallic via fence of the conventional SIW (Figure 101).

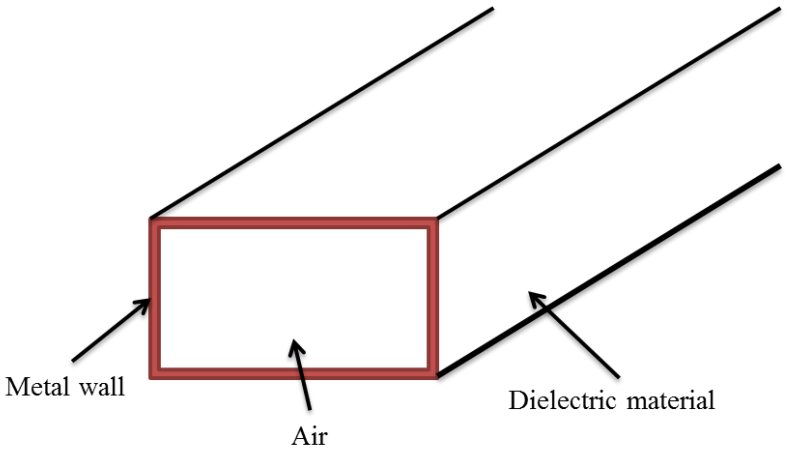

Figure 102 Air filled waveguide [167]

The main advantage of a substrate integrated waveguide is the fabrication of the whole circuit i.e. planar circuitry, transitions, rectangular waveguides, active components and antennas in planar form using planar processing techniques [161]. Secondly, substrate integrated waveguides confine the electromagnetic waves within the substrate and therefore can avoid the unwanted transmission losses at higher frequencies.

7.2.2 Research on Substrate Integrated Waveguides

A demonstration of a substrate integrated waveguide which was designed using green ceramic lamination technology was first reported in 1998 [165]. In this study, metallisation of top and bottom layers were achieved by printing of conductive paste and for the vertical metallisation, two rows of vias filled with conductive paste were used. The designed structures with different via hole pitch sizes were tested using a vector network analyser up to 110 GHz. The study found that the insertion loss increases with the via hole pitch size due to electromagnetic wave leakage through the via holes when the via hole pitch size is larger than a quarter of the test signal wavelength. Further developments of SIW structures have been carried out in terms of increasing frequency and minimising the total loss [168]. With the development of LTCC multilayer technology, SIWs that are used in microwave and millimetre wave filters, [169]–[173] and antennas [174]–[176] have been demonstrated in the literature. In these cases, SIWs were designed using two rows of metallised via holes which were embedded in the substrate and the layout of these via holes (diameter and the distance between two adjacent holes) was highly

dependent on the operating wavelength [177]. When frequency increases above 140 GHz, the fabrication of metallised via holes becomes difficult [178]. As a solution, research has been carried out to design air filled SIWs with continuous metallic side walls. An air filled rectangular waveguide which was fabricated using a photolithographic technique was reported in 2000 [179]. In this study, the metallic side walls were achieved using evaporated gold onto thick photoresist followed by gold electroplating for extra strength. A second photoresist layer was sprayed on top of the waveguide structure and this new resist layer was exposed and developed using a second mask to create accurately a slot in the top of the resist. The exposed gold was then etched away. The photoresist layer was removed using solvents to create the hollow waveguide. The fabricated waveguide was tested in 75–110 GHz using a vector network analyser and showed 0.2 dB loss per wavelength.

A substrate integrated waveguide operating at 140-190 GHz has been demonstrated [167] in 2009. The electrical performance showed total loss of around 0.13 dB/mm at the centre frequency of 150 GHz. The waveguide was designed for LTCC multilayer technology by stacking of pre-cut and metalized LTCC green tapes. Screen printing was used to metallise the top and bottom element of the waveguide structure for which the control of the thickness of the metal layer and the uniformity was challenging in the screen printing process. The alignment of LTCC green tapes needed extra care due to shrinkage of the LTCC material when sintering. Vertical metallisation was done for the middle element by filling the waveguide opening with metal paste while keeping it on a base foil using a stencil. The base foil and the excess conductive paste were removed with a rolling motion while leaving a thin conductive paste on the side walls. Metallised layers were then aligned and laminated at 10 MPa and 70°C for 20 minutes prior to the sintering at 875 ^{0}C for 20 minutes.

7.2.3 Metallisation of Microchannels and Cavity Structures

Microchannels and cavity structures are used in many applications such as microfluidic systems which are integrated in to lab on chip devices and waveguide structures. There are a wide variety of microfluidic systems including pressure sensors, chemical reactors, analytical devices etc. In many cases, these channel structures should be coated with metal layers, dielectric layers or catalyst layers depending on the application [180], [181].

The most common methods of metallising microchannels are based on conventional photolithography. In this process, the microchannels are built in various planar fabrication steps, with each step requiring a mask for selective metallisation [182]. Registration among layers and sealing between layers are important technical issues. Electroless plating of microchannels is a very promising approach as other metallising methods such as screen printing, sputter deposition, inkjet printing and electroplating are difficult to apply to these small 3-D structures. Several studies were reported in the literature to deposit metals on to the internal walls of closed channel structures using the electroless plating process.

Kim and co-workers studied electroless silver deposition inside glass capillaries [183]. The glass capillaries having dimensions of 1.1 mm inner diameter, 0.2 mm thickness, 75 mm length were immersed in an ethanolic $AgNO_3$ and butylamine reaction mixture and the container was vigorously shaken to achieve silver coating both inside and outside of the glass capillaries. The outside silver coating was then removed by wiping off with cotton wool. SEM images of the silver deposits showed the mean grain sizes of Ag nanostructures were increased with the molar ratio of butylamine used as the reductant. The analysis of Raman signals showed that the Ag coated capillary could be an efficient surface-enhanced Raman scattering (SERS) active substrate for microanalysis of chemicals.

Heuck et al. used electroless plating of silver to obtain thick, highly dense, conductive and structured layers on the surface of silicon dioxide rectangular capillaries (3 μm x 3 μm) to develop a scanning ion pipette with good adhesion to the capillary wall [184]. The main steps involved in their study were improving adhesion between the silicon dioxide surface and silver metal layer by an intermediate polymeric-mercaptopropyltrimethoxy-silane layer and achieving a thick metal layer by multiple plating.

In 2010, Paek and co-workers proposed a selective microfabrication of metal electrodes in a microchannel [185]. The channel dimensions were 600 μm × 200 μm × 5 mm. The technique was based both on silver electroless plating and on the rotation of laminar flows among three multiple fluids i.e. silver electroless plating solution, reducer solution and ethanol that had lower density compared to the other two solutions. The silver electrodes patterned by this solution were fabricated only on the wall of the micro-channel where the interface between plating solution and reducer solution made contact with the wall. Unlike the electroless copper plating process, silver electroless plating on glass does not require catalyst surface activation.

7.3 Research Methodology

Unlike in transmission lines, waveguide structures need a smooth and uniform metal layer to get the best performance with minimum transmission losses as mentioned in section 5.2.2. In the literature, surface roughness of the metal side walls accounted for the great proportion of the signal losses. Besides that, the fabrication process of those waveguides required several steps which are not cost effective and are time consuming when considering mass production. Use of electroless plating to metallise the LTCC cavity walls in the fired state would be promising in order to achieve a uniform thin metal layer. Also by changing the parameters such as concentration and temperature of the plating bath, it is possible to control the surface roughness and the thickness of the metal layer.

The research problem has arisen with the substrate integrated waveguide and system on substrate concept. As mentioned in the introduction, Low Temperature Co-fired Ceramic (LTCC) is a better candidate for employing multilayer technology which enables integration of passive and active components into the same substrate material. Although there is some information available for dielectric filled substrate integrated waveguides (SIW) in LTCC technology, the research on air-filled waveguide structures which will reduce further transmission losses needs more attention. The design aspects of SIW require minimum transmission losses for high frequency applications and low process cost from a manufacturing perspective.

7.3.1 Challenges of the Process

The main challenge of the process was selective copper deposition on to the internal walls of the channel structure. As mentioned earlier in chapter 2, the electroless plating process is usually carried out in a container by immersing test samples. In the current method the selective copper deposition was achieved by using a flow process. The steps involved in the plating process such as surface interaction with pre-dip solution, catalyst adsorption and also the electroless deposition could be varied in the flow process. The copper deposition process was initially established on glass tubes with the aim to extend the process to metallise LTCC micro channels in order to produce substrate integrated waveguide structures. Adhesion was a major issue when metallising glass tubes and surface pre-treatments to improve copper adhesion to the glass substrate were also considered. Furthermore, the surface roughness and the thickness of the metal deposit should be maintained and controlled as these parameters are responsible for the actual device

performance. The bath temperature, plating time and catalyst run time were controlled in order to obtain a continuous copper deposit. Following the initial trials, channel structures in LTCC were metallised. The channel openings were rectangular shaped and the next challenge was to connect silicon tubing on to a rectangular shaped aperture. Proper sealing of the connection had to be considered to prevent the solution leaking. The following approaches were considered to metallise the microchannel structures.

7.3.2 Research Approach

- Approach 1- In this approach, direct electroless Cu plating of glass tubes by circulating solutions was investigated in order to produce circular waveguide structures. Self-Assembled Monolayers (SAM) are found to be a promising solution for adhesion improvement between the Cu deposit and the glass substrate [186],[187]. Self-assembled monolayers are a group of organic compounds which have the capability of controlling physicochemical surface properties of materials. These compounds usually contain specific functional groups such as NH_2, OH, COOH, SO_3H, Ph etc. In the electroless plating process the Sn/Pd metallic core can be well adhered to the substrate via metal ligand bonds or electrostatic interactions between the substrate and these functional groups [188]. Silane pre-treatment to improve the copper adhesion to the glass substrate, Sn/Pd catalyst surface activation, and flow rate of solutions was studied. Once Cu was deposited in glass tubes, the signal propagation through these tubes was analysed electromagnetically. These latter measurements were carried out in collaboration with the project partners.
- Approach 2- NaOH pre-treatment process was employed on cleaned LTCC samples. Then the above process with some alterations was employed to deposit copper on to the internal walls of NaOH treated LTCC closed channels.
- Channel interconnection- The connector which connects the channel opening and the tubing which carries the solution was a key issue. Design and manufacture of a tubing system that could attach to the channel openings for the flow process without any solution leakage was also taken in to account. From the manufacturing point of view, the connection should be easy to implement in mass production. Due to this reason, the tubing was first connected to the channel openings using a clamp and the sealing was done using a rubber sheet in between the LTCC sample and the

tubing system. However, it was realised that the LTCC samples were not flat enough to maintain the seal and leaking of solutions was observed. As a result, double sided tape was applied in between the LTCC sample, rubber sheet and the tubing system.

7.4 Experimental Procedures

7.4.1 Metallisation of Glass tubes

A. Materials

In this experiment, Fisher scientific glass melting point tubes with outer diameter 1.8 mm to 2 mm and with different lengths were used. For the plating process, the same pre-dip, catalyst and electroless copper bath were used as described in Chapter 2 on LTCC metallisation. Sigma Aldrich 3-aminopropyltrimethoxy silane (APTS) was used to prepare a Self-Assembled Monolayer on the glass to improve the catalyst attachment.

B. Copper Deposition Process

Glass tubes were first cleaned with 10 Vol % Decon 90 solution in water following the procedures described in section 2.3.1. After rinsing and drying, these samples were then transferred into a 0.005 moldm^{-3} APTS solution. This solution was prepared by dissolving 0.18 ml of APTS in a mixture of 190 ml of methanol and 10 ml of distilled water. The samples were immersed in the APTS solution for 24 hours at room temperature and then rinsed with distilled water to remove excess APTS from the glass surface.

The copper deposition onto the internal walls of the glass capillaries was accomplished using a flow process shown schematically in Figure 103. Fluid flow was achieved using a suction pump attached to a Buchner funnel which was used as a solution trap. The other opening of the Buchner funnel was attached to one end of the glass tube to be plated using silicone tubing. The other end of the glass tube was attached to silicone tubing and the free end of the tubing was immersed in the solution beaker. The flow rates of the solution were controlled using a plastic valve attached to the silicone tubing which connected the glass capillary and the Buchner funnel. For the pre-dip and catalyst solutions the same set of apparatus was used and for the electroless copper solution a different set of apparatus was

used to avoid the plating of unwanted surfaces including tubing and Buchner flask. To activate the glass surface, pre-dip solution and Sn/Pd catalyst solution were flowed sequentially through the glass tube at room temperature with the aid of the vacuum pump. After the activation process, the glass tubes were rinsed thoroughly by passing distilled water at high flow rate. This was done by releasing the plastic valve completely. The electroless copper solution was placed on a hot plate and heated up to 40 ^{0}C and the temperature was controlled by a temperature probe immersed in the electroless solution. Then the electroless copper solution was passed through the glass tube. The flow rate of the pre-dip and catalyst solutions was kept at 60 ml/minute. The optimum flow rate of the electroless copper solution was obtained by passing different flow rates through the glass capillaries until the inside walls of the capillary were fully covered with electroless copper. The flow rates were calculated by measuring the solution collected in the Buchner funnel and the flow time. The pre-dip, catalyst and electroless copper solutions were prepared according to the procedures described in section 2.3.3 and 2.3.4 in chapter 2. The optimum flow time of the catalyst solution and the electroless copper solution was also investigated.

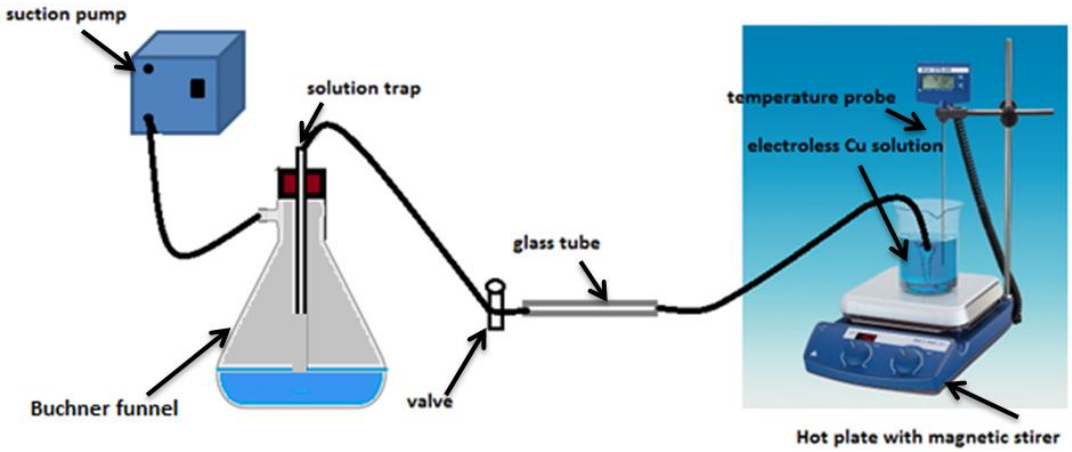

Figure 103 Experimental set up for electroless plating of glass tubes

7.4.2 Metallisation of LTCC Closed Channels

A. Interconnect to Closed Channel Structures

Closed channel structures with dimensions approx. 5 mm x 1 mm x 25 mm were pre-prepared in LTCC 9K7 material and fired according to the firing profile by partners at the University of Leeds. The samples were cleaned with 10 Vol% Decon 90 solution in water following the procedures described in section 2.3.1. To increase the roughness of the surface, these samples were then soaked in 4M NaOH for 24 hours. As these samples were

not tubular like the glass capillaries, a different method of connection was developed. The same layout of the channel openings was created in an acrylic sheet and a rubber sheet. Silicone tubing was attached to the openings of the acrylic sheet using glue. Initial attempts were to connect the acrylic sheet, rubber sheet and the LTCC sample together using a clamp, however, due to the solution leaking this method was rejected. The rubber sheet was therefore attached to the LTCC sample in such a way that the openings aligned using double sided adhesive tape and the acrylic sheet was then attached to the rubber sheet using double sided adhesive tape. Attachment of tubing and the sealing process is illustrated in Figure 104.

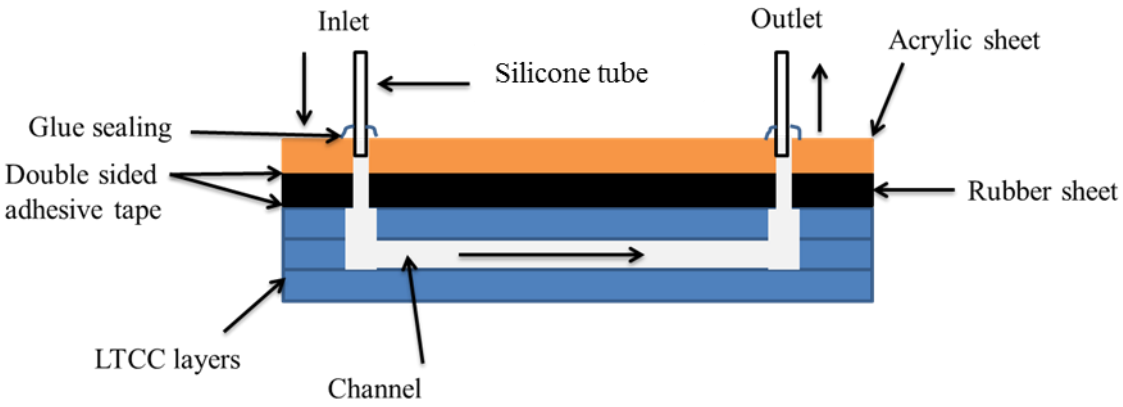

Figure 104 Cross section of the LTCC channel structure with the tube attachment

B. Copper Deposition Process

Using the same experimental set up used in section 7.4.1 the pre-dip solution was passed through the channel structure at 120 ml/hr for 5 minutes. Catalyst solution was passed through the channels for different time periods (2 min, 5 min, 10 min) to investigate its effect. The flow rate of the catalyst solution was kept at 60 ml/hr. Then the excess catalyst was rinsed by passing de-ionised water for 5 minutes and releasing the valve completely to get a higher flow rate. After the cleaning process, electroless copper solution was run through the LTCC channel for 1 hour at a flow rate of 120 ml/hr.

7.5 Results and Discussion

7.5.1 Electroless Copper Deposits on Glass Capillaries

In the initial experiments, the glass tubes were plated with electroless copper without APTS pre-treatment. Electroless copper was not observed on the internal walls of the glass tube without APTS pre-treatment showing that the silane treatment is an essential step for the process. The main challenge during the plating process was the coating of a uniform layer of electroless copper inside the capillary with sufficient thickness. The adhesion of the electroless copper to the internal walls of the glass capillary was found to depend both on the flow rate of the electroless solution and the deposition time. It was found that the copper deposit washed away with the higher flow rates. Different flow rates of the electroless copper solution were passed through the glass capillaries to find the optimum flow rate and the time taken to peel off the coating with the fluid flow was measured using a stop watch (Table 13).

Table 14 Electroless copper adhesion dependence on flow rate

Flow rate/ ml/hour	Coating coverage	Coating started to peel off at /seconds
216	Partially plated	65
189	Partially plated	103
155	Fully plated	139
120	Fully plated	196

Flow rate of the pre-dip and catalyst solutions were kept as low as possible at 60 ml/minute to enhance the surface activation while the flow rate of the electroless copper solution was kept higher to prevent the hydrogen gas building up inside the capillary due to the electroless reaction. However, when the flow rate of the electroless copper solution was higher (216 ml/hour), deposited copper started to peel off even before the internal walls of the glass capillary were fully coated with electroless copper. A similar observation was noted for the glass capillary plated with 189 ml/hour flow rate. The flow rate of the electroless copper solution was further reduced to 155 ml/hour and it was found that the

glass capillary was fully covered with the electroless copper. However, the copper coating started to peel off after 139 seconds. The flow rate was further lowered down to 120 ml/hour and the peeling off of the coating was observed at 196 seconds. When the flow rate dropped further air bubbles (hydrogen) started to trap inside the silicone tubing especially where the tubing was connected to the Buchner funnel. An example of a continuous uniform copper deposit only on the internal walls of the capillary is presented in Figure 105. The following sections discuss the thickness and the transmission loss of the plated capillaries.

Figure 105 Electroless copper deposited inside a glass tube

7.5.2 Thickness of Deposited Copper

The cross sectioning of glass samples using grinding and polishing is difficult due to the formation of glass chips. As a solution, a Focussed Ion Beam Scanning Electron Microscope (FIBSEM) was used to measure the coating thickness. This instrument consists of a high resolution field emission electron column and gallium source ion column which allows milling of cross sections (typically 20 x 5 microns) through samples and subsequent imaging using either electrons or ions. In this process, the plated glass tube was broken manually and a piece of broken glass (with Cu on the internal wall) was mounted on a carbon stub. The copper layer was connected to the carbon by silver paste to give continuous conductivity of the sample. The sample was then subjected to the FIBSEM analysis.

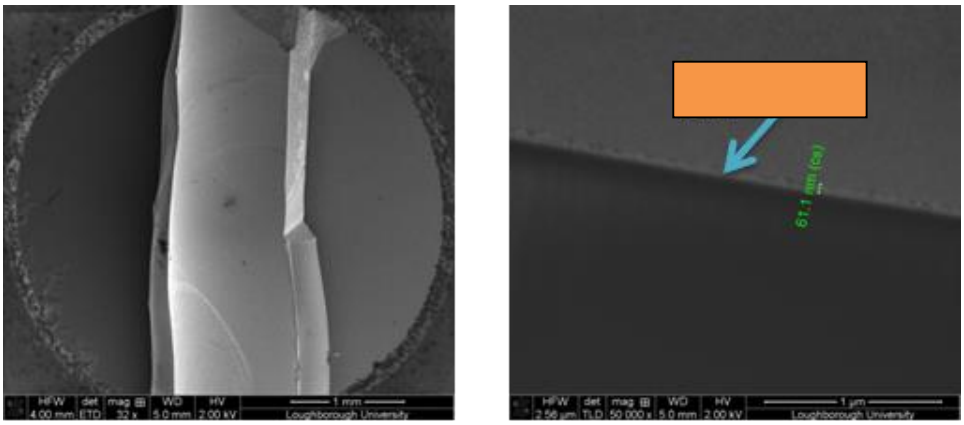

(a) (b)

Figure 106 FIBSEM micrographs of (a) broken glass tube mounted on Al stud (b) Cu layer

Figure 106 (a) shows the FIBSEM of the broken glass capillary. The analysis was carried out in the middle area of the sample. A continuous copper layer was observed (Figure 106 (b)). The maximum thickness of the electroless copper deposited on the inside walls of the glass capillary with the 120 ml/hour flow rate for 196 seconds was approximately 60 nm. A previous study [16] showed approximately 200 nm thick electroless copper deposits on a CMG flat glass substrate in 30 minutes, but this was using a different electroless bath system (Rohm and Haas Circuposit 4750 system). Another study [63] investigated the electroless plating thickness on flat CMG glass using bath system Circuposit 3350-1. In that work the copper coating thickness was approximately 1 μm after 25 minutes. However these glass substrates were bead blasted to introduce a rougher surface in order to increase the copper adhesion to the glass surface. The moving electroless solution and smooth surface may have been responsible for the limited coating thickness achieved on the internal walls of the glass capillaries.

7.5.2 Transmission Losses

Three glass tubes with different lengths (40 mm, 61 mm and 71 mm) were cut from 75 mm glass tubes and plated according to the procedures described above. Flow rate of the electroless copper was 120 ml/hour and these capillaries were plated for 180 seconds. After plating for 180 seconds, electroless copper was successfully deposited on the internal wall of the glass tubes. The transmission losses were measured at Imperial College by the project partners and the experimental results were compared with the simulation results. The test was carried out in the frequency range of 0.25 THz – 2.5 THz.

The transmission losses were experimentally measured using TetraView heads which have a Gaussian beam with a diameter of 2-3 mm. The simulation showed approximately a loss of 0.4 dB/0.1mm length which suggests 28 dB/70mm. However, the actual experimental results showed the loss to be lower than 10 dB for all three glass tubes. The drawback of the circular glass waveguide was the unwanted modes at the measured frequency range.

7.5.3 Electroless Cu Plating of LTCC Micro-channels

An example of a LTCC channel structure is shown in Figure 107. The closed channel structures were pre-created in the LTCC sample during the lamination process and fired according to the firing profile. This particular sample only has one channel structure, however some samples contained 3 or 5 channels embedded in the same sample. The rectangular holes in the middle of the sample are the opening of the channel and the channel goes across the sample. Other circular holes which can be seen in the LTCC sample are the registration pin holes used to align the LTCC layers.

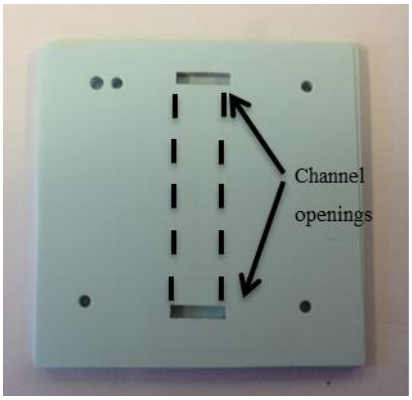

Figure 107 LTCC micro channel test structure

As described in Chapter 5 NaOH pre-treatment plays a part in adhesion improvement of electroless copper deposited on the fired LTCC substrate. The samples were first immersed in 4M NaOH solution for 24 hours at room temperature. As the closed channel in the test structure had relatively large dimensions (approx. 5 mm x 1 mm x 25 mm), the NaOH solution was flowed in to the channel structure by shaking the solution container. After the NaOH pre-treatment process the excess NaOH remaining inside the channel structure was rinsed thoroughly with de-ionized water.

To flow solutions through the channels an interface was prepared as described earlier. Figure 108 shows the LTCC sample which contained three closed channels running across

the sample. The tubing was attached to this sample as described in section 7.4.2. The catalyst solution is shown running through one of the channels in this example.

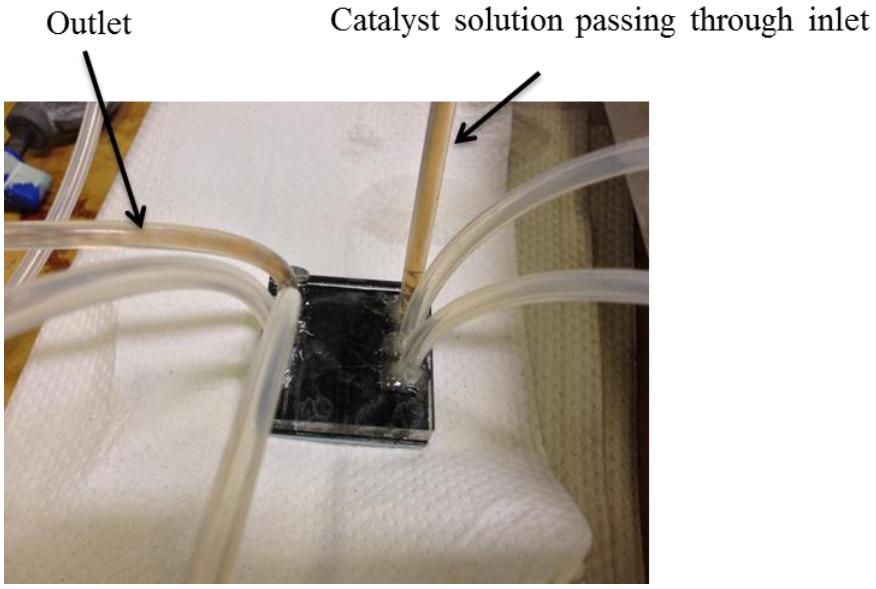

Figure 108 Attachment of tubing

Adsorption of catalyst on to the LTCC substrate is an essential part in the electroless process and the effect of flow time of the catalyst solution through the channel was investigated. The flow time of the pre-dip and the electroless copper solution was kept constant while the flow time of the catalyst solution was changed as shown in Table 14. Electroless copper solution was passed through the channel structures for one hour. After the deposition process, the continuity of the copper deposit was tested by means of electrical connectivity using a multimeter.

Table 15 Effect of flow time of catalyst solution on plating

	Flow time/ minutes			**Electrical connectivity**
Channel	Pre-dip	Catalyst	Electroless Cu solution	
1	5	2	60	no
2	5	5	60	yes
3	5	10	60	yes

Figure 109 shows the electroless deposits on LTCC channel structures. A very selective copper coating only on the channel structures was observed. The channel activated with

Sn/Pd catalyst for 2 minutes showed uncoated areas (Figure 109, No 1) and the other two channels showed uniform coating on the walls and the base of the channel opening. Both channels activated with Sn/Pd catalyst for 5 minutes and 10 minutes showed a positive multimeter signal confirming the electrical connectivity.

Figure 109 Copper plated LTCC closed channel structures

Optical micrographs of the base and the walls of the channel opening were taken and are shown in Figure 110. These micrographs show uniform and continuous electroless copper coating on the channel opening.

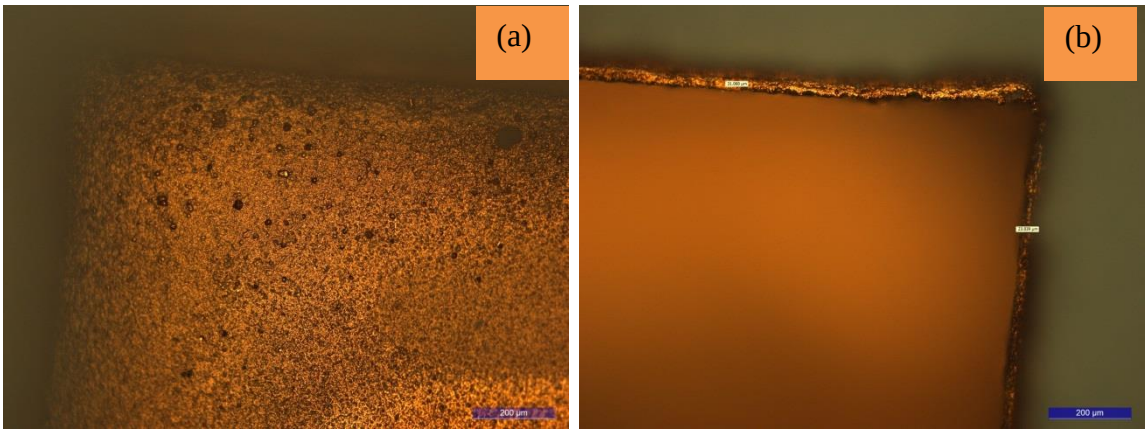

Figure 110 Optical micrograph of the (a) channel base and (b) wall

7.6 Conclusions

Methods to electrolessly plate the internal surface of glass and LTCC waveguides were established. The rate of flow of the electroless copper solution through the glass tubes was maintained at a low rate as the copper deposits tended to wash away with a high flow rate. It was also found that the electroless copper solution could only pass through the glass tube for 2-3 minutes otherwise the copper deposits peeled off. A thin layer of electroless copper (approx. 60 nm) was selectively deposited only on the internal wall of glass tubes. Application as circular glass waveguides showed low (<10dB) transmission losses in the terahertz region of the electromagnetic spectrum. A method was developed to deposit electroless copper on LTCC closed channel structures. Unfortunately, within the project, no measurements of electrical transmission of these samples were undertaken.

Chapter 8 Conclusions

The aim of the current research study was to investigate and develop an electroless copper metallisation technique for fired LTCC as an alternative to the conventional screen printing process in order to produce integrated passive components, circuit patterns and substrate integrated waveguide structures. To achieve this aim, selective copper metallisation including pattern formation on fired LTCC substrates and closed channel metallisation on both glass and LTCC was mainly considered. This chapter presents the conclusions highlighted in the previous chapters. The findings from this study make several contributions to the LTCC multilayer technology and are briefly stated here:

- Electroless copper was deposited on Sn/Pd activated fired LTCC surfaces. The deposit was homogenous and could achieve sufficient thickness. However the tape test results indicated poor adhesion between fired LTCC and electroless copper when no pre-treatment was applied.
- Chemical pre-treatment of fired LTCC was carried out using concentrated NaOH solution in order to improve the adhesion. The surface morphology of the fired LTCC was changed when using different concentrations of NaOH as well as different immersion times. Flake like features appeared on the LTCC surface with the NaOH pre-treatment and different surface and chemical analysis techniques suggested that these flake like features were originally dispersed in the ceramic material and appeared on the surface after the background material was selectively etched away. A material model of the NaOH treatment process was presented for fired LTCC based on the results obtained from chemical and surface analysis.
- Surface roughness of NaOH treated LTCC was studied using both Ra and volume parameters. It was found that Ra provides a poor representation of the LTCC surface. As an alternative, volume parameters were investigated and Vv, Vvv, Vvc, were found to give a better representation of the LTCC surface.

- Characterization of deposited electroless copper was carried out. The adhesion strength of the copper deposits on LTCC substrates treated with different concentration of NaOH was investigated using both tape test and scratch test. The results showed improved adhesion in all NaOH treated LTCC samples compared to untreated LTCC. Further investigation using XPS showed that, unlike untreated samples, NaOH treated samples showed some traces of copper adhered to the LTCC surface after the tape test. The role of the flake like structure on adhesion improvement was investigated. It was found that the flake like structures disappeared from the LTCC surface after the pre-dip and catalyst solution. It was therefore concluded that there is no effect of the flake like structure on adhesion improvement but, the roughness of the background surface of the LTCC may be responsible for the adhesion improvement.
- Excimer laser machining combined with the electroless plating process was employed for selective metallisation of LTCC. Complete working circuits and planar passive components including capacitor and inductor were demonstrated on fired LTCC. It was found that the copper plating rate depended on the laser parameters used. The process was further extended to design a resonator on LTCC. Limitations in the resolution of the features achievable were identified, especially when the separation between conductor lines dropped below 18 μm
- Electroless copper deposition onto the internal walls of glass capillaries and LTCC closed channel structures was investigated. Methods to connect tubing to glass tubes and SIW structures were established and electroless solutions were flowed through glass capillaries as well as LTCC closed channels to deposit copper selectively only on the internal walls of the channels. The thickness of the deposited copper on glass capillaries was 60 nm. The method was demonstrated as a promising solution to deposit electroless copper on the internal walls of closed channel structures in order to manufacture substrate integrated waveguides.

This research has thrown up many questions in need of further investigation.

- This research showed the potential for the deposition of electroless copper inside LTCC closed channel structures. Due to a lack of samples, the characterization of these deposits was not carried out in detail during this project. Further investigation to characterize the uniformity, thickness and the resistance of the deposited copper needs to be taken in to account.

- Fabrication of inductors and capacitors on fired LTCC (separation between conductor lines was approx. 50 μm) was demonstrated in this research. However it was found that when the separation between conductor lines dropped below 18 μm these separations started to connect with each other during the plating process. Further experiments need to be carried out to find the optimum metal line/space dimensions for capacitor and inductor fabrication and alternative laser processing and resist layer materials should be considered.
- As the generated substrate integrated waveguide structures and passive components are to be used in high frequency applications, future research should therefore concentrate on the detailed investigation of loss measurements of LTCC SIW and passive components in the expected frequency range.

References

[1] M. Norén, S. Brunner, C. Hoffmann, W. Salz, and K. Aichholzer, "Aspects of advanced thermal management for flip chip on low temperature cofired ceramics (LTCC)," *Solder. Surf. Mt. Technol.*, vol. 21, no. 2, pp. 24–27, 2009.

[2] R. Johannessen, F. Oldervoll, and F. Strisland, "High temperature reliability of aluminium wire-bonds to thin film, thick film and low temperature co-fired ceramic (LTCC) substrate metallization," *Microelectron. Reliab.*, vol. 48, no. 10, pp. 1711–1719, Oct. 2008.

[3] K. Wu, "Towards System-on-Substrate Approach For Future Millimeter-Wave and Photonic Wireless Applications," in *Proceedings of Asia-Pacific Microwave Conference*, Japan, pp.1895 - 1900 Dec. 2006.

[4] Z. Li, and K. Wu, "24-GHz Frequency-Modulation Continuous-Wave Radar Front-End System-on-Substrate," *IEEE Trans. Microw. Theory Tech.*, vol. 56, no. 2, pp. 278–285, 2008.

[5] D. M. Sheen, D. L. McMakin, and T. E. Hall, "Near Field Imaging at Microwave and Millimeter Wave Frequencies," *2007 IEEE/MTT-S Int. Microw. Symp.*, pp. 1693–1696, Jun. 2007.

[6] Emerson D. T.,The Work of Jagadis Chandra Bose: 100 Years of mm-wave Research IEEE Transactions on Microwave Theory and Techniques; Vol. 45, No. 12, pp. 2267-2273; Dec. 1997.

[7] W. Gautier, V. Ziegler, A. Stehle, B. Schoenlinner, U. Prechtel, and W. Menzel, "RF-MEMS Phased Array Antenna on Low-Loss LTCC Substrate for Ka-Band Data Link," in *Proceedings of European Microwave 39th Conference*, pp. 914–917,Oct 2009

[8] P. Pursula, T. Karttaavi, M. Kantanen, A. Lamminen, J. Holmberg, M. Lahdes, I. Marttila, M. Lahti, A. Luukanen, and T. Vähä-heikkilä, "60-GHz Millimeter-Wave Identification Reader," *IEEE Trans. Microw. Theory Tech.*, vol. 59, no. 4, pp. 1166–1173, 2011.

[9] A. Lamminen and J. Siiily, "77 GHz beam-switching high-gain end-fire antenna on L TCC," in *Conference Proceedings ICECom*, , pp. 1–4, 2010.

[10] R. C. Buchanan, Ceramic Materials for Electronics. New York: M. Dekker, 2004.

[11] C. A. Harper, *Electronic packaging and interconnection handbook*. New York: McGraw-Hill, 1991.

[12] W. D. Brown, Advanced Electronic Packaging : With Emphasis on Multichip Modules. New York: IEEE Press, 1999.

[13] J. H. Lau and S.-W. R. Lee, Chip Scale Package (CSP) : Design, Materials, Processes, Reliability, and Applications. London: McGraw-Hill, 1998.

[14] J. Coonrod, "Understanding When To Use FR-4 Or High Frequency Laminates," 2011.

[15] "RO3000 ® Series Circuit Materials,"[Online available]: http://www.rogerscorp.com/acs/producttypes/7/RO3000-Laminates.aspx

[16] X. Cui, "Electroless metallisation of glass for electrical interconnect applications," PhD Thesis, Loughborough University, 2009.

[17] L. S.-L. M.R. Gongora-Rubioa, P. Espinoza-Vallejosb, "Overview of low temperature co- ® red ceramics tape technology for meso-system technology (MsST)," *Sensors Actuators A*, vol. 89, pp. 222–241, 2001.

[18] R. R. Tummala, J. U. Knickerbocker, S. H. Knickerbocker, L. W. Herron, R. W. Nufer, R. N. Master, B. M. Kellner, C. H. Perry, J. N. Humenik, and T. F. Redmond, "High- performance ceramic / copper multilayer substrate with thin-film redistribution," *IBM J. Res. Dev.*, vol. 36, no. 5, pp. 889–904, 1992.

[19] R. R. Turnmala, "Ceramic and Glass-Ceramic Packaging in the 1990s," *J. Am. Ceram. Soc.*, vol. 74, no. 5, pp. 895–908, May 1991.

[20] H. Jantunen, T. Kangasvieri, J. Vähäkangas, and S. Leppävuori, "Design aspects of microwave components with LTCC technique," *J. Eur. Ceram. Soc.*, vol. 23, no. 14, pp. 2541–2548, Jan. 2003.

[21] T. Haas, C. Zeilmann, A. Bittner, and U. Schmid, Investigation on micromachining technologies for the realization of LTCC devices and systems, in *Proceedings of SPIE, ,* vol. 8066, pp.2011.

[22] P. Uhlig R. Kulke, M. Rittweger, "LTCC- Multilayer Ceramic for Wireless and Sensor Applications," pp. 1–8, 2001.

[23] A. Bittner and U. Schmid, "The porosification of fired LTCC substrates by applying a wet chemical etching procedure," *J. Eur. Ceram. Soc.*, vol. 29, no. 1, pp. 99–104, Jan. 2009.

[24] A. Bittner and U. Schmid, "Permittivity of LTCC substrates porousified with a wet chemical etching process," *Procedia Eng.*, vol. 5, pp. 327–330, Jan. 2010.

[25] P. K. Khanna, B. Hornbostel, M. Burgard, W. Schäfer, and J. Dorner, "Studies on three-dimensional moulding, bonding and assembling of low-temperature-cofired

ceramics for MEMS and MST applications," *Mater. Chem. Phys.*, vol. 89, no. 1, pp. 72–79, Jan. 2005.

[26] M. F. Shafique, , K. Saeed, D. P. Steenson, , and I. D. Robertson, "Laser Prototyping of Microwave Circuits in LTCC Technology," *IEEE Trans. Microw. Theory Tech.*, vol. 57, no. 12, pp. 3254–3261, 2009.

[27] P. E. Garrou and I. Turlik, *Multichip module technology handbook*. New York : McGraw-Hill, 1997.

[28] R. Mohd A. Lee, "Fabrication of 3D Microwave and Millimetre-Wave Components in LTCC Technology" PhD Thesis, University of Leeds, July2014.

[29] "DuPont Microcircuit Materials." [Online available] : http://www.dupont.com/content/dam/assets/products-and-services/electronic-electrical-materials/assets/datasheets/prodlib/LTCC_DesignGuide.pdf.

[30] L. J. Golonka, "Technology and applications of Low Temperature Cofired Ceramic (LTCC) based sensors and microsystems," Bulletin of the Polish Acadamy of Sciences and Technical Sciences vol. 54, no. 2, pp. 221-231, 2006.

[31] A. Bittner, N. Pagel, H. Seidel, and U. Schmid, "The Impact of Substrate Properties on the Electromigration Resistance of Sputter-Deposited Cu Thin Films," in *Proceedings of SPIE*, vol. 8066, 2011.

[32] P. W. Gian, X. Shan, Y. N. Liang, B. K. Lok, C. W. Lu, and B. L. Ooi, "High Aspect Pattern Formation by Integration of Micro Inkjetting and Electroless Plating," *DTIP MEMS MOEMS*, April, pp. 5–10, 2008.

[33] D. Jurkow, H. Roguszczak, and L. Golonka, "Cold chemical lamination of ceramic green tapes," *J. Eur. Ceram. Soc.*, vol. 29, no. 4, pp. 703–709, Mar. 2009.

[34] J. Kita, A. Dziedzic, L. J. Golonka, and T. Zawada, "Laser treatment of LTCC for 3D structures and elements fabrication," *Microelectron. Int.*, vol. 19, no. 3, pp. 14–18, 2002.

[35] Y. Lacrotte, J. P. Carr, R. W. Kay, and M. P. Y. Desmulliez, "LTCC Package Manufacturing Using Powder Blasting Technology," DTIP MEMS MOEMS, April, 2012.

[36] K. M. Nowak, H. J. Baker, and D. R. Hall, "Cold processing of green state LTCC with a CO_2 laser," *Appl. Phys. A*, vol. 84, no. 3, pp. 267–270, May 2006.

[37] X. Shan, S. H. Ling, H. P. Maw, C. W. Lu, and Y. C. Lam, "Micro Embossing of Ceramic Green Substrates for Micro Devices," *DTIP MEMS MOEMS*, April 2008.

[38] G. Wang, , E. C. Folk, and F. Barlow, "Fabrication of Microvias for Multilayer LTCC Substrates," *IEEE Trans. Electron. Packag. Manuf.*, vol. 29, no. 1, pp. 32–41, 2006.

[39] E. Steinhäuser, L. Stamp, and L. Brandt, “Chemical ‘kick start’ for the autocatalytic formaldehyde-free electroless copper plating process,” *Circuit World*, vol. 36, no. 2, pp. 20–23, 2010.

[40] H. Honma, “Plating technology for electronics packaging,” *Electrochim. Acta*, vol. 47, pp. 75–84, 2001.

[41] K. Kordás, A. E. Pap, J. Saavalainen, H. Jantunen, P. Moilanen, E. Haapaniemi, and S. Leppävuori, “Laser-Induced Surface Activation of LTCC Materials for Chemical Metallization,” *IEEE Trans. Adv. Packag.*, vol. 28, no. 2, pp. 259–263, 2005.

[42] A. Beikmohamadi, S. Stewart, J. Parisi, M. Mccombs, M. Smith, K. Souders, and J. C. Malerbi, “Electroplating and Electroless Plating Process Development for DuPont ™ GreenTape ™ 9K7 LTCC”, *IMAPS/ACerS 9th International Conference and Exhibition on* Ceramic Interconnect and Ceramic Microsystems Technologies April 2013,

[43] H. Xu, J. Brito, and O. A. Sadik, “Mechanism of Stabilizer Acceleration in Electroless Nickel at Wirebond Substrates,” *J. Electrochem. Soc.*, vol. 150, no. 11, pp. 816–822, 2003.

[44] I. Baskaran, T. S. N. S. Narayanan, and A. Stephen, “Effect of accelerators and stabilizers on the formation and characteristics of electroless Ni – P deposits,” *Mater. Chem. Phys.*, vol. 99, pp. 117–126, 2006.

[45] J. Shu, B. P. A. Grandjean, and S. Kaliaguine, “Effect of $Cu(OH)_2$ on Electroless Copper Plating,” *Ind. Eng. Chem. Res.*, vol. 5885, no. 1, pp. 1632–1636, 1997.

[46] H. R. Shemilt, “Electroless Copper Plating Troubleshooting,” *Circuit World*, vol. 1, no. 1, pp. 5–8, 1974.

[47] N. Kanani, " Electroplating and electroless plating of copper & its alloys" Stevenage: Finishing Publications, 2003.

[48] M. Paunovic and M. Schlesinger, *Fundamentals of electrochemical deposition*. Hoboken, N.J.: Wiley-Interscience, 2006.

[49] E. Natividad, E. Lataste, M. Lahaye, J. M. Heintz, and J. F. Silvain, “Chemical and morphological study of the sensitisation, activation and Cu electroless plating of Al_2O_3 polycrystalline substrate,” *Surf. Sci.*, vol. 557, no. 1–3, pp. 129–143, May 2004.

[50] F. Folser, “Applied PhysicsA " Electroless copper deposition on excimer-laser pretreated alumina,” *Appl. Phys. A*, vol. 213, pp. 209–213, 1994.

[51] X. Cui, D. A. Hutt, D. J. Scurr, and P. P. Conway, “The Evolution of Pd/Sn Catalytic Surfaces in Electroless Copper Deposition,” *J. Electrochem. Soc.*, vol. 158, no. 3, p. D172, 2011.

[52] T. Osaka and H. Takematsu, "A Study on Activation and Acceleration by Mixed $PdCl_2SnCl$ Catalysts for Electroless Metal Deposition," *J. Electrochem. Soc.*, vol. 127, no. 5, 1977.

[53] R. L. Cohen and K. W. West, "Generative and Stabilizing Processes in Tin-Palladium Sols and Palladium Sol Sensitizers," *J. Electrochem. Soc.*, vol. 120, no. 4, pp. 502–508, 1973.

[54] O. Holderer , T. Epicier ,C. Esnouf and G. Fuchs , "Direct Structural and Chemical Analysis of Individual Core - Shell (Pd, Sn) Nanocolloids," *J. Phys. Chem.*, vol. 107, no. 8, pp. 2–5, 2003.

[55] A. B. J. Meenan, N. M. D. Browna, and J. W. Wilsonb, "Characterisation of a PdCl2/SnCl2 electroless plating catalyst system adsorbed on barium titanate-based electroactive ceramics," *Appl. Surf. Sci.*, vol. 4332, no. 93, pp. 221–233, 1994.

[56] J. Li, M. J. O'Keefe, and T. J. O'Keefe, "Activation of non-metallic substrates for metal deposition using organic solutions," *Surf. Coatings Technol.*, vol. 205, no. 10, pp. 3134–3140, Feb. 2011.

[57] A. Hozumi, S. Asakura, A. Fuwa, N. Shirahata, and T. Kameyama, "Preparation of a well-defined amino-terminated self-assembled monolayer and copper microlines on a polyimide substrate covered with an oxide nanoskin.," *Langmuir*, vol. 21, no. 18, pp. 8234–42, Aug. 2005.

[58] W. Su, L. Yao, F. Yang, P. Li, J. Chen, and L. Liang, "Electroless plating of copper on surface-modified glass substrate," *Appl. Surf. Sci.*, vol. 257, no. 18, pp. 8067–8071, Jul. 2011.

[59] G. A. Shafeev, "Laser-assisted activation of dielectrics for electroless metal plating," *Appl. Phys. A Mater. Sci. Process.*, vol. 67, no. 3, pp. 303–311, Sept. 1998.

[60] K. C. Yung, C. Chen, and C. P. Lee, "Laser induced activation of circuit lines and via-holes on AlN for electroless metal plating," *Appl. Surf. Sci.*, vol. 257, no. 15, pp. 6601–6606, May 2011.

[61] "DuPont™ GreenTape™ 9K7." [Online Available]: http://www2.dupont.com/MCM/en_US/assets/downloads/prodinfo/GreenTape9K7DataSheet.pdf.

[62] R. Lacombe, *Adhesion measurement methods : theory and practice*. Boca Raton, FL: CRC/Taylor & Francis, 2005.

[63] B. He, "Characterization and improvement of copper / glass adhesion," PhD Thesis, Loughborough University, 2012.

[64] M. Paunovic, *Electroless deposition of copper*, 5th ed., vol. 1. 2010, pp. 433–446.

[65] R. Sard, B. T. Laboratories, and M. Hill, “The Nucleation , Growth , and Structure of Electroless Copper Deposits,” *J. Electrochem. Soc.*, no. 21, pp. 864–870.

[66] S. Nakahara, Y. Okinaka, and B. Laboratories, “MICROSTRUCTURE AND DUCT1 LITY OF ELECTROLESS COPPER DEPOSITS,” *Acta Met.*, vol. 3, no. 5, pp. 713–724, 1983.

[67] D. Hull and T. W. Clyne, *An introduction to composite materials*. Cambridge: Cambridge University Press, 1996.

[68] J. Comyn, *Adhesion science*. Cambridge: Royal Society of Chemistry, 1997.

[69] D. E. Packham, “Work of adhesion: contact angles and contact mechanics,” *Int. J. Adhes. Adhes.*, vol. 16, no. 2, pp. 121–128, May 1996.

[70] D. Packham, “Surface energy, surface topography and adhesion,” *Int. J. Adhes. Adhes.*, vol. 23, no. 6, pp. 437–448, Jan. 2003.

[71] H. Yoshiki, K. Hashimoto, and A. Fujishima, “Adhesion Mechanism of Electroless Copper Film Formed on Ceramic Substrates Using ZnO Thin Film as an Intermediate Layer,” *J. Electrochem. Soc.*, vol. 145, no. 5, pp. 1430–1434, 1998.

[72] S.-W. Choi, W.-B. Choi, Y.-H. Lee, B.-K. Ju, M.-Y. Sung, and B.-H. Kim, “The Analysis of Oxygen Plasma Pretreatment for Improving Anodic Bonding,” *J. Electrochem. Soc.*, vol. 149, no. 1, p. G8, 2002.

[73] A. Baldan, “Adhesively-bonded joints and repairs in metallic alloys, polymers and composite materials: Adhesives, adhesion theories and surface pretreatment,” *J. Mater. Sci.*, vol. 39, no. 1, pp. 1–49, Jan. 2004.

[74] R. L. Nuttall, J. P. Chem, R. Data, S. No, T. Osaka, T. Asada, E. Nakajima, and I. Koiwa, “Chemical Etching Properties of Highly Thermal Conductive AIN Ceramics for Electroless Ni-P Metallization,” *J. Electrochem. Soc.*, vol. 421, no. October, pp. 2578–2581, 1988.

[75] T. Jardiel, A. C. Caballero, J. F. Fernández, and M. Villegas, “Domain structure of $Bi_4Ti_3O_{12}$ ceramics revealed by chemical etching,” *J. Eur. Ceram. Soc.*, vol. 26, no. 13, pp. 2823–2826, Jan. 2006.

[76] M. Hubert, L. Calvez, F. Tessier, P. Lucas, and X.-H. Zhang, “Nanoporous surface of infrared transparent chalcogenide glass–ceramics by chemical etching,” *Mater. Res. Bull.*, vol. 47, no. 12, pp. 4076–4081, Dec. 2012.

[77] F. Yuan, “Etching Method for the Microstructure of LTCC,” *Mod. Appl. Sci.*, pp. 70–73, 2000.

[78] H. Horn, S. Beil, D. . Wesner, R. Weichenhain, and E. . Kreutz, “Excimer laser pretreatment and metallization of polymers,” *Nucl. Instruments Methods Phys. Res. Sect. B Beam Interact. with Mater. Atoms*, vol. 151, no. 1–4, pp. 279–284, May 1999.

[79] L. Tiejun, L. Qihong, D. Jingxing, W. Yunrong, Z. Jun, L. Jingru, Z. Zhiming, and S. Fanghong, "Improved adhesion of diamond coating on cobalt-cemented tungsten carbide hardmetal by using pulsed-UV-laser substrate surface pretreatment," *Appl. Surf. Sci.*, vol. 193, no. 1–4, pp. 102–119, Jun. 2002.

[80] H. K. Tonshoff and H. Kappel, "Surface Modification of Ceramics by Laser Machining," *Ann. CIRP*, vol. 47, pp.471-474, 1998.

[81] V. Oliveira, R. Vilar, and O. Conde, "Excimer laser ablation of Al_2O_3 – TiC ceramics : laser induced modifications of surface topography and structure," *Appl. Surf. Sci.*, vol. 97, pp. 831–836, 1998.

[82] "Material Safety Data Sheet 9K7 Green Tape." DuPont, pp. 1–11, 2011.

[83] B. Demri and D. Muster, "XPS study of some calcium compounds," *J. Mater. Process. Technol.*, vol. 55, no. 1995, pp. 311–314, 1994.

[84] K.M. Nair and S. Priya "DuPont™ Green Tape™ 9K7 Low Temperature Co-fired Ceramic (LTCC) Low Loss Dielectric System for High Frequency Microwave Applications" Advances in Electroceramic Materials II, Volume 221**,** pp212-216, 2010.

[85] G. Goch and H. N. Hansenl, "Quantitative Characterisation of Surface Texture," *CIRP Ann. - Manuf. Technol.*, vol. 49, no. 2, pp. 635–642, 2000.

[86] K. Stout and L. Blunt, "A contribution to the debate on surface classifications—random, systematic, unstructured, structured and engineered," *Int. J. Mach. Tools Manuf.*, vol. 41, no. 13–14, pp. 2039–2044, Oct. 2001.

[87] "Geometric Product Specifications (GPS) — Surface texture : Profile method - Nominal characteristics of contact (stylus) instruments," no. 1, 1998.

[88] R. Leach, "The Measurement of Surface Texture Using Stylus Instruments," 2001.

[89] S. Zahwi and A. M. Mekawi, "Some effects of stylus force on scratching surfaces," *Int. J. Mach. Tools Manuf.*, vol. 41, no. 13–14, pp. 2011–2015, Oct. 2001.

[90] R. Leach, "NanoSurf IV: traceable measurement of surface texture at the National Physical Laboratory, UK," *Int. J. Mach. Tools Manuf.*, vol. 41, no. 13–14, pp. 2113–2121, Oct. 2001.

[91] L. Deck and P. de Groot, "High-speed noncontact profiler based on scanning white-light interferometry.," *Appl. Opt.*, vol. 33, no. 31, pp. 7334–7342, Nov. 1994.

[92] U. Persson, "In-process measurement of surface roughness using light scattering," *Wear*, vol. 215, pp. 54–58, 1998.

[93] C. J. R. Sheppard and H. J. Matthews, “The extended-focus , auto-focus and surface-profiling techniques of confocal microscopy,” *J. Mod. Opt.*, vol. 35, no. 1, pp. 145–154, 1988.

[94] R. K. Leach, “Traceable measurement of suface texture in the optics industry,” *SPIE*, vol. 4411, no. 2002, pp. 177–183, Feb. 2002.

[95] R. Leach and A. Hart, “A comparison of stylus and optical methods for measuring 2D surface texture,” NPL Report, 2002.

[96] R. Leach, “Current Problems in the Field of Surface Texture Measurement,” NPL report, vol. 5436, pp. 0–3, 2001.

[97] “Good Practice Guide No . 116 The Measurement of Rough Surface Topography using Coherence,” NPL Report, 2010.

[98] “BSI Standards Publication Geometrical product specifications (GPS) — Surface texture : Areal Part 2 : Terms , definitions and surface.” 2012.

[99] R. K. Leach, “Good Practice Guide No. 37 The Measurement of Surface Texture using Stylus Instruments.”, NPL Report, 2014.

[100] R. K. Leach, “Measurement Good Practice Guide No. 108 Guide to the Measurement of Smooth Surface Topography using Coherence Scanning Interferometry.”

[101] “http://www.michmet.com/3d_s_functional_parameters.htm.” .

[102] A. N. N. Wennerberg, “The importance of surface roughness for implant incorparation,” *Int. J. Mach. Tools Manuf.*, vol. 38, no. 97, pp. 657–662, 1998.

[103] A. Wennerberg, R. Ohlsson, B. G. Rosén, and B. Andersson, “Characterizing three-dimensional topography of engineering and biomaterial surfaces by confocal laser scanning and stylus techniques.,” *Med. Eng. Phys.*, vol. 18, no. 7, pp. 548–56, Oct. 1996.

[104] E. Liew and M. Copper, “Signal Transmission Loss due to Copper Surface Roughness in High-Frequency Region,” no. 3.

[105] A. Zee and R. Massey, “Impact of surface treatment on high frequency signal loss characteristics,” *2009 4th Int. Microsystems, Packag. Assem. Circuits Technol. Conf.*, pp. 474–477, Oct. 2009.

[106] S. Hinaga, C. Systems, S. Jose, M. Y. Koledintseva, P. K. R. Anmula, and J. L. Drewniak, “Effect of Conductor Surface Roughness upon Measured Loss and Extracted Values of PCB Laminate Material Dissipation Factor,” in *Proceedins of technology conference IPC Expo/APEX*, 2009.

[107] B. He, D. P. Webb, J. Petzing, and R. Leach, “Improving plated copper adhesion for metallisation of glass PCBs,” *2011 12th Int. Conf. Electron. Packag. Technol. High Density Packag.*, pp. 1–5, Aug. 2011.

[108] J. Wang, N. R. Sottos, and R. L. Weaver, “Thin Film Adhesion Measurement by Laser Induced Stress Waves,” *J. Mech. Phys. Solids*, 2003.

[109] J. Strong, “Evaporated aluminum films for astronomical mirrors,” *Astron. Soc. Pacific*, vol. 2, no. 189, pp. 18–26, 1931.

[110] K. L. Mittal, “Adhesion measurement of thin films,” *Electrocompon. Sci. Technol.*, vol. 3, no. C, pp. 21–42, 1976.

[111] M. Charbonnier, Y. Goepfert, M. Romand, and D. Leonard, “Electroless Plating of Glass and Silicon Substrates Through Surface Pretreatments Involving Plasma-Polymerization and Grafting Processes,” *J. Adhes.*, vol. 80, no. 12, pp. 1103–1130, Dec. 2004.

[112] M. Charbonnier, M. Romand, Y. Goepfert, D. Léonard, and M. Bouadi, “Copper metallization of polymers by a palladium-free electroless process,” *Surf. Coatings Technol.*, vol. 200, no. 18–19, pp. 5478–5486, May 2006.

[113] R. R. Rye and A. J. Ricco, “Patterned Adhesion of Electrolessly Deposited Copper on Poly (tetrafluoroethylene),” *J. Electrochem. Soc.*, vol. 140, no. 6, 1993.

[114] S. Bhansali, D. K. Sood, and R. B. Zmood, “Selective electroless copper plating on silicon seeded by copper ion implantation,” *Thin Solid Films*, vol. 253, no. 1–2, pp. 391–394, Dec. 1994.

[115] M. Charbonnier, M. Romand, and Y. Goepfert, “Ni direct electroless metallization of polymers by a new palladium-free process,” *Surf. Coatings Technol.*, vol. 200, no. 16–17, pp. 5028–5036, Apr. 2006.

[116] S. J. Bull, “Failure mode maps in the thin scratch adhesion test,” *Tribol. Int.*, vol. 30, no. 7, 1997.

[117] O. S. Heavens, “Some factors influencing the adhesion of films produced by vacuum evaporation,” *lE J. Phys. rADIUM*, p. 355, 1950.

[118] P. Benjamin and C. Weaver, “Measurement of Adhesion of Thin Films,” *Proc. R. Soc. A Math. Phys. Eng. Sci.*, vol. 254, no. 1277, pp. 163–176, Feb. 1960.

[119] J. Sekler, P. A. Steinmann, and H. E. Hintermann, “The scratch test: different critical load determination techniques*,” *Surf. Coat. Technol.*, vol. 36, no. 1988, pp. 519–529, 1988.

[120] S. J. Bull, “Failure modes in scratch adhesion testing,” *Surf. Coatings Technol.*, vol. 50, no. 1, pp. 25–32, Jan. 1991.

[121] S. Soderberg, “Failure mode analysis of TiN-coated high speed steel: In situ scratch adhesion testing in the scanning electron microscope,” *Surf. Coat. Technol.*, vol. 41, pp. 31–49, 1990.

[122] Y. Xie and H. . Hawthorne, “Effect of contact geometry on the failure modes of thin coatings in the scratch adhesion test,” *Surf. Coatings Technol.*, vol. 155, no. 2–3, pp. 121–129, Jun. 2002.

[123] A. S. Maxwell, “Review of test methods for coating adhesion,” 2001.

[124] A. Harold, “Formulas the Skin Effect ,” in *proceedings of IRE*, 1942, pp. 299–311.

[125] T. S. Laverghetta, *Practical microwaves*. Englewood Cliffs, N.J.: Prentice Hall, 1996.

[126] S. Link and M. a. El-Sayed, *Shape and size dependence of radiative, non-radiative and photothermal properties of gold nanocrystals*, vol. 19, no. 3. 2000, pp. 409–453.

[127] J. Kim, S. H. Wen, D. Y.Jung, and R. W. Johnson, “Microstructure evolution during electroless copper deposition,” *IBM J. Res. Dev.*, vol. 28, no. 6, pp. 697–710, 1984.

[128] L. E. Khoong, Y. M. Tan, and Y. C. Lam, “Overview on fabrication of three-dimensional structures in multi-layer ceramic substrate,” *J. Eur. Ceram. Soc.*, vol. 30, no. 10, pp. 1973–1987, Aug. 2010.

[129] D. Rathnayake-Arachchige, D. A. Hutt, P. P. Conway, M. D’Auria, S. Lucyszyn, R. M. Lee, and I. D. Robertson, “Patterning of Electroless Copper Deposition on Low Temperature Co-fired Ceramic,” in *15th Electronic Packaging and technology conference*, 2013, pp. 630–634.

[130] S. Jia, M. Miao, R. Fangl, S. Guol, D. Hui, and Y. Jinl, “A 3D Micro-channel Cooling System Embedded in L TCC Packaging Substrate,” in *7th IEEE International Conference on Nano/Micro Engineered and Molecular Systems (NEMS)*, 2012, pp. 649–652.

[131] T. Tajima, H. Song, M. Yaita, K. Ajito, and N. Kukutsu, “300-GHz LTCC Horn Antennas Based on Antenna-in-package Technology,” in *Proceedings of the 43rd European Microwave Conference*, 2013, pp. 231–234.

[132] L. J. Golonka, T. Zawada, J. Radojewski, H. Roguszczak, and M. Stefanow, “LTCC Microfluidic System,” *Int. J. Appl. Ceram. Technol.*, vol. 3, no. 2, pp. 150–156, Mar. 2006.

[133] K.-I. Kim, J.-M. Kim, J.-M. Kim, G.-C. Hwang, C.-W. Baek, and Y.-K. Kim, “Packaging for RF MEMS devices using LTCC substrate and BCB adhesive layer,” *J. Micromechanics Microengineering*, vol. 16, no. 1, pp. 150–156, Jan. 2006.

[134] T. Rabe, P. Kuchenbecker, B. Schulz, and M. Schmidt, “Hot Embossing: An Alternative Method to Produce Cavities in Ceramic Multilayer,” *Int. J. Appl. Ceram. Technol.*, vol. 4, no. 1, pp. 38–46, Jan. 2007.

[135] W. Smetana, B. Balluch, G. Stangl, S. Lüftl, and S. Seidler, “Processing procedures for the realization of fine structured channel arrays and bridging elements by LTCC-Technology,” *Microelectron. Reliab.*, vol. 49, no. 6, pp. 592–599, Jun. 2009.

[136] G. Natarajan and J. N. Humenik, “3D Ceramic Microfluidic Device Manufacturing,” *J. Phys. Conf. Ser.*, vol. 34, pp. 533–539, Apr. 2006.

[137] G. Hagen and L. Rebenklau, “Fabrication of Smallest Vias in LTCC Tape,” *2006 1st Electron. Syst. Technol. Conf.*, pp. 642–647, 2006.

[138] T. Rabe, P. Kuchenbecker, B. Schulz, and M. Schmidt, “Hot Embossing: An Alternative Method to Produce Cavities in Ceramic Multilayer,” *Int. J. Appl. Ceram. Technol.*, vol. 4, no. 1, pp. 38–46, Jan. 2007.

[139] X. Shan, H. P. Maw, R. T. Tjeung, S. H. Ling, C. W. Lu, and R. Jachowicz, “Microstructure formation on low temperature co-fired ceramic green substrates using micro embossing,” *Microsyst. Technol.*, vol. 14, no. 9–11, pp. 1405–1409, Jan. 2008.

[140] K. Malecha and L. J. Golonka, “Microchannel fabrication process in LTCC ceramics,” *Microelectron. Reliab.*, vol. 48, no. 6, pp. 866–871, Jun. 2008.

[141] K. Malecha and L. J. Golonka, “Three-dimensional structuration of zero-shrinkage LTCC ceramics for microfluidic applications,” *Microelectron. Reliab.*, vol. 49, no. 6, pp. 585–591, Jun. 2009.

[142] Y. Fournier, O. Triverio, T. Maeder, and P. Ryser, “LTCC Free-standing Structures with Mineral Sacrificial Paste,” in *Proceedings of Ceramic Interconnect and Ceramic*, 2008.

[143] P. Espinoza-vallejos and J. Santiago-avilés, “Photolithographic Feature Fabrication in LTCC,” *Int. J. Microcircuits Electron. Packag.*, vol. 23, no. 3, 2000.

[144] D. Sciti, C. Melandri, and A. Bellosi, “Excimer laser-induced microstructural changes of alumina and silicon carbide,” *J. Mater. Sci.*, vol. 35, pp. 3799–3810, 2000.

[145] H. K. Tonshoff, A. Ostendorf, K. Korber, and K. Meyer, “Comparison of machining strategies for ceramics using frequency converted Nd : YAG and excimer lasers,” in *Second International Symposium on Laser Precision Microfabrication*, 2002, vol. 4426, pp. 408–411.

[146] J. Kita, A. Dziedzic, L. J. Golonka, and T. Zawada, “Laser treatment of LTCC for 3D structures and elements fabrication,” *Microelectron. Int.*, vol. 19, no. 3, pp. 14–18, 2002.

[147] G. (George) Chryssolouris, *Laser machining : theory and practice*. New York: Springer-Verlag, 1991.

[148] T. Baras, A. F. Jacob, and, "Manufacturing Reliability of LTCC Millimeter-Wave Passive Components," *IEEE Trans. Microw. Theory Tech.*, vol. 56, no. 11, pp. 2574–2581, 2008.

[149] J. J. Van Tassel and C. A. Randall, "Micron Scale Conductors and Integrated Passives in LTCC ' s by Electrophoretic Deposition."

[150] J. Müller, R. Perrone, H. Thust, K. Drüe, C. Kutscher, R. Stephan, J. Trabert, M. Hein, and D. Schwanke, "Technology Benchmarking of High Resolution Structures on LTCC for Microwave Circuits," in *Electronics Systemintegration Technology Conference*, 2006, pp. 111–117.

[151] S. Hildebrandt and K.-J. Wolter, "Thin film structuring on LTCC," *2008 31st Int. Spring Semin. Electron. Technol.*, pp. 526–530, May 2008.

[152] A. Dziedzic, "Electrical and structural investigations in reliability characterisation of modern passives and passive integrated components," *Microelectron. Reliab.*, vol. 42, no. 4–5, pp. 709–719, Apr. 2002.

[153] D. Nowak, "Simulations of passive components in LTCC technology," *2011 Int. Students Young Sci. Work. "Photonics Microsystems,"* pp. 99–102, Jul. 2011.

[154] M. Lahti, V. Lantto, and S. Leppävuori, "Planar Inductors on an LTCC Substrate Realized by the Gravure-Offset-Printing Technique," *IEEE Trans. Components Packag. Technol.*, vol. 23, no. 4, pp. 606–610, 2000.

[155] E. E. Hoppenjans and W. J. Chappell, "High Value Passive Component Integration in LTCC Technology," *2007 IEEE/MTT-S Int. Microw. Symp.*, pp. 1913–1916, Jun. 2007.

[156] H. Samavati, , A. Hajimiri, A. R. Shahani, G. N. Nasserbakht, and T. H. Lee, "Fractal Capacitors," *IEEE J. Solid state Circuits*, vol. 33, no. 12, pp. 2035–2041, 1998.

[157] M. T. Sebastian and H. Jantunen, "Low loss dielectric materials for LTCC applications: a review," *Int. Mater. Rev.*, vol. 53, no. 2, pp. 57–90, Mar. 2008.

[158] A. N. Samant and N. B. Dahotre, "Laser machining of structural ceramics—A review," *J. Eur. Ceram. Soc.*, vol. 29, no. 6, pp. 969–993, Apr. 2009.

[159] H. Hocheng and K. Y. Wang, *Analysis of excimer laser machining of micro patterns*. 2011.

[160] R. Crafer and P. J. Oakley, *Laser processing in manufacturing*. London: Chapman & Hall, 1993.

[161] M. Bozzi and L. Perregrini, "Modeling of Conductor, Dielectric, and Radiation Losses in Substrate Integrated Waveguide by the Boundary Integral-Resonant Mode Expansion Method," *IEEE Trans. Microw. Theory Tech.*, vol. 56, no. 12, pp. 3153–3161, Dec. 2008.

[162] Z. Li and K. Wu, "24GHz FMCW Radar Front-End System on Substrate," *2007 IEEE Radio Wirel. Symp.*, pp. 233–236, 2007.

[163] H. A. Atwater, *Introduction to microwave theory*. McGraw-Hill, 1962.

[164] N. J. Cronin, *Microwave and optical waveguides*. Bristol: Institute of Physics, 1995.

[165] H. Uchimura, T. Takenoshita, and M. Fujii, "Development of a 'laminated waveguide,'" *IEEE Trans. Microw. Theory Tech.*, vol. 46, no. 12, pp. 2438–2443, 1998.

[166] M. Bozzi, M. Pasian, L. Perregrini, and K. Wu, "On the Losses in Substrate Integrated Waveguides," in *Proceedings of European Microwave Conference*, 2007, no. October, pp. 384–387.

[167] T. Tick, J. Ja, M. Henry, C. Free, and H. Jantunen, "LTCC INTEGRATED AIR-FILLED WAVEGUIDES FOR G-BAND APPLICATIONS," *Microw. Opt. Technol. Lett.*, vol. 51, no. 1, pp. 176–178, 2009.

[168] M. Bozzi, L. Perregrini, K. Wu, and P. Arcioni, "Current and Future Research Trends in Substrate Integrated Waveguide Technology," *Radioengineering*, vol. 18, no. 2, pp. 201–209, 2009.

[169] H. Chien, T. Shen, T. Hung, and R. Wu, "Design ofA Vertically Stacked Substrate Integrated Folded-Waveguide Resonator Filter in LTCC," in *Proceedings of Asia-Pacific Microwave Conference*, 2007, pp. 2–5.

[170] P. Qiu, Y. Zhang, and B. Yan, "A Novel millimeter-wave Substrate Integrated Waveguide (SIW) filter buried in LTCC," *2008 Asia-Pacific Microw. Conf.*, pp. 1–4, Dec. 2008.

[171] P. Qiu, Z. Wang, and B. Yan, "Novel Ka-band Substrate Integrated Folded Waveguide (SIFW) Quasi-elliptic filters in LTCC," *2008 Asia-Pacific Microw. Conf.*, pp. 1–4, Dec. 2008.

[172] J. Chen, W. Hong, X. Chen, P. Yan, Q. Lai, and K. Wu, "SUBSTRATE INTEGRATED WAVEGUIDE FILTER," *Microw. Opt. Technol. Lett.*, vol. 50, no. 2, pp. 285–287, 2008.

[173] W. Tsai and R. Wu, "Tri-band Filter Design using Substrate Integrated Waveguide Resonators inLTCC," in *Microwave Symposium Digest (MTT)*, 2010, pp. 445–448.

[174] B. Sanadgol, S. Holzwarth, A. Milano, and R. Popovich, "60 GHz Substrate Integrated Waveguide Fed Steerable LTCC Antenna Array," pp. 2–5.

[175] J. Xu, Z. N. Chen, X. Qing, and W. Hong, “Bandwidth Enhancement for a 60 GHz Substrate Integrated Waveguide Fed Cavity Array Antenna on LTCC,” *IEEE Trans. Antennas Propag.*, vol. 59, no. 3, pp. 826–832, Mar. 2011.

[176] A.-C. Bunea, D. Neculoiu, M. Lahti, and T. Vaha-Heikkila, “94 GHz substrate integrated waveguide fed antenna in LTCC technology,” *2012 IEEE Asia-Pacific Conf. Antennas Propag.*, pp. 283–284, Aug. 2012.

[177] S. Ramesh and T. R. Rao, “High gain dielectric loaded exponentially tapered slot antenna array based on substrate integrated waveguide for V-band wireless communications,” *AEU - Int. J. Electron. Commun.*, pp. 8–15, Jul. 2014.

[178] S. W. Wong, K. Wang, , and Z. Chen, “Electric Coupling Structure of Substrate Integrated Waveguide (SIW) for the Application of 140-GHz Bandpass Filter on LTCC,” *IEEE Trans. Components Packag. Manuf. Technol.*, vol. 4, no. 2, pp. 316–322, 2014.

[179] J. W. Digby, C. E. Mcintosh, G. M. Parkhurst, B. M. Towlson, S. Hadjiloucas, J. W. Bowen, J. M. Chamberlain, R. D. Pollard, R. E. Miles, D. P. Steenson, L. S. Karatzas, N. J. Cronin, and S. R. Davies, “Fabrication and Characterization of Micromachined Rectangular Waveguide Components for Use at Millimeter-Wave and Terahertz Frequencies,” *IEEE Trans. Microw. Theory Tech.*, vol. 48, no. 8, pp. 1293–1302, 2000.

[180] Y. Matsuura, D. Miura, and M. Miyagi, “Fabrication of Copper Oxide-Coated Hollow Waveguides for CO_2 Laser Radiation,” *Appl. Opt.*, vol. 38, no. 9, p. 1700, Mar. 1999.

[181] R. Javaid, H. Kawanami, M. Chatterjee, T. Ishizaka, A. Suzuki, and T. M. Suzuki, “Fabrication of microtubular reactors coated with thin catalytic layer (M=Pd, Pd−Cu, Pt, Rh, Au),” *Catal. Commun.*, vol. 11, no. 14, pp. 1160–1164, Aug. 2010.

[182] P. J. A. Kenis, R. F. Ismagilov, and G. M. Whitesides, “Microfabrication inside capillaries using multiphase laminar flow patterning,” *Science (80-.).*, vol. 285, pp. 83–85, 1999.

[183] H. K. Park, H. B. Lee, and K. Kim, “A facile deposition of silver onto the inner surface of a glass capillary tube for micro-surface-enhanced Raman scattering measurements.,” *Appl. Spectrosc.*, vol. 61, no. 1, pp. 19–24, Jan. 2007.

[184] F. Heuck and U. Staufer, “Silver/silver-chloride electrode fabrication in closed micro-fluidic capillaries,” *Microelectron. Eng.*, vol. 87, no. 5–8, pp. 1383–1385, May 2010.

[185] S. H. Paek, Y. K. Choi, and D. S. Kim, “Selective microfabrication of silver electrodes inside a microchannel by multiphase laminar flow with density difference,” *Microelectron. Eng.*, vol. 87, no. 5–8, pp. 1375–1378, May 2010.

[186] W. Su, L. Yao, F. Yang, P. Li, J. Chen, and L. Liang, “Electroless plating of copper on surface-modified glass substrate,” *Appl. Surf. Sci.*, vol. 257, no. 18, pp. 8067–8071, Jul. 2011.

[187] Y. Chen, E. T. Kang, and K. G. Neoh, “Electroless Metallization of Glass Surfaces Functionalized by Silanization and Graft Polymerization of Aniline,” *Langmuir*, vol. 17, no. 23, pp. 7425–7432, 2001.

[188] P. Zhu, Y. Masuda, and K. Koumoto, “Seedless micropatterning of copper by electroless deposition on self-assembled monolayers,” *J. Mater. Chem.*, vol. 14, no. 6, p. 976, 2004.